Performance Evaluation and Waveform Design for MIMO Radar

Chaoran Du

A thesis submitted for the degree of Doctor of Philosophy.
The University of Edinburgh.
March 2010

Abstract

Multiple-input multiple-output (MIMO) radar has been receiving increasing attention in recent years due to the dramatic advantages offered by MIMO systems in communications. The amount of energy reflected from a common radar target varies considerably with the observation angle, and these scintillations may cause signal fading which severely degrades the performance of conventional radars. MIMO radar with widely spaced antennas is able to view several aspects of a target simultaneously, which realizes a spatial diversity gain to overcome the target scintillation problem, leading to significantly enhanced system performance. Building on the initial studies presented in the literature, MIMO radar is investigated in detail in this thesis.

First of all, a finite scatterers model is proposed, based on which the target detection performance of a MIMO radar system with arbitrary array-target configurations is evaluated and analyzed. A MIMO radar involving a realistic target is also set up, whose simulation results corroborate the conclusions drawn based on theoretical target models, validating in a practical setting the improvements in detection performance brought in by the MIMO radar configuration.

Next, a hybrid bistatic radar is introduced, which combines the phased-array and MIMO radar configurations to take advantage of both coherent processing gain and spatial diversity gain simultaneously. The target detection performance is first assessed, followed by the evaluation of the direction finding performance, *i.e.*, performance of estimating angle of arrival as well as angel of departure. The presented theoretical expressions can be used to select the best architecture for a radar system, particularly when the total number of antennas is fixed.

Finally, a novel two phase radar scheme involving signal retransmission is studied. It is based on the time-reversal (TR) detection and is investigated to improve the detection performance of a wideband MIMO radar or sonar system. Three detectors demanding various amounts of *a priori* information are developed, whose performance is evaluated and compared. Three schemes are proposed to design the retransmitted waveform with constraints on the transmitted signal power, further enhancing the detection performance with respect to the TR approach.

Declaration of originality

I hereby declare that the research recorded in this thesis and the thesis itself was composed and originated entirely by myself in the School of Engineering at The University of Edinburgh.

Chaoran Du

Acknowledgements

First of all, I would like to express my appreciation to my supervisors Dr. John S. Thompson and Dr. Yvan R. Petillot, for offering me the opportunity to pursue this project and for their excellent guidance and support during the course of my Ph.D. research. They are perfect gentlemen who are always nice, polite, responsible, and considerate. I have learned so much from them and working together with them is the most precious experience in my life.

I would also like to thank the financial support of the Scottish Funding Council for the Joint Research Institute (JRI) with Edinburgh and the Heriot-Watt Universities, which is a part of the Edinburgh Research Partnership (ERP), without which it would be impossible for me to complete this work.

My family have been the most important support for me. No words can express my deepest appreciation and gratitude to them and especially to my parents for their constant love and encouragement, which has helped me go through difficult times of completing this work. Thank you so much for believing in me at all times even when I had doubt about myself. I know you will always be there for me whenever I need, and I wish I can always make you very proud.

I would like to express my special appreciation to Tong Xu, who has been accompanying me for the last four years of my study overseas. Thank you so much for your patience, understanding, support, comfort, and most importantly your continuous love, especially during all the tough times.

Last but definitely not the least, I would like to thank all my friends at IDCOM for their continuous help and friendships. Without them, I would not have such a wonderful life in Edinburgh for the past four years.

Contents

List of figures

List of tables

Acronyms and abbreviations

2D	Two Dimensional
3D	Three Dimensional
ACRB	Average Cramer-Rao Bound
AoA	Angle of Arrival
AoD	Angle of Departure
APC	Armoured Personal Carrier
CAD	Computer Aided Design
CDF	Cumulative Distribution Function
CFAR	Constant False Alarm Rate
CRB	Cramer-Rao Bound
EM	Electro-Magnetic
FEKO	FEldberechnungbei Korpern mit beleibeiger Oberflache
GLRT	Generalized Likelihood Ratio Test
i.i.d.	Independent and Identically Distributed
KKT	Karush-Kuhn-Tucher
LCMV	Linearly Constrained Minimum Variance
LRT	Likelihood Ratio Test
MBT	Main Battle Tank
MF	Matched Filter
MI	Mutual Information
ML	Maximum Likelihood
MIMO	Multiple-Input Multiple-Output
MSC	Multiple Sidelobe Canceller
MSE	Mean-Square Error
MSL	Missile launcher
MTI	Moving Target Indication
MUSIC	MUltiple SIgnal Classification
MVDR	Minimum variance distortionless response
OFDM	Orthogonal Frequency Division Multiplexing

PDF	Probability Density Function
RCS	Radar Cross Section
SAR	Synthetic Aperture Radar
SCR	Signal to Clutter power Ratio
SNR	Signal to Noise Ratio
STR	Stinger launcher
SVD	Singular Value Decomposition
TDM	Time-Division Multiplexing
TR	Time Reversal
ULA	Uniform Linear Array

Nomenclature

a^{rc}	Reflectivity coefficient of a scatterer
c_0	The speed of light
$\mathbf{C_x}$	Covariance matrix of the vector $\mathbf{x}$
d^t	Distance between Tx 1 and the target
d^r	Distance between Rx 1 and the target
d^{tr}	Distance between Tx 1 and Rx 1 via the target
E_s	Total transmitted power from all the transmit antennas
$\mathbf{e}(f_q)$	Channel estimation error vector
$\mathbf{E}(f_q)$	Channel estimation error matrix
$\mathbf{h}$	Channel vector
$\mathbf{H}$	Channel matrix
$\mathbf{h}(f_q)$	Channel frequency response vector
$\mathbf{H}(f_q)$	Channel frequency response matrix
$\hat{\mathbf{h}}(f_q)$	Estimated Channel frequency response vector
$\hat{\mathbf{H}}(f_q)$	Estimated Channel frequency response matrix
$\mathcal{H}_0$	Null hypothesis that the target does not exist
$\mathcal{H}_1$	Alternate hypothesis that the target exists
M_t	Number of antenna arrays at transmitter of the hybrid bistatic radar
M_r	Number of antenna arrays at receiver of the hybrid bistatic radar
$\mathbf{n}(t)$	Time-domain additive white Gaussian noise vector of power σ_n^2
N_a	Number of antennas of array A in TR process
N_b	Number of antennas of array B in TR process
N_t	Number of antenna elements of the ULA at transmitter
N_r	Number of antenna elements of the ULA at receiver
N_s	Number of scatterers constituting the target
$\mathrm{Pr_D}$	Probability of detection
$\mathrm{Pr_{MD}}$	Probability of missed detection
$\mathrm{Pr_{FA}}$	Probability of false alarm
$\mathbf{r}(t)$	Time-domain receive signal vector with noise component

$\mathbf{s}(t)$	Time-domain transmit signal vector
$\mathbf{r}(f_q)$	Frequency-domain receive signal vector with noise component
$\mathbf{s}(f_q)$	Frequency-domain transmit signal vector
t	Time
T	Test statistic
$\mathbf{U}$	Matrix of eigenvectors
$\mathbf{x}$	Output of a bank of matched filters whose input is the received signal
$\boldsymbol{\alpha}$	Fading coefficient vector
Δ_t	Normalized transmit interelement spacing in wavelengths
Δ_{ta}	Normalized transmit array separation in wavelengths
Δ_r	Normalized receive interelement spacing in wavelengths
Δ_{ra}	Normalized receive array separation in wavelengths
Δx	Dimension of the target in the x-direction
Δy	Dimension of the target in the y-direction
η	Detector threshold
ι^2	Variance of the reflectivity coefficient of a scatterer
λ_c	Carrier wavelength
$\mathbf{\Lambda}$	Diagonal matrix of eigenvalues
σ	Standard deviation
τ	Time delay from the transmitter to receiver via the target
Φ^t	Angle of departure
$\hat{\Phi}^t$	Estimated angle of departure
Φ^{ta}	Azimuth of transmitter
Φ^{te}	Elevation of transmitter
Φ^r	Angle of arrival
$\hat{\Phi}^r$	Estimated angle of arrival
Φ^{ra}	Azimuth of receiver
Φ^{re}	Elevation of receiver
$\mathbf{\Psi}_t(\Phi^t)$	Transmitter steering vector
$\mathbf{\Psi}_r(\Phi^r)$	Receiver steering vector
(x, y)	(x,y)-coordinates of a scatterer
(x_0, y_0)	(x,y)-coordinates of the target center
(x^t, y^t)	(x,y)-coordinates of a transmit antenna

(x^r, y^r)	(x,y)-coordinates of a receive antenna
$\mathbf{0}_k$	$k \times 1$ all-zeros vector
$\mathbf{I}_k$	$k \times k$ identity matrix
δ_{ij}	Dirac delta function
$\mathrm{PDF}(\cdot)$	Probability density function
$\mathrm{CDF}(\cdot)$	Cumulative distribution function
$\digamma(\cdot)$	Characteristic function
$\Pr(\cdot)$	Probability value
$\sim$	Distributed as
$\mathcal{CN}(\boldsymbol{\mu}, \mathbf{C})$	Multivariate complex normal distribution with mean $\boldsymbol{\mu}$ and covariance matrix $\mathbf{C}$
χ^2_k	Central chi-square random variable with k degrees of freedom
$\chi'^2_k(\lambda)$	Non-central chi-square random variable with k degrees of freedom and non-centrality parameter λ
$\mathcal{F}_{\chi^2_k}$	CDF of a central chi-square random variable with k degrees of freedom
$\mathcal{F}^{-1}_{\chi^2_k}$	Inverse CDF of a central chi-square random variable with k degrees of freedom
$\Gamma(k, \theta)$	Gamma random variable with the shape parameter k and scale parameter θ
$\mathcal{F}_{\Gamma(k,\theta)}$	CDF of a Gamma random variable with parameters k and θ
$\mathcal{F}^{-1}_{\Gamma(k,\theta)}$	Inverse CDF of a Gamma random variable with parameters k and θ
$Q(x)$	Gaussian right-tail function
$Q^{-1}(x)$	Inverse Gaussian right-tail function
$\{\cdot\}^*$	Complex conjugate operation
$\{\cdot\}^T$	Matrix transpose operation
$\{\cdot\}^H$	Matrix Hermitian transpose operation
$\{\cdot\}^{-1}$	Matrix inverse operation
$\mathrm{diag}(\mathbf{a})$	A diagonal matrix with its diagonal given by the vector **a**
$\{\cdot\}^\dagger$	Moore-Penrose Pseudoinverse operation
$\mathrm{trace}\{\cdot\}$	Matrix trace operation
$\det\{\cdot\}$	Matrix determinant operation
$\lvert\cdot\rvert$	Modulus of a complex number
$\lVert\cdot\rVert$	Euclidean norm

$\|\cdot\|_F$	Frobenius norm
$\lfloor k \rfloor$	The largest integer smaller than k
$\mathrm{E}\{\cdot\}$	Statistical expectation operator
$\mathrm{var}\{\cdot\}$	Statistical variance operator
$\circledast$	Convolution
$\otimes$	Kronecker product
$\Re$	Real part
$\Im$	Imaginary part
$\cos(\cdot)$	Cosine function
$\sin(\cdot)$	Sine function
$\exp(\cdot)$	Exponential function
$J_k(z)$	Bessel functions of the first kind and integer order
$\mathrm{erf}(a+jb)$	Complex-valued error function

Chapter 1
Introduction

This thesis is devoted to the MIMO radar system taking advantage of spatial diversity gain. In this introductory chapter, the origin and motivation of this work will be provided in Section 1.1. Then Section 1.2 will summarize the objectives and main contributions of this thesis. Finally, an overview of the organisation of the remaining chapters will be presented in Section 1.3.

1.1 Introduction and Motivation

The term *RADAR* was originally an acronym for "*RAdio Detection And Ranging*" coined in 1941, and has become a standard English word today. The basic principle of a radar system is to transmit an electro-magnetic (EM) signal into space and receive echo signals reflected by targets, which are carefully processed to provide information about them. Early radar was developed at a rapid pace driven by military demands, but after World War II, radar has been used for diverse civilian purposes as well. The wide range of radar applications and developments in the signal processing domain stimulate radar researchers to design and implement more and more sophisticated radar systems in order to meet the increasing accuracy requirements.

In recent years, a concept termed multiple-input multiple-output (MIMO) radar has been attracting increasing attention, which was motivated by intensive research on MIMO wireless communications since 1990s. This is not surprising due to the fundamental similarity between communication systems and radar in that they both utilize antennas to transmit and receive EM signals. There is no explicit definition of MIMO radar as many different research groups have tackled MIMO radar problems from various perspectives. MIMO radar can be broadly defined as a radar system deploying multiple antennas to simultaneously transmit arbitrary waveforms and utilizing multiple antennas to receive signals which are then processed jointly. Researchers in this field have demonstrated considerable potential gains from MIMO radar in scintillation mitigation, resolution enhancement, and interference suppression, *etc*. By fully exploiting these benefits, MIMO radar is capable of significantly improving target detection,

parameter estimation, tracking and recognition performance compared with its conventional phased-array counterpart [1].

Motivated by breakthroughs in communications theory, one important notion of MIMO radar is proposed by Fishler *et al*. in [3] that the system performance can be dramatically enhanced by taking advantage of the *spatial diversity gain* provided by the array-target configuration. More specifically, such a gain is determined by the interelement spacing of the antenna array, the size of the target, and the distance between the antenna array and the target. Spatial diversity gain is one of the two major benefits realized by MIMO communication systems, and it is often achieved by transmitting the same signal through different sub-channels and combining the information at the receiver. Diversity gain is used to combat channel fading and thus enhance the link reliability of the system [4,5]. The same idea can be exploited in radar scenarios. It has long been understood that common radar targets are complex bodies, and large scintillations in the amount of energy reflected by a complex target can occur with only very small changes in the illuminating direction. The antennas of MIMO radar are widely separated such that different antennas observe different aspects of the target, and the target returns resulting from independent illuminations are combined together leading to a spatial diversity gain. This is similar to that obtained in the communication systems when the data is transmitted through independent channels. The underlying idea of diversity gain in MIMO radar is that any individual view of the target might have a small return with a significant probability, but by increasing the number of look directions, the probability that all directions have small returns can be very low [6]. The target deep fading or scintillation problem, which severely degrades the performance of conventional radars whose antennas are closely spaced, is overcome by taking advantage of spatial diversity gain, leading to a significantly enhanced target detection and parameter estimation performance of MIMO radar [7–10].

The MIMO model presented in the literature can only be adopted in radar systems with extreme configurations, and it is derived based on assumptions which may be not realistic in practice. In order to investigate performance of radar systems with arbitrary configurations, a new model has to be considered. In addition, since different configurations yield distinct system performance results, an immediate question “What is the best architecture for a radar system when the number of antennas is fixed?” needs to be answered. Moreover, for a radar system with a specified configuration, it is obvious that waveform design is a crucial problem as the choices of transmitted signals affect system performance considerably. The superiority of MIMO radar

and the questions mentioned above inspired the work documented in this thesis.

1.2 Objectives and Contributions of the Thesis

1.2.1 Objectives

The objective of the work presented in this thesis is to investigate the performance of a MIMO radar system taking advantage of spatial diversity gain. It aims to find out the effects that different configurations of a MIMO radar system have on detecting both theoretical and realistic targets. The next purpose is to seek the best architecture for a radar system with a fixed number of antennas, taking into account both target detection and direction finding performance. Finally, this work also aims to provide waveform and detector design schemes for a MIMO system to enhance target detection performance.

1.2.2 Contributions

The main contributions of this thesis can be summarized as follows:

- A finite scatterers model is introduced to solve the problem that the existing idealized statistical model proposed for MIMO radar can only be adopted in extreme scenarios. A closed form formula is derived to calculate the theoretical probability of detection for a MIMO radar having an arbitrary array-target configuration. This theoretical result makes it possible to predict the actual MIMO radar performance before implementing expensive experiments and avoiding time consuming simulations.

- Based on the finite scatterers model, a MIMO radar system is set up involving a realistic target which is a life-size land vehicle. The target detection performance of the system with different configurations is simulated, and the numerical results corroborate previous conclusions drawn based on theoretical and mathematical target models, validating in a practical setting the improvements in detection performance available from MIMO radar configurations. To the author's knowledge, this is the first effort of its kind in the open literature.

- A hybrid bistatic radar is introduced, which combines the phased-array and MIMO configurations to simultaneously take advantage of both coherent processing gain and spatial

diversity gain. This hybrid radar is a general system model and it can be utilized to describe various practical radar configurations, including the MIMO and phased-array configurations as special and extreme cases. Theoretical expressions are derived to evaluate both the target detection and direction finding performance of a hybrid radar, which can be used to select the best architecture for a given specific scenario, particularly when the total number of antennas is fixed.

- A modified detection process based on time-reversal (TR) detection, an approach to improve the detection performance of a radar system, is explored to overcome the latter's limitations. Three detectors requiring different amounts of *a priori* information are developed, whose theoretical thresholds and probabilities of detection are derived. Three schemes are proposed to design the retransmitted waveform with constraints on the transmitted signal power, further enhancing the system detection performance significantly compared with the TR approach.

1.3 Organisation of the Thesis

The rest of the thesis is organised as follows:

Chapter 2 presents the general principles and background knowledge related to the topic of this thesis. It starts with an introduction to the key components of a radar system, followed by a brief review of conventional radars employing multiple antennas. Then important signal processing approaches addressing the target detection and direction finding problems are discussed. After reviewing the current state of MIMO radar research, the time-reversal technique and its applications in radar for target detection are also discussed.

Chapter 3 evaluates the target detection performance of a MIMO radar system having an arbitrary array-target configuration. After a short discussion of the statistical MIMO model and its limitations, a finite scatterers model is introduced. MIMO radar with a theoretical target is then examined, and a closed form formula to calculate the theoretical probability of detection for such a system is derived, following which the analysis of two extreme channel models and simplified expressions of the formula for two special cases are provided. Finally, MIMO radar involving a realistic target is set up by using the data collected from previous research on target modelling, and the detection performance of the system with different configurations is simulated.

Chapter 4 studies a hybrid bistatic radar which combines the phased-array and MIMO configurations, providing a balance between coherent processing gain and spatial diversity gain. This chapter starts with the description of the hybrid radar configuration, along with its channel and signal models. Next, a closed form expression is derived to assess the theoretical probability of detection for different configurations of the hybrid radar system. In the end, the performance of the radar as a direction finding system is evaluated. An initialization process is first described, during which the angle of departure (AoD) is estimated. Then the angle of arrival (AoA) estimation is considered when the true AoD, or the estimated AoD obtained during the initialization stage is known at the transmitter, and for the latter, the effect the estimation error in AoD has on finding AoA is measured.

Chapter 5 investigates a MIMO detection process developed based on the time-reversal (TR) detection proposed in the literature to enhance radar target detection performance. Three detectors demanding different amounts of *a priori* information are discussed, whose theoretical thresholds and probabilities of detection are derived. Then, with constraints on transmitted signal power, three schemes are proposed to design the retransmitted waveform based on the noisy estimated channel and a parameter indicating the quality of the estimation. Lastly, a comparison of the performance of various detectors is done, followed by a comparison drawn between different waveform design schemes and the TR approach.

Chapter 6 summarises the whole thesis and states possible directions of future research.

Chapter 2
Background

In this chapter, we will present a discussion of some fundamental principles of radar required for this project, and a review of the work done by the research community in the emerging field of MIMO radar. The content of this chapter provides the reader with a basic background of the current work and will be frequently referred to in the rest of the thesis. This chapter will divide into two main parts, dealing separately with conventional and recently developed radars respectively. In the first part, some key concepts of a radar system will firstly be described, followed by an introduction to conventional radars utilizing multiple antennas as well as long-familiar approaches for target detection and direction finding problems. The second part will cover two new schemes that have appeared in the radar community, MIMO radar and the radar time-reversal technique, which can provide improved performance over conventional radars.

2.1 Basic Background of Radar

In this section, we will introduce some basic concepts of radar systems and briefly discuss three conventional multiple antenna radars. More details can be found in some classic textbooks, such as [11].

2.1.1 Tasks of Radar

The underlying concept of radar systems is that the transmitter emits electro-magnetic (EM) signals into an environment and the receiver collects the echoes reflected from objects. The reflected signals are then appropriately processed in order to detect the presence of targets and/or to extract as much information about the targets as possible. Early radar was developed for military applications such as surveillance of hostile targets and control of weapons to guide missiles and fighter aircraft. However, radar now has been widely employed for civilian applications including air traffic control, police detection of speeding traffic, marine and air navigation, detection and tracking of weather disturbances, *etc*. [11, 12]. Regardless of the broad ranges of applications, the two basic tasks of radar are:

Detection of the presence of reflecting targets, which is the most fundamental function of a radar system. To accomplish this task, an EM waveform is transmitted and it will be reflected by targets if they are present. The function of a detector is to decide whether the received signal is the reflected echo in noise (targets exist) or noise only (no target). If targets are detected, one may be interested in determining their characteristics, which leads to the second task of radar.

Extraction of information about targets from the received signals. The radar receiver measures the echoes reflected by the target, and several parameters of the target can be estimated by observing a series of measurements as a function of position, time, and frequency. Some of the most important parameters of a target being illuminated by a radar system are [11]:

- **Range**: Range is the distance between the radar system and the target. One approach to estimate the range is to transmit a short pulse and measure the time difference between the transmission and the reception of the echo signal. Another method is to transmit a *chirp* whose frequency changes with time, and then measure the difference in frequency by comparing the frequency of the received signal to the one currently being emitted, which gives the time difference and thus the range.
- **Angle**: The angle information, such as *angle of arrival* (AoA), indicates the direction of the target with respect to the radar system, and it specifies the exact target location when combined together with the range. The target direction finding problem is usually solved by processing the signals impinging on an antenna array, *i.e.*, spatial samples of the echo signal reflected by the target.
- **Velocity**: Measuring the velocity of targets is the main objective of several radar systems, such as the police speed radar. The velocity information is also used in a *moving target indication* (MTI) radar to separate the moving target echoes from the stationary clutter, and the latter is unwanted and can be very strong in many cases. The target motion relative to the radar system results in the *Doppler effect*, *i.e.*, frequency shift in the echo signal. The Doppler frequency can be estimated from the received echoes and consequently the velocity can be known.

Before we proceed to introduce the signal processing algorithms for target detection and parameter estimation, important properties of radar targets and sources of interference in radar

systems will be discussed first.

2.1.2 Radar Cross Section of Target

Scattering occurs when a target is illuminated by an EM wave, causing the incident energy to be re-radiated (scattered) in many different directions away from the target. The amount of energy scattered in the direction of the receiver is of chief interest in radar since it indicates how detectable the target is, and it is characterized by the target's radar cross section (RCS). The RCS of a target is the required area of a hypothetical perfectly reflecting sphere at the target location, such that the power actually received at the receiver is produced. The perfectly reflecting sphere means that it scatters the incident power isotropically. Scattering, and hence the RCS, depends on a large number of properties of both the target and the illuminating EM wave, including the material and absolute size of the target, target size relative to the wavelength of the EM wave, the incident angle and reflected angle, distance between the target and the transmitter and receiver, *etc.* [13].

Common types of radar targets such as aircraft, ships, and terrain, are complex bodies composed of many scatterers, and their RCS are complicated functions of the viewing aspect, the radar frequency, and also the range. Both experimental measurements and modelling simulations demonstrate that a small change in the target aspect of only a fraction of a degree may lead to scintillations of 15dB or more in the reflected energy [11]. In order to properly assess the effects of these scintillations, the RCS of a complex target is best described by an appropriate statistical model which is chosen according to assumptions about the nature of the target. There are several widely adopted statistical RCS models, for example, the Chi-square target model, the classical Swerling I - Swerling IV models, the Rice target model, *etc.* [12, 14].

2.1.3 Interference

Information about a target is carried by the signal reflected from the target which always experiences interference by undesired signals, degrading the system performance. Interference in radar has long been deeply studied and it can be divided into the following three categories:

Noise: Noise may be generated by internal sources such as electronic devices in the radar receiver, and/or by external sources like the background environment surrounding the

target and the receiver. Noise is always present and normally modelled as a random addition to the desired echo signal.

Clutter: Clutter is defined as unwanted radar echos, including reflections from ground, sea, clouds, rain, snow flakes, trees, birds, insects, and man-made structures, *etc*. [15]. It is an important task of the radar to distinguish clutter from the echo signals reflected by targets, and clutter sources in certain radar applications can be targets in other circumstances. Clutter is viewed as a passive interference since it is a response to the signals transmitted by the radar. In some scenarios, clutter could be so strong that the targets are difficult or even impossible to be detected. The modelling of clutter has been investigated in depth because a proper model is essential in clutter suppression, and there are several widely adopted statistical models fitting reality quite well, such as the Gaussian, Weibull, noncentral Chi-square, Log-normal, and K-distributed models [12, 16–18].

Jamming: Jamming arises from signals emitted by intentional hostile sources or unintentional friendly sources which use the same frequency range as the radar does. Jamming is considered as an active interference since it is transmitted by devices outside the radar and is generally independent of the radar signals. Jamming can severely degrade the usefulness of a radar by either masking real targets with high power noise (*confusion*), or producing false signals which appear as echoes from real targets (*deception*) [11].

2.1.4 Radar vs. Sonar

Although this thesis mainly focuses on radar, we notice that the underlying mathematical theories of radar and sonar are very similar. Thus, we briefly discuss the similarities and differences between these two remote sensing systems in this section.

Similar to the word radar, the term *SONAR* was originally an acronym for "*SOund Navigation And Ranging*", and has become a standard English word today. Working in the same way as a radar does, a sonar system transmits acoustic waves into an environment (usually underwater) from *projectors*, and then the echoes reflected from targets are received by *hydrophones*. The device being able to both transmit and receive acoustic signals is called a *transducer*, which is commonly utilized in sonar systems. The basic tasks of sonar are the same as that of radar: to detect the presence of targets and to extract information about targets from the received waves. In the sonar community, the energy reflected from a target is described by the *target strength*,

which, similar to the RCS of a radar target, is a function of the target size, material, and shape, *etc.* [19]. The performance of sonar is also degraded because of noise and interference. Possible noise sources are waves on the surface of the ocean, shipping traffic, sea-life such as shrimp, whales, and dolphins, the electronic devices in the receiver and so on [20]. Similar to clutter in radar, *reverberation* affects sonar performance significantly. Reverberation is defined as undesired received echoes due to scattering from objects in the sea, the bottom and surface of the ocean, *etc.*, and it is a response to the acoustic signals emitted by the sonar.

The fundamental difference between radar and sonar is the type of transmitted signal and propagation medium. Radar sends out EM waves propagating in air while sonar emits acoustic waves normally in water. This is because EM waves are severely attenuated underwater, while acoustic signals can penetrate water more easily. Hence, radar signals travel at a constant speed 3×10^8 meters per second, while sonar waves propagate at various velocities depending on the medium they are traveling through. The speed of acoustic waves in water is approximately 1500 meter per second, and it is no longer a constant value but a function of water temperature, salinity, and pressure (or ocean depth) [21]. This speed fluctuation makes the propagation of sonar signals very complicated and may lead to waveform distortion. Another difference between them is the operating frequency. The frequencies of radar systems are typically on the order of 1 GHz, while sonar systems operate at much lower frequencies, *i.e.*, less than 500kHz [22]. A low frequency is utilized in sonar because the absorption of acoustics strongly depends on frequency, and the higher the frequency, the greater the absorption, and thus the higher the sound attenuation for a given distance. We emphasize here that although in essence the mathematical expressions presented in this thesis can be used for both radar and sonar systems due to their similar underlying theories, Chapter 3 and Chapter 4 are more based on radar scenarios, while Chapter 5 is more suited to sonar environments.

2.1.5 Conventional Multiple Antenna Radars

Due to the presence of interference, some tasks of a radar may not be accomplished satisfactorily by a single antenna, and one solution is to employ an antenna array at the radar receiver and/or transmitter. Radar array processing has been a topic of intensive research and developed considerably for many years, and we will discuss three conventional multiple antenna radar systems in this section. Notice here that the antenna elements can be arranged in many ways to construct a linear, planar, or volumetric array, and the interelement spacings can be uniform,

non-uniform, or random [23]. In this thesis, we mainly consider the most widely known configuration, the uniform linear array (ULA), whose antenna elements are equally spaced along a straight line and are assumed to be omnidirectional. However, other typical array configurations can also be adopted in principle, such as circular arrays, parallel linear arrays, and arrays with three linear arms spaced at 120° with a common center [23]. Note here that, strictly speaking, the configuration considered in Chapter 4 is not an ULA but a linear array with unequal spacings.

2.1.5.1 Conventional Phased-Array Radar

A ULA is often employed at the receiver in the conventional phased-array radar, and it can also be used at the transmitter if the radar is active. We will discuss the processing at the receiver in this section, the transmission processing is very similar. As depicted in Figure 2.1, an N-element ULA with interelement spacing d is illuminated by a target located in the far field whose direction is specified by the angle Φ with respect to the perpendicular direction to the array. The far field assumption implies that the distance between the target and the receiver is much larger than the dimension of the antenna array such that a plane wave impinging on the array in the target direction Φ should be considered. We further assume that all the signals are narrowband, *i.e.*, the bandwidth of the incident wave is much smaller than the carrier frequency f_c. At time t, the antennas of the array spatially sample the received signal at different locations and the array outputs can be given by an $N \times 1$ vector:

$$\begin{aligned} &\mathbf{r}(t) = s_0(t) \cdot \mathbf{\Psi}(\Phi) + \mathbf{n}(t) \\ &\mathbf{\Psi}(\Phi) = \left[\begin{array}{cccc} 1 & \exp\left\{\frac{j2\pi d}{\lambda_c}\sin\Phi\right\} & \cdots & \exp\left\{\frac{j2\pi(N-1)d}{\lambda_c}\sin\Phi\right\} \end{array} \right]^T \end{aligned} \tag{2.1}$$

where the superscript T denotes the matrix transpose, $s_0(t)$ is the value of the signal arriving at the first antenna element which is viewed as a reference point, λ_c is the wavelength of the signal, and the $N \times 1$ vector $\mathbf{n}(t)$ is the additive noise at all the antennas. $\mathbf{\Psi}(\Phi)$ is an $N \times 1$ vector, which is usually referred to as the *steering vector* of the array in the direction Φ, and Φ is normally known as the *angle of arrival* (AoA). It is clear that the signals arriving at different antennas are the same except the phase terms $\exp\left\{\frac{j2\pi kd}{\lambda_c}\sin\Phi\right\}$, $k = 0, 1, ..., N-1$, which arise due to different propagating distances to the antennas, *i.e.*, the spatial delays with respect

to the reference point (Antenna Element 1) illustrated in Figure 2.1.

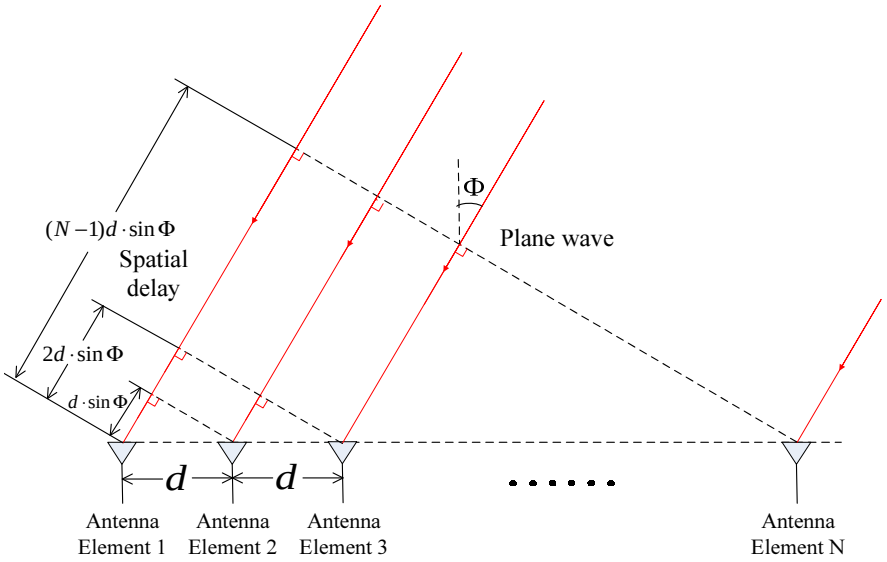

Figure 2.1: *Plane wave impinging on an uniform linear array (ULA)*

The receiver employs a *beamformer* to linearly combine the received signals with different weighting coefficients, and information about the target will be extracted based on the output of the beamformer which is given by:

$$\begin{aligned} x(t) &= \mathbf{w}^H \mathbf{r}(t) = s_0(t) \cdot \mathbf{w}^H \mathbf{\Psi}(\Phi) + \mathbf{w}^H \mathbf{n}(t) \\ &= s_0(t) \cdot \sum_{k=1}^{N} w_k^* \exp\left\{ \frac{j(k-1)2\pi d}{\lambda_c} \sin\Phi \right\} + \sum_{k=1}^{N} w_k^* n_k(t) \end{aligned} \tag{2.2}$$

where the superscripts $*$ and H stand for the complex conjugate and conjugate transpose operation, respectively. The scalar w_k is the k-th entry of the $N \times 1$ vector $\mathbf{w}$ and it is the weighting coefficient corresponding to the k-th antenna, and $n_k(t)$ is the k-th element of the noise vector $\mathbf{n}(t)$. The *beampattern* is the power of the beamformer output as a function of the direction along which it is measured and it can be defined as [24]:

$$B(\Phi) = \left\| \mathbf{w}^H \mathbf{\Psi}(\Phi) \right\|^2 = \mathbf{w}^H \mathbf{\Psi}(\Phi) \mathbf{\Psi}^H(\Phi) \mathbf{w} \tag{2.3}$$

where $\|\cdot\|$ represents the Euclidean norm. We show the beampattern of a conventional beam-

former which coheres a beam toward the direction $\Phi_0 = 0^\circ$ in Figure 2.2 as an example, and the arrays adopted are standard ULAs (interelement spacing $d = \frac{\lambda_c}{2}$) with 2, 4, 6, and 8 antennas. From Figure 2.2, we find that the more the antennas, the larger the array length, and thus, the higher the peak power and the narrower the beam. Observing (2.3) and Figure 2.2, it is clear that a beamformer has various gains for signals from different directions. Therefore, one can detect a target in the direction Φ_{tgt} by adopting a beamformer whose beampattern has large value at that angle, or cancel an interference from a certain angle by utilizing a beamformer having small beampattern in that direction. From (2.3), we know that a beamformer is able to produce a desired beampattern by controlling the weighting coefficients w_k. In the conventional phased-array radar, the weighting vector is chosen as $\mathbf{w} = \mathbf{\Psi}(\Phi_0)$, *i.e.*, the beamformer coheres a beam toward the direction of interest Φ_0. If the beam angle Φ_0 equals the target angle Φ, then a coherent processing gain $\mathbf{w}^H \mathbf{\Psi}(\Phi) = N$ can be realized. Since the weighting coefficients can be changed electronically, the conventional phased-array radar essentially realizes a radar with a directional antenna without any costly mechanical operations.

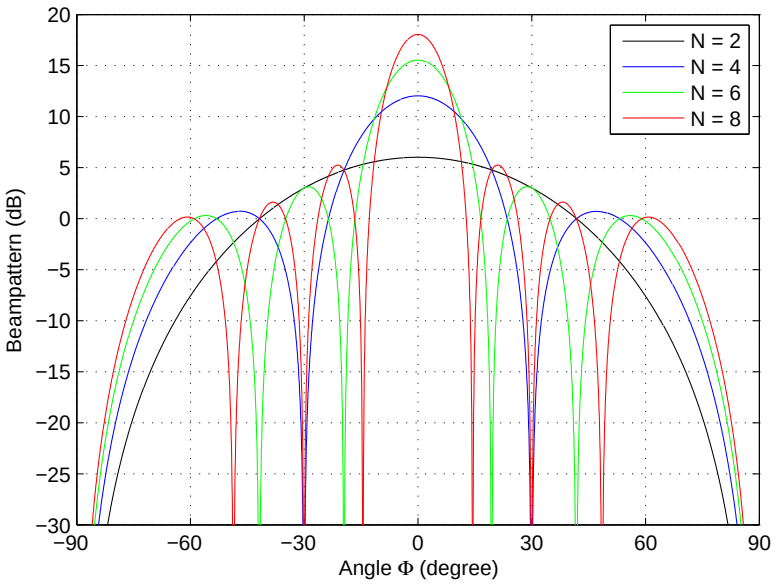

Figure 2.2: *The beampattern of a conventional beamformer aimed at 0°, and the arrays are standard N-element ULAs (interelement spacing $d = \frac{\lambda_c}{2}$) with different numbers of antennas N*

The angle Φ is normally restricted to the range $[-\pi/2, \pi/2]$, *i.e.*, only the wave propagating over the forward half of the antenna is considered [11]. Further define $\theta = \frac{2\pi d}{\lambda_c} \sin \Phi$ which is termed the *electrical angle*, and the beampattern can be rewritten as

$$B(\Phi) = \left\| \sum_{k=1}^{N} w_k^* \exp\left\{ \frac{j(k-1)2\pi d}{\lambda_c} \sin\Phi \right\} \right\|^2 = \left\| \sum_{k=1}^{N} w_k^* \exp\left\{ j(k-1)\theta \right\} \right\|^2 \tag{2.4}$$

If the value of θ lies outside the range $[-\pi, \pi]$, then there will be multiple values of Φ corresponding to the same θ, making it impossible to find the direction unambiguously. This spatial aliasing effect happens when the interelement spacing is larger than the half-wavelength $\frac{\lambda_c}{2}$. Therefore, we typically choose $d = \frac{\lambda_c}{2}$ such that $\theta = \frac{2\pi d}{\lambda_c} \sin\Phi = \pi \sin\Phi \in [-\pi, \pi]$, ensuring no aliasing exists in the beampattern.

2.1.5.2 Adaptive Array Radar

The conventional phased-array radar maximizes the output power for signals from a certain direction by utilizing a beamformer whose weighting coefficients are fixed and determined only by the locations of the antenna elements and the direction of interest [25]. The performance of this radar can be significantly degraded by strong directional interference, and thereby, an adaptive array radar is proposed. It adopts an adaptive beamformer which can adjust its weighting coefficients based on some optimality criterion which depends on the characteristics of the scene being observed, such as the target and clutter statistics. One simple example of the design criterion is to maximize the signal to noise ratio (SNR) [26]. Assume that the received array data is the sum of the desired signal component $\mathbf{s}$ and the unwanted noise component $\mathbf{n}$, whose covariance matrices are $\mathbf{C_s}$ and $\mathbf{C_n}$, respectively. The goal of this adaptive beamformer is to find the weighting vector $\mathbf{w}$ which maximizes the SNR, that is,

$$\max_{\mathbf{w}} \frac{\mathbf{w}^H \mathbf{C_s} \mathbf{w}}{\mathbf{w}^H \mathbf{C_n} \mathbf{w}} \tag{2.5}$$

Solving the above optimization problem yields the optimal weighting vector $\mathbf{w}_{opt}$ which is the eigenvector of the matrix $\mathbf{C_n}^{-1}\mathbf{C_s}$ corresponding to the largest eigenvalue. Here $\mathbf{C_n}^{-1}$ denotes the matrix inverse of $\mathbf{C_n}$.

The adaptive beamformer has long been studied and there are a large number of techniques [26–29], but the most well known is the *linearly constrained minimum variance* (LCMV) *beam-*

former proposed by Frost [30]. This algorithm minimizes the output power of the beamformer while constraining the responses of the beamformer to signals from directions of interest equal to specific values, which can be expressed as below:

$$\min_{\mathbf{w}} \mathbf{w}^H \mathbf{C_r} \mathbf{w} \qquad \text{s.t.} \mathbf{R}^H \mathbf{w} = \mathbf{f} \tag{2.6}$$

where $\mathbf{C_r}$ is the covariance matrix of the signals received by the antenna array, and the columns of the matrix $\mathbf{R}$ are the steering vectors of the array corresponding to the directions of interest and the entries of the vector $\mathbf{f}$ specify the desired responses. The above constraint optimization problem can be solved by the method of Lagrange multipliers as follows:

$$\mathbf{w}_{opt} = \mathbf{C_r}^{-1}\mathbf{R}(\mathbf{R}^H \mathbf{C_r}^{-1}\mathbf{R})^{-1}\mathbf{f} \tag{2.7}$$

For the special case of $\mathbf{R} = \mathbf{\Psi}(\Phi_0)$ and $\mathbf{f} = 1$, the above solution is the well known *minimum variance distortionless response* (MVDR) *beamformer* first derived by Capon in [31]. The steering vector $\mathbf{\Psi}(\Phi_0)$ is defined in (2.1) and the angle Φ_0 is the direction of the target. The MVDR beamformer avoids desired signal distortion in amplitude or phase while suppressing the unwanted interference.

Several adaptive algorithms have been developed for efficient implementation of adaptive beamformers [24, 30, 32], reducing the computational complexity which is primarily due to a matrix inversion operation. However, these algorithms require a large number of samples to reach the steady-state behavior when the number of antennas is large. An efficient technique to solve such a problem is reduced-rank adaptive filtering, and several algorithms were proposed [33–42]. The reduced-rank algorithm projects the received data vector onto a lower-dimensional subspace and performs the optimization within it, reducing the number of adaptive coefficients and extracting the most important characteristics of the processed data.

2.1.5.3 Multistatic Radar

A multistatic radar, also termed as a *multisite* or a *netted* radar, consists of several transmitters and receivers whose locations are sparsely separated such that different aspects of a target can be viewed simultaneously, bringing in a spatial diversity gain. Each of the possible transmitter-receiver pairs works just as an individual radar, which is capable of accomplishing target detection and/or estimation. The outcomes of the local processing are then delivered to a central processor through a communication link [43]. The central processor jointly fuses the outputs coming from all the transmitter-receiver pairs and provides a global result [44–46]. A statistical MIMO radar, which will be introduced in Section 2.3.1, can be viewed as a form of multistatic radar in a sense, but there are some differences between them. A statistical MIMO radar processes the signals picked up by all the receivers jointly, while the multistatic radar handles the received signals by a two-step approach including local processing in the initial stage and a decision fusion in the second stage.

2.2 Basic Review of Radar Signal Processing

Having introduced some basic concepts of a radar, this section will proceed to discuss basic approaches for the radar target detection and the direction finding problem, and more advanced methods developed recently will be deferred to the next section.

2.2.1 Target Detection Approach

The target detection problem in radar is to decide whether the received signals contain both the desired signal and noise or simply noise only, which can be described as follows:

$$\mathbf{r} = \begin{cases} \mathbf{n} & \mathcal{H}_0 \\ \mathbf{s}+\mathbf{n} & \mathcal{H}_1 \end{cases} \tag{2.8}$$

where $\mathbf{r}$, $\mathbf{s}$, and $\mathbf{n}$ represent the observed signals, the desired signals, and the noise, respectively. The *alternate hypothesis* $\mathcal{H}_1$ and *null hypothesis* $\mathcal{H}_0$ are that the target does or does not exist, respectively. Our goal is to find an appropriate function of the observed data and make the detection decision by comparing the value of the function with a pre-determined value, hoping

that the decision is correct most of the time. The detection process is usually expressed as

$$T(\mathbf{r}) \underset{<\mathcal{H}_0}{\overset{>\mathcal{H}_1}{}} \eta \tag{2.9}$$

where the function of the data $T(\mathbf{r})$ is termed as the *test statistic* or the *detection rule* and η is called the *threshold*. As shown in Table 2.1, four events are possible, two of which are erroneous and thereby unwanted. Since the noise, and thus the observed signals, are always assumed to be random variables, the performance of a target detector is commonly assessed by evaluating the possibilities the events would happen. Notice here that the observed signals $\mathbf{r}$ are assumed to be discrete samples, while in reality we normally observe continuous waveforms. The conversion can be easily done by a pre-processing, *e.g.*, matched-filtering the observed waveforms followed by appropriate sampling. The values of interest are the probability of false alarm $\mathrm{Pr_{FA}}$ (decide a target is present when it is not) and the probability of missed detection $\mathrm{Pr_{MD}}$ (decide no target exists when it does), and both error probabilities are expected to be as small as possible. Notice here that evaluating $\mathrm{Pr_{MD}}$ is equivalent to calculating the probability of detection $\mathrm{Pr_D}$ since their sum is always equal to one.

	$\mathcal{H}_0$: No target	$\mathcal{H}_1$: Target Exists
Decide No Target ($T < \eta$)	Correct	Type II Error (Missed Detection) $\mathrm{Pr_{MD}} = \mathrm{Pr}(T < \eta \mid \mathcal{H}_1)$
Decide Target Exists ($T \geq \eta$)	Type I Error (False Alarm) $\mathrm{Pr_{FA}} = \mathrm{Pr}(T \geq \eta \mid \mathcal{H}_0)$	Correct $\mathrm{Pr_D} = \mathrm{Pr}(T \geq \eta \mid \mathcal{H}_1) = 1 - \mathrm{Pr_{MD}}$

Table 2.1: *Decisions and probabilities of interest in target detection*

It is obvious that both error probabilities depend on the value of the threshold η, and as illustrated in Figure 2.3, increasing the threshold η can reduce $\mathrm{Pr_{FA}}$ but enlarging $\mathrm{Pr_{MD}}$, while $\mathrm{Pr_{MD}}$ can be decreased by reducing η at the expense of increasing $\mathrm{Pr_{FA}}$. Reducing both error probabilities simultaneously is impossible and there is a trade-off between them when choosing the threshold [47]. A common approach is to select the threshold η such that the probability of false alarm is fixed at a required value, and such a detector is referred to as *constant false alarm rate* (CFAR) detector. Recalling the definition $\mathrm{Pr_{FA}} = \mathrm{Pr}(T > \eta \mid \mathcal{H}_0)$, it is clear that the test statistic T has to be known in order to determine η from the value of $\mathrm{Pr_{FA}}$. We emphasize here that the test statistic is a function of the observed data and different choices of function

will lead to distinct detection performance results. We will next introduce several widely used approaches.

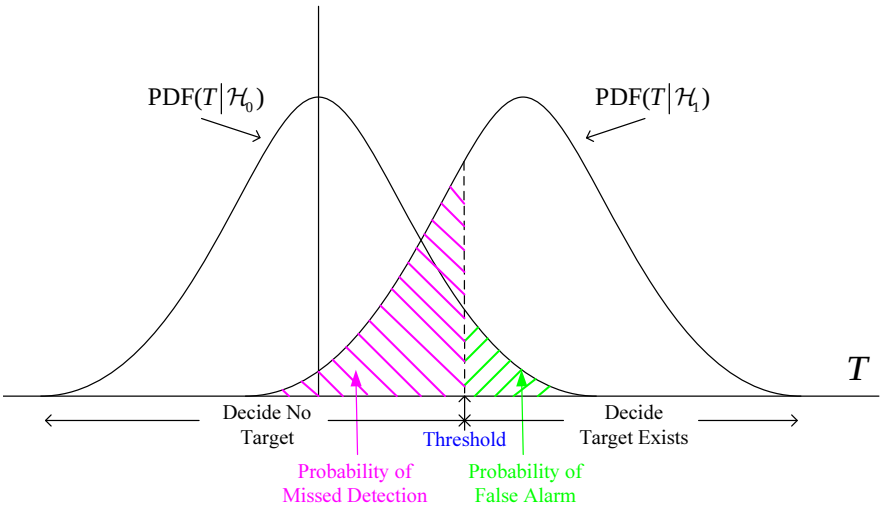

Figure 2.3: *Decision regions and Error probabilities*

The most classical approach is based on the Neyman-Pearson theorem, which states that for a given probability of false alarm $\mathrm{Pr}_{\mathrm{FA}}$, the detector maximizing the probability of detection Pr_{D} (equivalent to minimizing the probability of missed detection $\mathrm{Pr}_{\mathrm{MD}}$) is [47]

$$T_{\mathrm{LRT}}(\mathbf{r}) = \frac{\mathrm{PDF}(\mathbf{r}|\,\mathcal{H}_1)}{\mathrm{PDF}(\mathbf{r}|\,\mathcal{H}_0)} \underset{<\mathcal{H}_0}{>^{\mathcal{H}_1}} \eta \tag{2.10}$$

where the threshold η is determined from

$$\begin{aligned} &\mathrm{Pr}_{FA} = \mathrm{Pr}(T > \eta|\,\mathcal{H}_0) \\ &= \int_{\eta}^{+\infty} \mathrm{PDF}(T|\,\mathcal{H}_0)dT = \int_{\{\mathbf{r}:T(\mathbf{r})>\eta\}} \mathrm{PDF}(\mathbf{r}|\,\mathcal{H}_0)d\mathbf{r} \end{aligned} \tag{2.11}$$

where $\mathrm{PDF}(\mathbf{r}|\,\mathcal{H}_1)$ and $\mathrm{PDF}(\mathbf{r}|\,\mathcal{H}_0)$ denote the probability density function (PDF) of the observed data $\mathbf{r}$ under the alternate hypothesis $\mathcal{H}_1$ and null hypothesis $\mathcal{H}_0$, respectively. The test (2.10) is referred to as the *likelihood ratio test* (LRT). The LRT detector requires complete knowledge of the PDFs of the observed data under both hypotheses, which are not always possible in realistic scenarios. When unknown parameters exist in one or both PDFs, there are two

major approaches addressing the problem based on the LRT: the generalized likelihood ratio test (GLRT) and the Bayesian approach.

The GLRT views the unknown parameters as deterministic and replaces the unknowns by their maximum likelihood estimates (MLEs), which can be expressed as below [47]:

$$T_{\mathrm{GLRT}}(\mathbf{r}) = \frac{\mathrm{PDF}(\mathbf{r}|\,\hat{\boldsymbol{\theta}}_1, \mathcal{H}_1)}{\mathrm{PDF}(\mathbf{r}|\,\hat{\boldsymbol{\theta}}_0, \mathcal{H}_0)} \begin{array}{l} >^{\mathcal{H}_1} \\ <_{\mathcal{H}_0} \end{array} \eta \tag{2.12}$$

where $\boldsymbol{\theta}_1$ and $\boldsymbol{\theta}_0$ denote the unknown parameters included in PDFs under $\mathcal{H}_1$ and $\mathcal{H}_0$, respectively. $\hat{\boldsymbol{\theta}}_i$ is the MLE of $\boldsymbol{\theta}_i$ under $\mathcal{H}_i$ (maximizes $\mathrm{PDF}(\mathbf{r}|\,\boldsymbol{\theta}_i, \mathcal{H}_i)$), and $\mathrm{PDF}(\mathbf{r}|\,\theta_i, \mathcal{H}_i)$ is the PDF of the data $\mathbf{r}$ under $\mathcal{H}_i$ when $\boldsymbol{\theta}_i$ is known, where $i = 0$ or 1.

The Bayesian approach assumes that the unknown parameters $\boldsymbol{\theta}_0$ and $\boldsymbol{\theta}_1$ are random vectors with known prior PDFs $\mathrm{PDF}(\boldsymbol{\theta}_0)$ and $\mathrm{PDF}(\boldsymbol{\theta}_1)$, respectively, and the detector is given by [47]

$$T_{\mathrm{BLRT}}(\mathbf{r}) = \frac{\mathrm{PDF}(\mathbf{r}|\,\mathcal{H}_1)}{\mathrm{PDF}(\mathbf{r}|\,\mathcal{H}_0)} = \frac{\int \mathrm{PDF}(\mathbf{r}|\,\boldsymbol{\theta}_1, \mathcal{H}_1)\mathrm{PDF}(\boldsymbol{\theta}_1)d\boldsymbol{\theta}_\mathbf{1}}{\int \mathrm{PDF}(\mathbf{r}|\,\boldsymbol{\theta}_0, \mathcal{H}_1)\mathrm{PDF}(\boldsymbol{\theta}_0)d\boldsymbol{\theta}_0} \begin{array}{l} >^{\mathcal{H}_1} \\ <_{\mathcal{H}_0} \end{array} \eta \tag{2.13}$$

The Bayesian approach has the same optimality as the Neyman-Pearson test since the unconditional PDFs $\mathrm{PDF}(\mathbf{r}|\,\mathcal{H}_0)$ and $\mathrm{PDF}(\mathbf{r}|\,\mathcal{H}_1)$ no longer depend on the unknowns after the integrations. However, the multidimensional integration is always impossible to calculate in closed form, and it can be difficult to select proper prior PDFs for the unknown parameters. The GLRT is a practical approach when unknown parameters exist by virtue of its ease of implementation in realistic scenarios, although it cannot be claimed to be optimal in any sense.

2.2.2 Direction Finding Techniques

One of the most important parameters of a target is its direction with respect to the radar receiver, *i.e.*, AoA discussed in Section 2.1.5.1. A large number of techniques have been developed for AoA estimation and some of the most popular algorithms will be discussed in this section. As in Section 2.1.5.1, we focus our attention on the scenario that narrowband signals

impinge on an antenna array. Notice that only a single target is assumed to be present in (2.1), but here we extend that to the multiple targets case so that the signals received by the antenna array can be expressed by an $N \times 1$ vector as below:

$$\mathbf{r}(t) = \mathbf{\Theta}\mathbf{s}(t) + \mathbf{n}(t) \tag{2.14}$$

where the $K \times 1$ vector $\mathbf{s}(t)$ contains the signals impinging on the array from the K targets and the $N \times 1$ vector $\mathbf{n}(t)$ includes the additive white Gaussian noise received at each antenna. The k-th column of the $N \times K$ matrix $\mathbf{\Theta}$ is the steering vector of the antenna array corresponding to the k-th target, which is given by

$$\mathbf{\Psi}(\Phi_k) = \left[\begin{array}{cccc} 1 & \exp\{j\pi \sin\Phi_k\} & \cdots & \exp\{j\pi(N-1)\sin\Phi_k\} \end{array} \right]^T \tag{2.15}$$

Here Φ_k is the AoA of the k-th target and the antenna array is assumed to be an N-element ULA as shown in Figure 2.1 with interelement spacing $d = \frac{\lambda_c}{2}$. Note that K has to be smaller than N. The covariance matrix of $\mathbf{r}(t)$ is the basis of many algorithms, which is defined as

$$\mathbf{C_r} = \mathrm{E}\left\{\mathbf{r}(t)\mathbf{r}^H(t)\right\} = \mathbf{\Theta}\mathbf{C_s}\mathbf{\Theta}^H + \sigma_n^2\mathbf{I}_N \tag{2.16}$$

where the $K \times K$ matrix $\mathbf{C_s}$ is the covariance matrix of the signal vector $\mathbf{s}(t)$ and $\sigma_n^2\mathbf{I}_N$ is the covariance matrix of the white Gaussian noise vector, where $\mathbf{I}_K$ denotes the $K \times K$ identity matrix. Recall that acquiring the exact value of the second-order statistics of the data $\mathbf{C_r}$ requires infinite observation time, while in practice only a finite number of observation samples are available. If L snapshots of the data vector $\mathbf{r}(t)$ are known, a common approach to estimate $\mathbf{C_r}$ is to compute the sample covariance matrix as

$$\hat{\mathbf{C}}_\mathbf{r} = \frac{1}{L}\sum_{l=1}^{L}\mathbf{r}(t_l)\mathbf{r}^H(t_l) \tag{2.17}$$

where t_l is the time at which the l-th snapshot of the received signal $\mathbf{r}(t)$ is sampled. Direction finding techniques estimate the AoAs of targets through analyzing the structure of $\mathbf{C_r}$, and here we introduce several algorithms which are frequently employed.

- **Conventional Beamformer**

  The general idea of beamforming techniques is to "steer" the array in one direction at a time and measure the output power, and the AoA estimates are the locations of the highest peaks. The conventional (or *Bartlett*) beamformer [48] maximizes the power of the beamforming output for a given input signal, *i.e.*, the weighting vector $\mathbf{w}_{\mathrm{BF}} = \mathbf{\Psi}(\Phi)$, which produces the following output power spatial spectrum

$$P_{\mathrm{BF}}(\Phi) = \mathbf{w}_{\mathrm{BF}}^H \mathbf{C_r} \mathbf{w}_{\mathrm{BF}} = \mathbf{\Psi}^H(\Phi) \mathbf{C_r} \mathbf{\Psi}(\Phi) \tag{2.18}$$

  The resolution limit of the conventional beamformer prevent the separation of targets with close AoAs, and for an N-element ULA with interelement spacing d, the resolution is approximately $\frac{\lambda_c}{Nd}$ [49]. For example, by utilizing a standard ULA with 6 antennas and half-wavelength spacings, two targets whose angle separation is less than $\frac{1}{3}$ rad $\cong 19^\circ$ will not be resolved regardless of the available data quality or quantity.

- **Capon's Beamformer**

  In an attempt to separate closely spaced targets, Capon's beamformer (also known as the MVDR beamformer mentioned in Section 2.1.5.2) was proposed, whose weighting vector is appropriately chosen such that the total output power is minimized while the signal along the look direction passes the beamformer with unit response. Based on (2.7), the weighting vector can be expressed as follows:

$$\mathbf{w}_{\mathrm{Capon}} = \frac{\mathbf{C}_{\mathbf{r}}^{-1} \mathbf{\Psi}(\Phi)}{\mathbf{\Psi}^H(\Phi) \mathbf{C}_{\mathbf{r}}^{-1} \mathbf{\Psi}(\Phi)} \tag{2.19}$$

  The power spatial spectrum yielded by the weighting vector is given by

$$P_{\text{Capon}}(\Phi) = \mathbf{w}_{\text{Capon}}^H \mathbf{C_r} \mathbf{w}_{\text{Capon}} = \frac{1}{\mathbf{\Psi}^H(\Phi)\mathbf{C_r}^{-1}\mathbf{\Psi}(\Phi)} \tag{2.20}$$

Since the power contributed by the undesired interference coming from directions other than the look direction is minimized, the spectral leakage from nearby targets is attenuated. Hence, the Capon's spectrum has sharper peaks and thus better resolution compared with the conventional beamformer. There are many alternative algorithms for beamforming and the interested reader may refer to [25] for a comprehensive overview.

- **The MUSIC Algorithm**

The MUSIC (*MUltiple SIgnal Classification*) algorithm [50] analyzes the covariance matrix $\mathbf{C_r}$ by performing the eigendecomposition and dividing the eigenvalue/eigenvector pairs into two classes as below:

$$\mathbf{C_r} = \mathbf{\Theta C_s \Theta}^H + \sigma_n^2 \mathbf{I}_N = \mathbf{U_r \Lambda_r U_r}^H = \mathbf{U_s \Lambda_s U_s}^H + \sigma_n^2 \mathbf{U_n U_n}^H \tag{2.21}$$

where the $N \times N$ matrix $\mathbf{U_r}$ is a unitary matrix whose columns are eigenvectors and $\mathbf{\Lambda_r}$ is a diagonal matrix with N real and positive eigenvalues $\lambda_1, \lambda_2, \ldots, \lambda_N$ (in decreasing order) as its diagonal elements. Since K targets are assumed to be present and $\mathbf{C_s}$ is often assumed to be nonsingular, the matrix $\mathbf{\Theta C_s \Theta}^H$ has K positive eigenvalues and $N - K$ zero eigenvalues. It is clear that any vector orthogonal to $\mathbf{\Theta}$ is an eigenvector of $\mathbf{C_r}$ with eigenvalue σ_n^2 and there are $N - K$ linearly independent such vectors. Therefore, the eigenvalue/eigenvector pairs are partitioned into (a) the signal eigenvectors $\mathbf{U_s}$ whose columns are the eigenvectors corresponding to the largest K eigenvalues $\lambda_1 \geq \lambda_2 \geq \ldots \geq \lambda_K > \sigma_n^2$ and (b) the noise eigenvectors $\mathbf{U_n}$ whose columns are the eigenvectors corresponding to the remaining $N - K$ eigenvalues $\lambda_{K+1} = \lambda_{K+2} = \ldots = \lambda_N = \sigma_n^2$. Collectively, the eigenvectors $\mathbf{U_s}$ and $\mathbf{U_n}$ are ofen called the signal subspace and noise subspace, respectively. Since the columns of $\mathbf{U_n}$ (the noise eigenvectors) are orthogonal to $\mathbf{\Theta}$, hence, for all the K AoAs $\{\Phi_1, \Phi_2, \ldots, \Phi_K\}$, we have $\mathbf{U_n}^H \mathbf{\Psi}(\Phi_k) = \mathbf{0}$. The MUSIC power "spatial spectrum" is defined as

$$P_{\mathrm{MUSIC}}(\Phi) = \frac{1}{\mathbf{\Psi}^H(\Phi)\mathbf{U_n}\mathbf{U_n}^H\mathbf{\Psi}(\Phi)} \tag{2.22}$$

Although $P_{\mathrm{MUSIC}}(\Phi)$ is not a true power density spectrum, it exhibits peaks in the vicinity of the true AoAs [51]. Figure 2.4 illustrates the spectra of the conventional beamformer, Capon's beamformer, and the MUSIC algorithm when two targets exist, whose AoAs are 5° and 15°, respectively. Both signals have a SNR of 5dB, and all the three approaches use $L = 100$ data snapshots obtained from a ULA with 6 antennas using half-wavelength spacings. Observing the figure, we find that the conventional beamformer fails to resolve the targets since the angular separation in this case is 10°, which is smaller than the resolution limit of 19°. Capon's beamformer barely separates the targets, while the MUSIC algorithm produces two sharp peaks in the vicinity of the true AoAs.

It is clear that the MUSIC algorithm requires a search to find the target directions, which can be avoided by applying the Root-MUSIC approach [52] if the array is a ULA. The Root-MUSIC method is a polynomial-rooting version of the MUSIC technique, and instead of a search, the AoAs can be determined by computing the roots of a polynomial.

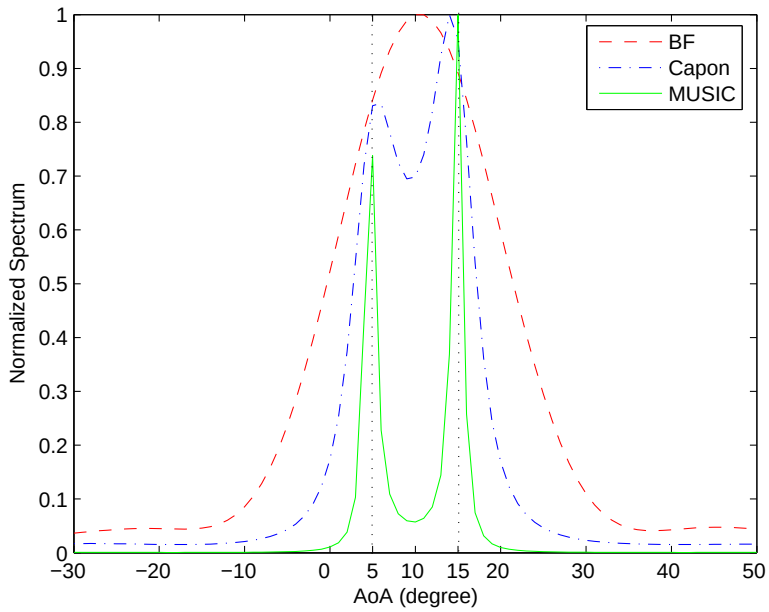

Figure 2.4: *A comparison of the spectral-based algorithms for AoA estimation when two targets exist. The true AoAs are indicated by dotted vertical lines.*

The MUSIC method is based on the assumption that $\mathbf{C_s}$ is nonsingular, which is invalid if the incident signals are coherent, *e.g.,* the signals result from the multipath effect. When this happens, $\mathbf{C_s}$ is singular and has zero eigenvalues. Thereby, it is impossible to distinguish some signal eigenvectors from the noise eigenvectors, and as a result, the noise subspace $\mathbf{U_n}$ is no longer orthogonal to the steering vectors in the matrix $\mathbf{\Theta}$ and the MUSIC method may fail to yield peaks at the correct locations.

- **Maximum Likelihood Methods**

Although the spectral-based algorithms discussed before are computationally attractive, they do not always provide sufficient accuracy, particularly for scenarios involving highly correlated or coherent signals. One way to solve this problem is to employ parametric approaches which directly estimate the AoAs by exploiting the underlying data model, and the most popular parametric approach is the maximum likelihood (ML) technique [53]. The *likelihood function* is the PDF of all the observation data given the unknown parameters. The ML estimates of the parameters are the arguments that maximize the likelihood function, since these values make the probability of the observations as large as possible. Here we take a case which is commonly considered in the literature as an example. Similar to (2.17), we denote by $\mathbf{s}(t_l)$ the l-th snapshot of the signals emitted from the K targets, where $l = 1, 2, ..., L$. It is assumed that the noise level σ_n^2, $\mathbf{s}(t_l)$, and a $K \times 1$ vector $\mathbf{\Phi}$, whose entries are the AoAs of the K targets Φ_1, Φ_2, ..., Φ_K, are unknown. Obviously, the matrix $\mathbf{\Theta}$ in (2.14) is a function of $\mathbf{\Phi}$ and we drop the argument of $\mathbf{\Theta}(\mathbf{\Phi})$ for notational convenience. Based on (2.14), the likelihood function can be expressed as below:

$$\mathcal{L}(\mathbf{\Phi}, \mathbf{s}(t_l), \sigma_n^2) = \prod_{l=1}^{L} \frac{1}{(\pi\sigma_n^2)^N} \exp\left\{ -\frac{1}{\sigma_n^2} \left[\mathbf{r}(t_l) - \mathbf{\Theta}\mathbf{s}(t_l)\right]^H \left[\mathbf{r}(t_l) - \mathbf{\Theta}\mathbf{s}(t_l)\right] \right\} \quad (2.23)$$

As mentioned before, the ML estimates of the parameters are the arguments maximizing the likelihood function, and thus, the optimization problem can be rewritten as

$$\min_{\mathbf{\Phi}, \mathbf{s}(t_l), \sigma_n^2} LN \cdot \log(\pi\sigma_n^2) + \frac{1}{\sigma_n^2} \sum_{l=1}^{L} \|\mathbf{r}(t_l) - \mathbf{\Theta}\mathbf{s}(t_l)\|^2 \quad (2.24)$$

Previous researchers had derived the ML estimates of the AoAs by solving (2.24), which can be given by [51]

$$\hat{\mathbf{\Phi}}_{\mathrm{ML}} = \arg\min_{\mathbf{\Phi}} \ \mathrm{trace}\left\{ \left[\mathbf{I}_N - \mathbf{\Theta} \left(\mathbf{\Theta}^H \mathbf{\Theta} \right)^{-1} \mathbf{\Theta}^H \right] \cdot \hat{\mathbf{C}}_{\mathbf{r}} \right\} \tag{2.25}$$

where $\hat{\mathbf{C}}_{\mathbf{r}}$ is the sample covariance matrix defined in (2.17). Note that for the special case when there is only one target, the above equation reduces to the conventional beamformer. Although the ML methods increase the estimation accuracy and robustness, they typically require a multidimensional search for the parameters of interest and can only be solved numerically, which may be too computationally expensive for practical use.

A large number of approaches for direction finding are documented in the literature, readers interested in this area may refer to [51,54–68] and references therein for detailed presentations.

2.3 Review of MIMO Radar

MIMO radar has been receiving increasing attention in recent years, and loosely speaking, it refers to an architecture that employs multiple antennas to simultaneously transmit waveforms and utilizes multiple antennas to receive the reflected signals which are then jointly processed. In general, MIMO radar systems can be classified into two categories according to their configurations: (a) statistical MIMO radar, and (b) colocated MIMO radar. The antennas of a statistical MIMO radar are widely separated in order to capture the spatial diversity of the target's RCS, while the antennas of the colocated MIMO radar are close enough such that all the elements view the same aspect of the target. It has been demonstrated that both MIMO radar systems have the ability to achieve significantly improved performance compared with the conventional phased-array or adaptive radars, and we will discuss some important aspects of MIMO radar in this section.

2.3.1 Statistical MIMO Radar

As mentioned in Section 2.1.2, large scintillations in the amount of energy reflected by a complex target can occur because of small changes in the target aspect. These scintillations are

responsible for signal fading, which may reduce the received energy to a level that does not allow reliable detection or estimation, severely degrading the system performance. The notion of the statistical MIMO radar is to employ widely separated antennas such that different antennas view various aspects of the target, capturing the spatial diversity of the target's RCS.

2.3.1.1 System Model

Due to the target's complex body and the large distance between the antennas, the point-like target model which is commonly adopted in radar is no longer adequate for a statistical MIMO radar. Therefore, a more accurate model has to be developed taking into account the spatial characteristics of the target. Fishler *et al.* [8] assumed that the target is composed of an infinite number of small scatterers that are distributed over an area S. The center of the target is denoted by S_0 whose coordinates are (x_0, y_0), and the target dimensions along the x and y axes are Δx and Δy, respectively. The scatterers are assumed to be random, isotropic and independent, and they are uniformly distributed over the area S. The complex reflectivity of each scatterer is modeled as a zero-mean, white, complex random variable with the same variance, and the sum of all the variances equals one such that the average energy returned from the target is normalized to one.

It is further assumed that the target is illuminated by N_t transmit antennas placed at arbitrary coordinates $T_k = (x_k^t, y_k^t)$, $k = 1, 2, ..., N_t$. The narrowband signal emitted from the k-th transmit antenna is assumed to be $\sqrt{\frac{E_s}{N_t}} s_k(t)$, where $\|s_k(t)\|^2 = 1$ and E_s is the total transmitted power. The normalizing coefficient is employed to make sure that the total transmitted power and the average received power at each element are not affected by the number of transmit antennas. The signals reflected by the target are collected by N_r receive antennas arbitrarily located at coordinates $R_l = (x_l^r, y_l^r)$, $l = 1, 2, ..., N_r$. Collectively denote the transmitted signals from the various transmitting elements and the signals collected by all the receive antennas by an $N_t \times 1$ vector $\mathbf{s}(t) = \begin{bmatrix} s_1(t) & s_2(t) & \cdots & s_{N_t}(t) \end{bmatrix}^T$ and an $N_r \times 1$ vector $\mathbf{r}(t) = \begin{bmatrix} r_1(t) & r_2(t) & \cdots & r_{N_r}(t) \end{bmatrix}^T$, respectively. The following expression is derived to describe the received signal vector [8]:

$$\mathbf{r}(t) = \sqrt{\frac{E_s}{N_t}} \underbrace{\text{diag}\left\{\mathbf{\Psi}_r(S_0)\right\} \cdot \text{A} \cdot \text{diag}\left\{\mathbf{\Psi}_t(S_0)\right\}}_{\mathbf{H}} \mathbf{s}(t-\tau) + \mathbf{n}(t) \tag{2.26}$$

where $\mathrm{diag}\{\mathbf{a}\}$ stands for a diagonal matrix with its diagonal given by the vector $\mathbf{a}$, and $\mathbf{n}(t) = \begin{bmatrix} n_1(t) & n_2(t) & \cdots & n_{N_r}(t) \end{bmatrix}^T$ is an $N_r \times 1$ vector representing the additive noise at all the receive antennas. Denote the distance between the k-th transmit antenna and the target center, and the distance between the target center and the l-th receive element by $d(T_k, S_0)$ and $d(R_l, S_0)$, respectively, where $k = 1, 2, ..., N_t$ and $l = 1, 2, ..., N_r$. $\tau = \frac{d(T_1,S_0)+d(R_1,S_0)}{c_0}$ is the propagation time delay from the first transmit antenna to the first receive antenna via the target center, and c_0 here is the speed of light. The $N_r \times 1$ vector $\mathbf{\Psi}_r(S_0)$ and the $N_t \times 1$ vector $\mathbf{\Psi}_t(S_0)$ are the receiver steering vector and transmitter steering vector, respectively, which are functions of the location of the target center $S_0 = (x_0, y_0)$ and can be expressed as below:

$$\begin{aligned}
\mathbf{\Psi}_r(S_0) &= \begin{bmatrix} 1 & \exp\left\{\frac{j2\pi f_c[d(R_1,S_0)-d(R_2,S_0)]}{c_0}\right\} & \cdots & \exp\left\{\frac{j2\pi f_c[d(R_1,S_0)-d(R_{N_r},S_0)]}{c_0}\right\} \end{bmatrix}^T \\
\mathbf{\Psi}_t(S_0) &= \begin{bmatrix} 1 & \exp\left\{\frac{j2\pi f_c[d(T_1,S_0)-d(T_2,S_0)]}{c_0}\right\} & \cdots & \exp\left\{\frac{j2\pi f_c\left[d(T_1,S_0)-d(T_{N_t},S_0)\right]}{c_0}\right\} \end{bmatrix}^T
\end{aligned} \tag{2.27}$$

Denote by α_{lk} the entry lying in the l-th row and the k-th column of the $N_r \times N_t$ matrix $\mathbf{A}$ in (2.26), and α_{lk} is the fading coefficient of the target between the k-th transmit element and the l-th receive antenna, accounting for the effects of all the small scatterers. Recalling that the complex reflectivities of the scatterers are assumed to be random variables, α_{lk} is approximately a complex normal random variable due to the central limit theorem, and it is shown in [8] that $\alpha_{lk} \sim \mathcal{CN}(0, 1)$. As indicated in (2.26), the transmitter and receiver steering vectors together with the fading coefficients comprise the $N_r \times N_t$ channel matrix $\mathbf{H}$, whose (l, k)-th entry is denoted by h_{lk}.

The idea of the statistical MIMO radar is to exploit the spatial diversity of the target's RCS, and for this to be possible, it is required that the fading coefficients α_{lk} for different transmit-receive antenna pairs are uncorrelated. Consider the (l, k)-th and the (j, i)-th entry of $\mathbf{A}$, it is proved in [8] that α_{lk} and α_{ji} are uncorrelated if at least one of the following four conditions holds:

$$\begin{aligned}
\frac{x_k^t}{d(T_k,S_0)} - \frac{x_i^t}{d(T_i,S_0)} > \frac{\lambda_c}{\Delta x}, \qquad \frac{y_k^t}{d(T_k,S_0)} - \frac{y_i^t}{d(T_i,S_0)} > \frac{\lambda_c}{\Delta y} \\
\frac{x_l^r}{d(R_l,S_0)} - \frac{x_j^r}{d(R_j,S_0)} > \frac{\lambda_c}{\Delta x}, \qquad \frac{y_l^r}{d(R_l,S_0)} - \frac{y_j^r}{d(R_j,S_0)} > \frac{\lambda_c}{\Delta y}
\end{aligned} \tag{2.28}$$

where λ_c is the carrier wavelength. In contrast, if the following four conditions are met jointly:

$$\begin{array}{ll} \frac{x_k^t}{d(T_k,S_0)} - \frac{x_i^t}{d(T_i,S_0)} \ll \frac{\lambda_c}{\Delta x}, & \frac{y_k^t}{d(T_k,S_0)} - \frac{y_i^t}{d(T_i,S_0)} \ll \frac{\lambda_c}{\Delta y} \\ \frac{x_l^r}{d(R_l,S_0)} - \frac{x_j^r}{d(R_j,S_0)} \ll \frac{\lambda_c}{\Delta x}, & \frac{y_l^r}{d(R_l,S_0)} - \frac{y_j^r}{d(R_j,S_0)} \ll \frac{\lambda_c}{\Delta y} \end{array} \tag{2.29}$$

then α_{lk} and α_{ji} are approximately fully correlated. These conditions have a simple physical interpretation. The spatial distributed target can be regarded as an "hypothetical" antenna with aperture Δ (Δ could be Δx or Δy for x- or y- direction), and thus its beamwidth is λ_c/Δ. If the spacing between two antennas is large enough such that they can not be illuminated by the target's beamwidth simultaneously, then they observe different aspects of the target with uncorrelated RCSs, *i.e.*, elements of $\mathbf{A}$ associated with these antennas are uncorrelated. Conversely, if two antennas are closely spaced and within the same beamwidth of the target, their corresponding entries of $\mathbf{A}$ are correlated. This concept is illustrated in Figure 2.5.

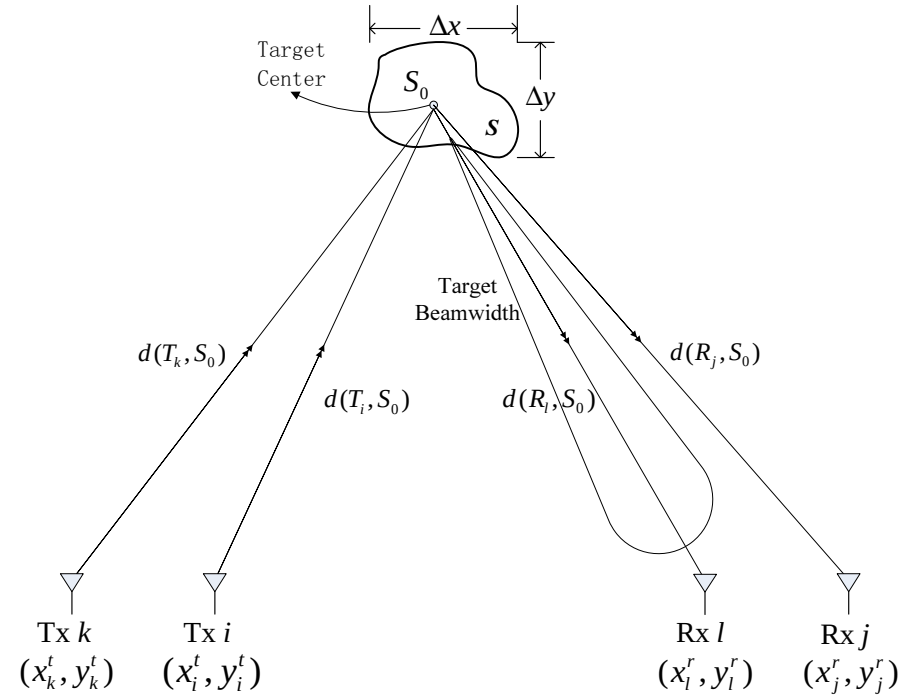

Figure 2.5: *Elements of the channel matrix are uncorrelated when the MIMO radar antennas fall in different beamwidths originating from the target [1]*

For the statistical MIMO radar, the interelement spacing between each pair of antennas obeys condition (2.28), and hence, all the entries of $\mathbf{A}$ are uncorrelated and $\alpha_{lk} \sim \mathcal{CN}(0,1)$. Note that

$[\mathrm{diag}\{\mathbf{\Psi}_r(S_0)\}\,\mathbf{A}\mathrm{diag}\{\mathbf{\Psi}_t(S_0)\}]$ has the same distribution as that of $\mathbf{A}$ since $\mathrm{diag}\{\mathbf{\Psi}_r(S_0)\}$ and $\mathrm{diag}\{\mathbf{\Psi}_t(S_0)\}$ are diagonal matrices with elements on the unit circle. Therefore, the received signal of the statistical MIMO model can be expressed as below:

$$\mathbf{r}(t) = \sqrt{\frac{E_s}{N_t}}\mathbf{H}\mathbf{s}(t-\tau) + \mathbf{n}(t) \tag{2.30}$$

where the entries of the $N_r \times N_t$ channel matrix $\mathbf{H}$ are independent and identically distributed (i.i.d.) random variables, and $h_{lk} \sim \mathcal{CN}(0,1)$. Defining a $N_rN_t \times 1$ channel vector $\mathbf{h}$ by stacking all the columns of $\mathbf{H}$ into a vector, the MIMO channel can also be expressed as $\mathbf{h} \sim \mathcal{CN}(\mathbf{0}_{N_rN_t}, \mathbf{I}_{N_rN_t})$, where $\mathbf{0}_k$ stands for a $k \times 1$ all-zeros vector.

For comparison purposes, we will briefly discuss the channel model for the configuration of the conventional phased-array radar. The array elements are densely spaced and every pair of antennas obeys condition (2.29), and hence, all the elements of $\mathbf{A}$ are fully correlated and the matrix can be given by $\mathbf{A} = \alpha\mathbf{1}_{N_r\times N_t}$. Here $\alpha \sim \mathcal{CN}(0,1)$ and $\mathbf{1}_{k\times l}$ denotes a $k \times l$ all-ones matrix. Hereby, based on (2.26), the channel matrix for the phased-array configuration can be expressed as $\mathbf{H} = \alpha\mathbf{\Psi}_r(S_0)\mathbf{\Psi}_t^T(S_0)$.

In addition, the statistical MIMO model can only be used for ideal array-target configurations where the interelement spacings are either large enough such that different antennas observe different aspects of the target or small enough that all the antennas view the same aspect. However, it is very possible that such conditions do not hold in practice and hence, the statistical MIMO model can no longer be adopted. Another model is required to be considered, and this problem will be solved in Chapter 3.

2.3.1.2 Diversity Gain

The statistical MIMO radar combines target returns resulting from independent illuminations, yielding a diversity gain which can be used to overcome target fading or scintillation. As discussed above, the fading coefficients of the paths between different transmit-receive antenna pairs are uncorrelated, and there are N_rN_t such paths responsible for the N_rN_t entries of the channel matrix $\mathbf{H}$. The signals emitted from different transmit antennas carry independent information about the target and are superposed yielding the received signals. Consequently,

the transmitted waveforms have to be properly selected enabling the separation between signals at the receiver. The most common choice is to transmit signals that are mutually orthogonal, that is, $\int s_l(t-\tau)s_k^*(t)dt = \delta_{lk}(\tau)$. Here $s_k(t)$ is the signal transmitted from the k-th antenna and δ_{lk} denotes the Dirac delta function. Let the received signals $\mathbf{r}(t)$ shown in (2.30) go through a bank of matched filters and denote the output by an $N_rN_t \times 1$ vector $\mathbf{x}$, then we have

$$[\mathbf{x}]_{(l-1)N_t+k} = \int r_l(t-\tau)s_k^*(t)dt = \sqrt{\frac{E_s}{N_t}}h_{lk} + n \tag{2.31}$$

where $k = 1, 2, ..., N_t$, $l = 1, 2, ..., N_r$, and n is the noise component. It is obvious that the noisy estimates of all the N_rN_t channel coefficients h_{lk} are extracted, and the statistical MIMO radar actually combines the results from N_rN_t statistically independent radars. It is known that the conventional phased-array radar coheres a beam toward the target direction in order to realize coherent processing gain, trying to overcome the scintillation problem by maximizing the received energy from the target. However, since the target fading coefficient for all transmit-receive antenna pairs are the same, and this individual view of the target might dramatically reduce the energy returned from the target with a significant probability. When this happens, the conventional approach would still fail even with a coherent processing gain. The statistical MIMO radar is an alternative to address the scintillation or deep fading problem. Although there is no coherent processing gain in a MIMO radar, it actually synthesizes many independent radars, each of which has an individual look at the target. Thereby, the whole system would suffer from deep fading only if the target fading for all the individual observed aspects are severe, which has a low probability. An intuitive question to ask is "Is it possible to take advantage of both coherent processing gain and spatial diversity gain simultaneously?", and we will answer this question in Chapter 4 by introducing a hybrid radar which combines the phased-array and MIMO radar configurations.

There are two applications that can benefit from the spatial diversity gain of MIMO radar presented in the literature. The first is the target detection problem studied in [7, 8], which illustrated that the MIMO radar outperforms the conventional phased-array radar whenever the probability of detection is at a reasonable level, *e.g.*, 0.8 or higher. The second application is the direction finding problem investigated in [3, 9], and the system considered has widely separated antennas at the transmitter to support the target spatial diversity and a standard antenna

array with half-wavelength intervals at the receiver to enable unambiguous AoA estimation. It is demonstrated that the performance of estimating AoA can be significantly improved by exploiting the spatial diversity gain offered by the MIMO configuration at the transmitter. For more benefits offered by the configuration having widely spaced antennas we refer the interested reader to [6, 10, 69].

2.3.1.3 Waveform Design Techniques

Orthogonal waveforms have been proven to be a good choice for transmission in a MIMO radar when the received signal is disturbed by additive white Gaussian noise and all the entries of the channel matrix $\mathbf{H}$ are independent complex Gaussian random variables with zero-mean and unit variance, *i.e.*, the covariance matrix of the channel vector $\mathbf{h}$ is an identity matrix. However, for a more general setting which takes the target angular spread into consideration, better waveforms are required to be designed to improve the system performance.

Yang and Blum [70] investigated waveform design for identification and classification of a distributed target, in other words, their goal is to find the waveform which leads to the best estimation of the target response. It is assumed that the target response vector (channel vector) remains static during the observation interval and it is a Gaussian random vector with zero-mean and a known covariance matrix. The components of the noise vector are assumed to be i.i.d. and complex Gaussian, with zero-mean and the same variance. The second-order statistics of the distributed target response contain information about the target and this fact has been exploited to find the optimum waveform. The waveform is designed under a constraint on the total transmitted power based on two criteria: (a) maximizing the mutual information between the random target response and the received signals; and (b) minimizing the value of minimum mean-square error (MMSE) in estimating the target response. It is demonstrated that both criteria lead to the same solution of the optimum waveform, which utilizes a waterfilling strategy to allocate the transmitted power.

De Maio and Lops [71] consider waveform design for detecting a distributed target in a disturbance which is not white due to the presence of clutter returns. It is assumed that the channel vector is a zero-mean Gaussian random vector whose covariance matrix is a scaled identity matrix, and the interference vector is a complex Gaussian random vector with zero-mean and a known covariance matrix. The optimum waveform is designed to maximize the Chernoff bound for the detection probability of the GLRT detector under a constraint on the signal to

clutter power ratio (SCR). In addition, the information-theoretic design criterion, maximizing the mutual information between the channel vector and the received waveforms, is also studied under the same SCR constraint, and the optimum solution found through both criteria are the same.

2.3.2 Colocated MIMO Radar

Unlike the statistical MIMO radar where antennas are widely separated to exploit the spatial diversity, the antennas of the colocated MIMO radar are close enough that all the elements view the same aspect of the target, and there are many papers investigating the merits of such a colocated MIMO radar, *e.g.*, [72–96]. The configuration of the colocated MIMO radar is similar to that of the conventional phased-array radar, but instead of transmitting scaled versions of a single waveforms, a colocated MIMO radar transmits independent probing signals via its multiple antennas, and this waveform diversity allows superior capabilities compared with its phased-array counterpart.

Transmitting independent waveforms simultaneously from the multiple transmit antennas of a MIMO radar and letting the received signals go through a bank of matched filters, the information of the propagation paths from each of the transmit antenna to each of the receive element can be extracted from the outputs of the matched filters. By appropriately utilizing the information, the colocated MIMO radar can improve the system performance by realizing a *virtual array* [72, 73, 87], and this concept is briefly explained as follows. Denoting the propagation time delay from the k-th transmit antenna to the target and from the target to the l-th receive element by τ_k^t and τ_l^r, respectively, the target response in the k-th matched filter output of the l-th receive antenna is $\alpha \exp\{-j2\pi f_c(\tau_k^t + \tau_l^r)\}$, where α is the target fading coefficient and $k = 1, 2, ..., N_t$, $l = 1, 2, .., N_r$. Obviously, both the transmit and receive antenna locations affect the time delay and thus the phase. There are $N_r N_t$ time delays for all of the matched filter outputs, and they can be viewed as the time delays corresponding to the antennas of a virtual array with $N_r N_t$ elements, whose steering vector is written as

$$\left[\begin{array}{cccccccc} e^{-j2\pi f_c(\tau_1^t+\tau_1^r)} & \dots & e^{-j2\pi f_c(\tau_1^t+\tau_{N_r}^r)} & e^{-j2\pi f_c(\tau_2^t+\tau_1^r)} & \dots & e^{-j2\pi f_c(\tau_{N_t}^t+\tau_{N_r}^r)} \end{array} \right]^T \quad (2.32)$$

Therefore, an $N_r N_t$-element virtual array is created by using only $N_r + N_t$ physical antennas.

The virtual array can be interpreted as the convolution of the transmit array and the receive array, as it is easy to understand that the transmitter steering vector convolved with the receiver steering vector gives the virtual steering vector [73].

Two configurations attracting the most attention are the filled and an overlapped linear virtual array. The filled linear virtual array is created by adopting a standard N_r-element ULA with half-wavelength interelement spacing as the receiver and a sparse N_t-element ULA as the transmitter whose interelement spacing is chosen as $\frac{N_r}{2}$ wavelength. It is clear that an N_rN_t-element virtual ULA is generated via the convolution, whose interelement spacing is half-wavelength. Hence, by wisely designing the locations of antennas, a virtual array with long aperture can be obtained using only a small number of physical antennas, dramatically increasing the spatial resolution [72] and improving parameter identifiability [77]. In contrast, if a standard ULA with half-wavelength spacing is employed at both the transmitter and receiver, the resulting virtual array is an overlapped linear virtual array, *i.e.*, more than one virtual element is at the same location. Selecting the standard ULA at the transmitter enables the radar to form a focused beam by emitting correlated waveforms [84], but transmit beamforming is impossible in the filled linear virtual array case because the large interelement spacing leads to aliasing. It has been shown that the overlapped linear virtual array configuration is able to enhance the flexibility for transmit beampattern design [78, 84, 85] and to improve the target detection and parameter estimation performance [82]. The work in this thesis focuses on the statistical MIMO radar, the reader may refer to a tutorial [75] for more details about the colocated MIMO radar.

2.4 Time-Reversal Techniques

The time-reversal (TR) technique, an extension to broadband signals of the phase-conjugation concept in optics, has attracted increasing interest for a broad range of applications for the last two decades. It has been indicated that applying TR in a radar system for target detection provides significant gains over conventional detection. In this section, we will start by discussing the basic principles of the TR approach, and move further to a brief introduction to TR detection in a radar system.

2.4.1 Basic principles of time-reversal techniques

The TR technique was first proposed as a solution to an important problem in the acoustic and ultrasound domains, focusing waves on targets through an inhomogeneous medium, which is difficult since the focusing can be strongly degraded due to the fluctuations of sound velocity in the propagating medium [97]. The idea of the TR technique is to convert a divergent wave reflected from a target into a convergent wave which focuses on the same target. As illustrated in Figure 2.6, the TR process includes three steps. In the first step, a waveform is radiated from the transducer array to the target through an inhomogeneous medium. The target generates a scattered waveform which propagates back through the inhomogeneous medium and is distorted. The second step is to record the waveforms received and measured by the transducer array for a time interval. In the last step, the recorded waveforms are time reversed and retransmitted into the medium, focusing on the target.

We next briefly explain why the TR technique provides inputs to the sensors of the transducer array that focus energy at the target location. The *diffraction impulse response* $h_{R_k}(S_0, t)$ measures the signal received at the target location S_0 after a Dirac delta function is applied to the k-th transducer at location R_k [98]. Similarly, the diffraction impulse response $h_{S_0}(R_k, t)$ is measured at the position of the k-th sensor after a source is excited at the target location S_0. The *reciprocity theorem*, valid in homogeneous as well as in inhomogeneous media, indicates that the respective positions of a source and an observer can be interchanged without altering the observed acoustic signal [99]. In other words, we have $h_{R_k}(S_0, t) = h_{S_0}(R_k, t)$. As shown in Figure 2.6, after the initial transmission, the target is illuminated and behaves as a source, and the signal observed at the k-th transducer is in proportion to $h_{S_0}(R_k, t)$. Consequently, the time reversed signal retransmitted from the k-th sensor in the third step is $h_{S_0}(R_k, T - t)$, and the total signal received at the target location is the superposition of the signals retransmitted from all the N sensors, which can be given by

$$r(S_0, t) = \sum_{k=1}^{N} h_{R_k}(S_0, t) \circledast h_{S_0}(R_k, T - t) = \sum_{k=1}^{N} h_{R_k}(S_0, t) \circledast h_{R_k}(S_0, T - t) \quad (2.33)$$

where $\circledast$ denotes the convolution. Clearly, all the signals from different sensors reach their maxima at the position S_0 at the same time T, leading to constructive interference and maximizing the signal energy at the target location. Therefore, TR technique provides the optimal

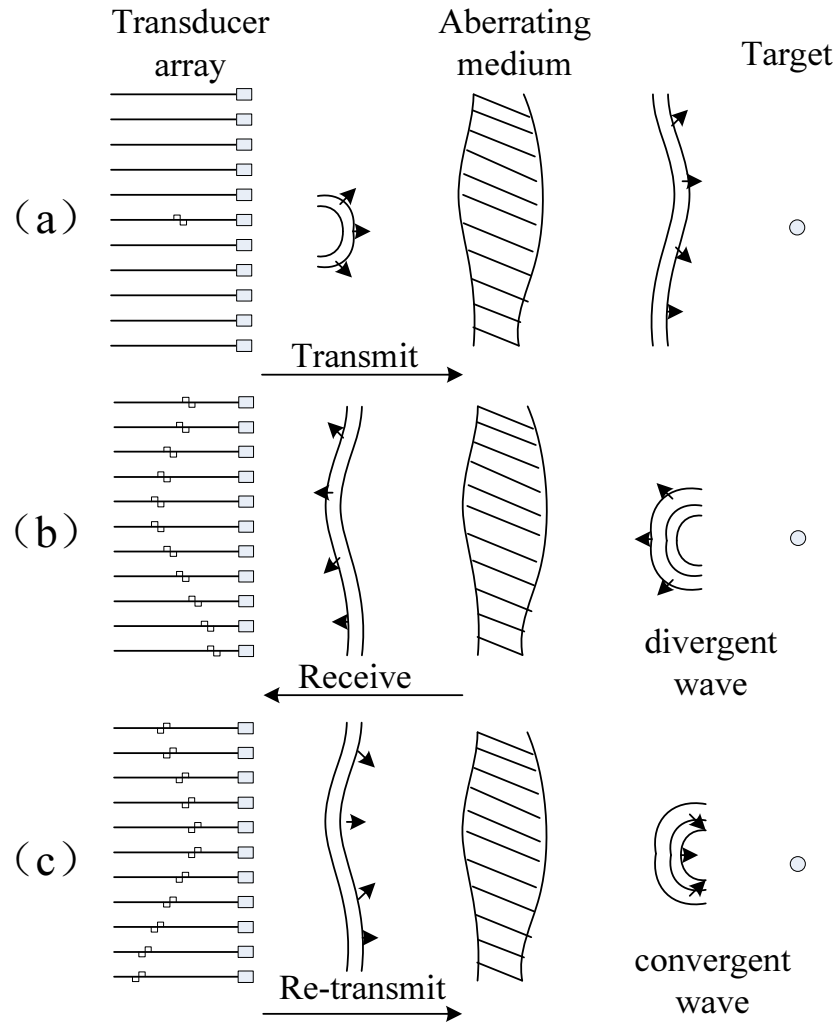

Figure 2.6: *Description of the TR process: (a) initial transmission, (b) record of the backscattered waveforms, (c) retransmission of the time reversed waveforms.*

solution for focusing energy through an inhomogeneous medium in the sense that it realizes the spatial-temporal matched filter to the propagation transfer function between the transducer array and the target [100].

The characteristics of the TR technique enable it to turn multipath effects, traditionally considered a drawback, into a benefit, which is very similar to the MIMO concept developed in communications. It has been shown that TR technique can improve the focusing quality by taking advantage of scattering and multipath in inhomogeneous media, *i.e.*, they demonstrate super-resolution focusing since the energy focuses on the target with much higher resolution than that in free-space [101–105]. We take a waveguide as an example to explain this unique

feature. As shown in Figure 2.7, each waveguide interface acts as a mirror and generates more paths in addition to the direct path from the real array to the target. By applying the method of images, the effect of a transducer array in a waveguide can be viewed as that of a set of virtual arrays in free-space, which are the images of the real array with respect to the waveguide interfaces. It is obvious that the resolution is much higher due to the existence of virtual arrays which increase the effective array aperture. Notice here that only the first reflections due to the presence of the two interfaces are depicted in Figure 2.7, but in fact the number of reflections required to be taken into account can be larger, depending on the distance from the target to the array [105].

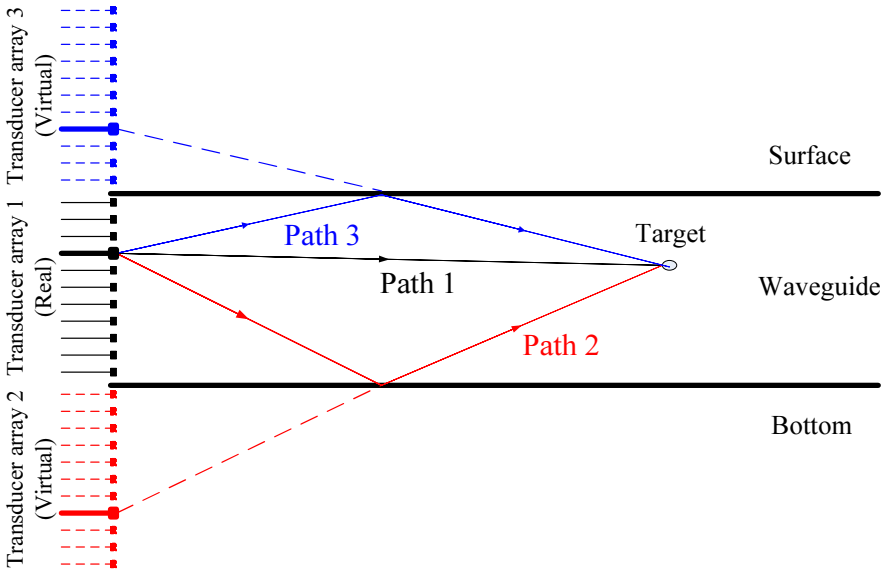

Figure 2.7: *Representation of the virtual transducer arrays in the waveguide.*

2.4.2 TR Detection in Radar

There are extensive publications studying the applications of TR in addition to focusing energy in acoustic and ultrasound domains, such as focusing in the electromagnetic domain [106], imaging in random media [107, 108], ultra-wideband communications [109–112], and computational imaging [113–117]. Recently, Moura *et al*. explored the radar target detection problem applying the TR technique, showing that TR detection provides significant gains over conventional detection [118–120]. The process of TR detection also involves three steps. Waveforms are first emitted from the transmitter, then the signals received by the receiver are measured, time reversed, energy normalized, and retransmitted, and finally the detector at the transmit-

ter makes the detection decision. The TR detection of a radar system with a single antenna as well as an antenna array was investigated, whose performance was examined with experimental measurements collected in a highly cluttered laboratory environment. It has been demonstrated that TR can dramatically improve target detection performance compared with conventional detection, which results from the fact that the waveform is reshaped to match the channel during the TR process, which is essentially a waveform design process. However, the retransmitted signal in Moura's algorithm contains noise components, and it is obvious that if the noise level is high, the TR technique is no longer a good choice. In addition, [118–120] did not derive analytical expressions for the threshold and probability of detection of the TR detection, which were determined by Monte Carlo simulations. These limitations of TR detection motivated the new schemes proposed in Chapter 5.

2.5 Conclusions

This chapter covered the fundamental knowledge required for analyzing a radar system. In the first part, the basic components and their characteristics in a radar system were studied, followed by a classification of conventional radars employing multiple antennas. A brief review of some well known signal processing approaches for target detection and direction finding problems were given, laying the foundation for the remainder of the thesis. In the second part, new schemes developed in radar were introduced, including the MIMO radar reported in the recent literature as well as systems utilizing time-reversal techniques. Their superiority over the conventional radar systems and their own limitations stimulated the present work, whose technical aspects will be discussed in the next three chapters.

Chapter 3
Detection Performance of MIMO Radar With Finite Scatterers Model

Previous researchers proposed a statistical MIMO model and investigated a radar system with several special array-target configurations, showing that MIMO radar can improve target detection performance significantly by exploiting spatial diversity. However, such model can only be adopted in extreme scenarios. In this chapter, we will introduce a system model in which the radar target is composed of a finite number of small scatterers, based on which the target detection performance of the system with different configurations is studied. A MIMO system involving a theoretical target is explored, and a closed form formula is derived to calculate the theoretical probability of detection for the system having an arbitrary array-target configuration. We also set up a MIMO radar system including a realistic target by making use of the data collected from previous research on ground target modelling.

3.1 Introduction

As mentioned in Chapter 2, Fishler *et al*. proposed a statistical MIMO radar model in [8] and demonstrated that MIMO techniques can be applied in radar scenarios to improve target detection performance by exploiting spatial diversity gain. In the statistical MIMO model, it is assumed that the distributed target has a rectangular shape and is composed of an infinite number of random and independent scatterers. All the scatterers are assumed to be uniformly distributed over the target area and their complex reflectivity coefficients are zero-mean random variables with the same distribution. Such a model is neither realistic nor convenient to be employed given that in practice the target actually comprises several significant scatterers at different spatial locations, which implies that a finite scatterers model should be used instead. Although in [3] the finite scatterers model is utilized, only a specific configuration is considered that the scatterers are assumed to be laid out as a linear array which is parallel to the antenna array. In addition, the statistical MIMO model can only be used for ideal array-target configurations where the interelement spacings are either large enough such that different antennas

observe different aspects of the target or small enough that all the antennas view the same aspect of the target. In other words, only extreme scenarios that the channel gains between different transmit-receive antenna pairs are totally uncorrelated or fully correlated are studied in [8]. However, it is very possible that such conditions do not hold in practice and hence, the statistical MIMO model can no longer be adopted and we need to resort to another model.

In this chapter, we investigate the target detection performance of a MIMO radar system with an arbitrary array-target configuration, assuming that the target is modelled as the sum of a finite number of independent scatterers. We first examine a radar system involving a theoretical target, for which the reflectivity coefficients of the scatterers are assumed to be zero-mean random variables. Unlike the ideal configurations discussed in [8] that all the channel gains have correlation coefficients 1 or 0, the channel gains between different antenna pairs of a general radar system have various degrees of correlation, which depend on the exact array-target configuration and can be measured by the correlation matrix of a vector containing all the entries of the channel matrix. Based on the calculated correlation matrix, a closed form formula is derived to evaluate the theoretical probability of detection for a MIMO radar having an arbitrary configuration, while [8] presents the detection performance for only four special configurations. This theoretical result makes it possible to predict the actual MIMO radar performance before implementing expensive experiments and avoiding time consuming simulations. Furthermore, the preferable MIMO array configuration could be selected for different scenarios by comparing the predicted performance of various configurations.

The assumption of the theoretical target model described above that the reflectivities of the scatterers are random variables is reasonable and useful from a theoretical and mathematical point of view. In order to have an impression of the effects the MIMO system has on detecting real targets, we next proceed to set up a MIMO radar including a realistic target by determining the reflectivity coefficients of the scatterers using the data collected from previous research on target modelling, and simulate the detection performance of the system with different configurations. To my best knowledge, this is the first effort of its kind in the open literature. The target considered here is a life-size land vehicle, which is modelled using a computer aided electro-magnetic (EM) simulator *FEldberechnungbei Korpern mit beleibeiger Oberflache* (FEKO) [121]. We emphasize here that although we are working with FEKO data, rather than "real" data collected from experimental field trials, the former is a common practical choice as the availability of the real data is very limited [121].

3.2 System Model

3.2.1 Channel Model

As shown in Figure 3.1, uniform linear arrays (ULA) of antennas are employed at both the transmitter and receiver with N_t and N_r elements, respectively. The interelement spacings are $\Delta_t\lambda_c$ and $\Delta_r\lambda_c$, where λ_c is the carrier wavelength and Δ_t and Δ_t are the normalized transmit and receive antenna spacing in wavelengths. We assume that all the signals are narrowband and that distances between scatterers and both the transmitter and receiver are much larger than the dimensions of the antenna arrays, that is, we operate in the far field.

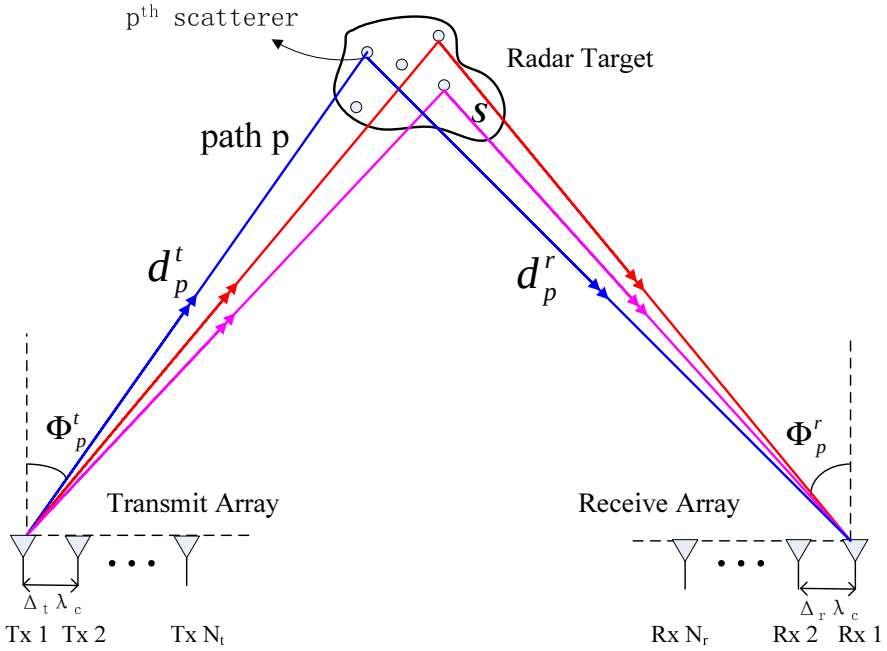

Figure 3.1: *Configuration of a MIMO radar system with the finite scatterers model*

In the finite scatterers model, a distributed target is assumed to be composed of a finite number of scatterers which are small enough to be viewed as point-like targets. As illustrated in Figure 3.1, it is assumed that there are N_s independent scatterers distributed over the target area S, and N_s is also the number of independent multipaths because of the assumption of a "single-bounce" propagation model. Path p is defined by the angle of departure (AoD) Φ_p^t, the angle of arrival (AoA) Φ_p^r, reflectivity coefficient of the p-th scatterer a_p^{rc}, and distance between Tx 1 and Rx 1 along the path $d_p^{tr} = d_p^t + d_p^r$.

Based on above assumptions, the $N_r \times N_t$ channel matrix $\mathbf{H}$ is given by [122]

$$\mathbf{H} = \sum_{p=1}^{N_s} a_p^{rc} \exp(-\frac{j2\pi d_p^{tr}}{\lambda_c}) \mathbf{\Psi}_r(\Phi_p^r) \mathbf{\Psi}_t^T(\Phi_p^t) \tag{3.1}$$

$$\mathbf{\Psi}_\varepsilon(\Phi_p^\varepsilon) = \begin{bmatrix} 1 \\ \exp\{j2\pi\Delta_\varepsilon \sin(\Phi_p^\varepsilon)\} \\ \vdots \\ \exp\{j2\pi(N_\varepsilon - 1)\Delta_\varepsilon \sin(\Phi_p^\varepsilon)\} \end{bmatrix} \tag{3.2}$$

In (3.2) ε represents either r or t.

3.2.2 Signal Model

It is supposed that the i-th antenna of the transmitter transmits a signal $\sqrt{\frac{E_s}{N_t}} s_i(t)$, where $\|s_i(t)\|^2 = 1$ and E_s is the total transmitted power. The normalizing coefficient is employed to make sure that the total transmitted power and the average received power at each element are not affected by the number of transmit antennas. Denote by an $N_r \times 1$ vector $\mathbf{r}(t) = \begin{bmatrix} r_1(t) & r_2(t) & \cdots & r_{N_r}(t) \end{bmatrix}^T$ the signals received at all the receiving elements, which can be described as follows:

$$\mathbf{r}(t) = \sqrt{\frac{E_s}{N_t}} \mathbf{H} \cdot \mathbf{s}(t - \tau) + \mathbf{n}(t) \tag{3.3}$$

where the $N_t \times 1$ vector $\mathbf{s}(t) = \begin{bmatrix} s_1(t) & s_2(t) & \cdots & s_{N_t}(t) \end{bmatrix}^T$ stands for the transmitted signals and the $N_r \times 1$ vector $\mathbf{n}(t) = \begin{bmatrix} n_1(t) & n_2(t) & \cdots & n_{N_r}(t) \end{bmatrix}^T$ represents the additive white Gaussian noise at all the receive antennas. Here we assume that $\mathbf{n}(t)$ is a zero-mean, complex Gaussian random vector process with correlation matrix $\sigma_n^2 \mathbf{I}_{N_r}$. Note here that τ is the time delay from the transmitter to the receiver via the target, and differences in time of arrival at the receive antennas are ignored for simplicity. We further assumed that the transmitted signals are mutually orthogonal, which is equivalent to the fact that $\int s_j(t - \tau) s_i^*(t) dt = \delta_{ij}(\tau)$.

Let the received signal $\mathbf{r}$ go through a bank of matched filters and denote the output by an $N_rN_t \times 1$ vector $\mathbf{x}$, that is, the $\{(i-1)N_t + j\}$-th entry of $\mathbf{x}$ is given by $[\mathbf{x}]_{(i-1)N_t+j} = \int r_i(t)s_j^*(t)dt$, where $i = 1, 2, ..., N_r$ and $j = 1, 2, ..., N_t$. Recalling that all the transmitted signals are orthogonal, it is not difficult to obtain the following expression

$$\mathbf{x} = \begin{cases} \mathbf{n} & \mathcal{H}_0 \\ \sqrt{\frac{E_s}{N_t}}\mathbf{h} + \mathbf{n} & \mathcal{H}_1 \end{cases} \tag{3.4}$$

where the alternate hypothesis $\mathcal{H}_1$ and null hypothesis $\mathcal{H}_0$ are that the target does or does not exist at delay τ, respectively. The $N_rN_t \times 1$ channel vector $\mathbf{h}$ is composed of all the entries of the channel matrix $\mathbf{H}$, and the $N_rN_t \times 1$ noise vector $\mathbf{n} \sim \mathcal{CN}(\mathbf{0}_{N_rN_t}, \sigma_n^2\mathbf{I}_{N_rN_t})$. The MIMO radar detector given by [8] can be written as below:

$$T = \|\mathbf{x}\|^2 \underset{<_{\mathcal{H}_0}}{>^{\mathcal{H}_1}} \eta \tag{3.5}$$

where η is a threshold ensuring the desired probability of false alarm $\mathrm{Pr}_{\mathrm{FA}}$. From (3.1) and (3.5), it is clear that the target detection decision will be made based on the value of the channel matrix, which is determined by the locations and reflectivity coefficients of the scatterers. Therefore, in the following two sections, we investigate the target detection performance of a MIMO radar system involving a theoretical target and a realistic target, respectively, and the only difference between them is the assumption of the locations and reflectivities of the scatterers. We emphasize here that the finite scatterers model itself has no limitation on the scatterers constituting the target except that each scatterer is required to be small enough such that they can be viewed as point-like targets.

3.3 MIMO Radar With a Theoretical Target

In this section, we explore a MIMO radar system having the same configuration as that shown in Figure 3.1, and the theoretical target considered here includes N_s random and independent scatterers which are uniformly distributed over the target area S. We assume that each reflec-

tivity coefficient a_p^{rc} can be a zero-mean complex Gaussian random variable with variance ι_p^2 and assume that the sum of all the variances equals to one. The last assumption is responsible for normalizing the average power reflected from the target to one. A formula to calculate the theoretical probability of detection for such a radar system will be derived first, following which is the analysis of two extreme channel models with respect to the level of correlation of the channel matrix, and then simplified expressions of the formula for two special cases are provided.

3.3.1 Detection Performance

From (3.4) and (3.5), it is easy to see that the probability of detection of the MIMO radar depends on the distributions of the test statistic $T = \|\mathbf{x}\|^2$ under both hypotheses. First of all, we consider T under the null hypothesis $\mathcal{H}_0$ and get

$$T = \|\mathbf{x}\|^2 = \sum_{i=1}^{N_r N_t} |n_i|^2 = \sum_{i=1}^{N_r N_t} \left(\Re^2[n_i] + \Im^2[n_i]\right) \tag{3.6}$$

where n_i is the i-th entry of the noise vector $\mathbf{n}$. Recalling that $\mathbf{n} \sim \mathcal{CN}(\mathbf{0}_{N_r N_t}, \sigma_n^2 \mathbf{I}_{N_r N_t})$, we can express the distribution of T directly by a chi-square random variable with $2N_r N_t$ degrees of freedom as follows:

$$T \sim \frac{\sigma_n^2}{2} \chi^2_{2N_r N_t} \qquad \text{Under } \mathcal{H}_0 \tag{3.7}$$

We next proceed to consider the test statistic T under the alternate hypothesis $\mathcal{H}_1$. First of all, an $N_r N_t \times 1$ vector $\mathbf{h_n} = \mathbf{h} + \sqrt{\frac{N_t}{E_s}}\mathbf{n}$ is defined, and thus $T = \|\mathbf{x}\|^2 = \frac{E_s}{N_t} \|\mathbf{h_n}\|^2$. It is easy to verify that $\mathbf{h_n}$ has zero mean, and the $N_r N_t \times N_r N_t$ square matrix $\mathbf{C_{h_n}} = \mathrm{E}\{\mathbf{h_n} \cdot \mathbf{h_n}^H\}$ is the covariance matrix of $\mathbf{h_n}$, that is, $\mathbf{h_n} \sim \mathcal{CN}(\mathbf{0}_{N_r N_t}, \mathbf{C_{h_n}})$. Recalling the assumption about the reflectivity coefficients and substituting (3.1) gives the (k, l)-th entry of the covariance matrix $\mathbf{C_{h_n}}$ as

$$\mathbf{C}_{\mathbf{h_n}}(k,l) = \sum_{m=1}^{N_s} \iota_m^2 \{\exp[j2\pi(p-u)\Delta_r \sin(\Phi_m^r)]\cdot \exp[j2\pi(q-v)\Delta_t \sin(\Phi_m^t)]\} + \frac{N_t}{E_s}\sigma_n^2\delta_{kl} \tag{3.8}$$

where $k = (p-1)N_t + q$, $l = (u-1)N_t + v$, $p, u = 1, 2, ..., N_r$, and $q, v = 1, 2, ..., N_t$. Therefore, for any set of parameters in the channel matrix given by (3.1), we can easily compute the covariance matrix $\mathbf{C}_{\mathbf{h_n}}$. Note that the covariance matrix $\mathbf{C}_{\mathbf{h_n}}$ is a Hermitian matrix and it can be factorized through its eigenvalue decomposition, *i.e.*,

$$\mathbf{C}_{\mathbf{h_n}} = \mathbf{U}_{\mathbf{h_n}} \cdot \mathbf{\Lambda}_{\mathbf{h_n}} \cdot \mathbf{U}_{\mathbf{h_n}}^H \tag{3.9}$$

where the $N_rN_t \times N_rN_t$ matrix $\mathbf{U}_{\mathbf{h_n}}$ is a unitary matrix whose columns are eigenvectors and $\mathbf{\Lambda}_{\mathbf{h_n}}$ is a diagonal matrix with N_rN_t real and nonnegative eigenvalues λ_1, λ_2,...,$\lambda_{N_rN_t}$ (in decreasing order) as its diagonal elements. We next define an $N_rN_t \times 1$ vector $\mathbf{h_{nu}} = \mathbf{U}_{\mathbf{h_n}}^H \mathbf{h_n}$, then according to the property of the linear transform of complex Gaussian random vectors, the distribution of $\mathbf{h_{nu}}$ is given by

$$\mathbf{h_{nu}} \sim \mathcal{CN}(\mathbf{0}_{N_rN_t}, \mathbf{U}_{\mathbf{h_n}}^H \cdot \mathbf{C}_{\mathbf{h_n}} \cdot \mathbf{U}_{\mathbf{h_n}}) = \mathcal{CN}(\mathbf{0}_{N_rN_t}, \mathbf{\Lambda}_{\mathbf{h_n}}) \tag{3.10}$$

Considering the fact that $\mathbf{\Lambda}_{\mathbf{h_n}}$ is the covariance matrix of $\mathbf{h_{nu}}$ and is a diagonal matrix, it is safe to conclude that all the elements of $\mathbf{h_{nu}}$ are uncorrelated and its i-th element has the distribution $\mathcal{CN}(0, \lambda_i)$. Finally, notice that

$$\|\mathbf{h_{nu}}\|^2 = \left\|\mathbf{U}_{\mathbf{h_n}}^H \mathbf{h_n}\right\|^2 = (\mathbf{U}_{\mathbf{h_n}}^H \mathbf{h_n})^H (\mathbf{U}_{\mathbf{h_n}}^H \mathbf{h_n}) = \mathbf{h_n}^H \mathbf{h_n} = \|\mathbf{h_n}\|^2 \tag{3.11}$$

Therefore, the original problem of calculating the distribution of $T = \|\mathbf{x}\|^2$ becomes the evaluation of $\|\mathbf{h_{nu}}\|^2$. The reason why we apply such a transform is that the elements of $\mathbf{x}$ could be correlated for some scenarios. The uncorrelated nature of the elements of $\mathbf{h_{nu}}$ simplifies the

calculation process dramatically.

According to the above analysis, the test statistic T can be viewed as the sum of a set of $N_r N_t$ independent weighted chi-square random variables $\left\{ \frac{E_s \lambda_i}{2N_t} \chi_2^2 \right\}$. The characteristic function is utilized in the following derivation because it provides a simple method for determining the PDF of a sum of independent random variables [123]. This approach is usually much easier than the direct calculation which demands PDF convolution, *i.e.*, the PDF of a sum of K independent random variables is the K-fold convolution of the PDF of each random variable. Further defining $c_i = \frac{E_s}{N_t} \lambda_i$, we can express the characteristic function of T as below [123]:

$$\digamma(v) = \prod_{i=1}^{N_r N_t} \frac{1}{1 - jvc_i} \tag{3.12}$$

Assume there are N distinct values $\{c_k\}$ of all the $N_r N_t$ values, and c_k has corresponding algebraic multiplicity μ_k [124]. Thus, (3.12) can be rewritten as

$$\digamma(v) = \prod_{k=1}^{N} \frac{1}{(1 - jvc_k)^{\mu_k}} \qquad \left(\sum_{k=1}^{N} \mu_k = N_r N_t \right) \tag{3.13}$$

Given the fact that the characteristic function of a random variable is the Fourier transform of the probability density function (PDF) of the random variable with a sign inverse in the complex component, it is possible to derive the PDF of T through the inverse Laplace transform of (3.13) with the substitution $z = -jv$. The following is the characteristic function expressed in the form of partial fraction expansions [124]:

$$\begin{aligned} \digamma(z) &= \prod_{k=1}^{N} \frac{1}{(1+c_k z)^{\mu_k}} = \frac{\prod_{k=1}^{N} \left(\frac{1}{c_k}\right)^{\mu_k}}{\prod_{k=1}^{N} (z+\frac{1}{c_k})^{\mu_k}} \\ &= \sum_{k=1}^{N} \left[\frac{A_{k,1}}{(z+\frac{1}{c_k})^{\mu_k}} + \frac{A_{k,2}}{(z+\frac{1}{c_k})^{\mu_k - 1}} + \cdots + \frac{A_{k,\mu_k}}{(z+\frac{1}{c_k})} \right] = \sum_{k=1}^{N} \sum_{l=1}^{\mu_k} \frac{A_{k,l}}{(z+\frac{1}{c_k})^{\mu_k - l + 1}} \end{aligned} \tag{3.14}$$

where the coefficient $A_{k,l}$ is given by

$$
\begin{aligned}
A_{k,l} &= \frac{1}{(l-1)!}\left[\frac{d^{l-1}}{dz^{l-1}}\left\{F(z)\cdot(z+\frac{1}{c_k})^{\mu_k}\right\}\right]\Big|_{z=-\frac{1}{c_k}} \\
&= \frac{1}{(l-1)!}\left[\frac{d^{l-1}}{dz^{l-1}}\frac{\prod_{p=1}^{N}\left(\frac{1}{c_p}\right)^{\mu_p}}{\prod_{p=1,p\neq k}^{N}(z+\frac{1}{c_p})^{\mu_p}}\right]\Bigg|_{z=-\frac{1}{c_k}}
\end{aligned}
\tag{3.15}
$$

The inverse Laplace transform of (3.14) gives rise to the PDF of T under $\mathcal{H}_1$ as below:

$$
\mathrm{PDF}(T|\,\mathcal{H}_1) = \sum_{k=1}^{N}\sum_{l=1}^{\mu_k}\frac{A_{k,l}}{(\mu_k-l)!}\cdot T^{(\mu_k-l)}\cdot\exp\left(-\frac{T}{c_k}\right) \tag{3.16}
$$

As mentioned before, for a given noise level, one common approach is to determine the threshold η based on the desired probability of false alarm $\mathrm{Pr_{FA}}$, and the probability of detection $\mathrm{Pr_D}$ is computed based on the value of η and the PDF of the test statistic T under $\mathcal{H}_1$. Both relations can be described using the following formulae:

$$
\mathrm{Pr_{FA}} = \Pr\left(T>\eta|\,\mathcal{H}_0\right) = \Pr\left(\frac{\sigma_n^2}{2}\chi^2_{2N_rN_t}>\eta\right) = \Pr\left(\chi^2_{2N_rN_t}>\frac{2\eta}{\sigma_n^2}\right) \tag{3.17}
$$

$$
\mathrm{Pr_D} = \Pr\left(T>\eta|\,\mathcal{H}_1\right) = \int_{\eta}^{+\infty}\mathrm{PDF}(T|\,\mathcal{H}_1)dT \tag{3.18}
$$

Substituting (3.16) into (3.18), we can express the probability of detection, by utilizing the upper incomplete Gamma function, as below:

$$
\mathrm{Pr_D} = \sum_{k=1}^{N}\sum_{l=1}^{\mu_k}A_{k,l}\cdot c_k^{\mu_k-l+1}\cdot\exp(-\tfrac{\eta}{c_k})\cdot\sum_{p=0}^{\mu_k-l}\frac{\left(\frac{\eta}{c_k}\right)^p}{p!} \tag{3.19}
$$

where the threshold η is easily calculated from (3.17) as

$$\eta = \frac{\sigma_n^2}{2} \mathcal{F}^{-1}_{\chi^2_{2N_rN_t}} (1 - \mathrm{Pr_{FA}}) \tag{3.20}$$

where $\mathcal{F}^{-1}_{\chi^2_k}$ denotes the inverse cumulative distribution function (CDF) of a chi-square random variable with k degrees of freedom. The above equations demonstrate that it is possible to predict the performance of MIMO radar system without implementing costly experiments. In addition, the comparison between the theoretical performance of different configurations provides us the principle based on which to design the best MIMO system for various scenarios. Below, we will further investigate the relationship between the correlation of the channel matrix and the distribution of eigenvalues $\{\lambda_i\}$, and then show the simplified expressions of $\mathrm{Pr_D}$ for two special cases.

We emphasize here that calculating the distributions of a sum of weighted chi-square random variables is a common problem encountered in statistics and engineering. The widely adopted technique is to approximate the linear summation by a single chi-square random variable with different degrees of freedom and an scaling factor, which are carefully chosen such that the first two moments remain the same [125–127]. However, in this section, the accurate PDF and CDF of the weighted sum are derived in closed form, which can be widely used in many practical applications.

3.3.2 Analysis of Extreme Channel Models

Recall that the additive white Gaussian noise is independent of the channel, then the covariance matrix $\mathbf{C_{h_n}}$ can be rewritten as

$$\mathbf{C_{h_n}} = \mathrm{E}\left[\mathbf{h_n} \cdot \mathbf{h_n}^H\right] = \mathrm{E}\left[\mathbf{h} \cdot \mathbf{h}^H\right] + \frac{N_t}{E_s}\sigma_n^2 \mathbf{I}_{N_rN_t} \tag{3.21}$$

That is, the covariance matrix $\mathbf{C_{h_n}}$ is actually the sum of the correlation matrix of the channel vector $\mathbf{h}$ including N_rN_t channel matrix entries $\{h_k\}$ and the scaled covariance matrix of the noise vector $\mathbf{n}$. Obviously, the eigenvalues $\{\lambda_i\}$ of $\mathbf{C_{h_n}}$ are closely related to the correlation matrix of the vector $\mathbf{h}$. This correlation matrix depends on the specific configuration of the

radar system. However, we can compute its value under the following two extreme cases.

3.3.2.1 Entries are totally uncorrelated

Invoking the assumption that the sum of all the variances of the reflectivity coefficients is one, it is not difficult to verify that $\mathrm{E}\left[h_k \cdot h_k^*\right] = 1$, in other words, the diagonal elements of the correlation matrix are one. Moreover, the totally uncorrelated condition illuminates that all the non-diagonal elements of $\mathrm{E}\left[\mathbf{h} \cdot \mathbf{h}^H\right]$ are zero. This results in the diagonal matrix $\mathbf{C}_{\mathbf{h_n}} = \left(1 + \frac{N_t}{E_s}\sigma_n^2\right)\mathbf{I}_{N_r N_t}$. Hence, there exists $N_r N_t$ eigenvalues $\{\lambda_i\}$, and they all have the same value $\lambda = 1 + \frac{N_t}{E_s}\sigma_n^2$. Making use of the simplified formula introduced in the next section, we can evaluate $\mathrm{Pr_D}$ easily.

3.3.2.2 Entries are fully correlated

Similar to the calculation in the previous subsection, we know that the diagonal elements of the correlation matrix are one. The condition of full correlation demonstrates that all the non-diagonal elements are also equal to one, that is, $\mathrm{E}\left[\mathbf{h} \cdot \mathbf{h}^H\right]$ is an all-ones matrix. Therefore, $\mathbf{C}_{\mathbf{h_n}}$ has $N_r N_t$ eigenvalues, in which $\lambda_1 = N_r N_t + \frac{N_t}{E_s}\sigma_n^2$ and the other $(N_r N_t - 1)$ eigenvalues have the same value $\lambda_2 = \frac{N_t}{E_s}\sigma_n^2$.

The magnitudes of the correlation values $\mathbf{C}_{\mathbf{h_n}}(k, l)$ in (3.8) depend on the distribution of the angles Φ^t and Φ^r of each path and the array interelement spacing. If Φ^t and Φ^r for all the paths are the same, then we get the fully correlated case. The correlation decreases as the range of angles increases for the same array spacing. For any non-zero angle spread, increasing antenna spacing has the effect of decreasing the correlation [122].

3.3.3 Formulae of $\mathrm{Pr_D}$ for Two Special Cases

Here, in order to simplify the computation, we display the compact form of (3.19) for two special cases: all the eigenvalues $\{\lambda_i\}$ are different or are the same.

3.3.3.1 Eigenvalues are different

In this case, the number of distinct eigenvalues is $N = N_r N_t$ and all the algebraic multiplicity μ_k are one. As a result, (3.16) is rewritten as

$$\mathrm{PDF}(T|\,\mathcal{H}_1) = \sum_{k=1}^{N_rN_t} \frac{\prod_{p=1,p\neq k}^{N_rN_t} \frac{c_k}{c_k-c_p}}{c_k} \cdot \exp\left(-\frac{T}{c_k}\right) \tag{3.22}$$

Substitute (3.22) into (3.18) leads to the following formula:

$$\mathrm{Pr_D} = \sum_{k=1}^{N_rN_t} \left(\prod_{p=1,p\neq k}^{N_rN_t} \frac{c_k}{c_k-c_p} \right) \cdot \exp(-\tfrac{\eta}{c_k}) \tag{3.23}$$

3.3.3.2 Eigenvalues are the same

In this case, the N_rN_t eigenvalues have the same value λ, so (3.12) can be expressed as below:

$$F(v) = \frac{1}{(1-jv\frac{E_s}{N_t}\lambda)^{N_rN_t}} \tag{3.24}$$

which results in the conclusion that $T = \|\mathbf{x}\|^2 \sim \frac{E_s\lambda}{2N_t}\chi^2_{2N_rN_t}$. Consequently, the probability of detection is given by

$$\mathrm{Pr_D} = 1 - \mathcal{F}_{\chi^2_{2N_rN_t}}\left(\frac{2N_t\eta}{E_s\lambda}\right) \tag{3.25}$$

where $\mathcal{F}_{\chi^2_k}$ denotes the CDF of a chi-square random variable with k degrees of freedom. This result matches equation (29) in [8].

3.4 MIMO Radar With a Realistic Target

The reflectivity coefficients of the scatterers composing the target are assumed to be zero-mean complex Gaussian random variables in the last section, which is a useful assumption from a theoretical point of view. In order to have an impression of the effects the MIMO radar has on

detecting real targets, we set up a MIMO radar system involving a realistic target in this section, and the locations and gains of the scatterers are determined by the data collected from previous research on modelling ground targets.

3.4.1 System Configuration

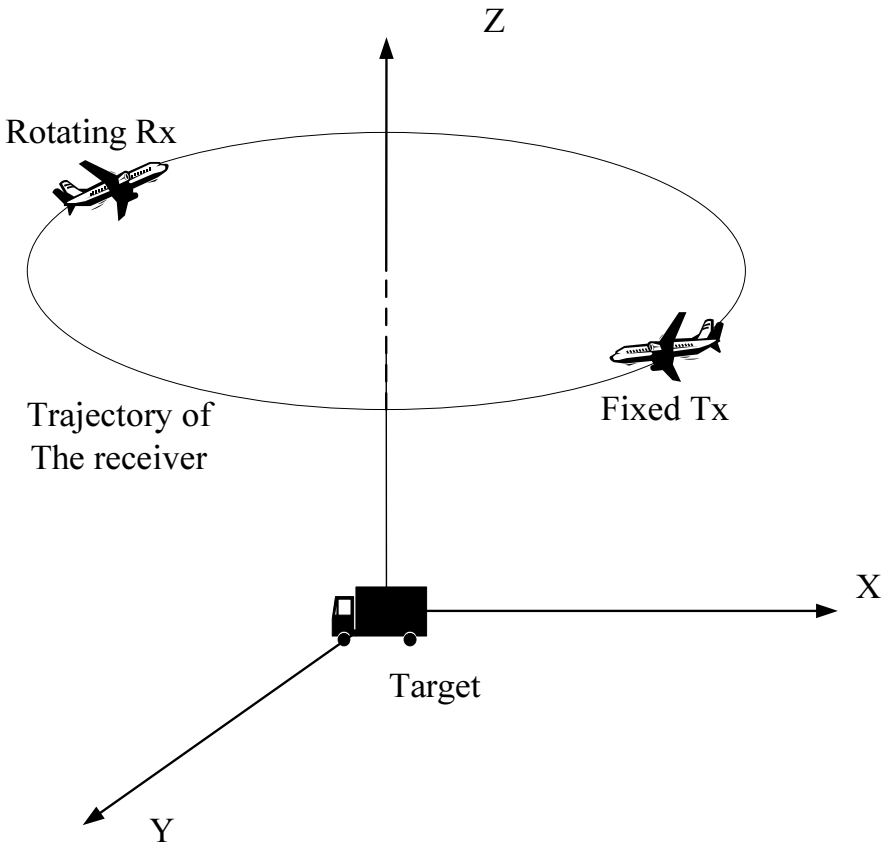

Figure 3.2: *Transmitter and receiver configuration during the FEKO simulations in [2]*

Mishra [121] modeled four types of life-size land vehicles using a computer aided EM simulator FEKO, and formatted bistatic synthetic aperture radar (SAR) images through appropriate post-processing of the results. These four targets are the armoured personal carrier (APC), the main battle tank (MBT), the stinger launcher (STR), and the land missile launcher (MSL). As illustrated in Figure 3.2, a system having a three dimensional (3D) configuration is simulated by Mishra. For each run, the 3D target is illuminated by the transmitter for a range of frequencies, and the transmitter is fixed at a certain azimuth and elevation with a given polarization. The EM simulator generates the surface current on the provided computer aided design (CAD) model of the target, based on which the scattered field in a given polarization at the receiver is obtained

and stored. The receiver has a fixed elevation and varying azimuth angle through 0° to 360° with a predetermined angular step. The FEKO data collected from each run then are post-processed, generating 2D SAR images of the target viewed by the fixed transmitter and rotating receiver with different azimuth. Figure 3.3 shows the bistatic SAR images of the MBT when the transmitter elevation and azimuth is 10° and 0°, respectively, and the receiver elevation is 10° and the receiver azimuth has four different values.

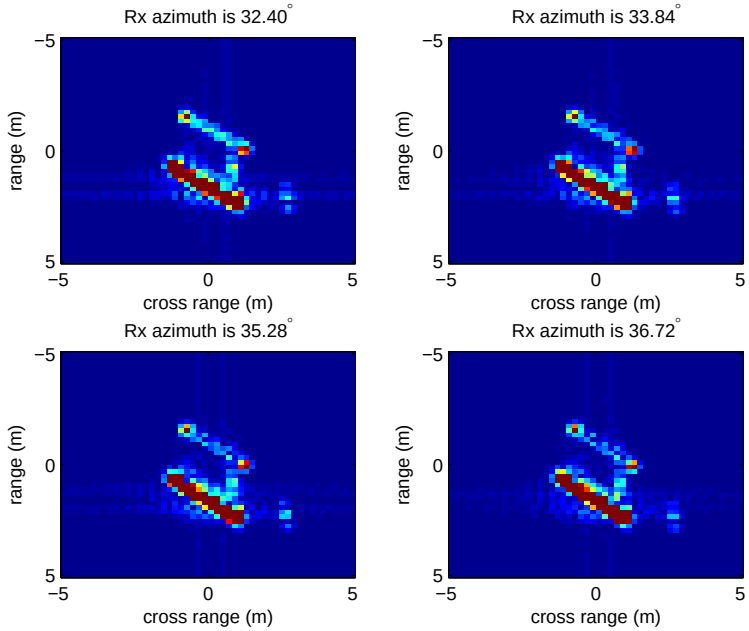

Figure 3.3: *Bistatic SAR images of the MBT for four values of the receiver azimuth*

For certain polarizations of the transmitter and receiver, several 50×50 matrices are available to form images of a given type of target viewed by a pair of transmitter and receiver at different locations. As the values of matrix entries indicate the reflectivities of different parts of the target, it is reasonable to assume that the target is composed of a finite number of point-like scatterers, whose reflectivity coefficients change as the locations of the transmitter and receiver vary. In other words, for each pair of transmitter and receiver locations, the target is modeled by a 10m by 10m rectangular area S as shown in Figure 3.4, in which there are 2,500 point-like scatterers $\{S_{p,q}\}$, whose reflectivity coefficients $\{a^{rc}_{p,q}\}$ are the values of the (p,q)-th entries of the corresponding 50×50 matrix. The origin of the xy-plane is at the center of the target, and the coordinates $(x_{p,q}, y_{p,q})$ of the scatterer $S_{p,q}$ are $(q \times 0.2 - 5.1, p \times 0.2 - 5.1)$.

Therefore, we set up the MIMO radar system as illustrated in Figure 3.5, where, as before,

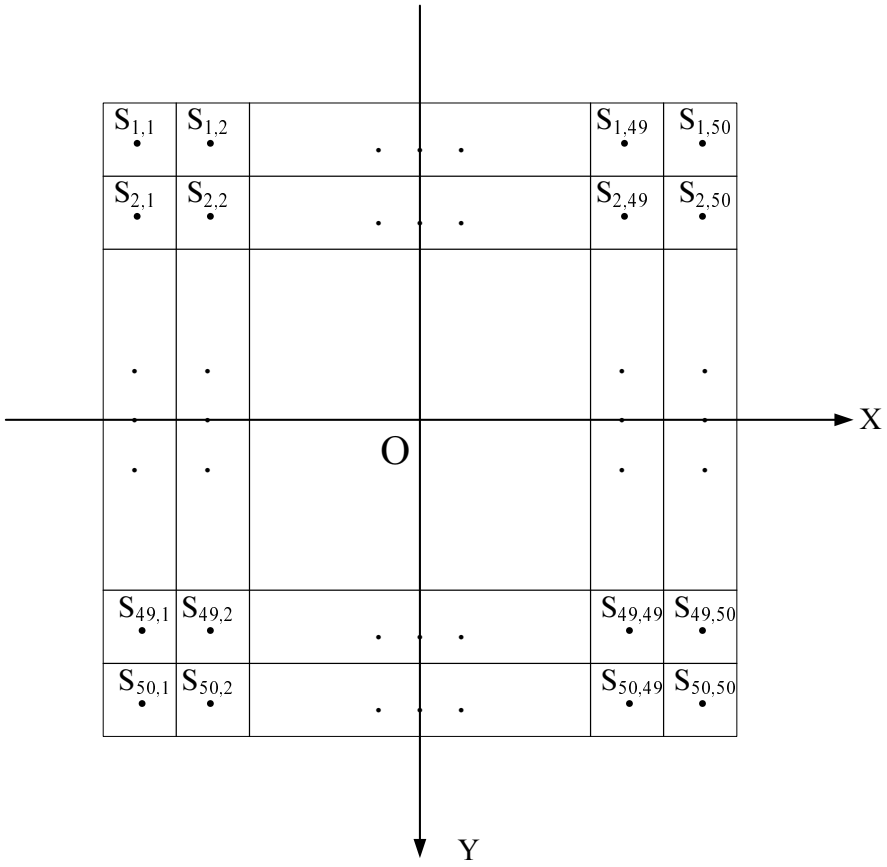

Figure 3.4: *Finite scatterers model of the realistic target*

ULAs are employed at both transmitter and receiver with N_t and N_r elements, respectively. The interelement spacings are $\Delta_t\lambda_c$ and $\Delta_r\lambda_c$, where λ_c is the carrier wavelength and Δ_t and Δ_r are the normalized transmit and receive antenna spacing in wavelengths. d_0^t and d_0^r are the distances between the centre of the target and the first antenna of the transmitting and receiving array, respectively. Notice the fact that these two values do not need to be the same. In Figure 3.5, the rectangular area S in the xy-plane is the 10m by 10m target model illustrated in Figure 3.4. Because of the limited FEKO data, the elevation of transmitter and receiver, Φ^{te} and Φ^{re}, can be either 10° or 15°, and the transmitter azimuth Φ^{ta} can be one of the following six values 0°, 60°, 120°, 180°, 240°, and 300°, while the receiver azimuth Φ^{ra} can be any one among 500 values, from 0° to 360° with a step of 0.72°. For any of the aforementioned system configuration, the target can be APC, MBT, STR, or MSL, and the polarizations of the transmitter and receiver can be either horizontal or vertical.

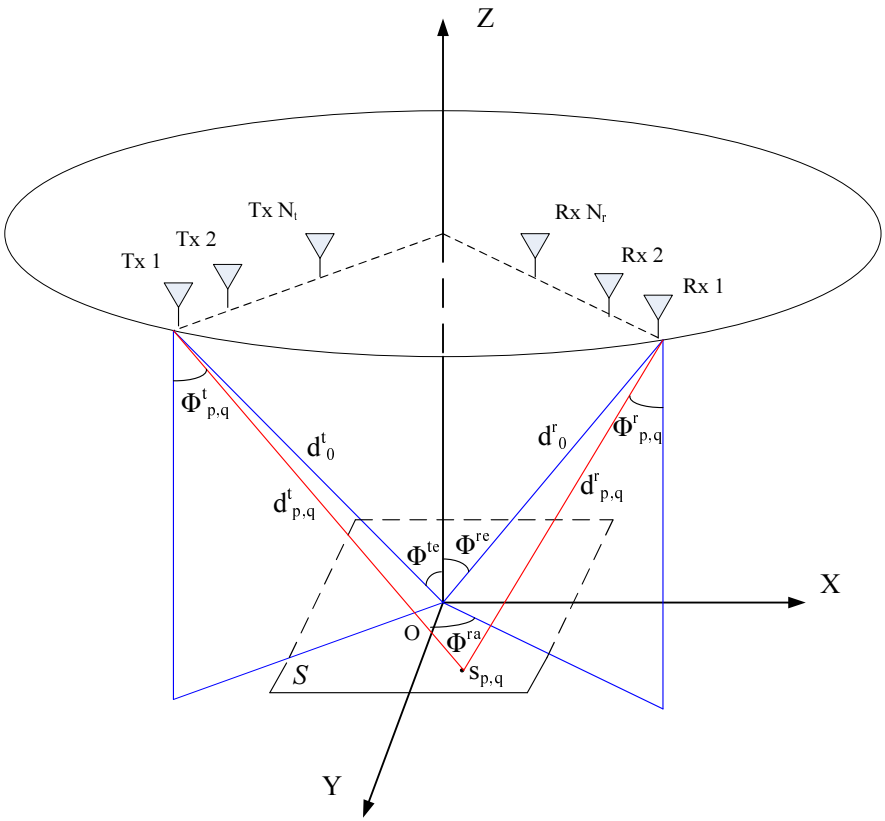

Figure 3.5: *Configuration of a MIMO radar system involving the realistic target*

3.4.2 System Model

As shown in Figure 3.5, the path through the scatterer $S_{p,q}$ is defined by AoD $\Phi^t_{p,q}$, AoA $\Phi^r_{p,q}$, reflectivity coefficient $a^{rc}_{p,q}$, distance between Tx 1 and $S_{p,q}$, $d^t_{p,q}$, and distance between $S_{p,q}$ and Rx 1, $d^r_{p,q}$. Then, similar to (3.1) and (3.2), for a MIMO radar having the configuration described in the last section with any combination of all the possible parameters, we can calculate the $N_r \times N_t$ channel matrix $\mathbf{H}$ as below:

$$\mathbf{H} = \sum_{p=1}^{50}\sum_{q=1}^{50} a^{rc}_{p,q} \exp(-\frac{j2\pi d^{tr}_{p,q}}{\lambda_c}) \mathbf{\Psi}_r(\Phi^r_{p,q}) \mathbf{\Psi}^T_t(\Phi^t_{p,q}) \tag{3.26}$$

$$\mathbf{\Psi}_{\varepsilon}(\Phi^{\varepsilon}_{p,q}) = \begin{bmatrix} 1 \\ \exp\{j2\pi\Delta_{\varepsilon}\sin(\Phi^{\varepsilon}_{p,q})\} \\ \vdots \\ \exp\{j2\pi(N_{\varepsilon}-1)\Delta_{\varepsilon}\sin(\Phi^{\varepsilon}_{p,q})\} \end{bmatrix} \tag{3.27}$$

where ε represents either r or t and $d^{tr}_{p,q} = d^{t}_{p,q} + d^{r}_{p,q}$ is the distance between Tx 1 and Rx 1 along the path through the scatterer $S_{p,q}$. In addition, geometrical computation gives us the following equations:

$$d^{\varepsilon}_{p,q} = \sqrt{(d^{\varepsilon}_{0}\sin\Phi^{\varepsilon e})^2 + (x_{\varepsilon} - x_{p,q})^2 + (y_{\varepsilon} - y_{p,q})^2} \tag{3.28}$$

$$\sin(\Phi^{\varepsilon}_{p,q}) = \frac{(d^{\varepsilon}_{p,q})^2 - (d^{\varepsilon}_{0})^2\cos(2\Phi^{\varepsilon e}) - x^2_{p,q} - y^2_{p,q}}{2d^{\varepsilon}_{0}\sin\Phi^{\varepsilon e}d^{\varepsilon}_{p,q}} \tag{3.29}$$

where $x_{\varepsilon} = d^{\varepsilon}_{0}\sin\Phi^{\varepsilon e}\sin\Phi^{\varepsilon a}$ and $y_{\varepsilon} = d^{\varepsilon}_{0}\sin\Phi^{\varepsilon e}\cos\Phi^{\varepsilon a}$. The transmitted signals are the same as that described in Section 3.2.2, and the output of a bank of matched filters $\mathbf{x}$, the MIMO radar detector, and the threshold of the detector η are shown in (3.4), (3.5), and (3.20), respectively. Therefore, together with the channel matrix $\mathbf{H}$ given by (3.26), we are able to measure the value of the vector $\mathbf{x}$, and the detection decision can be made by comparing $\|\mathbf{x}\|^{\mathbf{2}}$ with the threshold η.

Note here that the elements of the channel matrix $\mathbf{H}$ are assumed to be zero-mean complex Gaussian random variables in the theoretical target model discussed in the last section, and thus the theoretical probability of detection of a MIMO radar system can be derived. In the realistic target model, however, the channel gains are computed using the FEKO data and the distributions are unknown. Hence, we make the detection decision for each realization of $\mathbf{H}$ by viewing it as a deterministic matrix, and obtain the probability of detection of a MIMO radar system by averaging over multiple realizations. The approaches for generating multiple channel realizations using the available FEKO data will be described in detail in the next section.

3.5 Simulation Results

In this section, numerical results are presented showing the target detection performance of a MIMO radar system with different antenna spacings. We consider a radar system, regardless of the type of targets, having two transmit antennas and four receive antennas. The probability of false alarm is set to be a constant value $\mathrm{Pr_{FA}} = 10^{-6}$ and the SNR is defined as the ratio between the transmitted power E_s and the noise level per receiving element σ_n^2.

We start by investigating a MIMO radar system involving the theoretical target discussed in Section 3.3. It is assumed that the target area has circular shape with radius r_0, within which 64 scatterers are uniformly distributed. The carrier frequency of the signal is 10 GHz, and the size of the antenna array is much smaller than the distances between the target and both the transmitter and receiver, which are in the order of $3 \sim 5$ km.

First of all, we validate the theoretical results of the probability of detection $\mathrm{Pr_D}$ obtained from (3.19) for various configurations. Figure 3.6 depicts the theoretical probability of detection as a function of the average received SNR when $r_0 = 15$m, and the five configurations considered involve the two extreme models mentioned in Section 3.3.2 and three models whose array interelement spacings are 50, 100, and 200 wavelengths, respectively.

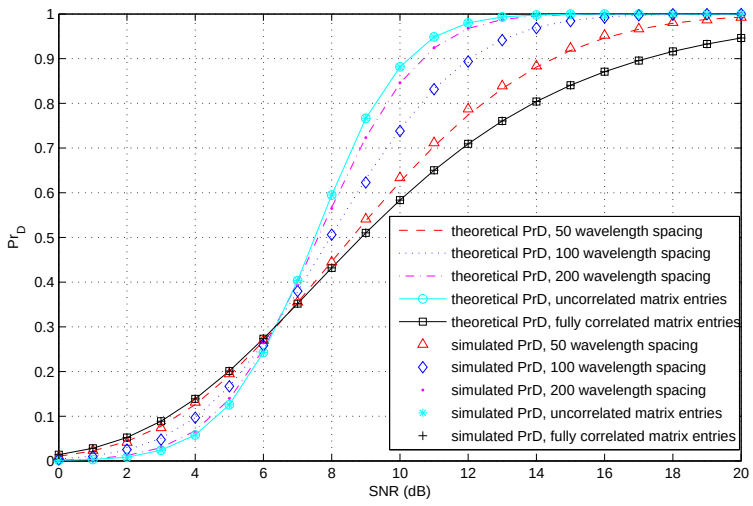

Figure 3.6: *Theoretical and simulated probability of detection as a function of the SNR for systems with 2 Tx and 4 Rx antennas, Tx/Rx interelement spacings varied simultaneously*

Figure 3.6 also shows the $\mathrm{Pr_D}$ recorded from Monte Carlo simulations for the same five sce-

narios, and the total number of tests for each case is 10,000. Obviously, the simulated results agree well with the theoretical values, which confirms the correctness of formula (3.19).

Observing the figure, we find that the curves corresponding to the two extreme channel models set bounds for the system performance. In other words, all the configurations with specific interelement spacings lie between these two ideal scenarios. Moreover, the performance curve is closer to the full correlation case as the spacing decreases, while closer to the uncorrelated case as the spacing becomes larger. This agrees with the analysis shown in Section 3.3.2 that for the same target having a non-zero angle spread, the larger the antenna spacing, the lower the channel matrix correlation, and thus the more spatial diversity gain can be realized.

It can be seen in Figure 3.6 that at low SNR, a system with densely spaced antennas outperforms the ones whose interelement spacing is large, while at high SNR the latter performs better. Furthermore, the system with large antenna spacing is always preferred when the detection performance is acceptable, *i.e.*, $\mathrm{Pr_D}$ is large enough. This is because at low SNR the received power affects target detection performance the most, while the number of diversity paths is the dominating factor at high SNR.

We next examine the target detection performance of a MIMO radar system with different configurations when the target is the realistic target introduced in Section 3.4. As mentioned before, the performance is measured based on multiple realizations of the channel matrix generated using the available FEKO data. Note the fact that there are several approaches to generate channel realizations, and here we just employ a simple one, as our major objective is to explore the advantages of a MIMO radar when a realistic target is considered.

In all the following simulations, the target studied is a MBT, the polarizations of both the transmitter and receiver are horizontal, the elevation of the receiver is 10°, and the elevation and azimuth of the transmitter is 10° and 0°, respectively. Numerical results for the scenarios with other combinations of the parameters can also be obtained using corresponding FEKO data. The carrier frequency of the signal is 1 GHz, and the channel matrix $\mathbf{H}$ is normalized such that the average energy returned from the target is one.

When the system parameters are fixed at the above values, 500 matrices with size 50×50 are available, whose entries are the reflectivity coefficients $\{a_{p,q}^{rc}\}$ of all the 2,500 scatterers $\{S_{p,q}\}$ composing the target. Each matrix corresponds to a receiver location with the azimuth Φ^{ra} varying from 0° to 360° at a step of 0.72°. We observe that those images, viewed by a fixed

transmitter and a rotating receiver whose azimuth changes within a small variation range, are quite similar. In other words, the coefficients $\{a_{p,q}^{rc}\}$ would not change dramatically for a few successive receiver azimuth steps when other parameters remain the same. Furthermore, from (3.26) to (3.29), it is obvious that, with the selected polarizations, elevations and azimuths of the transmitter and receiver, the values of $\{a_{p,q}^{rc}\}$ are fixed and the value of channel matrix $\mathbf{H}$ changes as the values of d_0^t and d_0^r, the distances between the center of the target and the first antenna of the transmitting and receiving array, vary. The conditions on choosing d_0^t and d_0^r are quite loose, as long as they are large enough that the system is operated in the far field, but not so large that the target would be viewed as a point target.

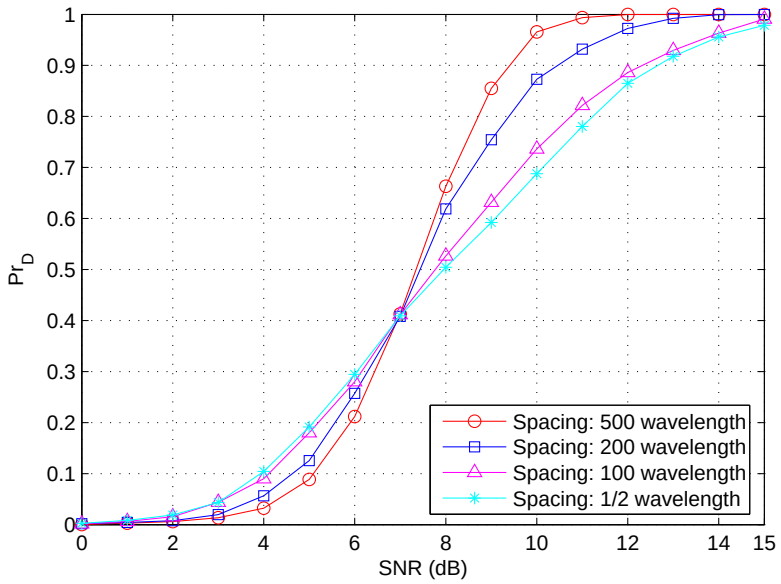

Figure 3.7: *Probability of detection as a function of the SNR for angular range I, 2 Tx and 4 Rx antennas, Tx/Rx interelement spacings varied simultaneously.*

The detection performance for various MIMO radar configurations is shown in Figure 3.7, and these systems are almost the same, except that the antenna spacings Δ_t and Δ_r are 0.5, 100, 200, and 500 wavelengths, respectively. For each configuration, we generate $3,000$ realizations of $\mathbf{H}$ by assigning 10 successive values to Φ^{ra} from $32.4°$ to $38.88°$ with a step of $0.72°$ (denoted range I), and allocating 300 arbitrary values to d_0^t and d_0^r respectively for each angular value. The values of d_0^t and d_0^r are selected to be between $3 \sim 5$ km. Observing the figure, we find that at low SNR, a system with densely spaced antennas outperforms the ones whose interelement spacing is large, while at high SNR the latter performs better. Furthermore, the system with large antenna spacing is always preferred when the detection performance is

acceptable, *e.g.*, $\mathrm{Pr_D} > 0.5$.

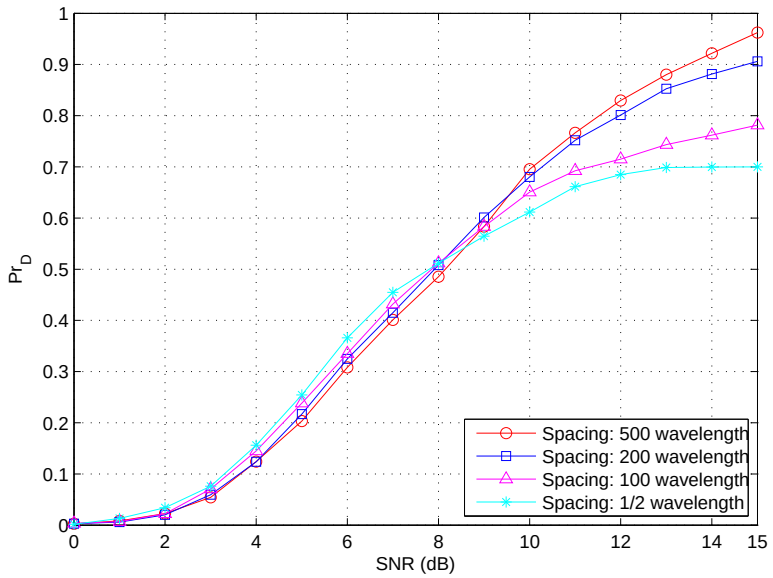

Figure 3.8: *Probability of detection as a function of the SNR for angular range II, 2 Tx and 4 Rx antennas, Tx/Rx interelement spacings varied simultaneously.*

Figure 3.8 depicts the detection performance of a MIMO radar system with different configurations. The difference between this figure and Figure 3.7 is the new angular range (range II) of the look angle, *i.e.*, 10 successive values are assigned to Φ^{ra} here from 176.4° to 182.88° with a step of 0.72°. Similar to Figure 3.7, we find from Figure 3.8 that the system with sparsely spaced arrays performs better at high SNR, and this configuration should always be chosen when $\mathrm{Pr_D} > 0.6$. This result agrees well with the conclusions drawn before from the numerical results of the system involving the theoretical target shown in Figure 3.6, where the realizations of the channel matrix are obtained based on theoretical and mathematical target models. However, it is obvious that the radar system has different detection performance from various observation angles, and the performance improvement brought in by the MIMO configuration is also different. Therefore, we next consider Figure 3.9, which displays the detection performance when the target is viewed from various receiver look angles at a fixed SNR value.

Before we proceed to discuss Figure 3.9, the second approach to generate multiple realizations of the channel matrix is introduced. It is clear that the receiver azimuth Φ^{ra} can only be one of the 500 values which are integer multiples of 0.72° when the data record is used directly. As mentioned before, $\{a^{rc}_{p,q}\}$ are similar for a few successive receiver azimuths when other param-

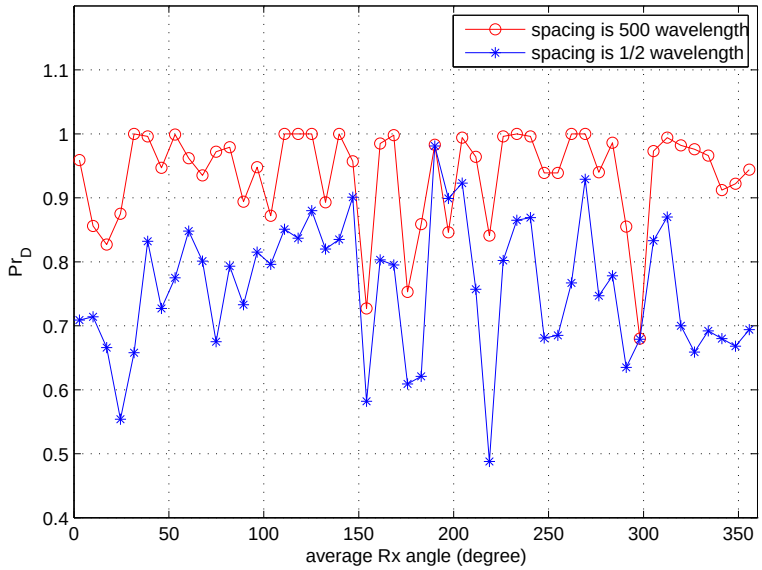

Figure 3.9: *Probability of detection as a function of the look angle at SNR=15dB for systems with 2 Tx and 4 Rx antennas, Tx/Rx interelement spacings varied simultaneously*

eters remain unchanged. Hence, we can generate several realizations of $\mathbf{H}$ where Φ^{ra} could be any value by using linear interpolation. In other words, for an arbitrary Φ_0^{ra} that is not an integer multiple of $0.72°$, we first find two values Φ_{L}^{ra} and Φ_{U}^{ra}, which is the lower and upper bound of Φ_0^{ra}, respectively. Here $\Phi_{\mathrm{L}}^{ra} = \left\lfloor \frac{\Phi_0^{ra}}{0.72°} \right\rfloor \times 0.72°$ and $\Phi_{\mathrm{U}}^{ra} = \Phi_{\mathrm{L}}^{ra} + 0.72°$, where $\lfloor k \rfloor$ represents the largest integer smaller than k. The reflectivity coefficients corresponding to Φ_{L}^{ra} and Φ_{U}^{ra} are available, denoted by $\{a_{p,q}^{rc,\mathrm{L}}\}$ and $\{a_{p,q}^{rc,\mathrm{U}}\}$, respectively. We calculate the reflectivity of each scatterer $a_{p,q}^{rc,0}$ when the receiver azimuth is Φ_0^{ra} by using interpolation between the corresponding two values of $a_{p,q}^{rc,\mathrm{L}}$ and $a_{p,q}^{rc,\mathrm{U}}$. Notice here that the real and imaginary parts of $\{a_{p,q}^{rc,0}\}$ are interpolated separately.

In the simulation yielding Figure 3.9, we divide $360°$ into 50 equal-sized angular sections and obtain the corresponding $\mathrm{Pr_D}$ values. Each $\mathrm{Pr_D}$ value comes from 3,000 realizations of $\mathbf{H}$ utilizing the interpolation approach mentioned before. These realizations are computed with different d_0^t and d_0^r, and various receiver azimuth chosen arbitrarily from the corresponding angle section. From Figure 3.9, it is obvious that, except for a few observation angles, a MIMO radar with large antenna spacing always provides better detection performance, and for most angles, the performance improvement resulting from the MIMO configuration is significant. For those few observation angles where the MIMO configuration is worse, the performance

difference is small, and we believe this is because the target scattering is not rich enough when it is viewed from those specific angles. In addition to the better average performance with the angle, we find from Figure 3.9 that the MIMO configuration also provides performance with less variability, *i.e.*, the performance is less dependent on the look angle, which makes it more attractive.

3.6 Conclusions

In this chapter we introduced the MIMO radar system assuming that the target is modelled as the sum of a finite number of independent small scatterers. Both theoretical and realistic targets were considered. For the theoretical target, a closed form formula to evaluate the theoretical probability of detection for a MIMO radar having an arbitrary array-target configuration was derived and it was validated by Monte Carlo simulations. This theoretical result makes it possible to predict the detection performance of the actual MIMO radar without time consuming simulations. For the realistic target, numerical results showing the target detection performance were presented, which was measured based on multiple realizations of the channel matrix generated utilizing the available FEKO data. Regardless of the target type, comparisons of the detection performance of a MIMO radar with different interelement spacings demonstrated that for a distributed target, the larger the antenna spacings, the lower the channel matrix correlation, and thus the more spatial diversity gain can be achieved. In addition, at low SNR, a system with densely spaced antennas outperforms the ones whose interelement spacing is large, while at high SNR the latter performs better. The system with large antenna spacing is always preferred when the detection performance is acceptable, *e.g.*, the probability of detection is higher than 0.6. All the results were consistent with the conclusions drawn in previous work which investigated a MIMO radar with special array-target configurations only.

Chapter 4
Detection and Direction Finding Performance of Hybrid Bistatic Radar

As mentioned in Chapter 2, previous researchers have demonstrated that the conventional phased-array radar provides coherent processing gain while the MIMO radar exploits spatial diversity gain to improve the target detection and direction finding performance. In this chapter, we will introduce a hybrid bistatic radar which combines these two configurations to take advantage of both types of gains. We will investigate the best architecture for such system, taking into account both target detection and direction finding performance. This radar system is a general model, which can be used to describe many practical array configurations, including the MIMO and phased-array radar as special and extreme cases. A closed form expression is derived to calculate the theoretical probability of detection for different configurations of the hybrid bistatic system, and the Cramer-Rao bound (CRB) and the mean-square error (MSE) of the maximum likelihood (ML) estimation for both angle of departure (AoD) and angle of arrival (AoA) are evaluated to assess the direction finding performance.

4.1 Introduction

The two major problems in radar theory are the target detection and parameter estimation problems. We emphasize here that rather than designing novel algorithms to solve these two problems, we mainly focus on the performance evaluation for a radar system in this thesis. Such an analysis makes it possible to find the best architecture for a specific scenario, and thus, the performance of a radar system can be enhanced by adopting an appropriate configuration.

In practice, the performance of a radar system is limited by target scintillations or "fading" [11]. As discussed in Chapter 2, for target detection, the conventional phased-array radar addresses this scintillation problem by cohering a narrow beam toward the target direction, which can realize coherent processing gain to maximize the received energy reflected by the target. For

direction finding, multiple independent snapshots are collected to average out scintillation effects in order to improve the estimation accuracy. The MIMO radar proposed by Fishler *et al.* in [8] can overcome the scintillation problem by exploiting spatial diversity gain. It is demonstrated in [8] that, for target detection, the MIMO radar system outperforms the phased-array radar at high SNR while the latter performs better when the SNR is low. It is also shown in [3] and [9] that the MIMO radar leads to a significant improvement in AoA estimation accuracy because of the diversity offered by widely-separated antennas at the transmitter. In this case, unlike the system used to detect targets, the receiver has to employ an array of closely-spaced elements in order to avoid ambiguous angle estimates.

In this chapter, we investigate the best architecture for a radar system which is used for both target detection and direction finding, particularly when the total number of transmitting and receiving antennas is fixed. A hybrid bistatic radar combines the phased-array and MIMO radar configurations, providing a balance between coherent processing gain and spatial diversity gain. In addition, the hybrid radar is a general system model, which can be used to describe various practical radar configurations, including the MIMO and phased-array configurations as special and extreme cases. The target is assumed to be spatially distributed, and both the finite scatterers model and the statistical model described in the last chapter are considered for a hybrid radar. Although the architecture of the multistatic coherent sparse aperture system proposed in [128] is similar to the hybrid bistatic radar, they utilized the point-like target assumption and focus on processing the received data at a central processor coherently rather than exploring the spatial diversity of the target. The system configuration discussed in [129] is the same as that in our work, but the major aim of [129] is to propose spatial spectral estimators to detect target and estimate parameters. In this chapter a parametric approach is applied and our emphasis is to explore the performance of the system accounting for both the diversity gain and the coherent processing gain in order to find the best configuration. In [129], the target direction is only denoted by a "target location parameter" whose manifold is not formally defined, and linearly independent waveforms are assumed to be transmitted from all the antennas. In our work, however, we define the target direction by two parameters, AoD and AoA, and assume that each array transmits one of a set of orthogonal waveforms and the antennas of each array work as a beamformer cohering a beam toward the AoD. In this way, as mentioned in [130], extra coherent processing gain can be achieved compared with the fully independent waveforms case at the price of estimating AoD first. We want to investigate the effect different configurations have on system performance and so we wish to measure the full gains that the hybrid radar

system can realize.

We first consider the target detection performance and a closed form formula is derived utilizing the statistical model, which can be used to predict the theoretical probability of detection for any hybrid radar configuration. It should be noted that [8], by contrast, only presents the detection performance for four special configurations. We also show that it is possible to model a realistic radar system using the finite scatterers model, which can perform just like the ideal hybrid radar under certain conditions. Then we introduce the initialization process during which the AoD is estimated, and assess the estimation performance by measuring the average CRB. This is because the transmitter needs to know the AoD at each phased-array in order to steer a beam toward the correct target direction to realize coherent processing gain. In the phased-array radar case considered in [8], perfect AoD information is assumed to be available but the method to obtain that is not described. Then the average and outage CRBs proposed in [9] for AoA estimation are extended to apply to the general case of a hybrid radar system assuming that the true AoD value is available at the transmitter. We focus our attention on the scenario that orthogonal waveforms and appropriate matched filters are employed, while in [9] the transmitted signals are modeled by a Gaussian random process. The extension of our results to the Gaussian waveform case in [9] is also briefly discussed. We also consider the scenario that the transmitter only knows the estimated AoD obtained during the "initialization" stage, and derive equations to evaluate the effect the estimation error in AoD has on finding AoA. The theoretical expressions presented in this chapter provide both the detection and estimation performance of a hybrid radar system. These equations can be used to select the best architecture for a given specific scenario, considering factors such as the number of antennas, the SNR values, and the required precision of the application.

4.2 System Model

4.2.1 Channel Model

As illustrated in Figure 4.1, the hybrid bistatic radar considered here has M_t antenna arrays at the transmitter and M_r arrays at the receiver, and the separation between antenna arrays at the transmitter and receiver are $\Delta_{ta}\lambda_c$ and $\Delta_{ra}\lambda_c$, respectively. Each array is a uniform linear array (ULA) of antennas with N_t elements at the transmitter and N_r elements at the receiver, and the interelement spacings are $\Delta_t\lambda_c$ and $\Delta_r\lambda_c$, respectively. Here λ_c is the carrier wavelength and

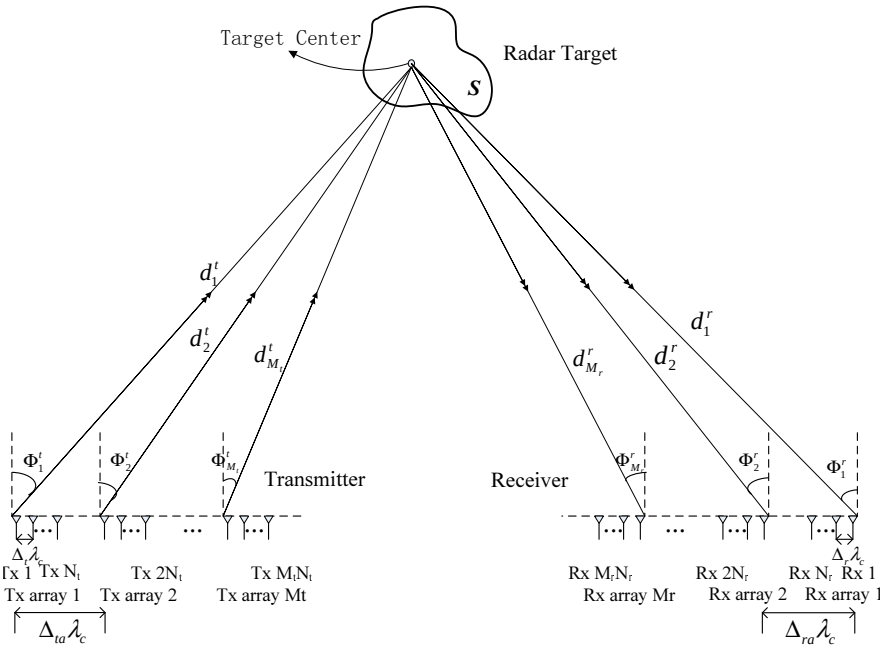

Figure 4.1: *Configuration of the hybrid bistatic radar system*

Δ_{ta}, Δ_{ra}, Δ_t, and Δ_r are normalized spacings in wavelengths. In order to realize coherent processing gain, it is required that the interelement spacings are small such that each antenna array has the same configuration as that of a conventional phased-array radar with N_t or N_r closely spaced sensors. Each phased-array is able to use a beamformer to steer toward any direction. To achieve spatial diversity gain, we assume that the separation between arrays at the transmitter and receiver are large enough that the whole radar system can be considered as an $M_r \times M_t$ MIMO radar. In other words, in the hybrid radar system we utilize an antenna array at the location where there is only one antenna in the conventional MIMO radar [8], so different antenna arrays observe different aspects of the target, while all the antennas in one array view the same aspect. All the signals are assumed to be narrowband. The channel matrix can be expressed by an $M_r N_r \times M_t N_t$ block matrix as below:

$$\mathbf{H} = \begin{bmatrix} \mathbf{H}_{11} & \mathbf{H}_{12} & \cdots & \mathbf{H}_{1M_t} \\ \mathbf{H}_{21} & \mathbf{H}_{22} & & \vdots \\ \vdots & & \ddots & \vdots \\ \mathbf{H}_{M_r 1} & \cdots & \cdots & \mathbf{H}_{M_r M_t} \end{bmatrix} \tag{4.1}$$

where the (u,p)-th block $\mathbf{H}_{up}$ is an $N_r \times N_t$ matrix which is given by

$$\begin{aligned}\mathbf{H}_{up} &= \alpha_{up}\mathbf{\Psi}_r(\Phi_u^r)\mathbf{\Psi}_t^T(\Phi_p^t) \\ \mathbf{\Psi}_\varepsilon(\Phi_\varsigma^\varepsilon) &= \begin{bmatrix} 1 \\ \exp\{j2\pi\Delta_\varepsilon \sin(\Phi_\varsigma^\varepsilon)\} \\ \vdots \\ \exp\{j2\pi(N_\varepsilon - 1)\Delta_\varepsilon \sin(\Phi_\varsigma^\varepsilon)\} \end{bmatrix}\end{aligned} \tag{4.2}$$

where α_{up} is the fading coefficient of the target between the p-th transmit array and the u-th receive array, ε and ς are either t and p or r and u, respectively, $p = 1, 2, ..., M_t$, and $u = 1, 2, ..., M_r$. Here Φ_p^t is the AoD of the path from the first element of the p-th transmit array to the center of the target area, and Φ_u^r is the AoA of the path from the target center to the first element of the u-th receive array. Here we adopt the statistical MIMO model proposed in [8], and hence a fading coefficient vector $\boldsymbol{\alpha}$ which is defined such that $[\boldsymbol{\alpha}]_{(u-1)M_t+p} \triangleq \alpha_{up}$ and $\boldsymbol{\alpha} \sim \mathcal{CN}(\mathbf{0}_{M_rM_t}, \mathbf{I}_{M_rM_t})$. Note here that the vector $\boldsymbol{\alpha}$ is the key MIMO definition, suggesting that each array constitutes one element of a MIMO system. On the other hand, (4.2) follows the phased-array definition, implying that each array itself works as a conventional phased-array radar.

Notice that the statistical MIMO model can only be utilized for a system combining the ideal phased-array and MIMO configurations, which do not exist in the real world. Therefore, a hybrid radar based on this model is actually an ideal system. In contrast, as mentioned in the last chapter, the finite scatterers model can be used to calculate the channel matrix of a radar system having an arbitrary array-target configuration described by specific parameters of locations and sizes of targets, transmitter and receiver. However, as discussed in Chapter 2, a finite scatterers model coincides with the statistical model of the ideal MIMO system if its parameters obey the condition that the so-called distance-dimension ratio, which is the ratio of the distances between the target and both the transmitter and receiver to the dimension of the target, is smaller than the normalized antenna spacing in wavelengths. In contrast, if the distance-dimension ratio is far larger than the normalized interelement spacing, then the corresponding finite scatterers model can be approximated as the statistical model of the ideal phased-array configuration. For mathematical tractability, we employ the statistical model to derive theoretical performance. As shown in Section 4.5, we can simulate a realistic hybrid radar using the finite scatterers model

with appropriate parameters, which performs in the same way as the ideal hybrid radar model above.

Furthermore, it is assumed that we operate in the "far field", but because of the configuration of the hybrid radar system, there are two ways to define the "far field" assumption depending upon the dimensions of the array separations:

(A1) The separations Δ_{ta} and Δ_{ra}, as well as the dimension of each transmitting and receiving antenna array, are much smaller than the distances between the target and both the transmitter and the receiver, that is, the whole system works in the far field. Therefore, the AoDs for all the M_tN_t transmit antenna elements are assumed to be the same, and similarly, the AoAs for all the M_rN_r receive antenna elements are assumed to have the same value.

(A2) The sizes of Δ_{ta} and Δ_{ra} cannot be neglected compared with the distances between the target and both the transmitter and the receiver, but the dimension of each antenna array is much smaller than those distances, *i.e.*, each antenna array individually works in the far field. In other words, there are M_t different values of AoDs corresponding to the M_t sub-arrays at the transmitter, but the N_t antenna elements within each sub-array have the same AoD. Similarly, there are M_r various AoAs for the M_r sub-arrays at the receiver, while the N_r antenna elements of each sub-array share the same AoA.

As mentioned before, the separations Δ_{ta} and Δ_{ra} have to be large enough such that different arrays observe different aspects of the target for both (A1) and (A2), that is the MIMO condition defined in equation (16) of [8] must hold. For the system shown in Figure 4.1, such a condition can be expressed as below:

$$\Delta_{ta} > \frac{d_1^t}{\Delta x}, \quad \Delta_{ra} > \frac{d_1^r}{\Delta x} \tag{4.3}$$

where d_1^t, d_1^r, and Δx denote the distance between the first element of the first transmit array and the target centre, the distance between the target centre and the first element of the first receive array, and the dimension of the target in the x-direction, respectively.

The assumption (A1) implies that the differences between the AoD Φ_p^t for different transmit arrays are so small that they can be neglected, *i.e.*, $\Phi_1^t \doteq \Phi_2^t \doteq \cdots \Phi_{M_t}^t$. Similarly, the AoA Φ_u^r

is also equal for all the M_r receiving arrays. From Figure 4.1, it is reasonable to say that such an approximation is proper if

$$\begin{aligned} \sin\Phi_1^t - \sin\Phi_{M_t}^t &\leq \epsilon \\ \sin\Phi_1^r - \sin\Phi_{M_r}^r &\leq \epsilon \end{aligned} \tag{4.4}$$

where ϵ is a small threshold chosen for a required precision, such as $\epsilon = 0.01, 0.001$. From (4.3) and (4.4), it is not difficult to see that if the following conditions hold jointly:

$$\begin{aligned} \frac{d_1^t}{\Delta x} < \Delta_{ta} &\leq \frac{x_0 - x_1^t - \frac{(y_0 - y_1^t)\left(\sin\Phi_1^t - \epsilon\right)}{\sqrt{1-\left(\sin\Phi_1^t - \epsilon\right)^2}}}{(M_t - 1)\lambda_c} \\ \frac{d_1^r}{\Delta x} < \Delta_{ra} &\leq \frac{x_1^r - x_0 - \frac{(y_0 - y_1^r)\left(\sin\Phi_1^r - \epsilon\right)}{\sqrt{1-\left(\sin\Phi_1^r - \epsilon\right)^2}}}{(M_r - 1)\lambda_c} \\ \sin\Phi_1^t = \tfrac{x_0 - x_1^t}{d_1^t}, &\quad \sin\Phi_1^r = \tfrac{x_1^r - x_0}{d_1^r} \end{aligned} \tag{4.5}$$

then the assumption (A1) is true. Here (x_0, y_0), (x_1^t, y_1^t), and (x_1^r, y_1^r) denote the coordinates of the target centre, the first antenna of the first transmit array, and the first antenna of the first receive array, respectively.

The assumption (A2) means that the AoDs and AoAs for various transmitting and receiving arrays are different, and we say (A2) is true when (4.3) holds while (4.4) is not met. It is possible that a few transmit or receive arrays have almost the same AoD or AoA while others are different, *i.e.*, the system is a hybrid of (A1) and (A2)[1]. We emphasize here that the system model presented in this section are suitable for both assumptions, and the differences between (A1) and (A2) will be discussed in later sections.

4.2.2 Signal Model

As discussed in the last section, we view the whole radar system as an $M_r \times M_t$ MIMO radar system. Therefore, we assume that each of the M_t transmit arrays transmits a different waveform, which are collectively denoted by an $M_t \times 1$ vector $\mathbf{b}(t) = [b_1(t), b_2(t), \cdots, b_{M_t}(t)]^T$.

[1]Such a scenario is not difficult to investigate using the formulae provided in the following sections.

In addition, each of the M_t transmit arrays can be regarded as the transmitter of a conventional phased-array radar with N_t antennas. That is, the p-th transmitting antenna array utilizes its corresponding beamformer to steer toward the estimated target direction $\tilde{\Phi}_p^t$ in order to obtain coherent processing gain for its waveform $b_p(t)$. The maximum processing gain that could be achieved by each transmit array is N_t, which can be realized when $\tilde{\Phi}_p^t$ equals the true target direction Φ_p^t. The transmitting beamformer of the p-th transmit array is denoted by an $N_t \times 1$ vector $\mathbf{a}_p^t = \mathbf{\Psi}_t^*(\tilde{\Phi}_p^t)$ and here $p = 1, 2, ..., M_t$. Therefore, the signals transmitted from the M_tN_t transmit antennas can be described by an $M_tN_t \times 1$ vector $\mathbf{s}(t)$ as below:

$$\mathbf{s}(t) = \sqrt{\frac{E_s}{M_tN_t}} \left[\begin{array}{cccc} (b_1(t)\mathbf{a}_1^t)^T & (b_2(t)\mathbf{a}_2^t)^T & \cdots & (b_{M_t}(t)\mathbf{a}_{M_t}^t)^T \end{array} \right]^T \tag{4.6}$$

where E_s is the total transmitted power from all the transmit antennas. The normalizing coefficient is used to make sure that the total transmitted power and the average received power at each sensor are not affected by the number of transmit antennas. We further assume that the transmit waveforms are mutually orthogonal over L samples, *i.e.*, $\int b_j(t-\tau)b_i^*(t)dt = L\delta_{ij}(\tau)$, where $L \geq M_t$. Note here that the transmitted signal model shown above does not apply to the "initialization" stage described in Section 4.4.1, during which the AoD is estimated.

Denote the received signals and the additive white Gaussian noise at all the receiver antennas by an $M_rN_r \times 1$ vector $\mathbf{r}(t) = [r_1(t), r_2(t), \cdots, r_{M_rN_r}(t)]^T$ and an $M_rN_r \times 1$ vector $\mathbf{n}(t) = [n_1(t), n_2(t), \cdots, n_{M_rN_r}(t)]^T$, respectively. Together with the channel matrix $\mathbf{H}$ given in (4.1), the received signal can be expressed as

$$\mathbf{r}(t) = \mathbf{H} \cdot \mathbf{s}(t-\tau) + \mathbf{n}(t) \tag{4.7}$$

where $\mathbf{n}(t)$ is assumed to be a zero-mean, complex Gaussian random vector process with correlation matrix $\sigma_n^2\mathbf{I}_{M_rN_r}$. Note here that τ is the time delay from the transmitter to the receiver via the target, and differences in time of arrival at the receive antennas are ignored for simplicity.

4.3 Target Detection Performance

In this section, we examine the target detection performance of the hybrid bistatic radar system, and a closed form expression to evaluate the theoretical probability of detection is derived.

In order to exploit coherent processing gain at both the transmitter and receiver to improve the target detection performance, we assume that the u-th receiving antenna array, similar to that of the transmitter, uses its corresponding beamformer to steer toward the estimated target direction $\tilde{\Phi}_u^r$. The maximum processing gain N_r is again realized when $\tilde{\Phi}_u^r$ is the same as the true target direction Φ_u^r. The receiving beamformer of the u-th receive array is denoted by an $N_r \times 1$ vector $\mathbf{a}_u^r = \mathbf{\Psi}_r^*(\tilde{\Phi}_u^r)$ and here $u = 1, 2, ..., M_r$. Therefore, from (4.1), (4.6), and (4.7), the output of the u-th beamformer is given by

$$\begin{aligned} r_u^b(t) &= (\mathbf{a}_u^r)^T \begin{bmatrix} r_{(u-1)N_r+1}(t) \\ r_{(u-1)N_r+2}(t) \\ \vdots \\ r_{uN_r}(t) \end{bmatrix} \\ &= \sqrt{\tfrac{E_s}{M_t N_t}} (\mathbf{a}_u^r)^T \sum_{p=1}^{M_t} \mathbf{H}_{up} \mathbf{a}_p^t b_p(t) + (\mathbf{a}_u^r)^T \mathbf{n}_u(t) \end{aligned} \tag{4.8}$$

where the $N_r \times 1$ vector $\mathbf{n}_u(t)$ denotes the additive white Gaussian noise at the elements of the u-th receiving array. Denote the output of a bank of matched filters by a $M_r M_t \times 1$ vector $\mathbf{x}$, that is, $[\mathbf{x}]_{(u-1)M_t+p} = \int r_u^b(t) b_p^*(t) dt$, where $u = 1, 2, ..., M_r$ and $p = 1, 2, ..., M_t$. Following [8], the radar detector can be written as

$$T = \|\mathbf{x}\|^2 \underset{<\mathcal{H}_0}{>^{\mathcal{H}_1}} \eta \tag{4.9}$$

where η is a threshold determined by the desired probability of false alarm $\mathrm{Pr_{FA}}$. Recalling the assumption that all the transmit waveforms are mutually orthogonal, we can obtain

$$[\mathbf{x}]_{(u-1)M_t+p} = \sqrt{\frac{E_s L^2}{M_t N_t}}(\mathbf{a}_u^r)^T \mathbf{H}_{up} \mathbf{a}_p^t + \int (\mathbf{a}_u^r)^T \mathbf{n}_u(t) b_p(t) dt \tag{4.10}$$

Assuming that all the beamformers steer toward the correct target direction, that is, $\tilde{\Phi}_p^t = \Phi_p^t$ and $\tilde{\Phi}_u^r = \Phi_u^r$, a full coherent processing gain of $N_r N_t$ can be realized. Substituting (4.2) into (4.10), it is not difficult to express the $M_r M_t \times 1$ vector $\mathbf{x}$ under both the null hypothesis $\mathcal{H}_0$ and alternate hypothesis $\mathcal{H}_1$ as below:

$$\mathbf{x} = \begin{cases} \mathbf{n} & \mathcal{H}_0 \\ \sqrt{\frac{E_s L^2}{M_t N_t}} N_r N_t \boldsymbol{\alpha} + \mathbf{n} & \mathcal{H}_1 \end{cases} \tag{4.11}$$

where the noise vector $\mathbf{n} \sim \mathcal{CN}(\mathbf{0}_{M_r M_t}, L N_r \sigma_n^2 \mathbf{I}_{M_r M_t})$ and the fading coefficient vector $\boldsymbol{\alpha} \sim \mathcal{CN}(\mathbf{0}_{M_r M_t}, \mathbf{I}_{M_r M_t})$. Therefore, the distributions of the test statistic T under both hypotheses are given by

$$T = \|\mathbf{x}\|^2 \sim \begin{cases} \frac{L N_r \sigma_n^2}{2} \chi^2_{2M_r M_t} & \mathcal{H}_0 \\ \left(\frac{E_s L^2 N_r^2 N_t^2}{2 M_t N_t} + \frac{L N_r \sigma_n^2}{2} \right) \chi^2_{2M_r M_t} & \mathcal{H}_1 \end{cases} \tag{4.12}$$

where χ_k^2 denotes a chi-square random variable with k degrees of freedom. As mentioned before, for a given noise level, the threshold η can be determined by $\mathrm{Pr_{FA}}$, while the probability of detection $\mathrm{Pr_D}$ is computed from the value of η and the distribution of the test statistic T under $\mathcal{H}_1$. Hereby, we can get

$$\begin{aligned} \mathrm{Pr_D} &= 1 - \mathcal{F}_{\chi^2_{2M_r M_t}} \left(\frac{2\eta}{\frac{E_s L^2 N_r^2 N_t^2}{M_t N_t} + L N_r \sigma_n^2} \right) \\ \eta &= \frac{L N_r \sigma_n^2}{2} \mathcal{F}^{-1}_{\chi^2_{2M_r M_t}} (1 - \mathrm{Pr_{FA}}) \end{aligned} \tag{4.13}$$

where $\mathcal{F}^{-1}_{\chi_k^2}$ and $\mathcal{F}_{\chi_k^2}$ denotes the inverse cumulative distribution function (CDF) and the CDF

of a chi-square random variable with k degrees of freedom, respectively. Here we assume that all the beamformers steer toward the true target direction, and the detection performance when only the estimated target direction is available will be provided at the end of Section 4.4.3.

The three systems discussed in [8] actually are special cases of the hybrid bistatic radar system, *i.e.*, the hybrid radar is the ideal MIMO radar when $N_t = N_r = 1$, the ideal phased-array radar when $M_t = M_r = 1$, and the ideal MISO radar when $N_t = M_r = 1$. The corresponding equations to calculate η and $\mathrm{Pr_D}$ for all these extreme scenarios derived from (4.13) match the results in equations (28), (29), (34), (35), (38) and (39), respectively, in [8]. Note the fact that previous theoretical results are derived utilizing the statistical model, which is appropriate only for ideal scenarios. In order to analyze the detection performance of a system with a more realistic configuration, we can extend the derivation provided in the last chapter for a MIMO radar to the hybrid radar system case employing the finite scatterers model.

4.4 Direction Finding Performance

In what follows, we examine the performance of the hybrid bistatic radar as a direction finding system to estimate the AoD and AoA based on the received signal reflected from the target. We emphasize here that the work presented in this thesis focuses on a single target scenario, and an extension to the multiple targets case is possible by adopting elaborately designed transmit waveforms and applying appropriate estimation techniques. This could be a promising area for future research since, to the author's knowledge, the effect of spatial diversity realized by a MIMO radar on the multiple targets scenario is not clear. From the viewpoint of estimation, the MSE of the estimator is a common measurement to compare the performance of different systems. However, the MSE depends on the specific approach adopted by the estimator. Thus, we focus our attention on the CRB of the hybrid radar system with various configurations, which provides a benchmark against which the performance of any unbiased estimator can be compared [131]. It is noted that we only consider a simple scenario where the target is viewed as a point source by each antenna array, which then estimates the target direction. However, our analysis could be extended to a more complicated problem of estimating the nominal direction of a distributed target [132, 133].

It is known that an array whose interelement spacings are larger than half-wavelength will suffer from the spatial aliasing effect [122, 134], which makes it impossible to estimate the

target direction unambiguously. Hence, here we assume that the interelement spacings of both the transmit and receive arrays are half-wavelength, that is, $\Delta_t = \Delta_r = 0.5$. In addition, in order to estimate the AoD and AoA, N_t and N_r cannot be equal to one since a single omni-directional antenna is unable to provide any angle information.

4.4.1 Initialization

In order to realize coherent processing gain, the transmitter needs to know the AoD in order to steer toward the target direction. Hence, an "initialization" stage is required with no *a priori* knowledge about the channel available, which is described as follows. If we only need to estimate the AoA and $N_t = 1$, *i.e.*, the transmitter is an array with widely-spaced antennas, then such initialization is unnecessary and we should estimate the AoA directly.

The transmitted signal model described in (4.6) cannot be employed in the procedure of estimating AoD since the direction knowledge of the transmitting beamformers is not known. Instead, during the "initialization" stage, orthogonal waveforms are transmitted from all the antennas to realize the AoD estimation [72, 87]. As a specific example of orthogonal waveforms, the time-division multiplexing (TDM) process is assumed to be utilized here, which is described as follows: At time t_1, the first element of the first transmitting antenna array transmits the signal s and the received signals at all the M_rN_r receiving antennas are stored. Then, at time t_2, the second antenna of the first array transmits s and again all the received signals are recorded. This operation is repeated until the last transmitting antenna is excited with the same signal s at time $t_{M_tN_t}$. Here we assumed that $|s|^2 = 1$, and the fading coefficients are assumed to be constant during the initialization process. We consider the far field assumption (A1) first and denote the AoD and AoA by Φ^t and Φ^r, respectively. According to (4.1) and (4.2), the signal received by the v-th element of the u-th receive array due to the excitation of s at the q-th antenna of the p-th transmit array is given by

$$r_{u,v}(t_w) = \psi_r(v) \cdot \alpha_{up} \cdot \psi_t(q) \cdot s + n \tag{4.14}$$

where $\psi_r(v) = \exp\{j\pi(v-1)\sin(\Phi^r)\}$; $\psi_t(q) = \exp\left\{j\pi(q-1)\sin(\Phi^t)\right\}$; $w = (p-1)N_t + q$; $u = 1, 2, ..., M_r$; $v = 1, 2, ..., N_r$; $p = 1, 2, ..., M_t$ and $q = 1, 2, ..., N_t$. After recording all the $M_rN_rM_tN_t$ received signals, we combine them into one $N_t \times 1$ data record with $M_rN_rM_t$

snapshots as shown below, based on which the AoD is estimated.

$$\begin{aligned}\mathbf{r}_{\text{init}}(k) &= \begin{bmatrix} r_{u,v}(t_{(p-1)N_t+1}) \\ r_{u,v}(t_{(p-1)N_t+2}) \\ \vdots \\ r_{u,v}(t_{pN_t}) \end{bmatrix} + \mathbf{n}(k) \\ &= \boldsymbol{\psi}_t(\Phi^t) \cdot \alpha_{up} \cdot \psi_r(v) \cdot s + \mathbf{n}(k)\end{aligned} \tag{4.15}$$

where $\boldsymbol{\psi}_t(\Phi^t) = \begin{bmatrix} \psi_t(1) & \psi_t(2) & \cdots & \psi_t(N_t) \end{bmatrix}^T$; $k = (u-1)N_rM_t + (v-1)M_t + p$; $u = 1, 2, ..., M_r$; $v = 1, 2, ..., N_r$ and $p = 1, 2, ..., M_t$. $\mathbf{n}(k) \sim \mathcal{CN}(\mathbf{0}_{N_t}, \sigma_n^2 \mathbf{I}_{N_t})$ and α_{up} is an entry of the $M_rM_t \times 1$ fading coefficient vector $\boldsymbol{\alpha}$. The estimated AoD $\hat{\Phi}^t$ is obtained by employing the ML estimator, which is given by [51]

$$\hat{\Phi}^t = \arg\max_{\Phi^{t\prime}} \sum_{k=1}^{M_rN_rM_t} \left| \boldsymbol{\psi}_t^H(\Phi^{t\prime}) \mathbf{r}_{\text{init}}(k) \right|^2 \tag{4.16}$$

As mentioned before, in order to compare the performance of any unbiased estimator, one can use the Cramer-Rao lower bound on the variance of any AoD estimator $\hat{\Phi}^t$, which is denoted by $\text{CRB}(\Phi^t \,|\boldsymbol{\alpha})$. The notation indicates that the value is conditioned on the unknown parameters $\boldsymbol{\alpha}$ [9]. Comparing (4.15) with equation (1.1a) in [64], we find that in this case, $\mathbf{r}_{\text{init}}(k)$, $\boldsymbol{\psi}_t(\Phi^t)$, $\alpha_{up}\psi_r(v)s$, $\mathbf{n}(k)$, and $M_rN_rM_t$ in (4.15) corresponds to the noisy data vector $y(t)$, the direction matrix $A(\theta)$, the signal amplitude $x(t)$, the additive noise $e(t)$, and the number of snapshots N in equation (1.1a), respectively. By using Theorem 4.1 provided in [64], the CRB conditioned on the fading coefficients can be expressed as

$$\text{CRB}(\Phi^t \,|\boldsymbol{\alpha}) = \frac{\sigma_n^2}{\|\boldsymbol{\alpha}\|^2} \cdot \frac{6}{N_rN_t\pi^2 \cos^2(\Phi^t)(N_t^2 - 1)} \tag{4.17}$$

Note here that $\|\boldsymbol{\alpha}\|^2 \sim \frac{1}{2}\chi^2_{2M_rM_t}$. Similar to [9], we can calculate the average CRB (ACRB) by averaging the CRB with respect to $\boldsymbol{\alpha}$, which is given by

$$\mathrm{ACRB}(\Phi^t) = \frac{\sigma_n^2}{(M_r M_t - 1)} \cdot \frac{6}{N_r N_t \pi^2 \cos^2(\Phi^t)(N_t^2 - 1)} \tag{4.18}$$

When the far field assumption (A2) is adopted, the AoDs for various transmitting arrays are different and all the AoDs need to be estimated separately. The AoD of the p-th transmitting array is estimated based on the $N_t \times 1$ data record with $M_r N_r$ snapshots, which is obtained from the received signals at all the $M_r N_r$ receiving antennas when each antenna of the p-th transmitting array is excited with the signal s in a TDM fashion. After a very similar derivation, we can obtain the conditional CRB and ACRB for each AoD under (A2). The equations are almost the same as (4.17) and (4.18), except that for the conditional CRB, $\|\boldsymbol{\alpha}\|^2 \sim \frac{1}{2}\chi^2_{2M_r}$, and for the ACRB, $(M_r M_t - 1)$ in (4.18) changes to $(M_r - 1)$.

4.4.2 AoA estimation with true AoD

Now we proceed to investigate the performance of the hybrid radar system for estimating the AoA Φ^r under (A1). Since the estimated AoD is available after the initialization process, we assume that each of the M_t transmitter arrays employs a beamformer to steer toward the target direction to exploit coherent processing gain. In order to examine the effects of the system configuration on the performance of estimating the AoA, we first assume that the transmitter knows the true target direction, *i.e.*, $\hat{\Phi}^t = \Phi^t$. The performance of the system when the error in estimating AoD is taken into account will be provided in the next section. During the observation period, it is assumed that the fading coefficients are constant while the transmitted waveforms are different for each snapshot.

In the hybrid radar system, we cannot estimate Φ^r by utilizing all the received signals directly, but by processing each receive antenna array's signals separately. This is because the separation between receiving antenna arrays are much larger than a half-wavelength. As was the case for target detection, we assume that the waveforms which are mutually orthogonal over L samples have been used as the transmit waveforms $\mathbf{b}(t)$. From (4.2), (4.6), and (4.7), the $N_r \times 1$ signals $\mathbf{r}_u$ received by the u-th receiving array are given by

$$\mathbf{r}_u(t) = \sqrt{\frac{E_s N_t}{M_t}} \boldsymbol{\psi}_r(\Phi^r) \boldsymbol{\alpha}_u^T \mathbf{b}(t - \tau) + \mathbf{n}_u(t) \tag{4.19}$$

where the k-th entry of the $N_r \times 1$ vector $\boldsymbol{\psi}_r(\Phi^r)$ is $\exp\{j\pi(k-1)\sin(\Phi^r)\}$, and $\boldsymbol{\alpha}_u = \begin{bmatrix} \alpha_{u1} & \alpha_{u2} & \cdots & \alpha_{uM_t} \end{bmatrix}^T$. Here $\boldsymbol{\alpha}_u \sim \mathcal{CN}(\mathbf{0}_{M_t}, \mathbf{I}_{M_t})$ and $\mathbf{n}_u(t) \sim \mathcal{CN}\left(\mathbf{0}_{N_r}, \sigma_n^2 \mathbf{I}_{N_r}\right)$. Then, by applying a matched filter of duration L samples for each distinct transmit waveform, *i.e.*, $\mathbf{x}_{up} = \int \mathbf{r}_u(t) b_p^*(t) dt$, and invoking the assumption that $\int b_j(t-\tau) b_i^*(t) dt = L\delta_{ij}(\tau)$, we can obtain a single snapshot which can be written as an $N_r \times 1$ vector

$$\mathbf{x}_{up} = \sqrt{\frac{E_s N_t L^2}{M_t}} \boldsymbol{\psi}_r(\Phi^r) \alpha_{up} + \mathbf{n}_{up} \tag{4.20}$$

where $u = 1, 2, ..., M_r$; $p = 1, 2, ..., M_t$, and $\mathbf{n}_{up} \sim \mathcal{CN}(\mathbf{0}_{N_r}, L\sigma_n^2 \mathbf{I}_{N_r})$. In this case, the SNR increases by a factor of L compared to what we would measure for one sample in isolation. Recall the fact that arrays at both the transmitter and receiver are separated far enough from each other that they view different aspects of the target, then the fading coefficients $\boldsymbol{\alpha}_u$ and $\boldsymbol{\alpha}_v$ for the u-th and v-th receiving arrays, respectively, are independent. Therefore, we can obtain a $M_r M_t \times 1$ vector $\boldsymbol{\alpha}$ by stacking all the M_r $\{\boldsymbol{\alpha}_u\}$ into a single column vector, and $\boldsymbol{\alpha} \sim \mathcal{CN}(\mathbf{0}_{M_r M_t}, \mathbf{I}_{M_r M_t})$. α_{up} in (4.20) is the $\{(u-1)M_t + p\}$-th entry of $\boldsymbol{\alpha}$. Since the elements of $\boldsymbol{\alpha}$ are independent, we can combine all the vectors $\mathbf{x}_{up}$ into one data record with $M_r M_t$ snapshots, based on which the AoA Φ^r is estimated.

Similar to the initialization stage, the ML estimator is applied to estimate the AoA $\hat{\Phi}^r$, which is given by [51]:

$$\hat{\Phi}^r = \arg\max_{\Phi^{r\prime}} \sum_{u=1}^{M_r} \sum_{p=1}^{M_t} \left| \boldsymbol{\psi}_r^H(\Phi^{r\prime}) \mathbf{x}_{up} \right|^2 \tag{4.21}$$

Comparing (4.20) with equation (1.1a) in [64], we note that $\mathbf{x}_{up}$, $\boldsymbol{\psi}_r(\Phi^r)$, $\sqrt{\frac{E_s N_t L^2}{M_t}}\alpha_{up}$, $\mathbf{n}_{up}$, and $M_r M_t$ in (4.20) correspond to the noisy data $y(t)$, the direction matrix $A(\theta)$, the signal amplitude $x(t)$, the additive noise $e(t)$, and the number of snapshots N in equation (1.1a), respectively. The CRB conditioned on $\boldsymbol{\alpha}$ can be calculated by using Theorem 4.1 provided in [64], which is written as

$$\mathrm{CRB}(\Phi^r \,|\boldsymbol{\alpha}) = \frac{6}{L\pi^2 \cos^2(\Phi^r)(N_r^2-1)} \cdot \frac{M_t \sigma_n^2}{E_s N_r N_t \left\|\boldsymbol{\alpha}\right\|^2} \tag{4.22}$$

Note here that $\left\|\boldsymbol{\alpha}\right\|^2 \sim \frac{1}{2}\chi^2_{2M_rM_t}$. The ACRB of Φ^r shown below is calculated by averaging (4.22) with regards to $\boldsymbol{\alpha}$.

$$\mathrm{ACRB}(\Phi^r) = \frac{6}{L\pi^2 \cos^2(\Phi^r)(N_r^2-1)} \cdot \frac{M_t \sigma_n^2}{E_s N_r N_t (M_r M_t - 1)} \tag{4.23}$$

From (4.23), it is obvious that the ACRB is unable to indicate the direction finding performance of the radar system when $M_r = M_t = 1$. Therefore, we proceed to examine the outage CRB proposed in [9], which is denoted by $\mathrm{CRB}_{out=p}(\Phi^r)$. Similar to the outage capacity defined in communications, the outage CRB for a given probability p means that the probability of finding an estimator whose MSE is less than $\mathrm{CRB}_{out=p}(\Phi^r)$ is smaller than $1-p$ [9]. Following [9], $\mathrm{CRB}_{out=p}(\Phi^r)$ can be evaluated from (4.22) by replacing $\left\|\boldsymbol{\alpha}\right\|^2$ with $\frac{1}{2}\mathcal{F}^{-1}_{\chi^2_{2M_rM_t}}(p)$.

As was the case for AoD estimation, AoAs for various receiving arrays are different under (A2), and all the AoAs are need to be estimated separately. In this case, we assume that all the transmitting arrays know the true target direction, and the AoA of the u-th receiving array is estimated based on the vector $\mathbf{x}_{up}$ with M_t snapshots. The equation of the conditional CRB for each AoA is almost the same as (4.22), except that $\left\|\boldsymbol{\alpha}\right\|^2 \sim \frac{1}{2}\chi^2_{2M_t}$. Using (M_t-1) instead of (M_rM_t-1) in the second term of (4.23) gives us the ACRB for each AoA under (A2).

Note here that although orthogonal waveforms are assumed to be adopted, the transmitted signals can also be modeled by a Gaussian random process in this hybrid radar system as that in [9], *i.e.*, $\mathbf{b}(t) \sim \mathcal{CN}\left(\mathbf{0}_{M_t}, \mathbf{I}_{M_t}\right)$. Here we assume that the power of each signal is unchanged compared to the orthogonal waveform case. When assumption (A1) is adopted, from (4.19), we can express the signals received by all the M_rN_r receiving antennas as below

$$\mathbf{r}(t) = \left[\begin{array}{cccc} \mathbf{r}_1^T(t) & \mathbf{r}_2^T(t) & \cdots & \mathbf{r}_{M_r}^T(t) \end{array}\right]^T = \sqrt{\tfrac{E_s N_t}{M_t}}\left[\mathbf{I}_{M_r} \otimes \boldsymbol{\psi}_r(\Phi^r)\right]\boldsymbol{\Omega}\mathbf{b}(t-\tau) + \mathbf{n}(t) \tag{4.24}$$

where the $M_r \times M_t$ matrix $\mathbf{\Omega} = \begin{bmatrix} \boldsymbol{\alpha}_1 & \boldsymbol{\alpha}_2 & \cdots & \boldsymbol{\alpha}_{M_r} \end{bmatrix}^T$ and $\mathbf{n}(t) \sim \mathcal{CN}(\mathbf{0}_{M_r N_r}, \sigma_n^2 \mathbf{I}_{M_r N_r})$. We further assume that $\mathbf{r}(t)$ has L independent snapshots, and based upon which the AoA Φ^r is estimated. Following a derivation similar to that provided in [135], we can obtain the CRB of Φ^r conditioned on $\mathbf{\Omega}$, which is given by

$$\mathrm{CRB}(\Phi^r|\mathbf{\Omega}) = \frac{6}{L\pi^2 \cos^2(\Phi^r)(N_r^2-1)} \left\{ \frac{E_s N_r N_t \|\mathbf{\Omega}\|_F^2}{M_t \sigma_n^2} M_t + \Re\left[\mathrm{trace}\left(\mathbf{I}_{M_t} + \frac{E_s N_r N_t}{M_t \sigma_n^2} \mathbf{\Omega}^H \mathbf{\Omega} \right)^{-1} \right] \right\}^{-1} \quad (4.25)$$

From (4.25), a closed form equation of the CRB conditioned on $\mathbf{\Omega}$ can be derived for two special cases: $M_t = 1$ or $M_r = 1$.

$$\mathrm{CRB}(\Phi^r|\mathbf{\Omega}) = \frac{6}{L\pi^2 \cos^2(\Phi^r)(N_r^2-1)} \cdot \left(\frac{M_t^2 \sigma_n^4}{E_s^2 N_r^2 N_t^2 \|\mathbf{\Omega}\|^4} + \frac{M_t \sigma_n^2}{E_s N_r N_t \|\mathbf{\Omega}\|^2} \right) \quad (4.26)$$

where $\|\mathbf{\Omega}\|^2 \sim \frac{1}{2}\chi^2_{2M_r M_t}$. Note here that the system considered in [9] is actually a special configuration of the hybrid radar when $M_r = N_t = 1$, and the corresponding equation for this scenario derived from (4.26) matches equation (26) provided in [9].

When assumption (A2) is adopted, the AoA of the u-th receiving array Φ_u^r is estimated based on the received signal vector $\mathbf{r}_u(t)$ with L snapshots. The covariance matrix of this signal is given by

$$\mathbf{C}_{\mathbf{r}_u} = \boldsymbol{\psi}_r(\Phi_u^r) \cdot \frac{E_s N_t}{M_t} \|\boldsymbol{\alpha}_u\|^2 \cdot \boldsymbol{\psi}_r^H(\Phi_u^r) + \sigma_n^2 \mathbf{I}_{N_r} \quad (4.27)$$

Comparing it with equation (1) in [135], we note that $\boldsymbol{\psi}_r(\Phi_u^r)$, $\frac{E_s N_t}{M_t} \|\boldsymbol{\alpha}_u\|^2$, and σ_n^2 in this equation corresponds to the direction matrix A, the signal covariance matrix P, and the common noise variance σ in equation (1) in [135], respectively. Hence, the CRB can be calculated by using equation (5) provided in [135]

$$\text{CRB}\left(\Phi^r \,|\boldsymbol{\alpha}\right) = \frac{6}{L\pi^2\cos^2(\Phi^r)(N_r^2-1)} \cdot \left(\frac{M_t^2\sigma_n^4}{E_s^2 N_t^2 N_r^2 \|\boldsymbol{\alpha}\|^4} + \frac{M_t\sigma_n^2}{E_s N_t N_r \|\boldsymbol{\alpha}\|^2}\right) \tag{4.28}$$

where $\|\boldsymbol{\alpha}\|^2 \sim \frac{1}{2}\chi^2_{2M_t}$. Comparing (4.26) with (4.22), and comparing (4.28) with the CRB equation of the scenario when orthogonal waveforms are transmitted under (A2), we find that both (4.26) and (4.28) have an additional term inversely proportional to $\|\boldsymbol{\alpha}\|^4$, which can be viewed as the "penalty" for using Gaussian random waveforms rather than orthogonal ones.

4.4.3 AoA estimation with estimated AoD

Since the CRB of AoD obtained before will not be zero, we know that the process of estimating AoD cannot be error-free, and the case discussed in last section is actually an ideal scenario. Therefore, we further investigate the direction finding performance of the hybrid radar under (A1) when the estimated AoD $\hat{\Phi}^t$ obtained during the "initialization" stage, instead of the true AoD value Φ^t, is available at the transmitter. In other words, each of the M_t transmitting antenna arrays utilizes a beamformer to steer toward the estimated target direction to exploit coherent processing gain. Given the fact that the ML estimator is asymptotically Gaussian distributed and achieves the CRB [131], it is reasonable to assume that the estimated AoD $\hat{\Phi}^t$ is a "truncated" Gaussian distributed, *i.e.*, $\hat{\Phi}^t \sim \mathcal{N}_t(\Phi^t, \sigma^2_\Phi)$, whose probability density function (PDF) is

$$\text{PDF}(\hat{\Phi}^t) = \frac{Q_{TG}}{\sqrt{2\pi\sigma^2_\Phi}} \exp\left\{-\frac{(\hat{\Phi}^t - \Phi^t)^2}{2\sigma^2_\Phi}\right\} \tag{4.29}$$

when $\hat{\Phi}^t \in \left[\Phi^t - \frac{\pi}{2}, \Phi^t + \frac{\pi}{2}\right]$ and equals to 0 elsewhere. The mean is the true value of the AoD, and for a certain realization of the fading coefficient vector $\boldsymbol{\alpha}$, the variance σ^2_Φ equals the conditional CRB of the AoD given by (4.17). Here Q_{TG} is a normalizing constant chosen to make $\text{PDF}(\hat{\Phi}^t)$ a density function depending on the value of Φ^t and σ^2_Φ, which is, however, very close to 1 for the scenarios considered here.

The error between $\hat{\Phi}^t$ and Φ^t reduces the coherent processing gain realized by the transmitting beamformers, which results in a decrease in the AoA estimation performance. We evaluate this

effect by considering the average coherent processing gain that could be achieved since $\hat{\Phi}^t$ is a random variable. After similar calculation as that for (4.19) to (4.22), the conditional CRB of AoA when the estimation error in AoD is included can be written as follows:

$$\begin{aligned} \mathrm{CRB}_{\mathrm{err}}(\Phi^r \,|\boldsymbol{\alpha}) &= \tfrac{6}{L\pi^2\cos^2(\Phi^r)(N_r^2-1)} \cdot \tfrac{M_t N_t \sigma_n^2}{E_s N_r \|\boldsymbol{\alpha}\|^2 P_t} \\ P_t &= \mathrm{E}\left[\left\|\boldsymbol{\psi}_t^T(\Phi^t)\mathbf{a}_t(\hat{\Phi}^t)\right\|^2\right] = \boldsymbol{\psi}_t^T(\Phi^t)\cdot\mathbf{C}_{\mathbf{a}_t}\cdot\boldsymbol{\psi}_t^*(\Phi^t) \end{aligned} \tag{4.30}$$

where $\mathbf{C}_{\mathbf{a}_t} = \mathrm{E}\left[\mathbf{a}_t(\hat{\Phi}^t)\mathbf{a}_t^H(\hat{\Phi}^t)\right]$, $\mathbf{a}_t(\hat{\Phi}^t) = \boldsymbol{\psi}_t^*(\hat{\Phi}^t)$, and the k-th element of the $N_t \times 1$ vector $\boldsymbol{\psi}_t(\Phi^t)$ is $\exp\left\{j\pi(k-1)\sin(\Phi^t)\right\}$. Then, the (m,n)-th entry of the $N_t \times N_t$ matrix $\mathbf{C}_{\mathbf{a}_t}$ is

$$\mathbf{C}_{\mathbf{a}_t}(m,n) = \mathrm{E}\left[\cos\left\{\pi(n-m)\sin(\hat{\Phi}^t)\right\}\right] + j\cdot\mathrm{E}\left[\sin\left\{\pi(n-m)\sin(\hat{\Phi}^t)\right\}\right] \tag{4.31}$$

Recall the assumption that $\hat{\Phi}^t \sim \mathcal{N}_t(\Phi^t, \sigma_\Phi^2)$, and make use of formulae provided in [136–138], the above equation becomes:

$$\begin{aligned} \mathbf{C}_{\mathbf{a}_t}(m,n) = J_0(z) + Q_{TG}\sum_{k=1}^{\infty} J_{2k}(z)\exp\left[-\tfrac{\sigma_\Phi^2(2k)^2}{2}\right]\times \\ \left\{\cos(2k\Phi^t)\mathcal{A}(2k,\sigma_\Phi) - \sin(2k\Phi^t)\mathcal{B}(2k,\sigma_\Phi)\right\} \\ + j\cdot Q_{TG}\sum_{k=0}^{\infty} J_{2k+1}(z)\exp\left[-\tfrac{\sigma_\Phi^2(2k+1)^2}{2}\right]\times \\ \left\{\sin\left[(2k+1)\Phi^t\right]\mathcal{A}(2k+1,\sigma_\Phi) + \cos\left[(2k+1)\Phi^t\right]\mathcal{B}(2k+1,\sigma_\Phi)\right\} \end{aligned} \tag{4.32}$$

where $J_k(z)$ is a Bessel function of the first kind and integer order [136], $z = \pi(n-m)$, and

$$\begin{aligned} \mathcal{A}(a,b) &= \Re\left\{\mathrm{erf}(\tfrac{\pi}{\sqrt{8}b} - j\tfrac{ab}{\sqrt{2}})\right\} - \Re\left\{\mathrm{erf}(-\tfrac{\pi}{\sqrt{8}b} - j\tfrac{ab}{\sqrt{2}})\right\} \\ \mathcal{B}(a,b) &= \Im\left\{\mathrm{erf}(\tfrac{\pi}{\sqrt{8}b} - j\tfrac{ab}{\sqrt{2}})\right\} - \Im\left\{\mathrm{erf}(-\tfrac{\pi}{\sqrt{8}b} - j\tfrac{ab}{\sqrt{2}})\right\} \end{aligned} \tag{4.33}$$

where $\mathrm{erf}(a+jb)$ is the complex-valued error function [136]. Substituting (4.32) and (4.33) into (4.30) gives the CRB of AoA conditioned on $\boldsymbol{\alpha}$ including the effect of the estimation error

in AoD. It is impossible to derive a closed-form equation of the corresponding ACRB. One way to obtain ACRB numerically is to generate a realization of $\boldsymbol{\alpha}$, calculate the conditional CRB of the AoD using (4.17) first, which is the value of σ_{Φ}^2, then evaluate the corresponding conditional CRB of the AoA from (4.30) to (4.33). Repeat this process for multiple realizations and compute the ACRB of the AoA by averaging over the conditional CRBs. However, such a procedure is time consuming, and hence, we employ another approach to calculate the ACRB approximately, and the numerical results provided in the next section validate that the approximate method works quite well. Firstly, calculate the ACRB of the AoD using (4.18). Then, substitute this value as σ_{Φ}^2 to (4.32) and denote the resulting matrix as $\mathbf{C}_{\mathrm{app}}^t$. Similar to (4.23), we evaluate the approximate ACRB of the AoA, taking into account the estimation error in AoD, as below:

$$\mathrm{ACRB}_{\mathrm{erra}}(\Phi^r) = \frac{6}{L\pi^2 \cos^2(\Phi^r)(N_r^2-1)} \cdot \frac{M_t N_t \sigma_n^2}{E_s N_r (M_r M_t - 1) \boldsymbol{\psi}_t^T(\Phi^t) \mathbf{C}_{\mathrm{app}}^t \boldsymbol{\psi}_t^*(\Phi^t)} \tag{4.34}$$

Similarly, we can obtain the approximate probability of detection $\mathrm{Pr_D}$ considering the estimation error in both AoD and AoA by replacing $N_r^2 N_t^2$ in the denominator of (4.13) by $\boldsymbol{\psi}_r^T(\Phi^r)\mathbf{C}_{\mathrm{app}}^r\boldsymbol{\psi}_r^*(\Phi^r) \times \boldsymbol{\psi}_t^T(\Phi^t)\mathbf{C}_{\mathrm{app}}^t\boldsymbol{\psi}_t^*(\Phi^t)$. Here $\mathbf{C}_{\mathrm{app}}^r$ is computed by substituting the value of ACRB of the AoA from (4.23) as σ_{Φ}^2 to (4.32), and replacing Φ^t in (4.32) by Φ^r.

When assumption (A2) is adopted and estimation errors exist in the AoD, we can derive the conditional and average CRBs of the AoA by following the same procedure leading to (4.30) and (4.34), which can be briefly described as below:

i) Compute the value of σ_{Φ}^2, which equals the conditional or average CRB of the AoD under (A2) provided in Section 4.4.1.

ii) Calculate the reduced coherent processing gain P_t by substituting the obtained σ_{Φ}^2 into (4.30) to (4.33).

iii) Derive the conditional or average CRB of the AoA when estimation errors exist in the AoD by multiplying $\frac{N_t^2}{P_t}$ by the corresponding CRBs of the AoA under (A2) when the transmitter knows the true AoD, which are provided in Section 4.4.2.

4.5 Simulation Results

In this section, numerical results yielded by simulations of a hybrid bistatic radar are provided. We examine the target detection performance first for a system with eight transmit antennas and eight receive antennas when the number of snapshots $L = 8$. The carrier frequency of the signal is 10 GHz, and the size of the antenna array is much smaller than the distances between the target and both the transmitter and receiver, which are on the order of $3 \sim 5$ km. The probability of false alarm is set to be a constant value $\mathrm{Pr}_{\mathrm{FA}} = 10^{-6}$ and the SNR is defined as the ratio between the transmitted power E_s and the noise level per receiving antenna σ_n^2. The far field assumption (A1) is employed in the simulations, and we assume that $\Phi^t = 45^\circ$ and $\Phi^r = 45^\circ$.

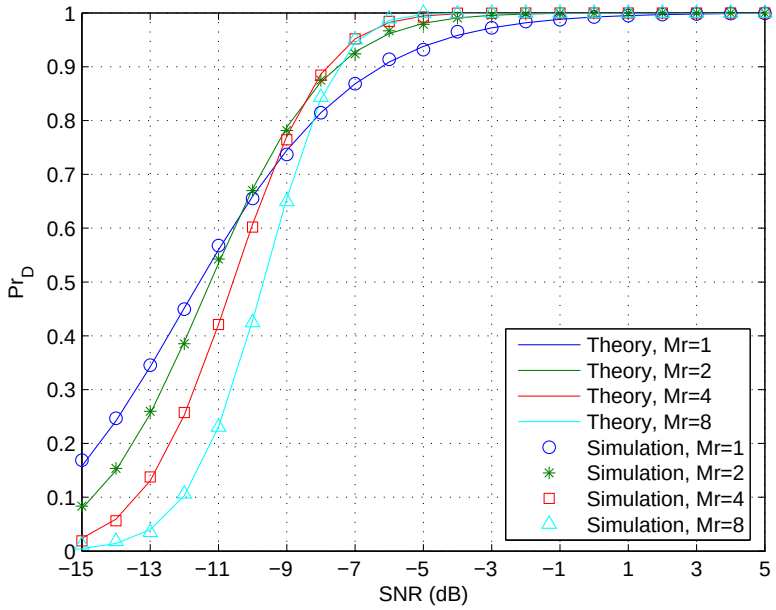

Figure 4.2: *Theoretical and simulated probability of detection as a function of the SNR for systems with 2 transmitting antenna arrays*

First of all, we validate the theoretical results of Pr_{D} obtained from (4.13) for various configurations. Figure 4.2 depicts the theoretical probability of detection as a function of the average received SNR when the number of the transmit arrays is two, *i.e.*, $M_t = 2$, and the number of receive arrays of the four configurations considered is 1, 2, 4, and 8, respectively. Figure 4.2 also shows the Pr_{D} recorded from simulations of the same four scenarios employing the finite scatterers model, and the total number of tests for each case is 10,000. It is assumed that

the target area has circular shape with radius $r_0 = 20$m, within which there are 64 scatterers. The normalized interelement spacing of each antenna array $\Delta_t = \Delta_r = 0.5$ and the array separation $\Delta_{ta} = \Delta_{ra} = 400$. In this case, the distance-dimension ratio mentioned in Section 4.2.1 is smaller than the normalized separations Δ_{ta} and Δ_{ra}. According to the description of the relationship between the finite scatterers model and the statistical model, all the antenna arrays in the considered scenario together constitute an ideal MIMO system. In contrast, each array itself can be viewed as an ideal phased-array configuration since the distance-dimension ratio is much larger than the interelement spacings Δ_t and Δ_r. Obviously, the simulated results agree well with the theoretical values calculated using the statistical model, which confirms the correctness of the formula (4.13).

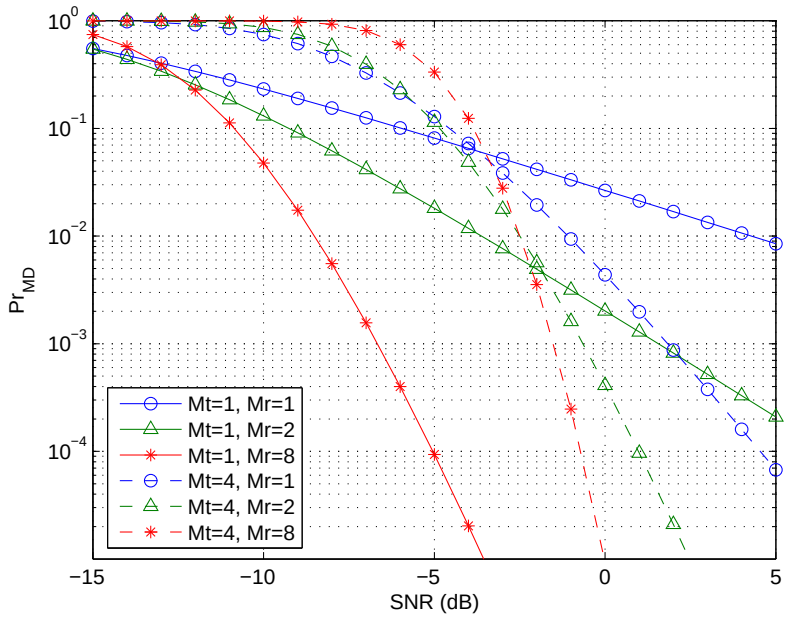

Figure 4.3: *Theoretical probability of missed detection as a function of the SNR for systems with various numbers of receiving antenna arrays*

Figure 4.3 and Figure 4.4 depict the theoretical probability of missed detection $\mathrm{Pr_{MD}}$ calculated by using (4.13) for various hybrid radar configurations.We consider different numbers of transmit and receive arrays, that is, M_t and M_r can be 1, 2, 4, or 8. The scenarios considered in Figure 4.3 have 2 values of M_t, and for each M_t, 3 different values of M_r are examined. From the figure, we find that the configuration with $M_r = 1$, *i.e.*, the phased-array receiver configuration, work best at low SNRs. As the SNR increases, the hybrid system with $M_r = 2$ outperforms the others. The receiver with one sparsely-spaced receive array ($M_r = 8, N_r = 1$)

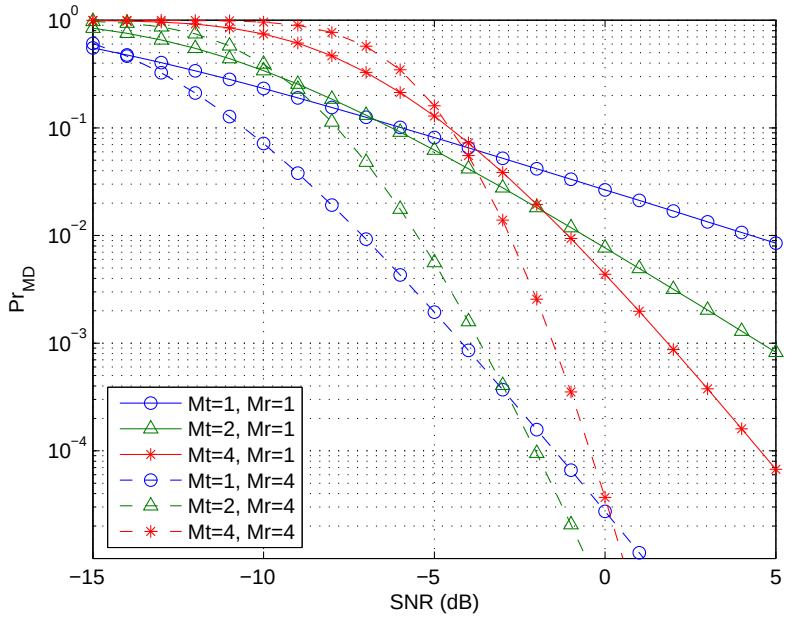

Figure 4.4: *Theoretical probability of missed detection as a function of the SNR for systems with various numbers of transmitting antenna arrays*

is always preferred when the detection performance is good, *e.g.*, $\mathrm{Pr}_{\mathrm{MD}}$ is less than 0.01. Then we compare the curves shown in Figure 4.4 corresponding to the radar systems having various M_t when M_r is fixed at 1 and 4. Similarly, the radar having the phased-array configuration at the transmitter performs the best at low SNR, but systems with larger M_t achieve lower $\mathrm{Pr}_{\mathrm{MD}}$ as the SNR increases. Furthermore, by comparing the three solid lines ($M_r = 1$) with the dotted lines ($M_r = 4$), it is clear that a larger value of M_r is always preferred when $\mathrm{Pr}_{\mathrm{MD}}$ is less than 0.1. However, this is not always the case for M_t, especially when M_r is large. In fact, the system with large M_t performs the best only at relatively high SNR, and at that SNR value $\mathrm{Pr}_{\mathrm{MD}}$ is comparatively low, *e.g.*, lower than 10^{-6}. In addition, observing these two figures, we can see that the improvement on detection performance by enlarging M_r for a fixed transmitter configuration is more obvious than that by increasing M_t when the receiver is unchanged. Therefore, a hybrid system, whose transmitter consists of a few antenna arrays and widely spaced elements at the receiver, provides better target detection performance than either the MIMO radar or the phased-array radar for practical values of $\mathrm{Pr}_{\mathrm{MD}}$, such as 0.01 and 0.001. Furthermore, these results suggest that it is possible to enhance the system performance by forming an adaptive MIMO radar. For example, the best architecture of a radar system can be predicted for every specific scenario, depending on the given number of antennas, the SNR value considered, the

required probability of false alarm, *etc.* Assuming we are capable of moving antenna elements to the desired locations in real time, a MIMO radar whose configuration is adaptively adjusted to provide the best performance can be realized.

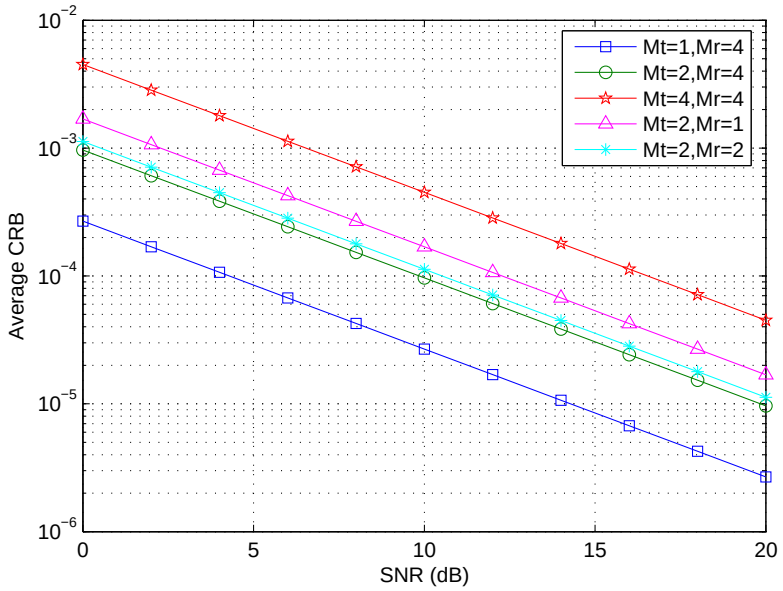

Figure 4.5: *Average CRB of AoD as a function of the SNR for a hybrid radar system with different configurations*

Next, we proceed to assess the direction finding performance of the hybrid radar system, which is again assumed to have a total of 8 transmitting and 8 receiving antennas. We first examine the performance of estimating AoD at the initialization stage. Notice that M_t cannot be 8 since no AoD estimation is possible when there is only one single antenna for each transmit array. Figure 4.5 shows the average CRB of AoD calculated by (4.18) for a hybrid radar system with various configurations. It is obvious that for the same M_r, the smaller the value of M_t, the lower the ACRB, while the ACRB decreases as M_r becomes larger for a fixed M_t. Therefore, in order to estimate the AoD more precisely, the phased-array configuration ($M_t = 1$) should be selected for the transmitter while increasing the number of receive arrays M_r improves performance. Figure 4.6 depicts the simulated average MSE of AoD for the same five scenarios as that in Figure 4.5, but this time using the ML estimator. It also shows the simulated result for the conventional phased-array radar, *i.e.*, $M_t = M_r = 1$, which is unable to be calculated by (4.18). Averaging the MSE $\left|\hat{\Phi}^t - \Phi^t\right|^2$ for 100,000 realizations of the channel matrix $\mathbf{H}$ defined in (4.1) gives the simulated results, where the estimated AoD $\hat{\Phi}^t$ is obtained from (4.16). Apparently, the theoretical ACRB curves in Figure 4.5 agree well with the corresponding simulated

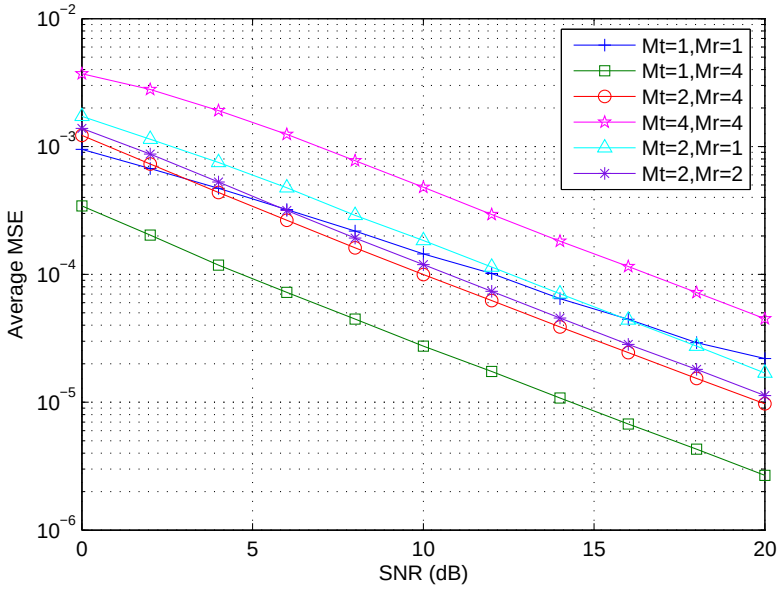

Figure 4.6: *Average MSE of the ML estimator for AoD as a function of the SNR for a hybrid radar system with different configurations*

average MSE curves shown in Figure 4.6, which validates the correctness of (4.18) and also indicates that the ML estimator utilized in these scenarios is an efficient estimation technique.

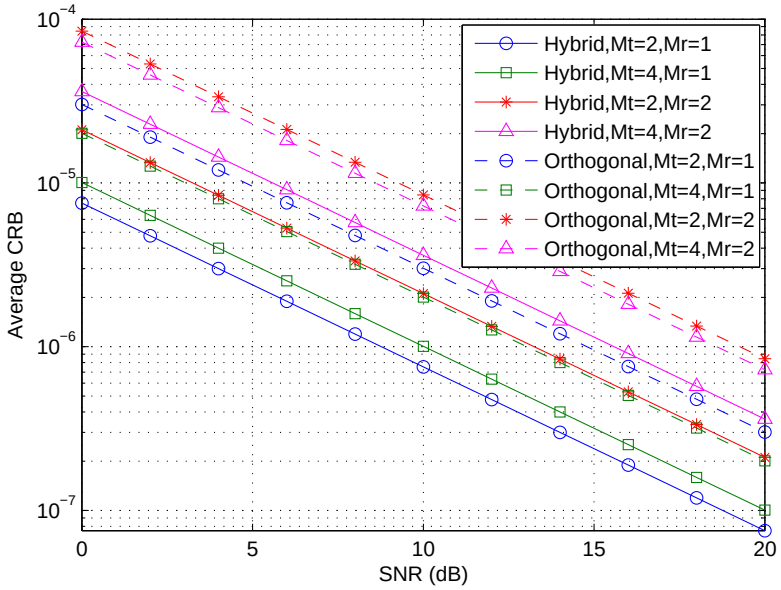

Figure 4.7: *Average CRB of AoA as a function of the SNR for two kinds of transmitting waveforms when the true AoD value is assumed to be available at the transmitter*

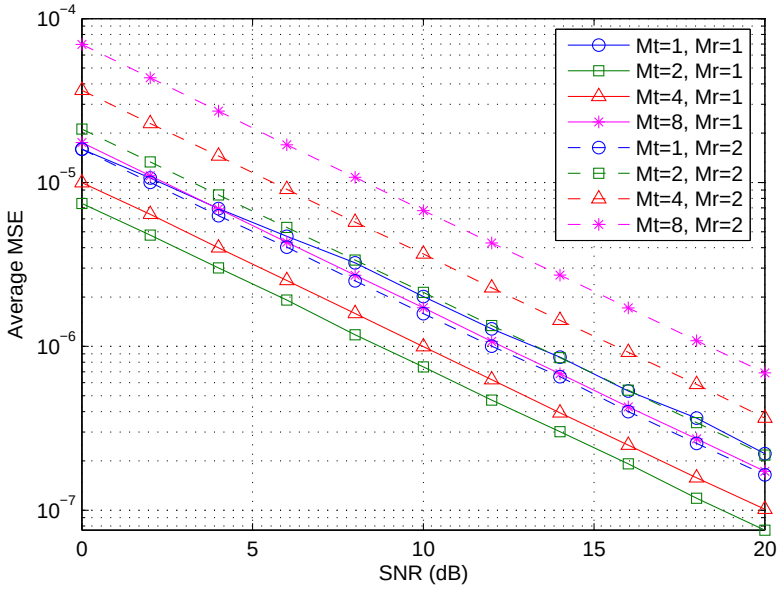

Figure 4.8: *Average MSE of the ML estimator for AoA as a function of the SNR when the true AoD value is assumed to be available at the transmitter*

Now we investigate the direction finding performance at the receiver. First of all, the performance of estimating AoA is examined when the true AoD value is assumed to be available at the transmitter. Here we assume that the number of snapshots L is 80, and M_t could be 1, 2, 4, or 8, while M_r could be 1, 2, or 4. The curves corresponding to "Hybrid" in Figure 4.7 are evaluated using (4.23), which show the average CRB of AoA when the hybrid signal (4.6) is adopted as the transmitting waveform. On the other hand, the curves corresponding to "Orthogonal" in Figure 4.7 show the average CRB of AoA for the same system configurations when the signals transmitted from all the M_tN_t antennas are mutually orthogonal. It is clear that the former provides better performance due to the coherent processing gain realized by the beamformers at the price of estimating the AoD first. Figure 4.8 shows the simulated average MSE of AoA for different systems employing the ML estimator. The estimated AoA is obtained from (4.21) and the simulated results are given by averaging the MSE $\left|\hat{\Phi}^r - \Phi^r\right|^2$ for 100,000 realizations of the channel matrix $\mathbf{H}$. Obviously, the theoretical ACRB results shown in Figure 4.7 agree well with the corresponding simulated curves in Figure 4.8, which validates the correctness of (4.23). Furthermore, we observe that the smaller the value of M_r, the better the estimation of AoA, and for the systems with the same receiver configuration $M_r = 1$, the one with $M_t = 2$ achieves the lowest average MSE, indicating that the total gain achieved by combining the spatial diversity gain provided by the 2 arrays and the coherent processing gain

obtained by the 4 antennas of each array outweighs the diversity gain, or the processing gain realized by the 8 antennas in the MIMO or the phased-array configurations.

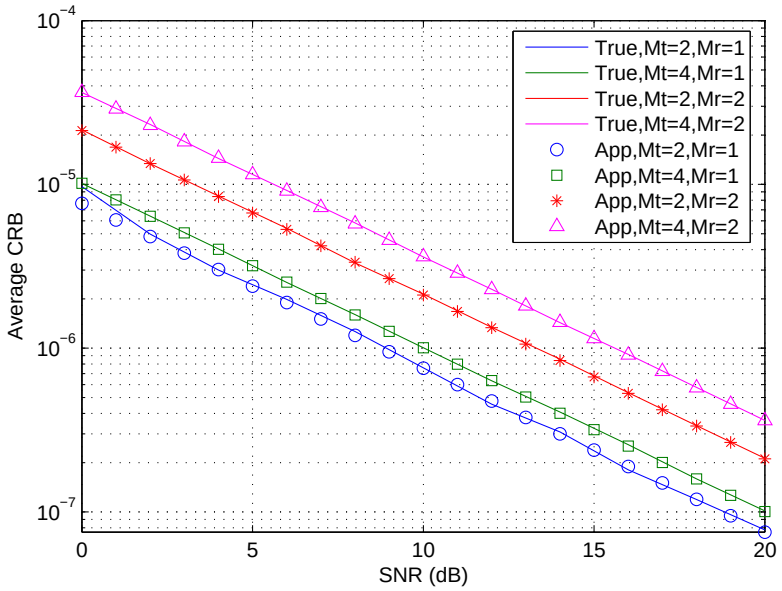

Figure 4.9: *True and approximate average CRB of AoA as a function of the SNR when only the estimated AoD value is available at the transmitter*

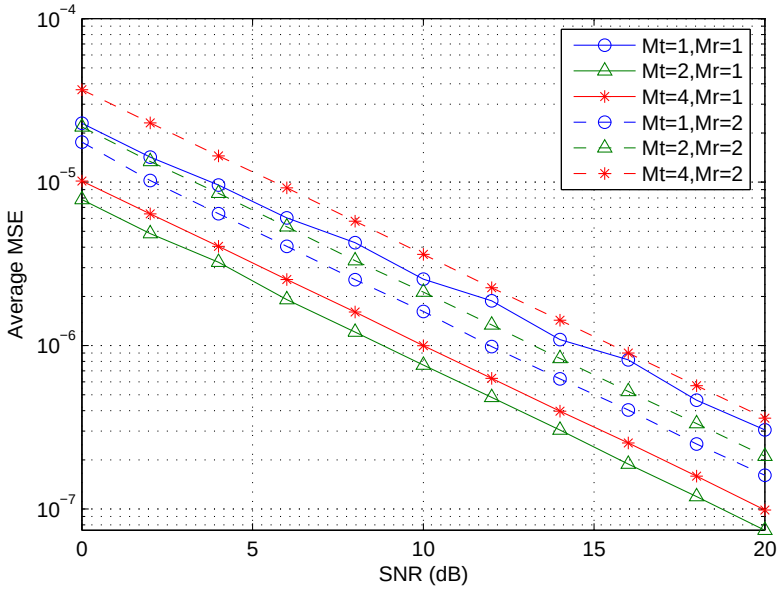

Figure 4.10: *Average MSE of the ML estimator for AoA as a function of the SNR when only the estimated AoD value is available at the transmitter*

We further explore the performance of finding Φ^r when the transmitter only knows the estimated AoD obtained during the initialization stage. In Figure 4.9, the curves corresponding to "True" show the ACRB of AoA obtained numerically using the first approach described in Section 4.4.3, while the curves corresponding to "App" depict the approximate ACRB of AoA when the second method is employed. Comparing the results, we find that the difference is quite small so that the second approach provides a useful CRB estimate. In addition, we present the simulated average MSE of AoA including the effect of estimation error in AoD in Figure 4.10. Here, the estimated AoD is obtained for each realization of channel matrix first, which is the direction the transmitting beamformers steer toward, then the ML estimator at receiver gives $\hat{\Phi}^r$ based on the received signal, and the average MSE is calculated by averaging $\left|\hat{\Phi}^r - \Phi^r\right|^2$ for 100,000 realizations. Obviously, Figure 4.9 agrees well with the corresponding curves in Figure 4.10, which validates the correctness of (4.30). Furthermore, comparing Figure 4.9 with Figure 4.7 and Figure 4.10 with Figure 4.8, we notice that the difference between the performance of the system with the true AoD and estimated AoD is small, indicating that the estimation error in AoD resulting from the initialization stage would not decrease the performance of estimating AoA dramatically. However, this conclusion is somewhat dependent on the array sizes and the number of snapshots available. Thereby, only the system with true AoD value is considered in the following simulations for simplicity and mathematical tractability.

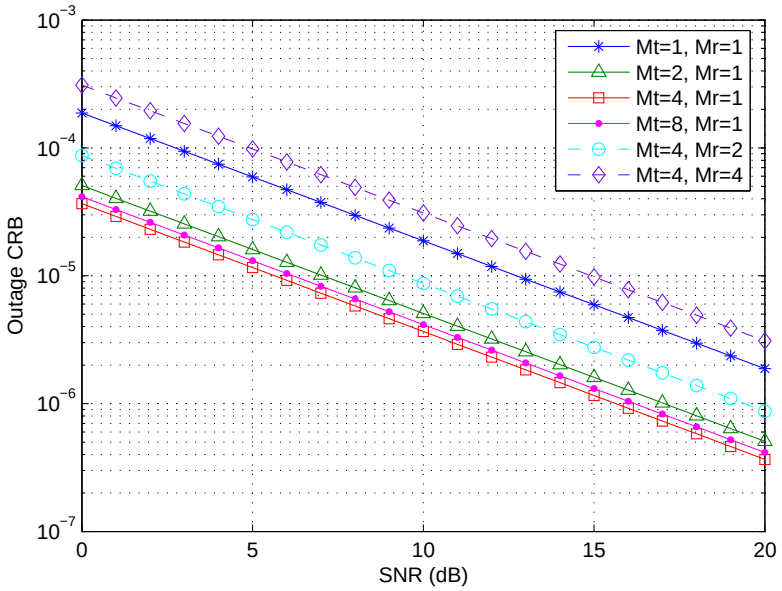

Figure 4.11: *Outage CRB of AoA as a function of the SNR for a hybrid radar system with different configurations when the outage probability* $p = 0.01$

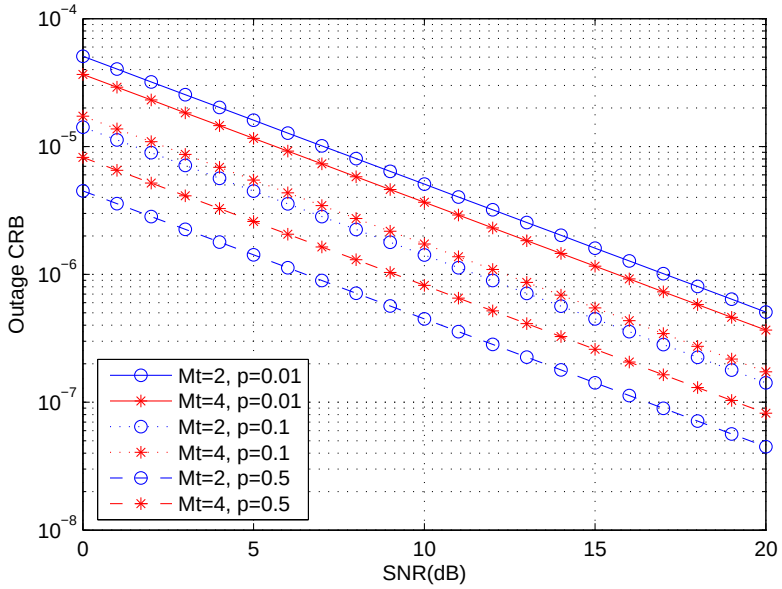

Figure 4.12: *Outage CRB of AoA as a function of the SNR for different values of outage probability p*

We will next compare the system performance by using the outage CRB rather than the ACRB since the latter does not exist when $M_r = M_t = 1$. Figure 4.11 shows the $\text{CRB}_{out}(\Phi^r)$ for various radar systems when $p = 0.01$. Observing the results for systems whose number of transmit arrays M_t is fixed at 4, we find that the radar with smaller M_r always performs better, which agrees with the conclusion drawn from Figure 4.7. Hence, an array with closely-spaced antennas is usually preferred at the receiver for estimating the AoA. Then we compare the performance of systems with the same M_r which is equal to 1. We see that the hybrid radar with 4 transmit arrays, each having 2 antennas, performs better than the system whose transmitting antennas are far from each other ($M_t = 8$) or are closely located ($M_t = 1$). Hence, applying the hybrid bistatic radar system can achieve better direction finding performance than using the MIMO or the phased-array configuration.

From previous results we find that when $M_r = 1$, the hybrid radar with 2 transmit arrays performs the best in terms of the average MSE, while the system with $M_t = 4$ should be chosen in order to achieve the lowest outage CRB for $p = 0.01$. In addition, we see from Figure 4.12 that when $M_r = 1$ and $p = 0.1$, the system with 2 transmit arrays outperforms the one having 4 arrays in the sense of outage CRB. In order to explain this, we further present in Figure 4.13 the CDF of the CRB for systems with $M_r = 1$ and $M_t = 1$, 2, 4, and 8 when the SNR is fixed at

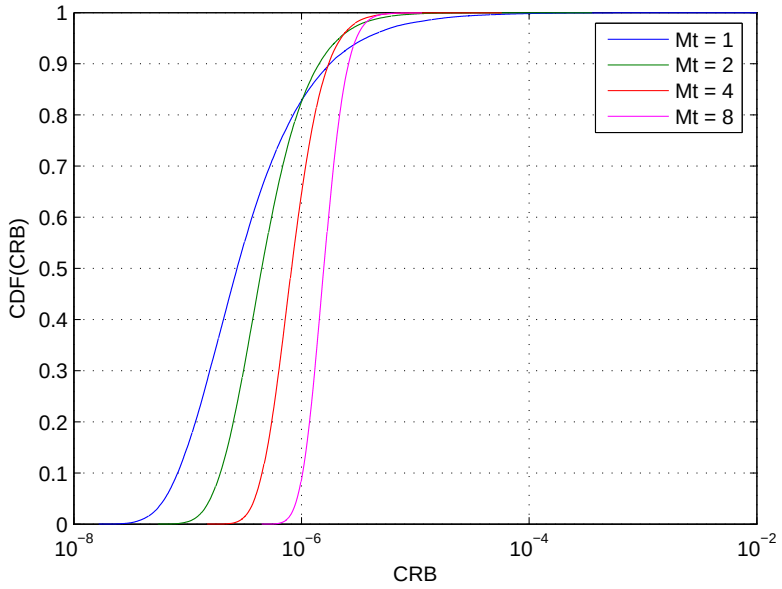

Figure 4.13: *CDF of the CRB of AoA at SNR=10dB for a hybrid radar system with different numbers of transmitting antenna array when the receiver has one antenna array ($M_r = 1$)*

10dB. Recalling the fact that the CRB is actually conditioned on a random variable $\|\boldsymbol{\alpha}\|^2$, which has the distribution $\frac{1}{2}\chi^2_{2M_rM_t}$, it is clear that the CRB itself is also a random variable whose distribution is affected by the values of M_t and M_r. Figure 4.13 illustrates that the comparison of the direction finding performance between different radar systems based on only the average MSE or only the outage CRB is not adequate, and the CDF of CRB should also be taken into account.

4.6 Discussion

In general, our analysis shows that a system with the phased-array configuration, either at the transmitter or receiver, has relatively better target detection performance at low SNR, while the system with the MIMO configuration is preferred at high SNR. The radar system having a sparsely-spaced receive array usually provides better detection performance for low probability of missed detection. However, it is possible that the system whose transmitter is a widely-spaced array works best only when the detection probability is equal to one, which is unnecessary or even impossible in the real radar system. Therefore, a hybrid radar, whose transmitter consists of a few antenna arrays and widely-spaced elements at the receiver, provides better tar-

get detection performance than either the MIMO radar or the phased-array radar for practical values of $\mathrm{Pr}_{\mathrm{MD}}$, such as 0.01 and 0.001.

In contrast, if a radar system is applied to find the target direction AoA, then the phased-array configuration is always preferred at the receiver, and the transmitter should also choose a hybrid configuration to improve the estimation performance. Regarding the estimation performance for the AoD, the phased-array configuration should be chosen at the transmitter while increasing the number of receive antenna arrays improves the estimation, which is the exact opposite of the best configuration for AoA estimation. Although the performance of estimating the AoD during the initialization process will affect the direction finding performance overall given the fact that the AoD information is needed to be known by the transmitter in order to cohere a beam toward the target direction, we validate that the estimation error in AoD caused by the initialization would not decrease the performance of estimating AoA significantly.

It can be seen that the best hybrid configuration for a radar system is not the same for different detection and estimation applications. A hybrid radar system, which is a compromise of these configurations, would be the best choice to optimize jointly the detection and estimation performance. The best hybrid radar configuration for a specific scenario varies depending on the given number of antennas, the SNR value considered, the required precision, *etc.*, which can be evaluated by the theoretical expressions presented in this chapter.

4.7 Conclusions

In this chapter we investigated the hybrid bistatic radar system, which is a combination of the conventional phased-array and MIMO radar configurations. We derived a closed form expression to evaluate the theoretical probability of detection of the system, and examined the performance of the hybrid radar to estimate the AoA by measuring the average and outage CRBs. The performance of estimating the AoD during the initialization process was also examined, and theoretical results were validated by simulations. For a radar system having a fixed number of transmitting and receiving antennas, which is used for both target detection and direction finding, we suggest that a hybrid configuration should be employed, and the total gain achieved by combining the spatial diversity gain provided by the antenna arrays together and the coherent processing gain obtained by each array outweighs the diversity gain, or the processing gain realized by the antennas in pure MIMO or phased-array configurations.

Chapter 5
Detector and Waveform Design for MIMO systems with Noisy Channel Estimation

We have studied the effects the configuration of a MIMO radar has on system performance in the previous chapters. Obviously, for a radar with a fixed architecture, system performance would be significantly affected by the choice of transmitted signals, and such a waveform design problem will be investigated in this chapter. As mentioned in Chapter 2, previous research has shown that time reversal (TR), which is developed in the acoustics domain, can also improve the detection performance of a radar system. However, the TR technique is no longer a good choice when the noise level is high since the retransmitted signal contains significant noise components. We will investigate a MIMO detection process similar to TR detection, during which a waveform designed using the estimated channel and a parameter indicating the quality of the estimation is retransmitted, and the detector determines the presence or absence of a target. Three detectors will be developed, whose theoretical thresholds and probabilities of detection will be derived. We will propose three schemes to design the retransmitted waveform with constraints on signal power, whose performance will be compared with the TR scheme.

5.1 Introduction

The TR technique, an extension of the concept of phase-conjugation in optics, has attracted increasing interest for a broad range of applications. The unique feature of TR is that it can turn multipath effects, traditionally considered a drawback, into a benefit, which is very similar to the MIMO concept. In the TR approach, a signal is first radiated through the medium, then the backscattered signal is recorded, time reversed, energy normalized, and retransmitted. As discussed in Chapter 2, this technique is not new, and there are extensive publications studying the applications of TR in the acoustic and ultrasound domains [99, 101, 139, 140], random media [107, 108], ultra-wideband communications [109, 110], and computational imaging [113–116]. Recently, Moura *et. al.* exploited the MIMO radar target detection problem

applying TR, showing that TR detection can considerably improve system performance compared with conventional detection [118–120]. This is because the waveform is reshaped to match the channel during the TR process, which is a waveform design process. However, the retransmitted signal in Moura's algorithm contains noise components, and it is clear that the TR scheme is no longer a good choice if the noise level is high. In addition, analytical expressions for the threshold and probability of detection of the TR detection were not derived in [118–120]. Instead these were determined by Monte Carlo simulations.

In this chapter, we investigate a MIMO detection process similar to TR detection. That is, during the probing phase, an incident wave is first radiated into the medium and an estimated channel matrix with estimation error is obtained. It is assumed that a parameter indicating the quality of the estimation is given *a priori*, which can be appropriately chosen depending on the noise level, the channel dynamics, and estimation strategies, *etc.* [141–143]. Then, a waveform designed using the estimated channel and the estimation quality parameter under power constraints, instead of the normalized TR signal used in Moura's scheme, is retransmitted. Finally the detector determines the presence or absence of a target. We first develop three detectors, whose theoretical thresholds and probabilities of detection are derived. Next, three criteria are proposed to design the retransmitted waveform under power constraints. Note here that similar to TR detection, it is assumed that the channel remains static during the probing and detection phases, *i.e.*, the scheme is only suited to low Doppler scenarios. The waveform design problem for a MIMO communication system maximizing the channel capacity when estimation error exists is studied in [141–143], and it is assumed that the estimated channel and the estimation error are independent. In this chapter, motivated by [141–143], we consider the waveform design problem for a radar (or sonar) system and assume that the estimation error is independent of the channel and their sum is the estimated channel. Although waveforms are designed for MIMO radar in [70,71], they only assumed that the second-order statistics of the channel matrix is known and this assumption is the basis for the algorithms which are developed. Here, however, we design the detector and the retransmitted waveform using an instantaneous estimated channel matrix.

5.2 System Model

We consider a wideband bistatic MIMO radar (or sonar) system including a pair of arrays A and B, which have N_a and N_b sensors, respectively. The channel frequency response matrix

is denoted by an $N_b \times N_a$ matrix $\mathbf{H}(f_q)$, $q = 1, 2, ..., Q_f$, where the (i, j)-th entry of $\mathbf{H}(f_q)$, $h_{ij}(f_q)$, is the frequency response of the channel between the i-th sensor of Array B and the j-th sensor of Array A at the discrete frequency f_q. It is assumed that the sequential frequencies f_q are at least one coherence bandwidth apart and hence the channel matrices at different frequencies are considered to be independent following [122]. We adopt the statistical MIMO model here, that is, the entries of the channel matrix are modeled as independent zero-mean complex Gaussian random variables, and they are normalized to have unit variance. Note that such a model has been utilized in [8] and [120], but the propagation mechanisms causing multipaths, which result in the random target response, are different. In [8], the distributed target itself leads to multipath propagation, while in [120], the multipaths are due to a rich scattering environment surrounding point-like targets.

As shown in Figure 5.1, the target detection process has two steps. During the probing phase, for the p-th snapshot, the i-th sensor of Array A transmits an incident wideband signal $s_{pi}(t)$ into the medium, whose discrete Fourier transform is $S_{pi}(f_q)$ at frequency f_q. The signal vector received by Array B for the p-th snapshot is

$$\mathbf{x}_p(f_q) = \mathbf{H}(f_q) \cdot \mathbf{s}_p(f_q) + \mathbf{n}_{1,p}(f_q) \tag{5.1}$$

where $\mathbf{n}_{1,p}(f_q)$ is the noise vector at Array B whose entries are assumed to be zero-mean complex Gaussian random variables with variance $\sigma_{n_1}^2$, and the $N_a \times 1$ signal vector $\mathbf{s}_p(f_q) = [S_{p1}(f_q), S_{p2}(f_q), \cdots, S_{pN_a}(f_q)]^T$. Here the superscript T denotes the transpose of a matrix. Based on all the P snapshots $\mathbf{x}_p(f_q)$, the estimated channel matrix $\hat{\mathbf{H}}(f_q)$ is obtained, whose (i, j)-th entry is expressed as

$$\hat{h}_{ij}(f_q) = h_{ij}(f_q) + e_{ij}(f_q) \tag{5.2}$$

where $e_{ij}(f_q)$ is the (i, j)-th element of the channel estimation error matrix $\mathbf{E}(f_q)$. Similar to [144], we assume that $e_{ij}(f_q)$ is a zero-mean complex Gaussian random variable which is independent of $h_{ij}(f_q)$ and has variance σ_e^2. Note here that knowing the value of σ_e^2 requires noise power estimation and knowledge of the estimation method and the waveform length dur-

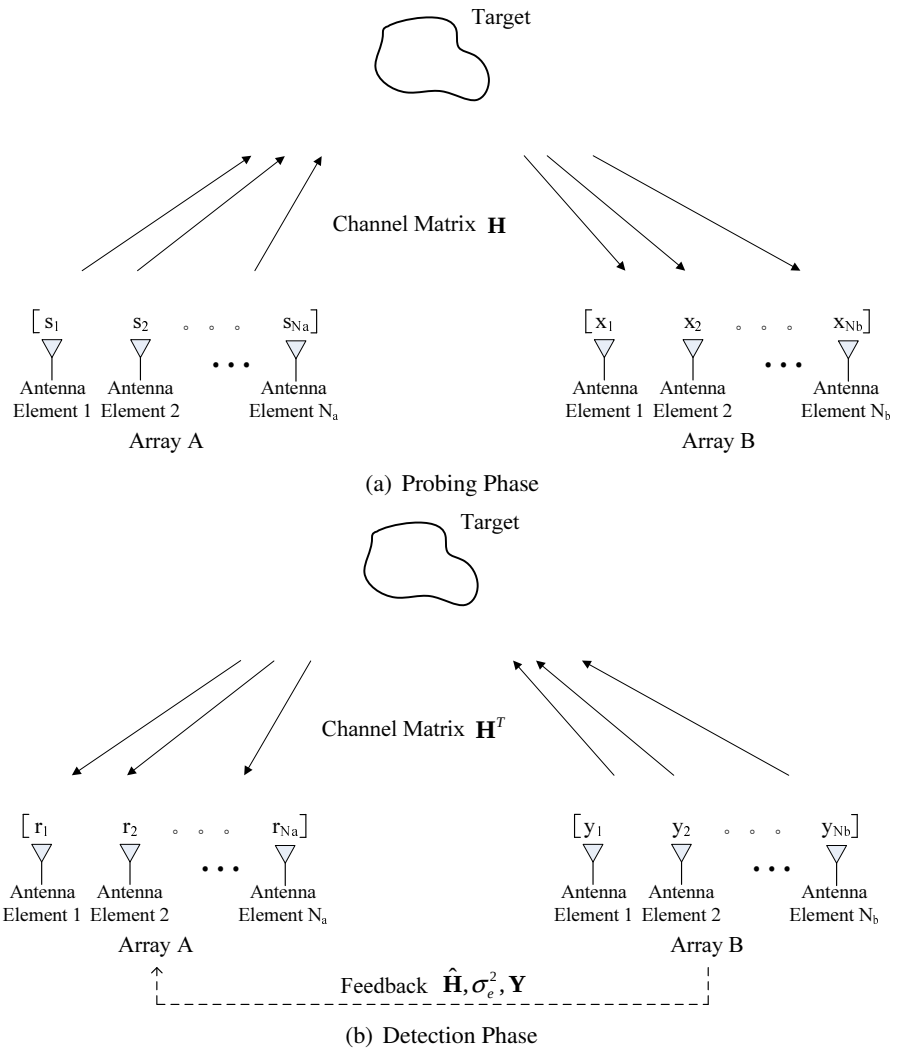

Figure 5.1: *Description of the (a) probing and (b) detection process of the MIMO system*

ing the probing phase. From (5.2), it is not difficult to see that $\hat{h}_{ij}(f_q)$ is a zero-mean complex Gaussian random variable with variance $1+\sigma_e^2$ and is dependent on $h_{ij}(f_q)$ with correlation coefficient $\frac{1}{\sqrt{1+\sigma_e^2}}$. Here, we define $\sigma_h^2 \triangleq \frac{1}{1+\sigma_e^2}$ to simplify mathematical expressions. Therefore, conditioned on $\hat{h}_{ij}(f_q)$, the random variable $h_{ij}(f_q)$ has mean $\sigma_h^2\hat{h}_{ij}(f_q)$ and variance $\sigma_h^2\sigma_e^2$.

Next, as shown in Figure 5.1(b), the signal $\mathbf{y}(f_q)$ designed based on $\hat{\mathbf{H}}(f_q)$ and σ_e^2 is retransmitted into the medium from Array B during the detection phase, and the detector at Array A determines the presence or absence of a target based on the received signal $\mathbf{r}(f_q)$ at all of the Q_f frequencies. Since the focus of this chapter is to design different detectors and retransmitted waveforms and study their effects on the target detection performance, we assume that, if it is

required, the estimated channel matrix $\hat{\mathbf{H}}(f_q)$, the estimation error variance σ_e^2, and the retransmitted waveform $\mathbf{Y}$ at Array B are fed back to Array A via a side channel, and we concentrate on analyzing the second detection stage.

It is assumed that Array B transmits M snapshots in the second phase, during which the channel remains the same. Denote the M snapshots received by the i-th sensor of Array A at frequency f_q and the corresponding additive white Gaussian noise components by $M \times 1$ vectors $\mathbf{r}_i(f_q)$ and $\mathbf{n}_i(f_q)$, respectively, which can be written as

$$\mathbf{r}_i(f_q) = \mathbf{Y}(f_q) \cdot \mathbf{h}_i(f_q) + \mathbf{n}_i(f_q) \tag{5.3}$$

where $i = 1, 2, ..., N_a$, $q = 1, 2, ..., Q_f$, and

$$\begin{aligned} \mathbf{Y}(f_q) &= \begin{bmatrix} \mathbf{y}_1(f_q) & \mathbf{y}_2(f_q) & \cdots & \mathbf{y}_M(f_q) \end{bmatrix}^T \\ \mathbf{H}(f_q) &= \begin{bmatrix} \mathbf{h}_1(f_q) & \mathbf{h}_2(f_q) & \cdots & \mathbf{h}_{N_a}(f_q) \end{bmatrix} \end{aligned} \tag{5.4}$$

where the $N_b \times 1$ vector $\mathbf{y}_m(f_q)$ is the m-th snapshot signal retransmitted from Array B at frequency f_q, and the entries of $\mathbf{n}_i(f_q)$ are assumed to be zero-mean complex Gaussian random variables with variance σ_n^2. Grouping the signals received by the i-th sensor of Array A at all the Q_f frequencies yields an $MQ_f \times 1$ vector $\mathbf{r}_i$, which is given by

$$\mathbf{r}_i = \begin{bmatrix} \mathbf{r}_i^T(f_1) & \mathbf{r}_i^T(f_2) & \cdots & \mathbf{r}_i^T(f_{Q_f}) \end{bmatrix}^T = \mathbf{Y} \cdot \mathbf{h}_i + \mathbf{n}_i \tag{5.5}$$

where the $MQ_f \times N_bQ_f$ matrix $\mathbf{Y}$, the $N_bQ_f \times 1$ vector $\mathbf{h}_i$, and the $MQ_f \times 1$ vector $\mathbf{n}_i$ can be expressed as below:

$$\mathbf{Y}=\begin{bmatrix} \mathbf{Y}(f_1) & \mathbf{0} & \cdots & \mathbf{0} \\ \mathbf{0} & \mathbf{Y}(f_2) & \cdots & \mathbf{0} \\ \vdots & \vdots & \ddots & \vdots \\ \mathbf{0} & \mathbf{0} & \cdots & \mathbf{Y}(f_{Q_f}) \end{bmatrix}, \quad \begin{matrix} \mathbf{h}_i=\begin{bmatrix} \mathbf{h}_i^T(f_1) & \mathbf{h}_i^T(f_2) & \cdots & \mathbf{h}_i^T(f_{Q_f}) \end{bmatrix}^T \\ \mathbf{n}_i=\begin{bmatrix} \mathbf{n}_i^T(f_1) & \mathbf{n}_i^T(f_2) & \cdots & \mathbf{n}_i^T(f_{Q_f}) \end{bmatrix}^T \end{matrix} \tag{5.6}$$

Similar to the channel vectors $\mathbf{h}_i$, we can obtain N_a estimated channel vectors $\hat{\mathbf{h}}_i$ and estimation error vectors $\mathbf{e}_i$ by stacking the corresponding columns of $\hat{\mathbf{H}}(f_q)$ and $\mathbf{E}(f_q)$ into $N_bQ_f \times 1$ columns, respectively, and $\hat{\mathbf{h}}_i = \mathbf{h}_i + \mathbf{e}_i$. Based on previous discussion, it is easy to see that

$$\mathbf{h}_i \left| \hat{\mathbf{h}}_i \sim \mathcal{CN}\left(\sigma_h^2\hat{\mathbf{h}}_i, \sigma_h^2\sigma_e^2\mathbf{I}_{N_bQ_f}\right), \quad \mathbf{n}_i \sim \mathcal{CN}\left(\mathbf{0}_{MQ_f}, \sigma_n^2\mathbf{I}_{MQ_f}\right) \right. \tag{5.7}$$

where $i = 1, 2, ..., N_a$, the separator "|" represents "conditioned on", and $\mathbf{0}_k$ and $\mathbf{I}_k$ stand for a $k \times 1$ all-zeros vector and a $k \times k$ identity matrix, respectively. The detector at Array A determines whether or not a target exists in the medium based on the values of all the N_a vectors $\mathbf{r}_i$. In this chapter, we restrict our attention to the design of the detector and the retransmitted waveform $\mathbf{Y}$, which will be explained in the following sections.

5.3 Detector Design

The target detection problem of the MIMO system can be described as follows:

$$\mathbf{r}_i = \begin{cases} \mathbf{n}_i & \mathcal{H}_0 \\ \mathbf{Y}\cdot\mathbf{h}_i + \mathbf{n}_i & \mathcal{H}_1 \end{cases} \tag{5.8}$$

where $i = 1, 2, ..., N_a$, and the alternate hypothesis $\mathcal{H}_1$ and null hypothesis $\mathcal{H}_0$ are that the target does or does not exist, respectively. From (5.5) and (5.7), it is obvious that the received signals $\mathbf{r}_i$ are complex Gaussian vectors under both hypotheses with different distributions given the estimated channel:

$$\mathbf{r}_i \sim \begin{cases} \mathcal{CN}\left(\mathbf{0}_{MQ_f}, \sigma_n^2 \mathbf{I}_{MQ_f}\right) & \mathcal{H}_0 \\ \mathcal{CN}\left(\mathbf{d}_i, \mathbf{C}\right) & \mathcal{H}_1 \end{cases} \tag{5.9}$$
$$\mathbf{d}_i = \sigma_h^2 \mathbf{Y}\hat{\mathbf{h}}_i, \;\; \mathbf{C} = \sigma_h^2 \sigma_e^2 \mathbf{Y}\mathbf{Y}^H + \sigma_n^2 \mathbf{I}_{MQ_f}$$

We develop three approaches to detect the target in this chapter: the conventional detector, the optimal detector, and the generalized likelihood ratio test (GLRT) detector. The theoretical threshold η and the probability of detection $\mathrm{Pr_D}$ of each detector will be derived in this section. Notice that in order to express the distribution of a weighted sum of several non-central chi-square random variables in a closed form equation, we use a common approximation technique [126] in the derivation for both the optimal detector and the GLRT detector. This approach approximates a weighted sum of non-central chi-square variables by a single central chi-square variable whose degrees of freedom and scaling factor are carefully chosen such that the first two moments remain the same.

5.3.1 Detector I: Conventional Detector

It is well known that the optimal detector for a known signal in white Gaussian noise is a matched filter [47], and such a detector is employed as Detector I, whose performance is examined when estimation errors exist in channel matrix. The conventional detector given by [47] can be expressed as

$$T_{\mathrm{I}} = \Re\left[\sum_{i=1}^{N_a} (\mathbf{Y}\hat{\mathbf{h}}_i)^H \bar{r}_i\right] \underset{<\mathcal{H}_0}{>^{\mathcal{H}_1}} \eta_{\mathrm{I}} \tag{5.10}$$

where the superscript H represents the conjugate transpose of a matrix and $\Re$ denotes the real part of a complex number. Notice here that the detector actually matches to the estimated channel $\hat{\mathbf{h}}_i$ instead of the true channel $\mathbf{h}_i$ as in [47] since only the noisy channel estimate is available. From (5.9) and (5.10), the distributions of the test statistic T_{I} under both hypotheses can be given by

$$T_{\mathrm{I}} \sim \begin{cases} \mathcal{N}\left(0, \frac{1}{2}\sum_{i=1}^{N_a} \Upsilon_{1i}\right) & \mathcal{H}_0 \\ \mathcal{N}\left(\sum_{i=1}^{N_a} \hat{\mathbf{h}}_i^H \mathbf{Y}^H \mathbf{d}_i, \frac{1}{2}\sum_{i=1}^{N_a} \{\Upsilon_{1i} + \Upsilon_{2i}\}\right) & \mathcal{H}_1 \end{cases} \tag{5.11}$$
$$\Upsilon_{1i} = \sigma_n^2 \hat{\mathbf{h}}_i^H \mathbf{Y}^H \mathbf{Y} \hat{\mathbf{h}}_i,\ \Upsilon_{2i} = \sigma_h^2 \sigma_e^2 \hat{\mathbf{h}}_i^H \mathbf{Y}^H \mathbf{Y}\mathbf{Y}^H \mathbf{Y} \hat{\mathbf{h}}_i$$

Therefore, for a given noise level, the threshold for the conventional detector η_{I} can be determined by the required probability of false alarm $\mathrm{Pr}_{\mathrm{FA}}$ following (5.11)

$$\eta_{\mathrm{I}} = \sqrt{\frac{\sigma_n^2}{2}\sum_{i=1}^{N_a} \hat{\mathbf{h}}_i^H \mathbf{Y}^H \mathbf{Y} \hat{\mathbf{h}}_i} \cdot Q^{-1}(\mathrm{Pr}_{\mathrm{FA}}) \tag{5.12}$$

From (5.10) and (5.12), it is obvious that Detector I requires knowledge of $\mathbf{Y}$ and $\hat{\mathbf{h}}_i$ at Array A in Figure 5.1 to decide the existence of targets. Based on (5.11) and (5.12), the theoretical probability of detection of Detector I $\mathrm{Pr}_{\mathrm{D,I}}$ can be written as

$$\mathrm{Pr}_{\mathrm{D,I}} = Q\left(\frac{\eta_{\mathrm{I}} - \sum_{i=1}^{N_a} \hat{\mathbf{h}}_i^H \mathbf{Y}^H \mathbf{d}_i}{\sqrt{\frac{1}{2}\sum_{i=1}^{N_a} \{\Upsilon_{1i} + \Upsilon_{2i}\}}}\right) \tag{5.13}$$

where the Gaussian right-tail function is defined as $Q(x) = \int_x^{+\infty} \frac{1}{\sqrt{2\pi}} \exp(-\frac{1}{2}t^2)dt$, and the function $Q^{-1}(x)$ denotes its inverse.

Next, we proceed to express the threshold and probability of detection in a second form, which is employed for waveform design discussed in the next section. Denote by $\mathbf{U}\mathbf{\Sigma}\mathbf{V}^H$ the singular value decomposition (SVD) of $\mathbf{Y}$, where the $MQ_f \times MQ_f$ matrix $\mathbf{U}$ and $N_bQ_f \times N_bQ_f$ matrix $\mathbf{V}$ are unitary matrices. When $M \geq N_b$, $\mathbf{\Sigma} = \begin{bmatrix} \mathbf{\Sigma}_1 & \mathbf{0} \end{bmatrix}^T$. Here $\mathbf{\Sigma}_1$ is an $N_bQ_f \times N_bQ_f$ diagonal matrix with n positive singular values $\varsigma_1, \varsigma_2, ..., \varsigma_n$ of $\mathbf{Y}$ (in decreasing order) on the diagonal and the all-zeros matrix has dimensions $N_bQ_f \times (M - N_b)Q_f$. While $M < N_b$, $\mathbf{\Sigma} = \begin{bmatrix} \mathbf{\Sigma}_2 & \mathbf{0} \end{bmatrix}$, and $\mathbf{\Sigma}_2$ is a $MQ_f \times MQ_f$ matrix with n singular values on the diagonal and the all-zeros matrix has dimensions $MQ_f \times (N_b - M)Q_f$. Here, n is the rank of $\mathbf{Y}$, *i.e.*, $n = \mathrm{rank}(\mathbf{Y}) \leq \min(MQ_f, N_BQ_f)$. Therefore, we can obtain the following expressions:

$$\begin{aligned}\sum_{i=1}^{N_a}\hat{\mathbf{h}}_i^H\mathbf{Y}^H\mathbf{Y}\hat{\mathbf{h}}_i &= \sum_{i=1}^{N_a}\hat{\mathbf{h}}_i^H\mathbf{V}\begin{bmatrix}\boldsymbol{\Xi} & \mathbf{0}\\ \mathbf{0} & \mathbf{0}\end{bmatrix}\mathbf{V}^H\hat{\mathbf{h}}_i\\ \sum_{i=1}^{N_a}\hat{\mathbf{h}}_i^H\mathbf{Y}^H\mathbf{Y}\mathbf{Y}^H\mathbf{Y}\hat{\mathbf{h}}_i &= \sum_{i=1}^{N_a}\hat{\mathbf{h}}_i^H\mathbf{V}\begin{bmatrix}\boldsymbol{\Xi}^2 & \mathbf{0}\\ \mathbf{0} & \mathbf{0}\end{bmatrix}\mathbf{V}^H\hat{\mathbf{h}}_i\end{aligned} \tag{5.14}$$

where the $n \times n$ diagonal matrix $\boldsymbol{\Xi} = \mathrm{diag}(\boldsymbol{\beta})$, and the k-th entry of the $n \times 1$ vector $\boldsymbol{\beta}$ is the square of the corresponding singular value of $\mathbf{Y}$, *i.e.*, $\beta_k = \varsigma_k^2$. Denote the k-th element of the vector $\mathbf{h}_i' = \mathbf{V}^H\hat{\mathbf{h}}_i$ by h_{ik}' and let $\rho_k = \sum_{i=1}^{N_a}|h_{ik}'|^2$, the above equations can be rewritten as

$$\sum_{i=1}^{N_a}\hat{\mathbf{h}}_i^H\mathbf{Y}^H\mathbf{Y}\hat{\mathbf{h}}_i = \sum_{k=1}^{n}\beta_k\rho_k, \qquad \sum_{i=1}^{N_a}\hat{\mathbf{h}}_i^H\mathbf{Y}^H\mathbf{Y}\mathbf{Y}^H\mathbf{Y}\hat{\mathbf{h}}_i = \sum_{k=1}^{n}\beta_k^2\rho_k \tag{5.15}$$

where $|\cdot|$ stands for the modulus of a complex number. Substituting (5.15) into (5.12) and (5.13), we can express the theoretical threshold and probability of detection of Detector I in the following form:

$$\eta_{\mathrm{I}} = \sqrt{\frac{\sigma_n^2}{2}\sum_{k=1}^{n}\beta_k\rho_k}\cdot Q^{-1}(\mathrm{Pr}_{\mathrm{FA}}), \mathrm{Pr}_{\mathrm{D,I}} = Q\left(\frac{\eta_{\mathrm{I}} - \sigma_h^2\sum_{k=1}^{n}\beta_k\rho_k}{\sqrt{\frac{1}{2}\left\{\sigma_h^2\sigma_e^2\sum_{k=1}^{n}\beta_k^2\rho_k + \sigma_n^2\sum_{k=1}^{n}\beta_k\rho_k\right\}}}\right) \tag{5.16}$$

5.3.2 Detector II: Optimal Detector

Next, we proceed to design Detector II, which is the likelihood ratio test (LRT) detector for the case when $\sigma_e^2 > 0$. The LRT detector is the optimal solution to the hypotheses testing problem in the Neyman-Pearson sense, *i.e.*, the detector maximizes Pr_{D} subject to a constraint on $\mathrm{Pr}_{\mathrm{FA}}$ [47]. The LRT can be stated as the following decision rule

$$L(\mathbf{r}) = \frac{\mathrm{PDF}(\mathbf{r}_1,\mathbf{r}_2,...,\mathbf{r}_{N_a}|\mathcal{H}_1)}{\mathrm{PDF}(\mathbf{r}_1,\mathbf{r}_2,...,\mathbf{r}_{N_a}|\mathcal{H}_0)} \begin{matrix}>^{\mathcal{H}_1}\\ <_{\mathcal{H}_0}\end{matrix} \eta \tag{5.17}$$

where $\mathrm{PDF}(\mathbf{r}_1,\mathbf{r}_2,...,\mathbf{r}_{N_a}|\mathcal{H}_1)$ and $\mathrm{PDF}(\mathbf{r}_1,\mathbf{r}_2,...,\mathbf{r}_{N_a}|\mathcal{H}_0)$ are the probability density functions (PDFs) of the data under hypotheses $\mathcal{H}_1$ and $\mathcal{H}_0$, respectively. Previous assumptions imply that the PDFs can be written as

$$\mathrm{PDF}(\mathbf{r}_1,\mathbf{r}_2,...,\mathbf{r}_{N_a}|\mathcal{H}_0) = \prod_{i=1}^{N_a} \frac{1}{(\pi\sigma_n^2)^{MQ_f}} \exp\left\{-\frac{1}{\sigma_n^2}\mathbf{r}_i^H\mathbf{r}_i\right\} \tag{5.18}$$

under $\mathcal{H}_0$ and

$$\mathrm{PDF}(\mathbf{r}_1,\mathbf{r}_2,...,\mathbf{r}_{N_a}|\mathcal{H}_1) = \prod_{i=1}^{N_a} \frac{1}{\pi^{MQ_f}\det(\mathbf{C})} \exp\left\{-(\mathbf{r}_i-\mathbf{d}_i)^H\mathbf{C}^{-1}(\mathbf{r}_i-\mathbf{d}_i)\right\} \tag{5.19}$$

under $\mathcal{H}_1$. Substituting (5.18) and (5.19) into (5.17), taking the logarithm of both sides, and incorporating the non-data-dependent term into the threshold, we decide $\mathcal{H}_1$ if

$$T' = \sum_{i=1}^{N_a}\left\{\mathbf{r}_i^H\mathbf{B}\mathbf{r}_i + \mathbf{r}_i^H\mathbf{g}_i + \mathbf{g}_i^H\mathbf{r}_i\right\} > \eta', \quad \mathbf{B} = \tfrac{1}{\sigma_n^2}\mathbf{I}_{MQ_f} - \mathbf{C}^{-1},\ \mathbf{g}_i = \mathbf{C}^{-1}\mathbf{d}_i \tag{5.20}$$

In order to analyze the distribution of the test statistic, a non-data-dependent term is added at both sides of (5.20), and the detector can be described as below:

$$\begin{aligned} T_{\mathrm{II}} &= \sum_{i=1}^{N_a}\left\{\mathbf{r}_i^H\mathbf{B}\mathbf{r}_i + \mathbf{r}_i^H\mathbf{g}_i + \mathbf{g}_i^H\mathbf{r}_i + \mathbf{g}_i^H\mathbf{B}^\dagger\mathbf{g}_i\right\} \\ &= \sum_{i=1}^{N_a}\left\{\left(\mathbf{r}_i+\mathbf{B}^\dagger\mathbf{g}_i\right)^H\cdot\mathbf{B}\cdot\left(\mathbf{r}_i+\mathbf{B}^\dagger\mathbf{g}_i\right)\right\} \begin{array}{l}>^{\mathcal{H}_1}\\<_{\mathcal{H}_0}\end{array} \eta_{\mathrm{II}} \end{aligned} \tag{5.21}$$

where the superscript † denotes the Moore-Penrose pseudoinverse. It is reasonable to assume that T_{II} under both hypotheses follows the Gamma distribution but with different parameters as it has a quadratic form in a Gaussian random variable, that is,

$$T_{\mathrm{II}} \sim \begin{cases} \Gamma\left(k_0, \theta_0\right) & \mathcal{H}_0 \\ \Gamma\left(k_1, \theta_1\right) & \mathcal{H}_1 \end{cases} \tag{5.22}$$

where $\Gamma\left(k, \theta\right)$ denotes the Gamma distribution with the shape parameter k and scale parameter θ. In order to calculate k_0 and θ_0, we first compute the mean and variance of the test statistic T_{II} under $\mathcal{H}_0$, which are given by

$$\begin{aligned} \mathrm{E}\left[T_{\mathrm{II}}\left|\mathcal{H}_0\right.\right] &= \sum_{i=1}^{N_a} \left\{\sigma_n^2 \mathrm{trace}(\mathbf{B}) + \mathbf{g}_i^H \mathbf{B}^\dagger \mathbf{g}_i\right\} \\ \mathrm{var}\left[T_{\mathrm{II}}\left|\mathcal{H}_0\right.\right] &= \sum_{i=1}^{N_a} \left\{\sigma_n^4 \mathrm{trace}(\mathbf{B}^H\mathbf{B}) + 2\sigma_n^2 \mathbf{g}_i^H \mathbf{g}_i\right\} \end{aligned} \tag{5.23}$$

Following (5.22), the threshold for Detector II based on the required $\mathrm{Pr}_{\mathrm{FA}}$ can be given by

$$\eta_{\mathrm{II}} = \mathcal{F}^{-1}_{\Gamma(k_0,\theta_0)}(1-\mathrm{Pr}_{\mathrm{FA}}), \quad k_0 = \tfrac{(\mathrm{E}[T_{\mathrm{II}}|\mathcal{H}_0])^2}{\mathrm{var}[T_{\mathrm{II}}|\mathcal{H}_0]}, \quad \theta_0 = \tfrac{\mathrm{var}[T_{\mathrm{II}}|\mathcal{H}_0]}{\mathrm{E}[T_{\mathrm{II}}|\mathcal{H}_0]} \tag{5.24}$$

where $\mathcal{F}^{-1}_{\Gamma(k,\theta)}$ denotes the inverse cumulative distribution function (CDF) of a Gamma random variable with parameters k and θ. From (5.21) and (5.24), it is clear that the implementation of Detector II requires knowledge of $\mathbf{Y}$, $\hat{\mathbf{h}}_i$, and σ_e^2 at Array A in Figure 5.1.

We next consider the test statistic T_{II} under the alternate hypothesis. Based on (5.9), the received signal under $\mathcal{H}_1$ can be rewritten as $\mathbf{r}_i = \mathbf{d}_i + \mathbf{w}_i$, where $i = 1, 2, ..., N_a$ and $\mathbf{w}_i \sim \mathcal{CN}\left(\mathbf{0}_{MQ_f}, \mathbf{C}\right)$. Hence, the test statistic T_{II} can be expressed as follows:

$$\begin{aligned} T_{\mathrm{II}} &= \sum_{i=1}^{N_a} \left\{\left(\mathbf{w}_i + \mathbf{d}_i + \mathbf{B}^\dagger \mathbf{g}_i\right)^H \mathbf{B} \left(\mathbf{w}_i + \mathbf{d}_i + \mathbf{B}^\dagger \mathbf{g}_i\right)\right\} \\ &= \sum_{i=1}^{N_a} \left\{\left[\mathbf{w}_i' + \mathbf{C}^{-\frac{1}{2}}\left(\mathbf{d}_i + \mathbf{B}^\dagger \mathbf{g}_i\right)\right]^H \mathbf{C}^{\frac{1}{2}} \mathbf{B} \mathbf{C}^{\frac{1}{2}} \left[\mathbf{w}_i' + \mathbf{C}^{-\frac{1}{2}}\left(\mathbf{d}_i + \mathbf{B}^\dagger \mathbf{g}_i\right)\right]\right\} \\ &= \sum_{i=1}^{N_a} \left\{\mathbf{w}_i'^H \mathbf{B}' \mathbf{w}_i' + \mathbf{w}_i'^H \mathbf{g}_i' + \mathbf{g}_i'^H \mathbf{w}_i' + \mathbf{g}_i'^H \mathbf{B}'^\dagger \mathbf{g}_i'\right\} \end{aligned} \tag{5.25}$$

where

$$\mathbf{w}_i' = \mathbf{C}^{-\frac{1}{2}}\mathbf{w}_i \sim \mathcal{CN}\left(\mathbf{0}_{MQ_f}, \mathbf{I}_{MQ_f}\right), \mathbf{B}' = \mathbf{C}^{\frac{1}{2}}\mathbf{B}\mathbf{C}^{\frac{1}{2}}, \mathbf{g}_i' = \mathbf{B}'\mathbf{C}^{-\frac{1}{2}}\left(\mathbf{d}_i + \mathbf{B}^{\dagger}\mathbf{g}_i\right) \quad (5.26)$$

Therefore, the mean and variance of T_{II} under $\mathcal{H}_1$ are given by

$$\begin{aligned} \mathrm{E}\left[T_{\mathrm{II}}\left|\mathcal{H}_1\right.\right] &= \sum_{i=1}^{N_a}\left\{\mathrm{trace}(\mathbf{B}') + \mathbf{g}_i'^H\mathbf{B}'^{\dagger}\mathbf{g}_i'\right\} \\ \mathrm{var}\left[T_{\mathrm{II}}\left|\mathcal{H}_1\right.\right] &= \sum_{i=1}^{N_a}\left\{\mathrm{trace}(\mathbf{B}'^H\mathbf{B}') + 2\mathbf{g}_i'^H\mathbf{g}_i'\right\} \end{aligned} \quad (5.27)$$

The theoretical probability of detection of the optimal detector can be expressed as follows based on (5.22):

$$\mathrm{Pr}_{\mathrm{D,II}} = 1 - \mathcal{F}_{\Gamma(k_1,\theta_1)}\left(\eta_{\mathrm{II}}\right), \quad k_1 = \frac{(\mathrm{E}[T_{\mathrm{II}}|\mathcal{H}_1])^2}{\mathrm{var}[T_{\mathrm{II}}|\mathcal{H}_1]}, \quad \theta_1 = \frac{\mathrm{var}[T_{\mathrm{II}}|\mathcal{H}_1]}{\mathrm{E}[T_{\mathrm{II}}|\mathcal{H}_1]} \quad (5.28)$$

where $\mathcal{F}_{\Gamma(k,\theta)}$ stands for the CDF of a Gamma random variable with parameters k and θ.

Similar to Detector I, we next express the threshold and probability of detection of Detector II using the second form which is more suited to waveform design. From (5.9) and (5.20), the following equations can be derived based on the SVD of $\mathbf{Y}$ mentioned in Section 5.3.1:

$$\begin{aligned} \mathbf{C} &= \mathbf{U}\begin{bmatrix} \sigma_h^2\sigma_e^2\mathbf{\Xi} + \sigma_n^2\mathbf{I}_n & \mathbf{0} \\ \mathbf{0} & \sigma_n^2\mathbf{I}_{MQ_f-n} \end{bmatrix}\mathbf{U}^H \\ \mathbf{B} &= \mathbf{U}\begin{bmatrix} \frac{1}{\sigma_n^2}\mathbf{I}_n - \left(\sigma_h^2\sigma_e^2\mathbf{\Xi} + \sigma_n^2\mathbf{I}_n\right)^{-1} & \mathbf{0} \\ \mathbf{0} & \mathbf{0} \end{bmatrix}\mathbf{U}^H \end{aligned} \quad (5.29)$$

Substituting (5.29) into (5.21), we can rewrite the test statistic under $\mathcal{H}_0$ as below:

$$\begin{aligned} T_{\mathrm{II}} &= \sum_{i=1}^{N_a} \mathbf{z}_{0i}^H \begin{bmatrix} \frac{1}{\sigma_n^2}\mathbf{I}_n - \left(\sigma_h^2\sigma_e^2\boldsymbol{\Xi} + \sigma_n^2\mathbf{I}_n\right)^{-1} & \mathbf{0} \\ \mathbf{0} & \mathbf{0} \end{bmatrix} \mathbf{z}_{0i} \\ &= \frac{1}{2}\sum_{i=1}^{N_a}\sum_{k=1}^{n} \frac{\sigma_e^2\beta_k}{\sigma_e^2\beta_k+\sigma_n^2(1+\sigma_e^2)} \left(2\left|z_{0ik}\right|^2\right) \qquad \text{Under } \mathcal{H}_0 \end{aligned} \tag{5.30}$$

where z_{0ik} is the k-th entry of the vector $\mathbf{z}_{0i} = \mathbf{U}^H\left(\mathbf{r}_i + \mathbf{B}^\dagger\mathbf{g}_i\right)/\sigma_n$. Denote as γ_{0ik} the k-th element of the vector $\mathbf{U}^H\mathbf{B}^\dagger\mathbf{g}_i/\sigma_n$, which is given by

$$\gamma_{0ik} = \frac{\sigma_h^2}{\sigma_n}\cdot\left(\frac{\sigma_e^2\beta_k}{\sigma_n^2\sigma_e^2\beta_k+\sigma_n^4(1+\sigma_e^2)}\right)^{-1}\cdot\left(\sigma_h^2\sigma_e^2\beta_k+\sigma_n^2\right)^{-1}\cdot\varsigma_k h'_{ik} = \frac{\sigma_n h'_{ik}}{\sigma_e^2\varsigma_k} \tag{5.31}$$

Following the fact that $\mathbf{z}_{0i} \sim \mathcal{CN}\left(\mathbf{U}^H\mathbf{B}^\dagger\mathbf{g}_i/\sigma_n, \mathbf{I}_{MQ_f}\right)$, we have

$$2\left|z_{0ik}\right|^2 \sim \chi_2^{'2}\left(2\left|\gamma_{0ik}\right|^2\right) = \chi_2^{'2}\left(\frac{2\sigma_n^2\left|h'_{ik}\right|^2}{\sigma_e^4\beta_k}\right) \tag{5.32}$$

where $\chi_k^{'2}(\lambda)$ denotes a non-central chi-square random variable with k degrees of freedom and non-centrality parameter λ. From (5.30) and (5.32), we know that the test statistic T_{II} under $\mathcal{H}_0$ is a weighted sum of non-central chi-square random variables, and thus, it can be approximated as below by using the approximation technique mentioned at the start of Section 5.3:

$$T_{\mathrm{II}} \sim \frac{1}{2}\sum_{i=1}^{N_a}\sum_{k=1}^{n}\frac{\sigma_e^2\beta_k}{\sigma_e^2\beta_k+\sigma_n^2(1+\sigma_e^2)}\chi_2^{'2}\left(\frac{2\sigma_n^2\left|h'_{ik}\right|^2}{\sigma_e^4\beta_k}\right) \doteq \theta_0\chi_{k_0}^2 \tag{5.33}$$

where χ_k^2 denotes a central chi-square random variable with k degrees of freedom. The condition that the first two moments of both sides of (5.33) are the same leads to

$$\begin{aligned}
&\tfrac{1}{2}\sum_{i=1}^{N_a}\sum_{k=1}^{n}\tfrac{\sigma_e^2\beta_k}{\sigma_e^2\beta_k+\sigma_n^2(1+\sigma_e^2)}\cdot\left(2+\tfrac{2\sigma_n^2\left|h'_{ik}\right|^2}{\sigma_e^4\beta_k}\right)=\theta_0 k_0\\
&\tfrac{1}{4}\sum_{i=1}^{N_a}\sum_{k=1}^{n}\tfrac{\sigma_e^4\beta_k^2}{[\sigma_e^2\beta_k+\sigma_n^2(1+\sigma_e^2)]^2}\cdot 2\cdot\left(2+\tfrac{4\sigma_n^2\left|h'_{ik}\right|^2}{\sigma_e^4\beta_k}\right)=2\theta_0^2 k_0
\end{aligned}\tag{5.34}$$

Solving the above equation for the parameters θ_0 and k_0 yields the following expressions:

$$\begin{aligned}
&\theta_0=\Omega_0/\mu_0,\qquad k_0=\mu_0^2/\Omega_0\\
&\mu_0=\tfrac{1}{2}\sum_{i=1}^{N_a}\sum_{k=1}^{n}\tfrac{\sigma_e^2\beta_k}{\sigma_e^2\beta_k+\sigma_n^2(1+\sigma_e^2)}\cdot\left(2+\tfrac{2\sigma_n^2\left|h'_{ik}\right|^2}{\sigma_e^4\beta_k}\right)=\sum_{k=1}^{n}\tfrac{N_a\sigma_e^4\beta_k+\sigma_n^2\rho_k}{\sigma_e^4\beta_k+\sigma_e^2\sigma_n^2(1+\sigma_e^2)}\\
&\Omega_0=\tfrac{1}{4}\sum_{i=1}^{N_a}\sum_{k=1}^{n}\tfrac{\sigma_e^4\beta_k^2}{[\sigma_e^2\beta_k+\sigma_n^2(1+\sigma_e^2)]^2}\cdot\left(2+\tfrac{4\sigma_n^2\left|h'_{ik}\right|^2}{\sigma_e^4\beta_k}\right)=\sum_{k=1}^{n}\tfrac{\beta_k\left(N_a\sigma_e^4\beta_k+2\sigma_n^2\rho_k\right)}{2[\sigma_e^2\beta_k+\sigma_n^2(1+\sigma_e^2)]^2}
\end{aligned}\tag{5.35}$$

Following (5.33), we can obtain the threshold for Detector II based on the choice of $\mathrm{Pr}_{\mathrm{FA}}$:

$$\eta_{\mathrm{II}}=\theta_0\mathcal{F}^{-1}_{\chi^2_{k_0}}\left(1-\mathrm{Pr}_{\mathrm{FA}}\right)\tag{5.36}$$

where $\mathcal{F}^{-1}_{\chi^2_k}$ is the inverse CDF of a central chi-square random variable with k degrees of freedom. We next consider the alternate hypothesis. Substituting (5.29) into (5.25) and letting $\mathbf{z}_{1i}=\mathbf{U}^H\left(\mathbf{w}'_i+\mathbf{C}^{-\frac{1}{2}}\left(\mathbf{d}_i+\mathbf{B}^\dagger\mathbf{g}_i\right)\right)$, we can express the test statistic T_{II} under $\mathcal{H}_1$ as below:

$$\begin{aligned}
T_{\mathrm{II}}&=\sum_{i=1}^{N_a}\mathbf{z}_{1i}^H\begin{bmatrix}\frac{1}{\sigma_n^2}\mathbf{I}_n-\left(\sigma_h^2\sigma_e^2\mathbf{\Xi}+\sigma_n^2\mathbf{I}_n\right)^{-1} & \mathbf{0}\\ \mathbf{0} & \mathbf{0}\end{bmatrix}\begin{bmatrix}\sigma_h^2\sigma_e^2\mathbf{\Xi}+\sigma_n^2\mathbf{I}_n & \mathbf{0}\\ \mathbf{0} & \sigma_n^2\mathbf{I}_{MQ_f-n}\end{bmatrix}\mathbf{z}_{1i}\\
&=\tfrac{1}{2}\sum_{i=1}^{N_a}\sum_{k=1}^{n}\tfrac{\sigma_h^2\sigma_e^2\beta_k}{\sigma_n^2}\left(2\left|z_{1ik}\right|^2\right)\qquad\text{Under }\mathcal{H}_1
\end{aligned}\tag{5.37}$$

where z_{1ik} is the k-th element of the vector $\mathbf{z}_{1i}$. Denote γ_{1ik} the k-th entry of the vector $\mathbf{U}^H\mathbf{C}^{-\frac{1}{2}}\left(\mathbf{d}_i+\mathbf{B}^\dagger\mathbf{g}_i\right)$, which is written as

$$\begin{aligned}\gamma_{1ik} &= \left(\sigma_h^2\sigma_e^2\beta_k+\sigma_n^2\right)^{-1/2}\left\{1+\left(\sigma_h^2\sigma_e^2\beta_k+\sigma_n^2\right)^{-1}\left(\frac{\sigma_e^2\beta_k}{\sigma_n^2\sigma_e^2\beta_k+\sigma_n^4(1+\sigma_e^2)}\right)^{-1}\right\}\frac{\varsigma_k h'_{ik}}{1+\sigma_e^2} \\ &= \left(\sigma_e^2\beta_k+\sigma_n^2(1+\sigma_e^2)\right)^{1/2}\cdot\frac{\sigma_h h'_{ik}}{\sigma_e^2\varsigma_k}\end{aligned} \tag{5.38}$$

Given $\mathbf{z}_{1i}\sim\mathcal{CN}\left(\mathbf{U}^H\mathbf{C}^{-\frac{1}{2}}\left(\mathbf{d}_i+\mathbf{B}^\dagger\mathbf{g}_i\right),\mathbf{I}_{MQ_f}\right)$, we have

$$2\left|z_{1ik}\right|^2\sim\chi_2'^2\left(2\left|\gamma_{1ik}\right|^2\right)=\chi_2'^2\left(\frac{2\sigma_h^2\left[\sigma_e^2\beta_k+\sigma_n^2(1+\sigma_e^2)\right]\left|h'_{ik}\right|^2}{\sigma_e^4\beta_k}\right) \tag{5.39}$$

From (5.37) and (5.39), the test statistic T_{II} under $\mathcal{H}_1$ is a weighted sum of non-central chi-square random variables, and similar to (5.33), we have the following central chi-square approximation:

$$T_{\mathrm{II}}\sim\frac{1}{2}\sum_{i=1}^{N_a}\sum_{k=1}^{n}\frac{\sigma_h^2\sigma_e^2\beta_k}{\sigma_n^2}\chi_2'^2\left(\frac{2\sigma_h^2\left[\sigma_e^2\beta_k+\sigma_n^2(1+\sigma_e^2)\right]\left|h'_{ik}\right|^2}{\sigma_e^4\beta_k}\right)\doteq\theta_1\chi_{k_1}^2 \tag{5.40}$$

Setting the first two moments of both sides of (5.40) to be the same yields

$$\begin{aligned}&\tfrac{1}{2}\sum_{i=1}^{N_a}\sum_{k=1}^{n}\tfrac{\sigma_h^2\sigma_e^2\beta_k}{\sigma_n^2}\cdot\left(2+\tfrac{2\sigma_h^2\left[\sigma_e^2\beta_k+\sigma_n^2(1+\sigma_e^2)\right]\left|h'_{ik}\right|^2}{\sigma_e^4\beta_k}\right)=\theta_1 k_1 \\ &\tfrac{1}{4}\sum_{i=1}^{N_a}\sum_{k=1}^{n}\tfrac{\sigma_h^4\sigma_e^4\beta_k^2}{\sigma_n^4}\cdot 2\cdot\left(2+\tfrac{4\sigma_h^2\left[\sigma_e^2\beta_k+\sigma_n^2(1+\sigma_e^2)\right]\left|h'_{ik}\right|^2}{\sigma_e^4\beta_k}\right)=2\theta_1^2 k_1\end{aligned} \tag{5.41}$$

The parameters θ_1 and k_1 can be solved from the above equation as below:

$$
\begin{aligned}
&\theta_1 = \Omega_1/\mu_1, \qquad k_1 = \mu_1^2/\Omega_1 \\
&\mu_1 = \tfrac{1}{2}\sum_{i=1}^{N_a}\sum_{k=1}^{n} \tfrac{\sigma_h^2\sigma_e^2\beta_k}{\sigma_n^2}\left(2 + \tfrac{2\sigma_h^2\left[\sigma_e^2\beta_k+\sigma_n^2(1+\sigma_e^2)\right]\left|h'_{ik}\right|^2}{\sigma_e^4\beta_k}\right) \\
&\quad = \tfrac{\sigma_h^2}{\sigma_n^2\sigma_e^2}\sum_{k=1}^{n}\left\{N_a\sigma_e^4\beta_k + \left(\sigma_h^2\sigma_e^2\beta_k + \sigma_n^2\right)\rho_k\right\} \\
&\Omega_1 = \tfrac{1}{4}\sum_{i=1}^{N_a}\sum_{k=1}^{n} \tfrac{\sigma_h^4\sigma_e^4\beta_k^2}{\sigma_n^4}\left(2 + \tfrac{4\sigma_h^2\left[\sigma_e^2\beta_k+\sigma_n^2(1+\sigma_e^2)\right]\left|h'_{ik}\right|^2}{\sigma_e^4\beta_k}\right) \\
&\quad = \tfrac{\sigma_h^4}{2\sigma_n^4}\sum_{k=1}^{n}\left\{N_a\sigma_e^4\beta_k^2 + 2\beta_k\left(\sigma_h^2\sigma_e^2\beta_k + \sigma_n^2\right)\rho_k\right\}
\end{aligned}
\tag{5.42}
$$

Based on (5.40), the theoretical probability of detection of Detector II can be given by

$$
\mathrm{Pr}_{\mathrm{D,II}} = 1 - \mathcal{F}_{\chi^2_{k_1}}\left(\tfrac{\eta_{\mathrm{II}}}{\theta_1}\right) \tag{5.43}
$$

where $\mathcal{F}_{\chi^2_k}$ is the CDF of a central chi-square random variable with k degrees of freedom.

5.3.3 Detector III: GLRT Detector

Detector III is the GLRT detector, which is a practical approach when unknown parameters exist [47]. The GLRT detector replaces the unknowns with their maximum likelihood (ML) estimates, and the decision rule is stated as

$$
\frac{\max\limits_{\mathbf{h}_1,\mathbf{h}_2,...,\mathbf{h}_{N_a}} \mathrm{PDF}(\mathbf{r}_1,\mathbf{r}_2,...,\mathbf{r}_{N_a}\,|\mathcal{H}_1,\mathbf{h}_1,\mathbf{h}_2,...,\mathbf{h}_{N_a})}{\mathrm{PDF}(\mathbf{r}_1,\mathbf{r}_2,...,\mathbf{r}_{N_a}\,|\mathcal{H}_0)} \underset{<\mathcal{H}_0}{>\mathcal{H}_1} \eta \tag{5.44}
$$

where $\mathrm{PDF}(\mathbf{r}_1,\mathbf{r}_2,...,\mathbf{r}_{N_a}\,|\mathcal{H}_1,\mathbf{h}_1,\mathbf{h}_2,...,\mathbf{h}_{N_a})$ is the PDF of the data under $\mathcal{H}_1$ when the vectors $\mathbf{h}_i$ are known. Taking the logarithm of (5.44), we can recast the GLRT rule as

$$
\sum_{i=1}^{N_a}\mathbf{r}_i^H\mathbf{r}_i - \sum_{i=1}^{N_a}\min_{\mathbf{h}_1,\mathbf{h}_2,...,\mathbf{h}_{N_a}}\left\|\mathbf{r}_i - \mathbf{Y}\mathbf{h}_i\right\|^2 \underset{<\mathcal{H}_0}{>\mathcal{H}_1} \eta' \tag{5.45}
$$

where $\|\cdot\|$ stands for the Euclidean norm. The second term in (5.45) achieves the minimum when [131]

$$\tilde{\mathbf{h}}_i = \left(\mathbf{Y}^H\mathbf{Y}\right)^\dagger \mathbf{Y}^H\mathbf{r}_i \tag{5.46}$$

where $i = 1, 2, ..., N_a$. Therefore, after some algebra, the GLRT detector is given by

$$T_{\mathrm{III}} = \sum_{i=1}^{N_a} \frac{2\mathbf{r}_i^H\mathbf{Y}\left(\mathbf{Y}^H\mathbf{Y}\right)^\dagger\mathbf{Y}^H\mathbf{r}_i}{\sigma_n^2} \begin{array}{l} >^{\mathcal{H}_1} \\ <_{\mathcal{H}_0} \end{array} \eta_{\mathrm{III}} \tag{5.47}$$

Invoking the SVD of $\mathbf{Y}$, T_{III} under $\mathcal{H}_0$ can be written as

$$T_{\mathrm{III}} = \sum_{i=1}^{N_a}\left(\tfrac{2}{\sigma_n^2}\mathbf{r}_i^H\mathbf{U}\begin{bmatrix}\mathbf{I}_n & \mathbf{0}\\ \mathbf{0} & \mathbf{0}\end{bmatrix}\mathbf{U}^H\mathbf{r}_i\right) = \sum_{i=1}^{N_a}\sum_{k=1}^{n}\tfrac{2}{\sigma_n^2}\left|\psi_{0ik}\right|^2 \sim \chi^2_{2nN_a} \tag{5.48}$$

The above result comes from the fact that the vector $\boldsymbol{\psi}_{0i} = \mathbf{U}^H\mathbf{r}_i \sim \mathcal{CN}\left(\mathbf{0}_{MQ_f}, \sigma_n^2\mathbf{I}_{MQ_f}\right)$ and ψ_{0ik} is the k-th element of $\boldsymbol{\psi}_{0i}$. Following (5.48), we can obtain the threshold for the GLRT detector based on the choice of $\mathrm{Pr}_{\mathrm{FA}}$:

$$\eta_{\mathrm{III}} = \mathcal{F}^{-1}_{\chi^2_{2nN_a}}\left(1 - \mathrm{Pr}_{\mathrm{FA}}\right) \tag{5.49}$$

From (5.47) and (5.49), only the value of $\mathbf{Y}$ is required to be known for Detector III at Array A in Figure 5.1. We next calculate the distribution of T_{III} under $\mathcal{H}_1$. Let the vector $\boldsymbol{\psi}_{1i} = \mathbf{U}^H\mathbf{C}^{-\frac{1}{2}}\mathbf{r}_i$ and we can rewrite (5.47) as

$$
\begin{aligned}
T_{\mathrm{III}} &= \sum_{i=1}^{N_a} \tfrac{2}{\sigma_n^2} \left\{ \boldsymbol{\psi}_{1i}^H \mathbf{U}^H \mathbf{C}^{\frac{1}{2}} \mathbf{Y} \left(\mathbf{Y}^H \mathbf{Y} \right)^{\dagger} \mathbf{Y}^H \mathbf{C}^{\frac{1}{2}} \mathbf{U} \boldsymbol{\psi}_{1i} \right\} \\
&= \sum_{i=1}^{N_a} \tfrac{2}{\sigma_n^2} \boldsymbol{\psi}_{1i}^H \begin{bmatrix} \sigma_h^2 \sigma_e^2 \boldsymbol{\Xi} + \sigma_n^2 \mathbf{I}_n & \mathbf{0} \\ \mathbf{0} & \mathbf{0} \end{bmatrix} \boldsymbol{\psi}_{1i} = \sum_{i=1}^{N_a} \sum_{k=1}^{n} \tfrac{1}{\sigma_n^2} \left(\sigma_h^2 \sigma_e^2 \beta_k + \sigma_n^2 \right) \left(2 \left| \psi_{1ik} \right|^2 \right)
\end{aligned} \tag{5.50}
$$

where ψ_{1ik} is the k-th entry of the vector $\boldsymbol{\psi}_{1i}$. Denote λ_{1ik} the k-th element of the vector $\mathbf{U}^H \mathbf{C}^{-1/2} \mathbf{d}_i$, which is given by

$$
\lambda_{1ik} = \left(\sigma_h^2 \sigma_e^2 \beta_k + \sigma_n^2 \right)^{-\frac{1}{2}} \cdot \sigma_h^2 \varsigma_k h'_{ik} \tag{5.51}
$$

Following the fact that $\boldsymbol{\psi}_{1i} \sim \mathcal{CN} \left(\mathbf{U}^H \mathbf{C}^{-\frac{1}{2}} \mathbf{d}_i, \mathbf{I}_{MQ_f} \right)$, we have

$$
2 \left| \psi_{1ik} \right|^2 \sim \chi_2^{'2} \left(2 \left| \lambda_{1ik} \right|^2 \right) = \chi_2^{'2} \left(\tfrac{2\sigma_h^2 \beta_k \left| h'_{ik} \right|^2}{\sigma_e^2 \beta_k + \sigma_n^2 (1+\sigma_e^2)} \right) \tag{5.52}
$$

From (5.50) and (5.52), it is clear that T_{III} is a weighted sum of several non-central chi-square random variables, and similar to (5.33), the test statistic can be approximated as a central chi-square random variable as follows:

$$
T_{\mathrm{III}} \sim \frac{1}{\sigma_n^2} \sum_{i=1}^{N_a} \sum_{k=1}^{n} \left(\sigma_h^2 \sigma_e^2 \beta_k + \sigma_n^2 \right) \chi_2^{'2} \left(\frac{2\sigma_h^2 \beta_k \left| h'_{ik} \right|^2}{\sigma_e^2 \beta_k + \sigma_n^2 (1+\sigma_e^2)} \right) \doteq \frac{\alpha}{\sigma_n^2} \chi_l^2 \tag{5.53}
$$

The condition that the first two moments of both sides of (5.53) are the same leads to

$$
\begin{aligned}
\sum_{k=1}^{n} \sum_{i=1}^{N_a} \left\{ \left(\sigma_h^2 \sigma_e^2 \beta_k + \sigma_n^2 \right) \cdot \left(2 + \tfrac{2\sigma_h^2 \beta_k \left| h'_{ik} \right|^2}{\sigma_e^2 \beta_k + \sigma_n^2 (1+\sigma_e^2)} \right) \right\} &= \alpha l \\
\sum_{k=1}^{n} \sum_{i=1}^{N_a} \left\{ \left(\sigma_h^2 \sigma_e^2 \beta_k + \sigma_n^2 \right)^2 \cdot 2 \cdot \left(2 + \tfrac{4\sigma_h^2 \beta_k \left| h'_{ik} \right|^2}{\sigma_e^2 \beta_k + \sigma_n^2 (1+\sigma_e^2)} \right) \right\} &= 2\alpha^2 l
\end{aligned} \tag{5.54}
$$

Solving the above equation for the parameters α and l yields the following expressions:

$$\begin{aligned}
&\alpha = b/a, \qquad l = a^2/b \\
&a = \sum_{k=1}^{n} 2\left\{N_a\left(\sigma_h^2\sigma_e^2\beta_k + \sigma_n^2\right) + \sigma_h^4\beta_k\rho_k\right\} \\
&b = \sum_{k=1}^{n} 2\left\{N_a\left(\sigma_h^2\sigma_e^2\beta_k + \sigma_n^2\right)^2 + 2\sigma_h^4\left(\sigma_h^2\sigma_e^2\beta_k + \sigma_n^2\right)\beta_k\rho_k\right\}
\end{aligned} \tag{5.55}$$

Hence, based on (5.53), the theoretical probability of detection of Detector III can be written as

$$\mathrm{Pr}_{\mathrm{D,III}} = 1 - \mathcal{F}_{\chi_l^2}\left(\frac{\eta_{\mathrm{III}}\sigma_n^2}{\alpha}\right) \tag{5.56}$$

5.4 Waveform Design

In this section, we propose three approaches to design the retransmitted waveform $\mathbf{Y}$ in order to improve the system detection performance. Notice here that all the schemes discussed in this section are under the transmit power constraint $\mathrm{trace}(\mathbf{Y}\mathbf{Y}^H) = ME_s$ which limits the total transmitted power.

5.4.1 Conventional Signal Scheme

We first introduce the conventional signal (CS) scheme similar to that in [118, 119] for comparison purposes in the numerical results presented in the next section. In the CS scheme, the same waveform is retransmitted from Array B regardless of the available channel information. In this chapter, we assume that the k-th element of the retransmitted signal vector $\mathbf{y}_m(f_q)$ in (5.4) is given by

$$y_{mk}(f_q) = \sqrt{\frac{E_s}{N_b Q_f}}\exp\left[j2\pi(k-1)(q-1)/Q_f\right] \tag{5.57}$$

where $k = 1, 2, ..., N_b$, $q = 1, 2, ..., Q_f$, and the normalization factor is employed here to meet

the power constraint.

5.4.2 Time Reversal Scheme

Before introducing the proposed waveform designs, we first briefly describe the TR scheme proposed in [118–120]. It is assumed that the number of snapshots during the probing and detection phases are the same, and for each snapshot, Array A transmits an incident waveform and the signals received by Array B are recorded, time reversed, power normalized, and transmitted back into the medium by Array B. The signal vector received by Array B at frequency f_q for the m-th snapshot is denoted by $\mathbf{x}_m(f_q)$ in (5.1), and the m-th retransmitted TR signal is given by

$$\mathbf{y}_m(f_q) = k_m \mathbf{x}_m^*(f_q) = k_m \left[\mathbf{H}^*(f_q)\mathbf{s}_m^*(f_q) + \mathbf{n}_{1,\mathrm{m}}^*(f_q)\right], \quad k_m = \sqrt{\frac{E_s}{\sum_{q=1}^{Q_f} \|\mathbf{x}_m(f_q)\|^2}} \tag{5.58}$$

where the superscript $*$ stands for the complex conjugate and k_m is a normalization factor to meet the power constraint. The conjugation here results from the fact that time reversal in the time domain corresponds to phase conjugation in the frequency domain up to a phase shift (see, *e.g.*, [99]).

It is assumed that the noise level at Array B, *i.e.*, the variance of the white Gaussian noise $\mathbf{n}_{1,\mathrm{m}}(f_q)$, is known in [118–120]. In this chapter, instead, we assume that the estimated channel matrix $\hat{\mathbf{H}}(f_q)$ and the estimation error variance σ_e^2 are known. In order to fairly compare the performance of different waveform schemes, we modified the TR scheme as follows:

$$\mathbf{y}_m(f_q) = \sqrt{E_s \Big/ \sum_{q=1}^{Q_f} \left\|\hat{\mathbf{H}}(f_q)\mathbf{s}_m(f_q)\right\|^2} \left[\hat{\mathbf{H}}^*(f_q)\mathbf{s}_m^*(f_q)\right] \tag{5.59}$$

Such a modification actually approximates $\mathbf{x}_m(f_q)$ as $\hat{\mathbf{H}}(f_q)\mathbf{s}_m(f_q)$, which is reasonable since $\hat{\mathbf{H}}(f_q)$ is estimated based on $\mathbf{x}_m(f_q)$ and σ_e^2 is a function of the noise level at Array B. We name this modified TR scheme as the matched-filter (MF) scheme in this chapter in order

to avoid confusion. Following the procedure mentioned in Section 5.2, we can generate the retransmitted MF signal matrix $\mathbf{Y}_{MF}$ by assembling all the MQ_f vectors $\mathbf{y}_m(f_q)$ appropriately. In general, the incident waveform can be any signal and in the simulations we adopt $s_{mk}(f_q) = \exp\left[j2\pi(k-1)(q-1)/Q_f\right]$ in (5.59) as in [120]. Here $s_{mk}(f_q)$ is the k-th entry of the vector $\mathbf{s}_m(f_q)$ and $k = 1, 2, ..., N_a$, $q = 1, 2, ..., Q_f$.

5.4.3 Waveform Design A: MF Upper Scheme

As demonstrated in [118–120], the TR scheme improves the system detection performance significantly. Our goal in this section is to further improve the performance by designing a waveform based on the MF scheme above, in order to maximize an upper bound of $\mathrm{Pr_D}$ for the GLRT detector. Before we proceed to the waveform design, several parameters are defined similar to (5.49) and (5.50):

$$\begin{aligned}
&\eta_{\mathrm{L}} = \mathcal{F}^{-1}_{\chi^2_{2N_a}}\left(1-\mathrm{Pr_{FA}}\right), \;\; \eta_{\mathrm{U}} = \mathcal{F}^{-1}_{\chi^2_{2\vartheta N_a}}\left(1-\mathrm{Pr_{FA}}\right) \\
&T_{\mathrm{U}} = \sum_{i=1}^{N_a}\sum_{k=1}^{\vartheta}\tfrac{1}{\sigma_n^2}\left(\sigma_h^2\sigma_e^2\beta_k+\sigma_n^2\right)\left(2\left|\psi_{1ik}\right|^2\right) \\
&\quad = T_{\mathrm{III}} + \sum_{i=1}^{N_a}\sum_{k=n+1}^{\vartheta}\tfrac{1}{\sigma_n^2}\left(\sigma_h^2\sigma_e^2\beta_k+\sigma_n^2\right)\left(2\left|\psi_{1ik}\right|^2\right) \triangleq T_{\mathrm{III}} + T_{\mathrm{D}}
\end{aligned} \tag{5.60}$$

where $\vartheta = \min(N_b Q_f, MQ_f)$ and the second term in the last row is defined as T_{D}. Since n is the rank of $\mathbf{Y}$ and β_k is the square of the k-th singular value of $\mathbf{Y}$, we have $1 \le n \le \vartheta$ and $\beta_k = 0$ when $k > n$. Therefore, $2\left|\psi_{1ik}\right|^2 \sim \chi_2'^2\left(2\left|\lambda_{1ik}\right|^2\right) = \chi_2^2$ for $k > n$ and hence $T_{\mathrm{D}} \sim \chi^2_{2N_a(\vartheta-n)}$. It is not difficult to derive the following inequalities:

$$\eta_{\mathrm{U}} \ge \eta_{\mathrm{III}} \ge \eta_{\mathrm{L}} > 0, \quad T_{\mathrm{U}} = T_{\mathrm{III}} + T_{\mathrm{D}}, \quad T_{\mathrm{III}} > 0, \quad T_{\mathrm{D}} \ge 0 \tag{5.61}$$

The reason for defining the above parameters is that the goal of the waveform design is to derive the optimal value of the matrix $\mathbf{Y}$ based on a certain criterion. Therefore, it is impossible to know the rank of the "designed" $\mathbf{Y}$ before the waveform design process, and thereby the threshold and test statistic in (5.49) and (5.50) can not be employed directly during the design process because of the unknown value of n. Following (5.61), we can derive the required upper

bound of $\mathrm{Pr_D}$ for the GLRT detector as below:

$$\mathrm{Pr_D} = \Pr\{T_{\mathrm{III}} \geq \eta_{\mathrm{III}}\} \leq \Pr\{T_{\mathrm{III}} \geq \eta_{\mathrm{L}}\} \leq \Pr\{T_{\mathrm{U}} \geq \eta_{\mathrm{L}}\} \leq \mathrm{E}[T_{\mathrm{U}}]/\eta_{\mathrm{L}} \tag{5.62}$$

where the last inequality arises from Markov's inequality [145]. Taking the expectation of T_{U} in (5.60) yields

$$\mathrm{E}[T_{\mathrm{U}}] = \frac{2\sigma_h^4}{\sigma_n^2} \sum_{k=1}^{\vartheta} \left\{ N_a \sigma_n^2 \left(1+\sigma_e^2\right)^2 + \left[N_a \sigma_e^2 \left(1+\sigma_e^2\right) + \rho_k \right] \beta_k \right\} \tag{5.63}$$

where $\rho_k = \sum_{i=1}^{N_a} |h'_{ik}|^2 = \sum_{i=1}^{N_a} \mathbf{v}_k^H \hat{\mathbf{h}}_i \hat{\mathbf{h}}_i^H \mathbf{v}_k$ and $\mathbf{v}_k$ is the k-th right-singular vector of $\mathbf{Y}_{MF}$ introduced in the last section. Note here that the entries of $\boldsymbol{\beta}$ are actually the eigenvalues of the Hermitian matrix $\mathbf{Y}\mathbf{Y}^H$, and thus, the power constraint can be rewritten as

$$\sum_{k=1}^{\vartheta} \beta_k = ME_s, \;\; \beta_k \geq 0, \;\; k = 1, 2, ..., \vartheta \tag{5.64}$$

Therefore, the design criterion under the power constraint can be expressed as the following constrained maximization problem:

$$\max_{\boldsymbol{\beta}} \sum_{k=1}^{\vartheta} \left[N_a \sigma_e^2 \left(1+\sigma_e^2\right) + \rho_k \right] \beta_k, \quad \text{s.t.} \sum_{k=1}^{\vartheta} \beta_k = ME_s, \beta_k \geq 0, k = 1, 2, ..., \vartheta \tag{5.65}$$

Considering the fact that $[N_a \sigma_e^2 \left(1+\sigma_e^2\right) + \rho_k]$ is positive and taking into account the constraints, we can derive the following equation employing Abel's inequality [146]:

$$\begin{aligned}&\sum_{k=1}^{\vartheta}\left[N_a\sigma_e^2\left(1+\sigma_e^2\right)+\rho_k\right]\beta_k \leq \max\left\{\beta_1,\beta_1+\beta_2,...,\sum_{k=1}^{\vartheta}\beta_k\right\}\cdot\max\left\{N_a\sigma_e^2\left(1+\sigma_e^2\right)+\rho_k\right\}\\&= ME_s\cdot\left[N_a\sigma_e^2\left(1+\sigma_e^2\right)+\max\left\{\rho_k\right\}\right]\end{aligned} \tag{5.66}$$

Observing the above equation, it is easy to understand that the maximization of (5.65) is achieved by allocating all the available power to the eigenvalue β_k which corresponds to the largest ρ_k.

5.4.4 Waveform Design B: MF Lower Scheme

Now we consider the second waveform design from the viewpoint of maximizing a lower bound of $\mathrm{Pr_D}$ for the GLRT detector based on the MF scheme. Similar to the last section, (5.61) leads to

$$\mathrm{Pr_D}=\Pr\left\{T_{\mathrm{III}}\geq\eta_{\mathrm{III}}\right\}\geq 1-\Pr\left\{T_{\mathrm{III}}\leq\eta_{\mathrm{U}}\right\}\geq 1-\frac{\Pr\{T_{\mathrm{III}}+T_{\mathrm{D}}\leq 2\eta_{\mathrm{U}}\}}{\Pr\{T_{\mathrm{D}}\leq\eta_{\mathrm{U}}\}} \tag{5.67}$$

In addition, recalling the distribution of T_{D} and the definition of η_{U}, we have

$$\Pr\left\{T_{\mathrm{D}}\leq\eta_{\mathrm{U}}\right\}=1-\Pr\left\{\chi^2_{2N_a(\vartheta-n)}\geq\eta_{\mathrm{U}}\right\}\geq 1-\Pr\left\{\chi^2_{2N_a\vartheta}\geq\eta_{\mathrm{U}}\right\}=\mathrm{Pr_{FA}} \tag{5.68}$$

Substituting (5.68) into (5.67) and utilizing Markov's inequality again, we can derive the required lower bound of $\mathrm{Pr_D}$ for the GLRT detector as follows:

$$\mathrm{Pr_D}\geq 1-\frac{\Pr\{T_{\mathrm{U}}\leq 2\eta_{\mathrm{U}}\}}{\mathrm{Pr_{FA}}}=1-\frac{\Pr\left\{e^{-\sigma_n^2T_{\mathrm{U}}}\geq e^{-2\sigma_n^2\eta_{\mathrm{U}}}\right\}}{\mathrm{Pr_{FA}}}\geq 1-\frac{\mathrm{E}\left[e^{-\sigma_n^2T_{\mathrm{U}}}\right]}{e^{-2\sigma_n^2\eta_{\mathrm{U}}}\cdot\mathrm{Pr_{FA}}} \tag{5.69}$$

Due to the fact that $\left[-\left(\sigma_h^2\sigma_e^2\beta_k+\sigma_n^2\right)\right]<0$ and given the statistical independence of $2\left|\psi_{1ik}\right|^2$ for different values of i and k, the following equation can be obtained for the moment generating function of the non-central chi-square distribution:

$$\begin{aligned}\mathrm{E}\left[e^{-\sigma_n^2 T_{\mathrm{U}}}\right] &= \prod_{k=1}^{\vartheta}\prod_{i=1}^{N_a}\mathrm{E}\left[e^{-\left(\sigma_h^2\sigma_e^2\beta_k+\sigma_n^2\right)\left(2|\psi_{1ik}|^2\right)}\right] \\ &= \prod_{k=1}^{\vartheta}\prod_{i=1}^{N_a}\frac{\exp\left(\frac{-2\sigma_h^4\beta_k|h'_{ik}|^2}{1+2\left(\sigma_h^2\sigma_e^2\beta_k+\sigma_n^2\right)}\right)}{1+2\left(\sigma_h^2\sigma_e^2\beta_k+\sigma_n^2\right)} = \prod_{k=1}^{\vartheta}\frac{\exp\left(\frac{-2\sigma_h^4\beta_k\rho_k}{1+2\left(\sigma_h^2\sigma_e^2\beta_k+\sigma_n^2\right)}\right)}{\left[1+2\left(\sigma_h^2\sigma_e^2\beta_k+\sigma_n^2\right)\right]^{Na}}\end{aligned} \tag{5.70}$$

Taking the logarithm and making use of the inequality $\log(1+x) > \frac{x}{1+x}$ when $x > -1$ and $x \neq 0$, we can express the problem of maximizing the lower bound of $\mathrm{Pr_D}$ with the power constraint as below:

$$\max_{\boldsymbol{\beta}} \sum_{k=1}^{\vartheta}\left\{\frac{2\beta_k\rho_k+2N_a\left(\sigma_h^2\sigma_e^2\beta_k+\sigma_n^2\right)}{1+2\left(\sigma_h^2\sigma_e^2\beta_k+\sigma_n^2\right)}\right\}, \quad \text{s.t.} \sum_{k=1}^{\vartheta}\beta_k = ME_s, \beta_k \geq 0, k = 1, 2, ..., \vartheta \tag{5.71}$$

We solve the above constrained optimization problem by using the method of Lagrange multipliers [24] and applying the Karush-Kuhn-Tucker (KKT) conditions [147]. The solution for the waveform design criterion (5.71) can be written as

$$\beta_k = \frac{1+2\sigma_n^2}{2\sigma_h^2\sigma_e^2}\left(\frac{\sqrt{2\rho_k+4\rho_k\sigma_n^2+2N_a\sigma_h^2\sigma_e^2}}{1+2\sigma_n^2}\xi - 1\right)^+ \tag{5.72}$$

where $(a)^+ \triangleq \max(0, a)$ and ξ is chosen such that the power constraint is met:

$$\sum_{k=1}^{\vartheta}\left(\frac{\sqrt{2\rho_k+4\rho_k\sigma_n^2+2N_a\sigma_h^2\sigma_e^2}}{1+2\sigma_n^2}\xi - 1\right)^+ = \frac{2ME_s\sigma_h^2\sigma_e^2}{1+2\sigma_n^2} \tag{5.73}$$

It is clearly seen from above equation that this design scheme actually utilizes the waterfilling strategy [122] to allocate the transmitted power, and the larger the ρ_k is, the more power is allocated to the corresponding β_k.

REMARK 1: Both waveform designs introduced above select the values of β_k according to

the ρ_k values, which are determined by the estimated channel vectors as well as the right-singular vectors of $\mathbf{Y}_{MF}$. Recalling the physical explanation of the SVD, we can split the design procedure into two separate parts. The "path directions" of the designed waveform are determined by the MF scheme, and the waveform design A and B allocate the retransmitted power to each direction according to the "path quality" following different design criteria. We emphasize this by naming the design schemes as "MF upper" and "MF lower", respectively. The reason for utilizing the MF scheme, *i.e.*, a modified TR scheme, is that [118–120] have shown that TR is able to significantly improve the detection performance, and we want to achieve further performance improvements. Furthermore, although the theoretical derivation for both schemes are based on the GLRT detector, Detector I and II can also be employed when the designed waveforms are retransmitted from Array B, and their performance can be easily calculated using the formulae (5.13) and (5.28) or (5.16) and (5.43).

5.4.5 Waveform Design C: Mutual Information (MI) Scheme

In this section, we design the waveform by maximizing the lower bound of the mutual information (MI) between the retransmitted and received signals. First of all, rewrite the $N_aQ_f \times 1$ received signal vector for one snapshot as

$$\mathbf{r}=\left[\mathbf{r}^T(f_1),\mathbf{r}^T(f_2),\cdots,\mathbf{r}^T(f_{Q_f})\right]^T=\mathbf{H}_Q^T\mathbf{y}+\mathbf{n},\ \mathbf{y}=\left[\mathbf{y}^T(f_1),\mathbf{y}^T(f_2),\cdots,\mathbf{y}^T(f_{Q_f})\right]^T \quad (5.74)$$

where the $N_a \times 1$ vector $\mathbf{r}(f_q)$ and the $N_b \times 1$ vector $\mathbf{y}(f_q)$ contain the signals received by all the N_a antennas of Array A and the signals retransmitted from all the N_b antennas of Array B at frequency f_q, respectively. The elements of the $N_aQ_f\times 1$ noise vector $\mathbf{n}$ are zero-mean complex Gaussian random variables with variance σ_n^2. The $N_bQ_f\times N_aQ_f$ matrix $\mathbf{H}_Q$ is a block diagonal matrix with the Q_f matrices $\mathbf{H}(f_q)$ arranged sequentially along its main diagonal blocks. We also define the $N_bQ_f \times N_aQ_f$ estimated channel matrix $\hat{\mathbf{H}}_Q$ in the same way. Assuming $\mathbf{y}$ is a random vector, the considered MI is

$$I\left(\mathbf{r},\mathbf{y}|\,\hat{\mathbf{H}}_Q\right)=h\left(\mathbf{y}|\,\hat{\mathbf{H}}_Q\right)-h\left(\mathbf{y}|\,\mathbf{r},\hat{\mathbf{H}}_Q\right) \quad (5.75)$$

where $h(\cdot)$ stands for the differential entropy. The above MI can be interpreted as the amount of uncertainty in the received signal $\mathbf{r}$ which is removed by knowing $\mathbf{y}$ given $\hat{\mathbf{H}}_Q$. Intuitively, the larger the MI, the less uncertain the received signal, and thus the better the system performance. Following the conclusion stated in Appendix I in [141] that the second term on the right-hand side of (5.75) is upper bounded by the entropy of a Gaussian random variable whose variance is equal to the mean square error of the linear MMSE estimate of $\mathbf{y}$ given $\mathbf{r}$ and $\hat{\mathbf{H}}_Q$, we can derive the lower bound of the MI as below:

$$\begin{aligned} I\left(\mathbf{r},\mathbf{y}|\hat{\mathbf{H}}_Q\right) &\geq \log_2 \frac{\det(\pi e \mathbf{C}_{\mathbf{y}})}{\det\left(\pi e \mathbf{C}_{\mathbf{y}|\mathbf{r},\hat{\mathbf{H}}_Q}\right)} = \log_2 \frac{\det(\pi e \mathbf{C}_{\mathbf{y}})}{\det\left(\pi e \left[\mathbf{C}_{\mathbf{y}} - \sigma_h^4 \mathbf{C}_{\mathbf{y}} \hat{\mathbf{H}}_Q^* \left(\sigma_h^4 \hat{\mathbf{H}}_Q^T \mathbf{C}_{\mathbf{y}} \hat{\mathbf{H}}_Q^* + \mathbf{C}_\omega\right)^{-1} \hat{\mathbf{H}}_Q^T \mathbf{C}_{\mathbf{y}}\right]\right)} \\ &= \log_2 \det\left(\mathbf{I}_{N_b Q_f} + \sigma_h^4 \hat{\mathbf{H}}_Q^* \mathbf{C}_\omega^{-1} \hat{\mathbf{H}}_Q^T \mathbf{C}_{\mathbf{y}}\right) \triangleq I_{\mathrm{L}}\left(\mathbf{r}, \mathbf{y} | \hat{\mathbf{H}}_Q\right) \end{aligned} \tag{5.76}$$

where $\det(\cdot)$ represents the determinant of a matrix, $\mathbf{C}_{\mathbf{y}}$ stands for the covariance matrix of $\mathbf{y}$ given $\hat{\mathbf{H}}_Q$, and $\mathbf{C}_{\mathbf{y}|\mathbf{r},\hat{\mathbf{H}}_Q}$ denotes the covariance matrix of $\mathbf{y}$ given $\mathbf{r}$ and $\hat{\mathbf{H}}_Q$. The $N_a Q_f \times N_a Q_f$ matrix $\mathbf{C}_\omega$ is a block diagonal matrix, whose q-th diagonal block is a $N_a \times N_a$ matrix $\left[\sigma_h^2 \sigma_e^2 P(f_q) + \sigma_n^2\right] \cdot \mathbf{I}_{N_a}$ and $P(f_q) = \mathrm{E}\left[\mathbf{y}^H(f_q)\mathbf{y}(f_q)\right]$. Note that the Hermitian matrix $\hat{\mathbf{H}}^*(f_q)\hat{\mathbf{H}}^T(f_q)$ can be factorized through its eigenvalue decomposition, *i.e.*,

$$\hat{\mathbf{H}}^*(f_q)\hat{\mathbf{H}}^T(f_q) = \boldsymbol{\mathcal{V}}(f_q)\boldsymbol{\mathcal{D}}(f_q)\boldsymbol{\mathcal{V}}^H(f_q) \tag{5.77}$$

where the $N_b \times N_b$ matrix $\boldsymbol{\mathcal{V}}(f_q)$ is a unitary matrix whose columns are eigenvectors and $\boldsymbol{\mathcal{D}}(f_q)$ is a diagonal matrix with N_b real and nonnegative eigenvalues $\Lambda_{q1}, \Lambda_{q2}, \cdots, \Lambda_{qN_b}$ (in decreasing order) as its diagonal entries. We next define the $N_b Q_f \times N_b Q_f$ block diagonal matrices $\boldsymbol{\mathcal{G}}_Q$ and $\boldsymbol{\mathcal{V}}_Q$, whose q-th diagonal blocks are $\sigma_h^4 \boldsymbol{\mathcal{D}}(f_q) / \left[\sigma_n^2 + \sigma_h^2 \sigma_e^2 P(f_q)\right]$ and $\boldsymbol{\mathcal{V}}(f_q)$, respectively. Recalling that $\det(\mathbf{I}_a + \mathbf{AB}) = \det(\mathbf{I}_b + \mathbf{BA})$, the lower bound of the MI in (5.76) can be rewritten as

$$I_{\mathrm{L}}\left(\mathbf{r}, \mathbf{y} | \hat{\mathbf{H}}_Q\right) = \log_2 \det\left[\mathbf{I}_{N_b Q_f} + \boldsymbol{\mathcal{V}}_Q \boldsymbol{\mathcal{G}}_Q \boldsymbol{\mathcal{V}}_Q^H \mathbf{C}_{\mathbf{y}}\right] = \log_2 \det\left[\mathbf{I}_{N_b Q_f} + \boldsymbol{\mathcal{G}}_Q \boldsymbol{\mathcal{Q}}\right] \tag{5.78}$$

where $\boldsymbol{\mathcal{Q}} = \boldsymbol{\mathcal{V}}_Q^H \mathbf{C}_\mathbf{y} \boldsymbol{\mathcal{V}}_Q$ is an $N_b Q_f \times N_b Q_f$ matrix. Hadamard's inequality states that given an $N \times N$ positive semi-definite Hermitian matrix $\mathbf{A}$ with (i,j)-th entry a_{ij}, then $\det(\mathbf{A}) \leq \prod_{i=1}^{N} a_{ii}$ and the equality is achieved if and only if $\mathbf{A}$ is diagonal [70]. Thus, (5.78) achieves its maximum value when $\mathbf{I}_{N_b Q_f} + \boldsymbol{\mathcal{G}}_Q \boldsymbol{\mathcal{Q}}$ is diagonal. Remembering that the diagonal matrix $\boldsymbol{\mathcal{G}}_Q$ has nonnegative diagonal entries and $\mathbf{C}_\mathbf{y}$ is a covariance matrix, we conclude that $\boldsymbol{\mathcal{Q}}$ must be a diagonal matrix whose $\{(q-1)N_b + k\}$-th diagonal element is a nonnegative value $\mathcal{Q}_{qk}$, $q = 1, 2, ..., Q_f$ and $k = 1, 2, ..., N_b$. In addition, the power constraint is given by

$$E_s = \mathrm{E}\left[\mathbf{y}^H \mathbf{y}\right] = \mathrm{trace}\left(\mathbf{C}_\mathbf{y}\right) = \mathrm{trace}\left(\boldsymbol{\mathcal{Q}}\right) \tag{5.79}$$

Therefore, the waveform design criterion maximizing the lower bound of the MI under the power constraint can be expressed as below:

$$\begin{aligned} &\max_{\boldsymbol{\mathcal{Q}}} \sum_{q=1}^{Q_f} \sum_{k=1}^{N_b} \log_2 \left\{ 1 + \frac{\sigma_h^4 \Lambda_{qk} \mathcal{Q}_{qk}}{\sigma_n^2 + \sigma_h^2 \sigma_e^2 P(f_q)} \right\} \\ &\text{s.t.} \quad \sum_{q=1}^{Q_f} \sum_{k=1}^{N_b} \mathcal{Q}_{qk} = E_s, \quad \mathcal{Q}_{qk} \geq 0, \quad q = 1, 2, ..., Q_f, \quad k = 1, 2, ..., N_b \end{aligned} \tag{5.80}$$

Notice here that by virtue of the presence of $P(f_q) = \mathrm{E}\left[\mathbf{y}^H(f_q)\mathbf{y}(f_q)\right] = \sum_{k=1}^{N_b} \mathcal{Q}_{qk}$ in the denominator, (5.80) is not a concave function. However, for a fixed set of values for $P(f_q)$, the function becomes concave and thus it can be directly optimized. Hence, an iterative algorithm is proposed here, and the values of $P(f_q)$ are updated in each iteration until the algorithm converges. We initialize the algorithm by allocating equal power to all the Q_f frequencies, that is, $P(f_q, 0) = E_s/Q_f$ for $q = 1, 2, ..., Q_f$. For the i-th iteration ($i \geq 1$), replacing $P(f_q)$ in (5.80) by $P(f_q, i-1)$ and applying the KKT conditions [147] leads to the solution

$$\mathcal{Q}_{qk}(i) = \left(\zeta(i) - \frac{\sigma_n^2 + \sigma_h^2 \sigma_e^2 P(f_q, i-1)}{\sigma_h^4 \Lambda_{qk}} \right)^+ \tag{5.81}$$

where the water-level $\zeta(i)$ can be found by solving

$$\sum_{q=1}^{Q_f}\sum_{k=1}^{N_b}\left(\zeta(i)-\frac{\sigma_n^2+\sigma_h^2\sigma_e^2P(f_q,i-1)}{\sigma_h^4\Lambda_{qk}}\right)^+=E_s \tag{5.82}$$

Then, the values of $P(f_q)$ for the i-th iteration are updated as $P(f_q,i)=\sum_{k=1}^{N_b}\mathcal{Q}_{qk}(i)$ and the iteration ends if $\max|P(f_q,i)-P(f_q,i-1)|\leq\varepsilon$ for all the Q_f frequencies, where ε is a threshold with small value. After the values of $\mathcal{Q}_{qk}$ are determined, we have the covariance matrix $\mathbf{C_y}=\boldsymbol{\mathcal{V}}_Q\boldsymbol{\mathcal{Q}}\boldsymbol{\mathcal{V}}_Q^H$.

Notice here that when $N_a<N_b$, a small modification is required to be made to the above algorithm. Obviously, $\Lambda_{qk}=0$ for $k=N_a+1,N_a+2,...,N_b$, and from (5.80), it is clear that the corresponding $\mathcal{Q}_{qk}$ should be equal to zero in order to maximize the lower bound. Thus, when $N_a<N_b$, the limit of k is changed from N_b to N_a in (5.80)-(5.82) and the values of $\mathcal{Q}_{qk}$ are determined for $k=1,2,...,N_a$ using the algorithm mentioned before. Next, setting $\mathcal{Q}_{qk}=0$ for $k=N_a+1,N_a+2,...,N_b$ gives us the $N_bQ_f\times N_bQ_f$ diagonal matrix $\boldsymbol{\mathcal{Q}}$.

Once $\mathbf{C_y}$ is determined, we generate a set of deterministic vectors $\{\mathbf{y}_1,\mathbf{y}_2,\cdots,\mathbf{y}_M\}$ as the retransmitted signals vectors for the M snapshots. These vectors are appropriately designed such that their covariance matrix remains as $\mathbf{C_y}$. The block diagonal structure of $\mathbf{C_y}$ implies that the retransmitted signals at different frequencies are mutually orthogonal. Such orthogonality can be realized, for example, by designing the retransmitted signal using the orthogonal frequency division multiplexing (OFDM) scheme [148]. Denoting the k-th column of $\boldsymbol{\mathcal{V}}(f_q)$ by $\mathbf{v}_k(f_q)$, we generate the signals retransmitted from Array B at frequency f_q for the m-th snapshot by using an orthogonal basis as below:

$$\mathbf{y}_m(f_q)=\sum_{k=1}^{N_b}\mathbf{v}_k(f_q)\sqrt{\mathcal{Q}_{qk}}\mathcal{O}_{km},\qquad\sum_{m=1}^{M}\mathcal{O}_{km}\mathcal{O}_{lm}^*=M\delta_{kl} \tag{5.83}$$

where $m=1,2,...,M$, $k,l=1,2,...,N_b$, and δ_{kl} represents the Dirac delta function. The $N_bQ_f\times 1$ signal vector $\mathbf{y}_m$ is obtained by sequentially stacking all the Q_f vectors $\mathbf{y}_m(f_q)$ into a vector. Walsh codes are adopted as the basis functions in the simulations, but any other orthogonal bases could also be employed in principle. From (5.83), we can calculate that the

covariance matrix of the generated vectors equals $\mathbf{C_y}$ and the power constraint has been met. After all the M snapshots $\{\mathbf{y}_m\}$ are generated, the retransmitted signal matrix $\mathbf{Y}$ can be easily obtained by reshaping $\{\mathbf{y}_m\}$ appropriately. Its corresponding system performance for all the three detectors can be evaluated using the formulae provided in Section 5.3.

REMARK 2: From the simulation we find that normally the iterative algorithm converges after a few iterations (less than 20 for $\varepsilon = 0.001$). However, at very low signal-to-noise ratios (SNRs) and when the difference between the largest two values of Λ_{qk} is very small, the algorithm can enter an endless loop by allocating all the power to their corresponding power allocations $\mathcal{Q}_{qk}$ in turn. From (5.81), it is not difficult to understand that this problem can happen when the difference between the numerators for two successive iterations $\sigma_e^2\left(1+\sigma_e^2\right)|P(f_q,i)-P(f_q,i-1)|$ is large enough. The lower the SNR, the larger the value of σ_e^2, and this is the reason why such a problem only occurs at very low SNRs. To solve this problem, we terminate the algorithm if the number of iterations exceeds a selected value and choose the results obtained in the last iteration as the final solution. This approach is reasonable since if there are two coefficients Λ_{qk} having similar values, then allocating the power to either of them leads to similar system performance.

5.5 Numerical Results and Discussion

In this section, we present numerical results showing the target detection performance of a MIMO system with different detectors and different retransmitted waveforms. We set $\mathrm{Pr_{FA}} = 0.001$ and define the SNR as $\mathrm{SNR} = E_s/\sigma_n^2$ with E_s normalized to 1. As mentioned before, the value of σ_e^2 depends on the estimation method and the waveform length during the probing phase, which is inversely proportional to the SNR at Array B [144]. Since we focus on the detection phase and system performance when channel estimation errors exist, we assume that the noise level at Array B is in proportion to that at Array A and set $\sigma_e^2 = \sigma_n^2$ in all the simulations. Notice here that the algorithms for both the detector and waveform designs are based on the estimated channel $\hat{\mathbf{H}}(f_q)$, which is the sum of the true channel and the estimation error. Therefore, we utilize a semi-analytical approach to obtain the system performance. In other words, we generate $10,000$ realizations of the true channel and the estimation error matrix, calculate the corresponding $\mathrm{Pr_D}$ for each realization using (5.16), (5.43), and (5.56), and obtain the theoretical system detection performance by averaging $\mathrm{Pr_D}$ over all the realizations. The system performance recorded from Monte Carlo simulations is also presented to validate the

correctness of the derived formulae. For each realization of the estimated channel matrix, we generate 10,000 independent received signals, compute their test statistics, and compare them with the threshold. The percentage of the number of times that the test statistic exceeds the threshold is the simulated probability of detection.

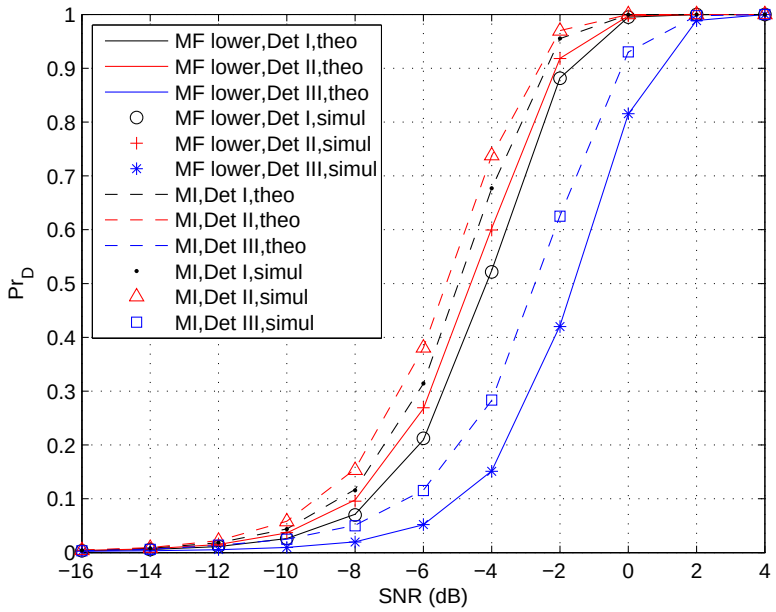

Figure 5.2: *Theoretical and simulated probability of detection as a function of the SNR for systems with different detectors when* $N_a = N_b = 4$ *and* $M = 5$

We first examine the performance of a system with four sensors at both Arrays A and B, choosing $M = 5$ and $Q_f = 6$ for simulation purposes only. Notice here that the number of snapshots M only applies to the detection phase, and the waveform transmitted from Array A during the probing phase is not specified, but leads to the situation that the estimation error variance $\sigma_e^2 = \sigma_n^2$. Figure 5.2 depicts the detection performance of the system employing different detectors when two kinds of designed waveforms, the MF lower and MI schemes, are adopted. Obviously, the simulated results agree well with the theoretical values, validating the correctness of the derived formulae. Comparing the curves corresponding to the same retransmitted waveform, we find that Detector II performs the best under any circumstance, which is consistent with the fact that Detector II is the optimal detector in the Neyman-Pearson sense. In addition, the performance difference between Detector I and Detector II decreases as the SNR becomes higher, *i.e.*, σ_e^2 is smaller. This can be explained by the fact that both the optimal detector when the channel matrix is known and Detector I are in the form of matched filters, and

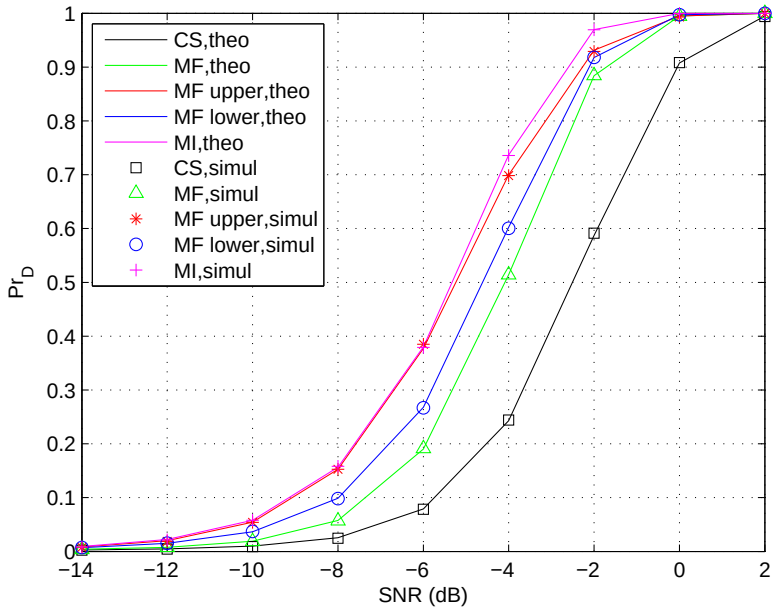

Figure 5.3: *Theoretical and simulated probability of detection as a function of the SNR for systems with different retransmitted waveforms when $N_a = N_b = 4$, $M = 5$, and Detector II is employed*

the only difference is that the former matches to the true channel $\mathbf{H}$ while the latter matches to the estimated channel $\hat{\mathbf{H}}$ [47]. When σ_e^2 has a small value, the estimation error in the estimated channel is insignificant, and thus the difference between the performance of Detector I and the optimal performance should be small. Furthermore, it is easily seen that Detector III performs the poorest at low SNR but is similar to the optimal detector when the SNR is high. This is because the GLRT detector actually estimates the unknown parameters first and then makes the detection decision based on them. Intuitively, the lower the SNR, the worse the estimation, which degrades the detection performance. However, although Detector II performs the best, it requires knowledge of $\mathbf{Y}$, $\hat{\mathbf{h}}_i$, and σ_e^2 at Array A. In contrast, as mentioned in Section 5.3, the implementation of Detector I needs the information of $\mathbf{Y}$ and $\hat{\mathbf{h}}_i$, while for Detector III only $\mathbf{Y}$ is required to be known.

We next compare the detection performance of the systems retransmitting different waveforms as shown in Figure 5.3 and Figure 5.4 for low and high SNRs, respectively. Here, Detector II is employed for all the scenarios, and any difference in performance arises from the designed waveforms only. In order to demonstrate the advantage of the MF scheme, we also present the system performance when the CS scheme is adopted. It is clear that there is very good agree-

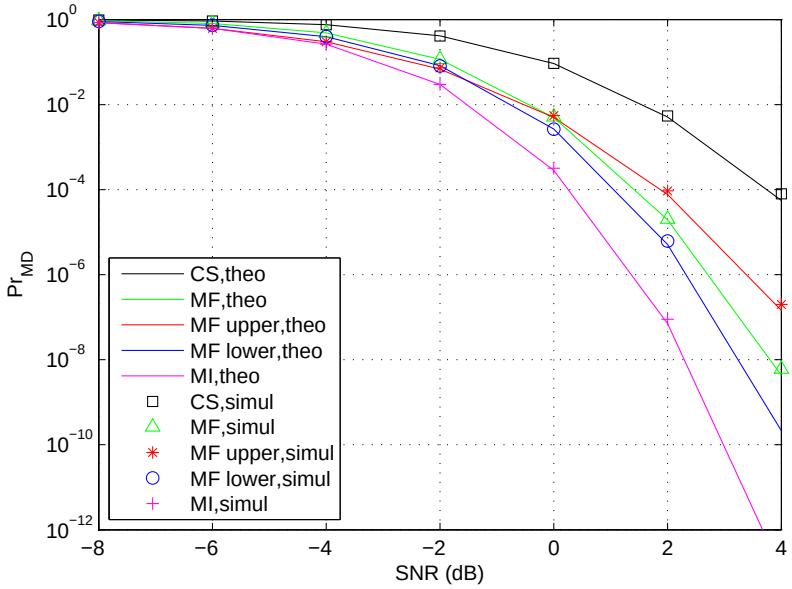

Figure 5.4: *Theoretical and simulated probability of missed detection as a function of the SNR for systems with different retransmitted waveforms when $N_a = N_b = 4$, $M = 5$, and Detector II is employed*

ment between the theoretical and simulated performance. Obviously, the MF scheme provides much better performance than the CS approach, and all the three proposed waveform designs further improve the system performance significantly with respect to the MF scheme. We start by comparing the MF upper and lower schemes. At low SNR, the MF upper is superior, while the MF lower is preferred when SNR is high. In addition, the MF lower always outperforms the MF approach, but the MF upper performs worse than the MF scheme when SNR is high enough. Such results are reasonable since one should concentrate all the available power on the path with the best quality in order to overcome the high level of noise at low SNR, which is the idea of the MF upper method. As the SNR becomes higher, the noise level and consequently the estimation error variance σ_e^2 decreases, and thus allocating power to several paths according to their amplitudes, *i.e.*, the waterfilling strategy utilized in the MF lower approach, leads to better detection reliability because of the spatial diversity gain. Furthermore, it is clear from Figure 5.3 and Figure 5.4 that the MI scheme outperforms all the other waveform designs and should be selected for precise target detection, *e.g.*, for probability of detection $\mathrm{Pr_D} \geq 0.7$. Although all the three designed waveforms provide significant performance improvements, we point out that such enhancement is achieved at the price of knowing the quality of channel estimation σ_e^2 *a priori*.

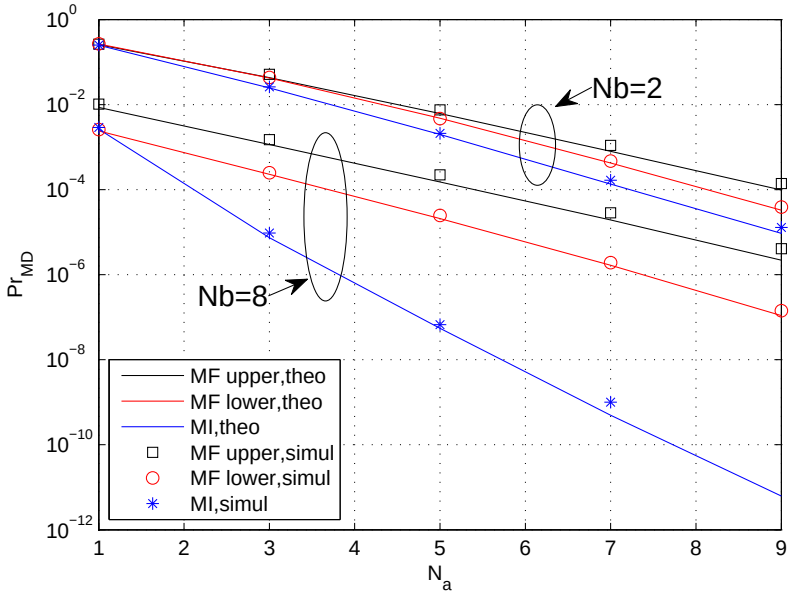

Figure 5.5: *Theoretical and simulated probability of missed detection as a function of N_a for systems with different retransmitted waveforms when $M = 5$, SNR $= 0$dB, and Detector II is employed*

We proceed to investigate the impact of the number of antennas at Array A N_a, the number of antennas at Array B N_b, and the number of snapshots M on the detection performance for the proposed three waveform designs. The SNR is fixed at 0dB for the next three figures, and the number of snapshots M equals 5 for Figure 5.5 and Figure 5.6. First of all, it is clear that for all the scenarios considered in Figure 5.5, Figure 5.6, and Figure 5.7, the MI scheme provides the best detection performance, and the MF lower approach outperforms the MF upper method. Next, we compare the slopes of the curves corresponding to different waveforms for the same N_b in Figure 5.5, and the larger the slope is, the more effect N_a has on the corresponding waveform design. In other words, for the same increase in the value of N_a, the MI scheme provides the greatest performance improvement, and the MF lower method achieves more enhancement than the MF upper approach does. Similarly, we can draw the same conclusions for both N_b and M by observing Figure 5.6 and Figure 5.7. Therefore, the MI scheme is the best among the three waveform design approaches since it not only performs the best but also realizes the largest performance enhancement for the same increase in the value of N_a, N_b, or M. In that sense, the MF lower scheme is also better than the MF upper approach.

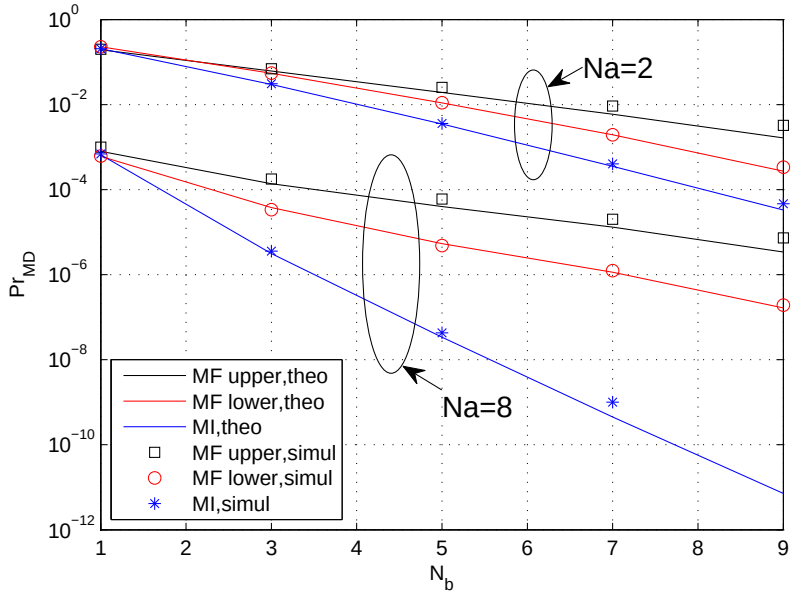

Figure 5.6: *Theoretical and simulated probability of missed detection as a function of N_b for systems with different retransmitted waveforms when $M = 5$, SNR $= 0$dB, and Detector II is employed*

5.6 Conclusions

In this chapter, we investigated the target detection performance of a bistatic wideband MIMO system, whose detection process is similar to the TR procedure. Based on the estimated channel and the estimation error variance obtained during the probing phase, the retransmitted waveform and the detector were designed. Three detectors were developed, whose theoretical thresholds and probabilities of detection were derived. Three schemes were proposed to design the retransmitted waveform with a power constraint, which maximizes the upper and lower bound of the probability of detection of the GLRT detector, and the lower bound of the MI between the retransmitted signal and the received signal, respectively. Numerical results showing the detection performance of a MIMO system involving the designed detectors and retransmitted waveforms were presented. It was demonstrated that the optimal detector performs the best but it requires more *a priori* information than the conventional detector does. The performance difference between the conventional and the optimal detector increases as the estimation quality becomes poorer. The GLRT detector performs the poorest at low SNR but demands the least amount of *a priori* information. All the three waveform design approaches further improve the system performance with respect to the MF approach at the price of knowing the quality of

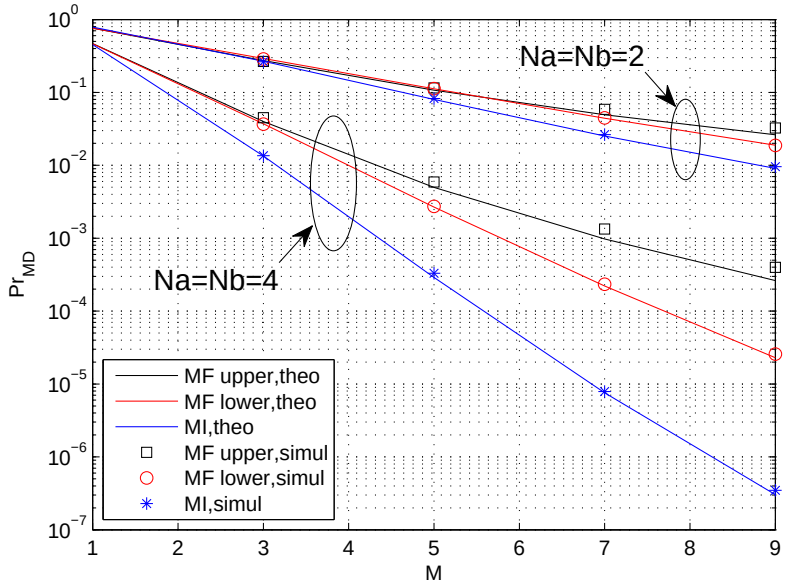

Figure 5.7: *Theoretical and simulated probability of missed detection as a function of M for systems with different retransmitted waveforms when SNR $= 0dB$ and Detector II is employed*

channel estimation *a priori*. The MF upper scheme works the best at low SNR, but is outperformed by the MF lower approach as the SNR increases. However, the MI scheme consistently provides the maximum target detection probability in all the simulation scenarios that were tested.

Chapter 6
Conclusions

This thesis has been concerned with the performance evaluation and waveform design for MIMO radar which takes advantage of spatial diversity gain. This concluding chapter will give a summary of the results from previous chapters as well as the main contributions of this thesis in Section 6.1. Some suggestions for possible future directions of the current research will be discussed in Section 6.2.

6.1 Summary of Results

One of the major interests behind the present project was to overcome the limitations of the statistical MIMO model proposed for MIMO radar in the literature. The finite scatterers model is one solution, based on which the target detection performance of a MIMO radar system with arbitrary array-target configurations was evaluated in Chapter 3. First of all, a theoretical target model was examined, the reflectivity coefficients of whose scatterers were assumed to be independent, identically distributed zero-mean random variables. Unlike the ideal configurations that all the channel gains have correlation coefficients 1 or 0, the channel gains between different antenna pairs of a general radar system have various degrees of correlation, which depend on the exact array-target configuration. Based on the correlation matrix, a closed form result was derived to calculate the theoretical probability of detection for a MIMO radar system. Two extreme channel models where all the channel gains are totally uncorrelated or fully correlated were analyzed, and the simplified expressions of the formula for two special cases were provided. Numerical results were presented showing the probabilities of detection of a MIMO radar system with five configurations, including the two extreme cases. The curves corresponding to the two extreme channel models set bounds for the system performance, and the performance curve is closer to the full correlation case as the spacing decreases, while it is closer to the uncorrelated case as the antenna array spacing becomes larger. Furthermore, at low SNR, a system with densely spaced antennas outperforms large interelement spacing. Conversely, widely spaced antennas perform better at high SNR and are always preferred when

the detection performance is acceptable. Next, a MIMO radar system involving a realistic target was set up by determining the reflectivity coefficients of the scatterers using the data collected from previous research on target modelling. The considered target is a life-size land vehicle modelled using a computer aided electromagnetic (EM) simulator FEKO. Numerical results of the system with different configurations were displayed, corroborating previous conclusions based on the theoretical and mathematical target model. This work has validated in a practical setting the improvements in detection performance available from MIMO radar configurations.

Previous researchers have shown that the conventional phased-array radar provides coherent processing gain while the MIMO radar exploits spatial diversity gain, and a hybrid radar which combines these two configurations to take advantage of both types of gains was investigated in Chapter 4. This radar system is a general model and it can be used to describe many practical configurations, including the MIMO and phased-array radar as special cases. A closed form expression was first derived to evaluate the theoretical probability of detection of the system. Next, the performance of the hybrid radar as a direction finding system was examined. An initialization stage was introduced, during which angle of departure (AoD) is estimated, and the performance is assessed by measuring the average Cramer-Rao bound (CRB). Then the performance of the hybrid radar for estimating the angle of arrival (AoA) was evaluated by computing the average and outage CRBs when the true AoD is assumed to be known at the transmitter. The corresponding CRBs for AoA estimation were also calculated when only the estimated AoD obtained during the initialization stage is available at the transmitter, that is, the effect the estimation error in AoD has on finding AoA was taken into account. Numerical results demonstrated that a hybrid radar, whose transmitter consists of a few antenna arrays and widely spaced elements at the receiver, provides the best detection performance for practical values of probability of missed detection, such as 0.01 and 0.001. Simulations also showed that for a radar system applied to find AoA, the architecture that the transmitter has a hybrid configuration and the receiver has the phased-array configuration is the best choice. Regarding the AoD estimation, the phased-array configuration should be selected at the transmitter while increasing the number of receive antenna arrays improves the performance, which is the exact opposite of the best configuration for AoA estimation. Although the performance of the AoD estimation affects the direction finding performance overall given the fact that the AoD information is required at the transmitter to cohere a beam toward the target direction, we investigated several simulation scenarios where it was shown that the estimation error in AoD caused by the initialization would not decrease the AoA estimation performance significantly.

Consequently, the best configuration for a radar system is not the same for different applications, and a hybrid radar which is a compromise of these configurations would be the best choice to jointly optimize the detection and estimation performance. The total gain achieved by combining the spatial diversity gain provided by the antenna arrays together with the coherent processing gain obtained by each array outweighs the diversity gain, or the processing gain realized by the antennas in pure MIMO or phased-array configurations.

After studying the effect the radar configuration has on system performance, the waveform design problem for a MIMO radar system was explored in Chapter 5. The target detection performance of a wideband MIMO system was considered, whose detection process is similar to the time-reversal (TR) detection proposed in the literature. TR detection provides dramatic gains over conventional detection since the transmitter reshapes the waveform to match the channel during the TR process, which is a simple form of waveform design. Here, instead of the normalized TR signal, a waveform is designed based on the noisy estimated channel and a parameter indicating the quality of the estimation. This waveform is retransmitted, and then a detector determines the presence or absence of a target. Three detectors were developed: the conventional detector, the optimal detector, and the generalized likelihood ratio test (GLRT) detector. Closed form formulae were derived to compute the theoretical threshold and probability of detection of each detector. Simulations showed that the optimal detector performs the best but it demands more *a priori* information than the conventional detector does. The performance difference between the two increases as the estimation quality becomes poorer. Although the GLRT detector performs the worst at low SNR, it requires the least amount of *a priori* information and it obtains similar performance to the optimal detector when SNR is high enough. Three schemes were proposed to design the retransmitted waveform with constraints on transmitted signal power: the MF upper and MF lower schemes maximize the upper and lower bound of the probability of detection of the GLRT detector, respectively, and the MI scheme maximizes the lower bound of the mutual information (MI) between the retransmitted signal and the received signal. Numerical results illustrated that the MF scheme, a modified TR approach, performs much better than the conventional signal (CS) scheme, and all the three designed waveforms bring in further performance improvements with respect to the MF approach at the cost of knowing the quality of channel estimation *a priori*. In addition, the MF upper scheme is always preferred at low SNR, which is outperformed by the MF lower approach as the SNR increases, and the MI scheme should be selected for precise target detection.

6.2 Future Work

There are several directions that can be extended around the topics involved in this thesis. Some suggestions are listed below:

- In Chapter 3, the theoretical probability of detection for a MIMO radar system was derived based on the assumption that the target RCS fading has a zero-mean complex Gaussian distribution. An interesting research area is to extend the analysis to other widely adopted statistical RCS models, such as the Chi-square target model and the Rice target model, examining if the MIMO configuration can still provide superior performance due to spatial diversity gain. In addition, the target detection performance of MIMO radar was evaluated without taking into account the effects of clutter and jamming, and the noise level was always assumed to be known, which were unrealistic in real-life systems. Consequently, one future research area is to design an optimal detector when clutter and jamming exist and/or the noise level is unknown, and assess the corresponding performance of a MIMO radar system with different configurations. Again, realistic target models can then be substituted for the theoretical target, allowing us to have an impression of the realistic benefits of MIMO radar.

- We focused our attention on investigating the impact of the radar configuration on system performance in Chapter 4, thus a simple transmitted waveform was adopted and each antenna array worked as a conventional phased-array radar. Recall that the colocated MIMO radar explored in depth in the current literature has the same configuration as the conventional phased-array radar does, and it is capable of exploiting the waveform diversity to provide increased flexibility and performance gains. A promising area for future research is to combine the statistical MIMO radar and the colocated MIMO radar, that is, study a system which has the same architecture as the hybrid radar but transmitting colocated MIMO waveforms from each phased-array and applying sophisticated signal processing approaches to the received signals. For example, extend the probing signal design proposed in [78] to the hybrid radar scenario and/or applying adaptive techniques for radar imaging introduced in [82] to the received signals. It is possible to further enhance the detection capability, parameter estimation accuracy, resolution, and jammer resistance, *etc.*, by simultaneously taking advantage of spatial diversity gain and waveform diversity gain provided by both types of MIMO radar.

- Theoretically speaking, the schemes proposed in Chapter 5 can be adopted in any MIMO system, radar or sonar, as long as the channel remains static during the probing and detection phases. In addition, it has been demonstrated that TR techniques have a wide range of underwater applications. Hence, an interesting future topic is to implement experiments, instead of doing simulations, on those schemes in a sonar scenario, experimentally validating their superiority as well as the realizability of a MIMO sonar. Moreover, due to the characteristics of TR techniques, it is possible to exploit its potential in applications such as parameter estimation and target localization. Furthermore, only the very original TR approach has been applied to MIMO systems, and there are many developed TR techniques in the current literature, *e.g.*, decomposition of the time reversal operator (DORT) approach [140], MUSIC TR [115], likelihood TR [113]. How to apply these methods in MIMO system and provide performance gains would be another promising research field.

- The MIMO radar with widely spaced antennas enables simultaneous observations of a target from several perspectives, providing us more information about the target features. Thereby, MIMO radar possesses potential for moving target detection, target tracking, and target classification. How to exploit these potentials could be another future topic.

References

[1] J. Li and P. Stoica, *MIMO radar signal procesing*. New Jersey: John Wiley & Sons, 2009.

[2] A. K. Mishra, *Ground target classification for airborne bistatic radar*. PhD thesis, Dept. Eng. Elect., Univ. Edinburgh, Edinburgh, UK, 2006.

[3] E. Fishler, A. Haimovich, R. S. Blum, D. Chizhik, L. J. Cimini, and R. A. Valenzuela, "MIMO radar: An idea whose time has come," *Proc. of the IEEE Int. Conf. on Radar*, pp. 71–78, Apr. 2004.

[4] D. Gesbert, M. Shafi, D. Shiu, P. J. Smith, and A. Naguib, "From theory to practice: An overview of MIMO space-time coded wireless systems," *IEEE J. Sel. Areas Commun.*, vol. 21, pp. 71–78, Apr. 2003.

[5] A. Paulraj, D. A. Gore, R. U. Nabar, and H. Bolcskei, "An overview of MIMO communications - A key to gigabit wireless," *Proc. IEEE*, vol. 92, pp. 198–218, Feb. 2004.

[6] A. M. Haimovich, R. S. Blum, and L. J. Cimini, "MIMO radar with widely separated antennas," *IEEE Signal Process. Mag.*, vol. 25, pp. 116–129, Jan. 2008.

[7] E. Fishler, A. Haimovich, R. S. Blum, L. J. Cimini, D. Chizhik, and R. A. Valenzuela, "Performance of MIMO radar systems: Advantages of angular diversity," *Proc. 38th Asilomar Conf. Signals, Systems, Computers, Pacific Grove, CA*, vol. 1, pp. 305–309, Nov. 2004.

[8] E. Fishler, A. Haimovich, R. S. Blum, L. J. Cimini, D. Chizhik, and R. A. Valenzuela, "Spatial diversity in radars-Models and detection performance," *IEEE Trans. Signal Process.*, vol. 54, pp. 823–838, Mar. 2006.

[9] N. H. Lehmann, E. Fishler, A. M. Haimovich, R. S. Blum, D. Chizhik, L. J. Cimini, and R. A. Valenzuela, "Evaluation of transmit diversity in MIMO-Radar direction finding," *IEEE Trans. Signal Process.*, vol. 55, pp. 2215–2225, May 2007.

[10] N. Lehmann, *Some contributions on MIMO radar*. PhD thesis, New Jersey Institute of Technology, 2006.

[11] M. Skolnik, *Introduction to radar systems*. New York: McGraw-Hill, 2nd ed., 1980.

[12] F. E. Nathanson, J. P. Reilly, and M. N. Cohen, *Radar design principles*. New York: McGraw-Hill, 2nd ed., 1991.

[13] N. Levanon, *Radar principles*. New York: Wiley, 1st ed., 1988.

[14] M. Skolnik, *Radar handbook*. New York: McGraw-Hill, 1st ed., 1970.

[15] G. Kulemin, *Millimeter-wave radar targets and clutter*. Boston: Artech House, 2003.

[16] S. H. Yueh and J. A. Kong, "K - distribution and polarimetric terrain radar clutter," *Journal of Electromagnetic Waves and Applications*, vol. 3, no. 8, pp. 747–768, 1989.

[17] D. A. Shnidam, "Generalized radar clutter model," *IEEE Trans. Aerosp. Electron. Syst.*, vol. 35, pp. 857–865, Jul. 1999.

[18] D. K. Barton, *Modern radar systems analysis*. Boston: Artech House, 1988.

[19] R. J. Urick, *Principles of underwater sound*. New York: McGraw-Hill, 3rd. ed., 1983.

[20] G. M. Wenz, "Acoustic ambient noise in the ocean: spectra and sources," *IEEE J. Acoust. Soc. Am.*, vol. 34, pp. 1936–1956, Dec. 1962.

[21] K. V. Mackenzie, "Nine-term equation for sound speed in the oceans," *IEEE J. Acoust. Soc. Am.*, vol. 70, pp. 807–812, Sept. 1981.

[22] M. McKay and S. Zisk, "Radar and sonar: A primer for the geophysically-challenged," *Hawaii Center for Volcanology Newsletter*, vol. 2, Dec. 1994. [Online]. Available: http://www.soest.hawaii.edu/GG/HCV/NEWSV2N1/mackay1.html.

[23] H. L. V. Trees, *Optimum array processing*. New York: John Wiley, 1st ed., 2003.

[24] S. Haykin, *Adaptive filter theory*. Upper Saddle River, NJ: Prentice-Hall PTR, 4th ed., 2002.

[25] B. D. Van Veen and K. M. Buckley, "Beamforming: A versatile approach to spatial filtering," *IEEE ASSP Magzine*, pp. 4–24, Apr. 1988.

[26] R. Monzingo and T. Miller, *Introduction to adaptive arrays*. New York: Wiley and Sons, 1980.

[27] S. P. Applebaum and D. J. Chapman, "Adaptive arrays with main beam constraints," *IEEE Trans. Antennas Propag.*, vol. 24, pp. 650–662, Sept. 1976.

[28] B. Widrow, P. E. Mantey, L. J. Griffiths, and B. B. Goode, "Adaptive antenna systems," *Proc. IEEE*, vol. 55, pp. 2143–2159, Dec. 1967.

[29] P. W. Howells, "Intermediate frequency sidelobe canceller," U.S. Patent 3202990, Aug. 1965.

[30] I. O. L. Frost, "An algorithm for linearly constrained adaptive array processing," *Proc. IEEE*, vol. 60, pp. 926–935, Aug. 1972.

[31] J. Capon, "High-resolution frequency-wavenumber spectrum analysis," *Proc. IEEE*, vol. 57, pp. 1408–1418, 1969.

[32] L. S. Resende, J. M. T. Romano, and M. G. Bellanger, "A fast least-squares algorithm for linearly constrained adaptive filtering," *IEEE Trans. Signal Process.*, vol. 44, pp. 1168–1174, May 1996.

[33] J. S. Goldstein, I. S. Reed, and L. L. Scharf, "A multistage representation of the Wiener filter based on orthogonal projections," *IEEE Trans. Inf. Theo.*, vol. 44, pp. 2943–2959, Nov. 1998.

[34] M. L. Honig and J. S. Goldstein, "Adaptive reduced-rank interference suppression based on the multistage Wiener filter," *IEEE Trans. Comm.*, vol. 50, pp. 986–994, Jun. 2002.

[35] H. Qian and S. N. Batalama, "Data record-based criteria for the selection of an auxiliary vector estimator of the MMSE/MVDR filter," *IEEE Trans. Comm.*, vol. 51, pp. 1700–1708, Oct. 2003.

[36] D. A. Pados and S. N. Batalama, "Joint space-time auxiliary vector filtering for DS/CDMA systems with antenna arrays," *IEEE Trans. Comm.*, vol. 47, pp. 1406–1415, Sept. 1999.

[37] R. C. de Lamare and R. Sampaio-Neto, "Reduced-rank adaptive filtering based on joint iterative optimization of adaptive filters," *IEEE Signal Process. Letters*, vol. 14, pp. 980–983, Dec. 2007.

[38] R. C. de Lamare, "Adaptive reduced-rank LCMV beamforming algorithms based on joint iterative optimization of filters," *Electronics Letters*, vol. 44, Apr. 2008.

[39] R. Fa, R. C. de Lamare, and D. Zanatta-Filho, "Reduced-rank STAP algorithm for adaptive radar based on joint iterative optimization of adaptive filters," *Proc. 42th Asilomar Conf. Signals, Systems, Computers, Pacific Grove, CA*, pp. 533–537, Oct. 2008.

[40] R. Fa and R. C. de Lamare, "Reduced-rank STAP algorithm for adaptive radar based on basis-functions approximation," *IEEE 15th Workshop on Statistical Signal Processing*, pp. 89–92, Aug. 2009.

[41] L. Wang and R. C. de Lamare, "A new approach to reduced-rank DOA estimation based on joint iterative subspace optimization and grid search," *16th Int. Conf. Digital Signal Process.*, pp. 1–6, Jul. 2009.

[42] L. Wang and R. C. de Lamare, "Adaptive reduced-rank constrained constant modulus beamforming algorithms based on joint iterative optimization of filters," *IEEE 15th Workshop on Statistical Signal Processing*, pp. 153–156, Aug. 2009.

[43] V. S. Chernyak, *Fundamentals of multisite radar systems*. New York: Gordon and Breach, 1998.

[44] P. Viswanath and P. K. Varshney, "Distributed detection with multiple sensors I: Fundamentals," *Proc. IEEE*, vol. 85, pp. 54–63, Jan. 1997.

[45] R. S. Blum, S. A. Kassam, and H. V. Poor, "Distributed detection with multiple sensors II: Advanced topics," *Proc. IEEE*, vol. 85, pp. 64–79, Jan. 1997.

[46] R. S. Blum, "Distributed detection for diversity reception of fading signals in noise," *IEEE Trans. Inf. Theory*, vol. 48, pp. 158–164, Jan. 1999.

[47] S. M. Kay, *Fundamentals of statistical signal proceesing: Detection Theory*. Upper Saddle River, NJ: Prentice-Hall PTR, 1993.

[48] D. H. Johnson, "The application of spectral estimation methods to bearing estimation problems," *Proc. IEEE*, vol. 70, pp. 1018–1028, Sept. 1982.

[49] P. Stoica and R. L. Moses, *Introduction to spectral analysis*. Upper Saddle River, NJ: Prentice-Hall PTR, 1997.

[50] R. O. Schmidt, "Multiple emitter location and signal parameter estimation," *IEEE Trans. Antennas Propag.*, vol. 34, pp. 276–280, Mar. 1986.

[51] H. Krim and M. Viberg, "Two decades of array signal processing research," *IEEE Signal Process. Mag.*, vol. 13, pp. 67–94, Jul. 1996.

[52] A. J. Barabell, "Improving the resolution performance of eigenstructure-based direction-finding algorithms," *IEEE Int. Conf. Acoustic, Speech, and Signal Processing. (ICASSP '83)*, pp. 336–339, 1983.

[53] P. Stoica and K. C. Sharman, "Maximum likelihood methods of direction-of-arrival estimation," *IEEE Trans. Acoust., Speech, and Signal Process.*, vol. 38, pp. 1132–1143, Jul. 1990.

[54] S. Haykin, J. P. Reilly, V. Kezys, and E. Vertatschitsch, "Some aspects of array signal processing," *Proc. IEE - F*, vol. 139, pp. 1–26, Feb. 1992.

[55] R. Kumaresan and D. W. Tufts, "Estimation of arrival of multiple plane waves," *IEEE Trans. Aerosp. Electron. Syst.*, vol. 19, pp. 123–133, Jan. 1983.

[56] R. Roy, A. Paulraj, and T. Kailath, "ESPRIT - A subspace rotation approach to estimation of parameters of cisoids in noise," *IEEE Trans. Acoust., Speech, and Signal Process.*, vol. 34, pp. 1340–1342, Oct. 1986.

[57] B. Ottersten, M. Viberg, and T. Kailath, "Performance analysis of the total least squares ESPRIT algorithm," *IEEE Trans. Signal Process.*, vol. 39, pp. 1122–1135, May 1991.

[58] M. Viberg and B. Ottersten, "Sensor array processing based on subspace fitting," *IEEE Trans. Signal Process.*, vol. 39, pp. 1110–1120, May 1991.

[59] B. Ottersten, M. Viberg, and T. Kailath, "Analysis of subspace fitting and ML techniques for parameter estimation from sensor array data," *IEEE Trans. Signal Process.*, vol. 40, pp. 590–600, Mar. 1992.

[60] D. J. Jeffries and D. R. Farrier, "Asymptotic results for eigenvector methods," *Proc. IEE - F*, vol. 132, pp. 589–594, Dec. 1986.

[61] B. D. Rao and K. V. S. Hari, "Performance analysis of root-MUSIC," *IEEE Trans. Acoust., Speech, and Signal Process.*, vol. 37, pp. 1939–1949, Dec. 1989.

[62] B. Porat and B. Friedlander, "Direction finding algorithms based on higher-order statistics," *IEEE Trans. Signal Process.*, vol. 39, pp. 2016–2023, Sept. 1991.

[63] B. Porat and B. Friedlander, "Analysis of the asymptotic relative efficiency of the MUSIC algorithm," *IEEE Trans. Acoust., Speech, and Signal Process.*, vol. 36, pp. 532–543, Apr. 1988.

[64] P. Stoica and A. Nehorai, "MUSIC, maximum likelihood, and Cramer-Rao bound," *IEEE Trans. Acoust., Speech, and Signal Process.*, vol. 37, pp. 720–741, May 1989.

[65] P. Stoica and A. Nehorai, "MUSIC, maximum likelihood, and Cramer-Rao bound: Further results and comparisons," *IEEE Trans. Acoust., Speech, and Signal Process.*, vol. 38, pp. 2140–2150, Dec. 1990.

[66] P. Stoica and A. Nehorai, "Performance study of conditional and unconditional direction-of-arrival estimation," *IEEE Trans. Acoust., Speech, and Signal Process.*, vol. 38, pp. 1783–1795, Oct. 1990.

[67] T. J. Shan, M. Wax, and T. Kailath, "On spatial smoothing for directional-of-arrival estimation of coherent signals," *IEEE Trans. Acoust., Speech, and Signal Process.*, vol. 33, pp. 806–811, Aug. 1985.

[68] S. U. Pillai and B. H. Kwon, "Forward/backward spatial smoothing techniques for coherent signal identification," *IEEE Trans. Acoust., Speech, and Signal Process.*, vol. 37, pp. 8–15, Jan. 1989.

[69] N. Lehmann, A. Haimovich, R. S. Blum, and L. J. Cimini, "High resolution capability of MIMO radar," *Proc. 40th Asilomar Conf. Signals, Systems, Computers, Pacific Grove, CA*, pp. 25–30, Nov. 2006.

[70] Y. Yang and R. S. Blum, "MIMO radar waveform design based on mutual information and minimum mean-square error estimation," *IEEE Trans. Aerosp. Electron. Syst.*, vol. 43, pp. 330–343, Jan. 2007.

[71] A. De Maio and M. Lops, "Design principles of MIMO radar detectors," *IEEE Trans. Aerosp. Electron. Syst.*, vol. 43, pp. 886–898, Jul. 2007.

[72] D. W. Bliss and K. W. Forsythe, "Multiple-input multiple-output (MIMO) radar and imaging: degrees of freedom and resolution," *Proc. 37th Asilomar Conf. Signals, Systems, Computers, Pacific Grove, CA*, vol. 1, pp. 54–59, Nov. 2003.

[73] K. W. Forsythe, D. W. Bliss, and G. S. Fawcett, "Multiple-Input Multiple-Output (MIMO) radar performance issues," *Proc. 38th Asilomar Conf. Signals, Systems, Computers, Pacific Grove, CA*, pp. 310–315, Nov. 2004.

[74] K. W. Forsythe and D. W. Bliss, "Waveform correlation and optimization issues for MIMO radar," *Proc. 39th Asilomar Conf. Signals, Systems, Computers, Pacific Grove, CA*, pp. 1306–1310, Nov. 2005.

[75] J. Li and P. Stoica, "MIMO radar with colocated antennas," *IEEE Signal Process. Mag.*, vol. 24, pp. 106–114, Sept. 2007.

[76] J. Li and P. Stoica, "MIMO radar - diversity means superiority," *Proc. 14th Annual Workshop on Adaptive Sensor Array Procesing, MIT Lincoln Laboratory, Lexington, MA*, June 2006.

[77] J. Li, P. Stoica, L. Xu, and W. Roberts, "On parameter identifiability of MIMO radar," *IEEE Signal Process. Lett.*, vol. 14, pp. 968–971, Dec. 2007.

[78] J. Li, P. Stoica, and Y. Xie, "On probing signal design for MIMO radar," *Proc. 40th Asilomar Conf. Signals, Systems, Computers, Pacific Grove, CA*, 2006.

[79] J. Li, L. Xu, P. Stoica, K. W. Forsythe, and D. W. Bliss, "Range compression and waveform optimization for MIMO radar: A Cramer-Rao bound based study," *IEEE Trans. Signal Process.*, vol. 56, pp. 218–232, Jan. 2008.

[80] L. Xu, J. Li, and P. Stoica, "Target detection and parameter estimation for MIMO radar systems," *IEEE Trans. Aerospace Electron. Syst.*, vol. 44, pp. 927–939, Jul. 2008.

[81] L. Xu, J. Li, and P. Stoica, "Adaptive techniques for MIMO radar," *Proc. 4th IEEE Workshop on Sensor Array and Multi-channel Processing, Waltham, MA*, Jul. 2006.

[82] L. Xu, J. Li, and P. Stoica, "Radar imaging via adaptive MIMO techniques," *EUSIPCO*, 2006. Available: fttp://www.sal.ufl.edu/xuluzhou/EUSIPCO2006.pdf.

[83] L. Xu, J. Li, P. Stoica, K. W. Forsythe, and D. W. Bliss, "Waveform optimization for MIMO radar: A Cramer-Rao bound based study," *IEEE Int. Conf. Acoustic, Speech, and Signal Processing. (ICASSP '07)*, Apr. 2007.

[84] D. R. Fuhrmann and G. San Antonio, "Transmit beamforming for MIMO radar systems using partial signal correlations," *Proc. 38th Asilomar Conf. Signals, Systems, Computers, Pacific Grove, CA*, vol. 1, pp. 295–299, 2004.

[85] D. R. Fuhrmann and G. San Antonio, "Transmit beamforming for MIMO radar systems using signal cross-correlation," *IEEE Trans. Aerospace Electron. Syst.*, vol. 44, pp. 171–186, Jan. 2008.

[86] D. Rabideau and P. Parker, "Ubiquitous MIMO multifunctino digital array radar," *Proc. 37th Asilomar Conf. Signals, Systems, Computers, Pacific Grove, CA*, Nov. 2003.

[87] F. C. Robey, S. Coutts, D. Weikle, J. C. McHarg, and K. Cuomo, "MIMO radar theory and experimental results," *Proc. 38th Asilomar Conf. Signals, Systems, Computers, Pacific Grove, CA*, vol. 1, pp. 300–304, Nov. 2004.

[88] I. Bekkerman and J. Tabrikian, "Target detection and localization using MIMO radars and sonars," *IEEE Trans. Signal Process.*, vol. 54, pp. 3873–3883, Oct. 2006.

[89] J. Tabrikian, "Barankin bounds for target localization by MIMO radars," *Proc. 4th IEEE Workshop on Sensor Array and Multi-channel Processing, Waltham, MA*, Jul. 2006.

[90] J. Tabrikian and I. Bekkerman, "Transmission diversity smoothing for multi-target localization," *IEEE Int. Conf. Acoustic, Speech, and Signal Processing. (ICASSP '05), Philadelphia, PA*, vol. 4, pp. 1041–1044, Mar. 2005.

[91] B. Friedlander, "Waveform design for MIMO radars," *IEEE Trans. Aerosp. Electron. Syst.*, vol. 43, pp. 1227–1238, Jul. 2007.

[92] C. Y. Chen and P. P. Vaidyanathan, "A subspace method for MIMO radar space-time adaptive proceesing," *IEEE Int. Conf. Acoustic, Speech, and Signal Processing. (ICASSP '07)*, vol. 2, pp. 925–928, Apr. 2007.

[93] C. Y. Chen and P. P. Vaidyanathan, "MIMO radar waveform optimization with prior information of the extended target and clutter," *IEEE Trans. Signal Process.*, vol. 57, pp. 3533–3544, Sept. 2009.

[94] C. Y. Chen and P. P. Vaidyanathan, "MIMO radar ambiguity properties and optimization using frequency-hopping waveforms," *IEEE Trans. Signal Process.*, vol. 56, pp. 5926–5936, Dec. 2008.

[95] C. Y. Chen and P. P. Vaidyanathan, "MIMO radar space-time adaptive proceesing using prolate spheroidal wave functions," *IEEE Trans. Signal Process.*, vol. 56, pp. 623–635, Feb. 2008.

[96] C. Y. Chen and P. P. Vaidyanathan, "Joint MIMO radar waveform and receiving filter optimization," *IEEE Int. Conf. Acoustic, Speech, and Signal Processing. (ICASSP '09)*, pp. 2073–2076, Apr. 2009.

[97] C. Prada, J. L. Thomas, and M. Fink, "The iterative time reversal process: Analysis of the convergence," *IEEE J. Acoust. Soc. Am.*, vol. 97, pp. 62–71, Jan. 1995.

[98] M. Fink and J. F. Cardoso, "Diffraction effects in pulse-echo measurements," *IEEE Trans. Sonics Ultrason.*, vol. 31, no. 4, pp. 313–329, 1984.

[99] M. Fink, "Time reversal of ultrasonic fields - part I: Basic principles," *IEEE Trans. Ultrason., Ferroelectr., Freq. Control*, vol. 39, pp. 555–566, Sept. 1992.

[100] C. Dorme and M. Fink, "Focusing in the transmit-receive mode through inhomogeneous media: The time reversal matched filter approach," *IEEE J. Acoust. Soc. Am.*, vol. 98, pp. 1155–1162, Aug. 1995.

[101] M. Fink, "Time reversed acoustics," *Phys. Today*, vol. 50, no. 3, pp. 34–40, 1997.

[102] N. Mordant, C. Prada, and M. Fink, "Highly resolved detection and selective focusing in a waveguide using the DORT method," *IEEE J. Acoust. Soc. Am.*, vol. 105, pp. 2634–2642, May 1999.

[103] P. Roux and M. Fink, "Time reversal in a waveguide: Study of the temporal and spatial focusing," *IEEE J. Acoust. Soc. Am.*, vol. 107, pp. 2418–2429, May 2000.

[104] T. Folegot, C. Prada, and M. Fink, "Resolution enhancement and separation of reverberation from target echo with the time reversal operator decomposition," *IEEE J. Acoust. Soc. Am.*, vol. 113, pp. 3155–3160, Jun. 2003.

[105] J. G. Minonzio, D. Clorennec, A. Aubry, T. Folegot, T. Pelican, C. Prada, J. Rosny, and M. Fink, "Application of the DORT method to the detection and characterization of two targets in a shallow water wave-guide," *Proc. Oceans 2005 Europe*, 2005.

[106] G. Lerosey, J. Rosny, A. Tourin, G. Montaldo, and M. Fink, "Time reversal of electromagnetic waves," *Phys. Rev. Lett.*, vol. 92, p. 193904, May 2004.

[107] C. Oestges, A. D. Kim, G. Papanicolaou, and A. J. Paulraj, "Characterization of space-time focusing in time-reversed random fields," *IEEE Trans. Antennas Propag.*, vol. 53, pp. 283–293, Jan. 2005.

[108] L. Borcea, G. Papanicolaou, C. Tsogka, and J. Berryman, "Imaging and time reversal in random media," *Inverse Problems*, vol. 18, pp. 1247–1279, 2002.

[109] R. C. Qiu, "A theory of time-reversed impulse multiple-input multiple-output (MIMO) for ultra-wideband (UWB) communications," in *IEEE International Conf. Ultra Wideband (ICUWB06)*, (BOSTON, MA), Sept. 2006. invited paper.

[110] R. C. Qiu, C. Zhou, N. Guo, and J. Q. Zhang, "Time reversal with MISO for ultra-wideband communications: Experimental resutls," *IEEE Antennas Wireless Propag. Lett.*, vol. 5, pp. 269–273, 2006.

[111] C. Zhou, N. Guo, B. M. Sadler, and R. C. Qiu, "Performance study on time reversed impulse MIMO for UWB communications based on measured spatial UWB channels," *Military Commun. Conf. (MILCOM2007)*, pp. 1–6, Oct. 2007.

[112] H. T. Nguyen, I. Z. Kovacs, and P. C. F. Eggers, "A time reversal transmission approach for multiuser UWB communications," *IEEE Trans. Antennas Propag.*, vol. 54, pp. 3216–3224, Nov. 2006.

[113] G. Shi and A. Nehorai, "Maximum likelihood estimation of point scatterers for computational time-reversal imaging," *Commun. Inf. Syst.*, vol. 5, no. 2, pp. 227–256, 2005.

[114] G. Shi and A. Nehorai, "A relationship between time-reversal imaging and maximum-likelihood scattering estimation," *IEEE Trans. Signal Process.*, vol. 55, pp. 4707–4711, Sept. 2007.

[115] A. J. Devaney, "Super-resolution processing of multi-static data using time reversal and MUSIC," *unpublished*, 2000. [Online]. Available: http://www.ece.neu.edu/faculty/devaney.

[116] S. K. Lehman and A. J. Devaney, "Transmission mode time-reversal super-resolution imaging," *IEEE J. Acoust. Soc. Am.*, vol. 113, pp. 2742–2753, May 2003.

[117] E. A. Marengo, F. K. Gruber, and F. Simonetti, "Time-reversal MUSIC imaging of extended targets," *IEEE Trans. Image Process.*, vol. 16, pp. 1967–1984, Aug. 2007.

[118] J. M. F. Moura and Y. Jin, "Detection by time reversal: Single antenna," *IEEE Trans. Signal Process.*, vol. 55, pp. 187–201, Jan. 2007.

[119] J. M. F. Moura, Y. Jin, D. Stancil, J. G. Zhu, A. Cepni, Y. Jiang, and B. Henty, "Array processing using time reversal: Experimental and performance," *IEEE Int. Conf. Acoustic, Speech, and Signal Processing. (ICASSP '06)*, vol. 4, pp. 1053–1056, May 2006.

[120] Y. Jin, J. M. F. Moura, and N. O'Donoughue, "Time reversal transmission in MIMO radar," *Proc. 41th Asilomar Conf. Signals, Systems, Computers, Pacific Grove, CA*, pp. 2204–2208, 2007.

[121] A. K. Mishra and B. Mulgrew, "Database generation of bistatic ground target signatures," *IEEE/ACES Conference on Wireless Communication and Applied Computational Electromagnetics*, pp. 523–528, Apr. 2005.

[122] D. Tse and P. Viswanath, *Fundamentals of wireless communication*. New York: Cambridge University Press, 2005.

[123] J. G. Proakis, *Digital communications*. Boston: McGraw-Hill, 4th ed., 2001.

[124] N. S. Nise, *Control systems engineering*. Redwood City: The Benjamin/Cummings Pub. Co., 1992.

[125] Q. T. Zhang and D. P. Liu, "A simple capacity formula for correlated diversity Rician fading channels," *IEEE Commun. Lett.*, vol. 6, pp. 481–483, Nov. 2002.

[126] G. E. P. Box, "Some theorems on quadratic forms applied in the study of analysis of variance problems," *The Annals of Mathematical Statistics*, vol. 25, pp. 290–302, Jun. 1954.

[127] J. P. Imhof, "Computing the distribution of quadratic forms in normal variables," *Biometrika*, vol. 48, no. 3-4, pp. 419–426, 1961.

[128] D. R. Kirk, J. S. Bergin, P. M. Techau, and J. E. Don Carlos, "Multi-static coherent sparse aperture approach to precision target detection and engagement," *IEEE International Radar Conference*, pp. 579–584, May 2005.

[129] L. Xu and J. Li, "Iterative generalized-likelihood ratio test for MIMO radar," *IEEE Trans. Signal Process.*, vol. 55, pp. 2375–2385, June 2007.

[130] A. S. Fletcher and F. C. Robey, "Performance bounds for adaptive coherence of sparse array radar," presented at the 11th Conf. Adaptive Sensors Array Processing, Lexington, MA, Mar. 2003.

[131] S. M. Kay, *Fundamentals of statistical signal proceesing: Estimation Theory*. Upper Saddle River, NJ: Prentice-Hall PTR, 1993.

[132] S. Valaee, B. Champagne, and P. Kabal, "Parametric localization of distributed sources," *IEEE Trans. Signal Process.*, vol. 43, pp. 2144–2153, Sept. 1995.

[133] R. Raich, J. Goldberg, and H. Messer, "Bearing estimation for a distributed source: Modeling, inherent accuracy limitations and algorithms," *IEEE Trans. Signal Process.*, vol. 48, pp. 429–441, Feb. 2000.

[134] A. M. Sayeed, "Deconstructing multiantenna fading channels," *IEEE Trans. Signal Process.*, vol. 50, pp. 2563–2579, Oct. 2002.

[135] P. Stoica, E. G. Larsson, and A. B. Gershman, "The stochastic CRB for array processing: A textbook derivation," *IEEE. Signal Process. Lett.*, vol. 8, pp. 148–150, May 2001.

[136] M. Abramowitz and I. A. Stegun, *Handbook of mathematical functions*. New York: Dover, 1965.

[137] J. Fuhl, A. F. Molisch, and E. Bonek, "Unified channel model for mobile radio systems with smart antennas," *IEE Proc. -Radar, Sonar, Navig.*, vol. 145, pp. 32–41, Feb. 1998.

[138] J. Fuhl, *Smart antennas for second and third generation mobile communications systems*. PhD thesis, Technical University, Vienna, 1997.

[139] C. Prada, F. Wu, and M. Fink, "The iterative time reversal mirror: A solution to self-focusing in the pulse echo mode," *IEEE J. Acoust. Soc. Am.*, vol. 90, pp. 1119–1129, Aug. 1991.

[140] C. Prada, S. Manneville, D. Spoliansky, and M. Fink, "Decomposition of the time reversal operator: Detection and selective focusing on two scatterers," *IEEE J. Acoust. Soc. Am.*, vol. 99, pp. 2067–2076, Apr. 1996.

[141] T. Yoo and A. Goldsmith, "Capacity and power allocation for fading MIMO channels with channel estimation error," *IEEE Trans. Inf. Theory*, vol. 52, pp. 2203–2214, May 2006.

[142] T. E. Klein and R. G. Gallager, "Power control for the additive white Gaussian noise channel under channel estimation errors," *in Proc. IEEE Int. Symp. Inf. Theory (ISIT)*, p. 304, Jun. 2001.

[143] A. Soysal, *Optimum transmit strategies for Gaussian multi-user MIMO systems with partial CSI and noisy channel estimation*. PhD thesis, University of Maryland, 2008.

[144] V. Tarokh, A. Naguib, N. Seshadri, and A. R. Calderbank, "Space-time codes for high data rate wireless communication: Performance criteria in the presence of channel estimation errors, mobility, and multiple paths," *IEEE Trans. Commun.*, vol. 47, pp. 199–207, Feb. 1999.

[145] T. M. Cover and J. A. Thomas, *Elements of information theory*. New York: Wiley, 2nd. ed., 2005.

[146] [Online]. Available: http://mathworld.wolfram.com/Abelsinequality.html.

[147] S. Boyd and L. Vandenberghe, *Convex optimization*. New York: Cambridge University Press, 2004.

[148] A. F. Molisch, *Wireless communications*. Chichester: John Wiley & Sons, 2006.

Appendix A
Original Publications

The author of this thesis has the following accepted or submitted publications during the course of her Ph.D. research:

A.1 Journal Papers

- Chaoran Du, John S. Thompson, and Yvan R. Petillot, "Detector and Waveform Design for MIMO Radar and Sonar Systems with Noisy Channel Estimation," Submitted to *IEEE Transactions on Signal Processing*.
- Chaoran Du, John S. Thompson, and Yvan R. Petillot, "Predicted Detection Performance of MIMO Radar," *IEEE Signal Processing Letters*, vol. 15, pp. 83-86, 2008.

A.2 Conference Papers

- Chaoran Du, John S. Thompson, Bernard Mulgrew, and Yvan R. Petillot, "Detection Performance of MIMO Radar with Realistic Target Models," in *Proceeding of RADAR 2009 International Conference*, 12-16 Oct., 2009, Bordeaux, France.
- Chaoran Du, John S. Thompson, and Yvan R. Petillot, "Detection and Direction Finding Performance of Hybrid Bistatic Radar," in *Proceeding of RADAR 2009 International Conference*, 12-16 Oct., 2009, Bordeaux, France.
- Chaoran Du, John S. Thompson, and Yvan R. Petillot, "Detector and Waveform Design of MIMO System," in *Proceeding of 3rd International Conference & Exhibition of Underwater Acoustic Measurements: Technologies & Results*, 21-26 Jun., 2009, Nafplion, Greece, (invited paper).

The original publications are included in the following pages.

Detector and Waveform Design for MIMO Radar and Sonar Systems with Noisy Channel Estimation

Chaoran Du, *Student Member, IEEE,* John S. Thompson, *Member, IEEE,* Yvan R. Petillot

Abstract

It has been shown that time reversal (TR), which is developed in the acoustics domain, can also improve the detection performance of a radar system. However, the TR technique is no longer a good choice when the noise level is high since the retransmitted signal contains significant noise components. We investigate a multiple-input multiple-output (MIMO) detection process similar to TR detection, during which a waveform designed using the estimated channel and a parameter indicating the quality of the estimation is retransmitted, and the detector determines the presence or absence of a target. We develop three detectors, whose theoretical thresholds and probabilities of detection are derived in closed form. Three schemes are proposed to design the retransmitted waveform with constraints on signal power. We compare the detection performance of different detectors, showing that the detector performing the best has the highest complexity, while the detector with the poorest performance requires the least amount of *a priori* information. Numerical results also show that all the three designed waveforms can further improve the system performance significantly compared with the TR approach, but such enhancement is gained at the price of knowing the quality of channel estimation *a priori*.

C. Du and J. S. Thompson are with the Institute for Digital Communications, Joint Research Institute for Signal & Image Processing, School of Engineering, University of Edinburgh, Edinburgh, EH9 3JL, UK.(e-mail: C.Du@ed.ac.uk, John.Thompson@ed.ac.uk; Tel: +44(0)131 6505655; Fax: +44(0)131 6506554)

Y. Petillot is with the Joint Research Institute for Signal & Image Processing, School of Engineering and Physical Sciences, Heriot-Watt University, Edinburgh, EH14 4AS, UK. (e-mail: Y.R.Petillot@hw.ac.uk; Tel: +44(0)131 4518277; Fax: +44(0)131 4514155)

We acknowledge the support of the Scottish Funding Council for the Joint Research Institute with Edinburgh and the Heriot-Watt Universities, which is a part of the Edinburgh Research Partnership (ERP). Chaoran Du gratefully acknowledges the support of the ERP in funding her PhD studies.

Index Terms

MIMO, time-reversal, target detection, detector design, waveform design

I. Introduction

The time-reversal (TR) technique has attracted increasing interest for a broad range of applications. The unique feature of TR is that it can turn multipath effects, traditionally a considered drawback, into a benefit, which is very similar to the MIMO concept. In the TR approach, a signal is radiated through the medium, then the backscattered signal is recorded, time reversed, and retransmitted. This technique is not new, Fink *et. al.* applied TR to focus energy on scatterers through an inhomogeneous medium two decades ago [1], [2], demonstrating super-resolution in the acoustic and ultrasound domains. There are also extensive publications studying the applications of TR, such as random media [3], ultra-wideband communications [4], and computational imaging [5], [6]. Recently, Moura *et. al.* explored the MIMO radar detection using TR, showing that TR detection provides significant gains over conventional detection [7]–[9]. This results from the fact that the transmitter reshapes the waveform to match the channel during the TR process, which is a waveform design process. However, the retransmitted signal in Moura's algorithm contains noise components, and obviously the TR technique is no longer a good choice when the noise level is high. Furthermore, [7]–[9] did not derive analytical expressions for the threshold and probability of detection of the TR detection, which are determined by Monte Carlo simulations.

We investigate a MIMO detection process similar to TR detection in this paper. That is, during the probing phase, an incident wave is transmitted into the medium and an estimated channel matrix with estimation error is obtained. It is assumed that a parameter indicating the estimation quality is given *a priori*, which can be appropriately chosen depending on the noise level, the channel dynamics, and estimation strategies, *etc.* [10]–[12]. Then, a waveform designed based on the estimated channel and the estimation quality parameter under power constraints, instead of the normalized TR signal used in Moura's scheme, is retransmitted, and finally the detector determines the presence or absence of a target. Note here that similar to TR detection, it is assumed that the channel remains static during the probing and detecting phases, *i.e.*, the scheme is only suited to low doppler scenarios. The waveform design problem for a MIMO communication system maximizing the channel capacity when estimation error exists is explored in [10]–[12], and it is assumed that the estimated channel and the estimation error are independent. In this paper, we assume that the estimation error is independent of the channel and their sum is the estimated channel. Although the waveforms are designed for MIMO radar in [13] [14],

they only assumed that the second-order statistics of the channel matrix is known and based on which the algorithms are developed. Here, however, we design the detector and the waveform according to the value of an instantaneous estimated channel matrix.

This paper is organized as follows. We first introduce the system model of the MIMO system. Three detectors are formulated in Section III, whose theoretical thresholds and probabilities of detection are expressed in closed form formulae. We then propose three criteria to design the retransmitted waveform under power constraints. Section V presents the numerical results to compare the detection performance of a MIMO system with different detectors and retransmitted waveforms. Finally, we give some discussion and draw conclusions.

II. System Model

We consider a wideband bistatic MIMO radar (or sonar) system including a pair of arrays A and B, which has N_a and N_b sensors, respectively. The channel frequency response matrix is denoted by an $N_b \times N_a$ matrix $\bar{H}(f_q)$, $q = 1, 2, ..., Q_f$, where the (i, j)-th entry of $\bar{H}(f_q)$, $h_{ij}(f_q)$, is the frequency response of the channel between the i-th sensor of Array B and the j-th sensor of Array A at the discrete frequency f_q. It is assumed that the sequential frequencies f_q are one coherence bandwidth apart and hence the channel matrices at different frequencies are considered to be independent [15]. We adopt the statistical MIMO model here, that is, the entries of the channel matrix are modeled as independent zero-mean complex Gaussian random variables, and they are normalized to have unit variance. Note that such a model has been utilized in [9] and [16], but the propagation mechanisms causing multipaths, which result in the random target response, are different. In [9], the multipaths are due to a rich scattering environment surrounding point-like targets, while in [16], the distributed target itself leads to multipath propagation.

As shown in Fig.1, the target detection process has two steps. During the probing phase, for the p-th snapshot, the i-th sensor of Array A transmits an incident wideband signal $s_{pi}(t)$ into the medium, whose discrete Fourier transform is $S_{pi}(f_q)$ at frequency f_q. The signal vector received by Array B for the p-th snapshot is

$$\bar{x}_p(f_q) = \bar{H}(f_q) \cdot \bar{s}_p(f_q) + \bar{\varpi}_p(f_q) \tag{1}$$

where $\bar{\varpi}_p(f_q)$ is the noise vector at Array B whose entries are assumed to be zero-mean complex Gaussian random variables with variance σ_ϖ^2, and the $N_a \times 1$ signal vector $\bar{s}_p(f_q) = [S_{p1}(f_q), S_{p2}(f_q), \cdots, S_{pN_a}(f_q)]^T$. Here the superscript T denotes matrix transpose. Based on all the P snapshots $\bar{x}_p(f_q)$, the estimated

channel matrix $\hat{\bar{H}}(f_q)$ is obtained, whose (i,j)-th entry is expressed as

$$\hat{h}_{ij}(f_q) = h_{ij}(f_q) + e_{ij}(f_q) \tag{2}$$

where $e_{ij}(f_q)$ is the (i,j)-th element of the channel estimation error matrix $\bar{E}(f_q)$. We assume that $e_{ij}(f_q)$ is a zero-mean complex Gaussian random variable which is independent of $h_{ij}(f_q)$ and has variance σ_e^2. Note here that knowing the value of σ_e^2 requires noise power estimation and knowledge of the estimation method and the waveform length during the probing phase. From (2), we know that $\hat{h}_{ij}(f_q)$ is a zero-mean complex Gaussian random variable with variance $1+\sigma_e^2$ and is dependent on $h_{ij}(f_q)$ with correlation coefficient $1/\sqrt{1+\sigma_e^2}$. Therefore, conditioned on $\hat{h}_{ij}(f_q)$, the random variable $h_{ij}(f_q)$ has mean $\sigma^2\hat{h}_{ij}(f_q)$ and variance $\sigma^2\sigma_e^2$. Here, we define $\sigma^2 \triangleq \frac{1}{1+\sigma_e^2}$.

Next, as shown in Fig.1(b), the signal $\bar{y}(f_q)$ designed based on $\hat{\bar{H}}(f_q)$ and σ_e^2 is retransmitted from Array B during the detecting phase, and the detector at Array A determines whether or not a target exists based on the received signal $\bar{r}(f_q)$ at all of the Q_f frequencies. Since the focus of this paper is to design different detectors and retransmitted waveforms and study their effects on the detection performance, we assume that, if it is required, the estimated channel matrix $\hat{\bar{H}}(f_q)$, the estimation error parameter σ_e^2, and the retransmitted waveform $\bar{Y}$ at Array B are fed back to Array A via a side channel, and we concentrate on analyzing the second detection stage.

It is assumed that Array B transmits M snapshots in the second phase, during which the channel remains the same. Denote the M snapshots received by the i-th sensor of Array A at frequency f_q and the corresponding additive white Gaussian noise components by $M\times 1$ vectors $\bar{r}_i(f_q)$ and $\bar{n}_i(f_q)$, respectively, which can be written as

$$\bar{r}_i(f_q) = \bar{Y}(f_q)\cdot\bar{h}_i(f_q) + \bar{n}_i(f_q) \tag{3}$$

where $i = 1,2,...,N_a$, $q = 1,2,...,Q_f$, and

$$\begin{aligned}\bar{Y}(f_q) &= \left[\begin{array}{cccc} \bar{y}_1(f_q) & \bar{y}_2(f_q) & \cdots & \bar{y}_M(f_q)\end{array}\right]^T \\ \bar{H}(f_q) &= \left[\begin{array}{cccc} \bar{h}_1(f_q) & \bar{h}_2(f_q) & \cdots & \bar{h}_{N_a}(f_q)\end{array}\right]\end{aligned} \tag{4}$$

where the $N_b\times 1$ vector $\bar{y}_m(f_q)$ is the m-th snapshot signal retransmitted from Array B at frequency f_q, and the entries of $\bar{n}_i(f_q)$ are assumed to be zero-mean complex Gaussian random variables with variance σ_n^2. Grouping the signals received by the i-th sensor of Array A at all the Q_f frequencies yields an $MQ_f\times 1$ vector $\bar{r}_i$, which is given by

$$\bar{r}_i = \left[\begin{array}{cccc} \bar{r}_i^T(f_1) & \bar{r}_i^T(f_2) & \cdots & \bar{r}_i^T(f_{Q_f})\end{array}\right]^T = \bar{Y}\bar{h}_i + \bar{n}_i \tag{5}$$

where the $N_bQ_f \times 1$ vector $\bar{h}_i$ and the $MQ_f \times 1$ vector $\bar{n}_i$ are obtained by sequentially stacking all the Q_f vectors $\bar{h}_i(f_q)$ and $\bar{n}_i(f_q)$ into columns, respectively. The $MQ_f \times N_bQ_f$ matrix $\bar{Y}$ is a block diagonal matrix with the Q_f matrices $\bar{Y}(f_q)$ arranged sequentially along its main diagonal blocks. Similar to the channel vectors $\bar{h}_i$, we can obtain N_a estimated channel vectors $\hat{\bar{h}}_i$ and estimation error vectors $\bar{e}_i$ by stacking the corresponding columns of $\hat{\bar{H}}(f_q)$ and $\bar{E}(f_q)$ into $N_bQ_f \times 1$ columns, respectively, and $\hat{\bar{h}}_i = \bar{h}_i + \bar{e}_i$. Based on previous discussion, it is easy to see that

$$\begin{aligned} \bar{h}_i \left| \hat{\bar{h}}_i \right. &\sim \mathcal{CN}\left(\sigma^2 \hat{\bar{h}}_i, \sigma^2 \sigma_e^2 \bar{I}_{N_bQ_f}\right) \\ \bar{n}_i &\sim \mathcal{CN}\left(\bar{0}_{MQ_f}, \sigma_n^2 \bar{I}_{MQ_f}\right) \end{aligned} \tag{6}$$

where $i = 1, 2, ..., N_a$, the separator "|" represents "conditioned on", and $\bar{0}_k$ and $\bar{I}_k$ stand for a $k \times 1$ all-zeros vector and a $k \times k$ identity matrix, respectively. The detector at Array A determines whether or not a target exists based on the values of all the N_a vectors $\bar{r}_i$. In this paper, we restrict our attention to the design of the detector and the retransmitted waveform $\bar{Y}$, which will be explained in the following sections.

III. Detector Design

The target detection problem of the MIMO system can be described as follows:

$$\bar{r}_i = \begin{cases} \bar{n}_i & \mathcal{H}_0 \\ \bar{Y} \cdot \bar{h}_i + \bar{n}_i & \mathcal{H}_1 \end{cases} \tag{7}$$

where $i = 1, 2, ..., N_a$, and the alternate hypothesis $\mathcal{H}_1$ and null hypothesis $\mathcal{H}_0$ are that the target does or does not exist, respectively. From (5) and (6), it is obvious that the received signals $\bar{r}_i$ are complex Gaussian vectors under both hypotheses with different distributions given the estimated channel:

$$\begin{aligned} \bar{r}_i &\sim \begin{cases} \mathcal{CN}\left(\bar{0}_{MQ_f}, \sigma_n^2 \bar{I}_{MQ_f}\right) & \mathcal{H}_0 \\ \mathcal{CN}\left(\bar{d}_i, \bar{C}\right) & \mathcal{H}_1 \end{cases} \\ \bar{d}_i &= \sigma^2 \bar{Y} \hat{\bar{h}}_i, \quad \bar{C} = \sigma^2 \sigma_e^2 \bar{Y} \bar{Y}^H + \sigma_n^2 \bar{I}_{MQ_f} \end{aligned} \tag{8}$$

In this paper, we develop three approaches to detect the target, and the theoretical threshold η and the probability of detection $\mathrm{Pr_D}$ of each detector will be derived in this section. Notice that in order to express the distribution of a weighted sum of several noncentral chi-square random variables in a closed form equation, we use a common approximation technique [17] in the derivation for both Detector II and Detector III. This approach approximates a weighted sum of chi-square variables by a single one with different degree of freedom and a scaling factor, which are carefully chosen such that the first two moments remain the same.

A. Detector I: Conventional Detector

It is well known that the optimal detector for a known signal in white Gaussian noise is a matched filter [18], and such a detector is employed as Detector I, whose performance is examined when estimation errors exist in channel matrix. The conventional detector given by [18] can be expressed as

$$T_{\mathrm{I}} = \mathrm{Re}[\sum_{i=1}^{N_a} (\bar{Y}\hat{\bar{h}}_i)^H \bar{r}_i] \underset{<\mathcal{H}_0}{>^{\mathcal{H}_1}} \eta_{\mathrm{I}} \tag{9}$$

where the superscript H represents the conjugate transpose of a matrix. Notice here that the detector actually matches to the estimated channel $\hat{\bar{h}}_i$ instead of the true channel $\bar{h}_i$ as in [18] since only the noisy channel estimation is available. From (8) and (9), the distributions of the test statistic T_{I} under both hypotheses can be given by

$$\begin{aligned} T_{\mathrm{I}} &\sim \begin{cases} \mathcal{N}\left(0, \frac{1}{2}\sum_{i=1}^{N_a} \Upsilon_{1i}\right) & \mathcal{H}_0 \\ \mathcal{N}\left(\sum_{i=1}^{N_a} \hat{\bar{h}}_i^H \bar{Y}^H \bar{d}_i, \frac{1}{2}\sum_{i=1}^{N_a} \{\Upsilon_{1i} + \Upsilon_{2i}\}\right) & \mathcal{H}_1 \end{cases} \\ \Upsilon_{1i} &= \sigma_n^2 \hat{\bar{h}}_i^H \bar{Y}^H \bar{Y} \hat{\bar{h}}_i, \;\; \Upsilon_{2i} = \sigma^2 \sigma_e^2 \hat{\bar{h}}_i^H \bar{Y}^H \bar{Y} \bar{Y}^H \bar{Y} \hat{\bar{h}}_i \end{aligned} \tag{10}$$

Before we proceed to derive the theoretical threshold and probability of detection, we denote the singular value decomposition (SVD) of $\bar{Y}$ by $\bar{U}\bar{\Sigma}\bar{V}^H$, where the $MQ_f \times MQ_f$ matrix $\bar{U}$ and $N_bQ_f \times N_bQ_f$ matrix $\bar{V}$ are unitary matrices. When $M \geq N_b$, $\bar{\Sigma} = \begin{bmatrix} \bar{\Sigma}_1 & \bar{0} \end{bmatrix}^T$. Here $\bar{\Sigma}_1$ is an $N_bQ_f \times N_bQ_f$ diagonal matrix with n positive singular values $\varsigma_1, \varsigma_2, ..., \varsigma_n$ of $\bar{Y}$ (in decreasing order) on the diagonal and the all-zeros matrix has dimensions $N_bQ_f \times (M - N_b)Q_f$. While $M < N_b$, $\bar{\Sigma} = \begin{bmatrix} \bar{\Sigma}_2 & \bar{0} \end{bmatrix}$, and $\bar{\Sigma}_2$ is a $MQ_f \times MQ_f$ matrix with n singular values on the diagonal and the all-zeros matrix has dimensions $MQ_f \times (N_b - M)Q_f$. Here, n is the rank of $\bar{Y}$, *i.e.*, $n = \mathrm{rank}(\bar{Y}) \leq \min(MQ_f, N_BQ_f)$. Therefore, we can obtain the following expressions:

$$\begin{aligned} \sum_{i=1}^{N_a} \hat{\bar{h}}_i^H \bar{Y}^H \bar{Y} \hat{\bar{h}}_i &= \sum_{i=1}^{N_a} \hat{\bar{h}}_i^H \bar{V} \begin{bmatrix} \bar{\Xi} & \bar{0} \\ \bar{0} & \bar{0} \end{bmatrix} \bar{V}^H \hat{\bar{h}}_i \\ \sum_{i=1}^{N_a} \hat{\bar{h}}_i^H \bar{Y}^H \bar{Y} \bar{Y}^H \bar{Y} \hat{\bar{h}}_i &= \sum_{i=1}^{N_a} \hat{\bar{h}}_i^H \bar{V} \begin{bmatrix} \bar{\Xi}^2 & \bar{0} \\ \bar{0} & \bar{0} \end{bmatrix} \bar{V}^H \hat{\bar{h}}_i \end{aligned} \tag{11}$$

where the $n \times n$ diagonal matrix $\bar{\Xi} = \mathrm{diag}(\bar{\beta})$, and the k-th entry of the $n \times 1$ vector $\bar{\beta}$ is the square of the corresponding singular value of $\bar{Y}$, *i.e.*, $\beta_k = \varsigma_k^2$. Denote the k-th element of the vector $\bar{h}_i' = \bar{V}^H \hat{\bar{h}}_i$

by h'_{ik} and let $\rho_k = \sum_{i=1}^{N_a} |h'_{ik}|^2$, the above equations can be rewritten as

$$\begin{aligned} \sum_{i=1}^{N_a} \hat{\bar{h}}_i^H \bar{Y}^H \bar{Y} \hat{\bar{h}}_i &= \sum_{k=1}^{n} \beta_k \rho_k \\ \sum_{i=1}^{N_a} \hat{\bar{h}}_i^H \bar{Y}^H \bar{Y} \bar{Y}^H \bar{Y} \hat{\bar{h}}_i &= \sum_{k=1}^{n} \beta_k^2 \rho_k \end{aligned} \tag{12}$$

where $|\cdot|$ stands for the modulus of a complex number. For a given noise level, the threshold for the conventional detector η_{I} can be determined by the required probability of false alarm $\mathrm{Pr_{FA}}$ following (10) and (12) as below:

$$\eta_{\mathrm{I}} = \sqrt{\frac{\sigma_n^2}{2} \sum_{k=1}^{n} \beta_k \rho_k} \cdot Q^{-1}(\mathrm{Pr_{FA}}) \tag{13}$$

From (9) and (13), it is obvious that Detector I requires knowledge of $\bar{Y}$ and $\hat{\bar{h}}_i$ at Array A in Fig.1 to decide the existence of targets. Based on (10) and (13), the theoretical probability of detection of Detector I $\mathrm{Pr_{D,I}}$ can be given by

$$\mathrm{Pr_{D,I}} = Q\left(\frac{\eta_{\mathrm{I}} - \sigma^2 \sum_{k=1}^{n} \beta_k \rho_k}{\sqrt{\frac{1}{2}\left\{ \sigma^2 \sigma_e^2 \sum_{k=1}^{n} \beta_k^2 \rho_k + \sigma_n^2 \sum_{k=1}^{n} \beta_k \rho_k \right\}}} \right) \tag{14}$$

where the functions $Q(x)$ and $Q^{-1}(x)$ denote the Gaussian right-tail function and its inverse, respectively.

B. Detector II: Optimal Detector

Next, we proceed to design Detector II, which is the likelihood ratio test (LRT) detector for the case when $\sigma_e^2 > 0$. The LRT detector is the optimal solution to the hypotheses testing problem in the Neyman-Pearson sense, *i.e.*, the detector maximizes $\mathrm{Pr_D}$ subject to a constraint on $\mathrm{Pr_{FA}}$ [18]. The LRT can be stated as the following decision rule

$$L(\bar{r}) = \frac{p(\bar{r}_1, \bar{r}_2, ..., \bar{r}_{N_a} | \mathcal{H}_1)}{p(\bar{r}_1, \bar{r}_2, ..., \bar{r}_{N_a} | \mathcal{H}_0)} \underset{<\mathcal{H}_0}{>\mathcal{H}_1} \eta \tag{15}$$

where $p(\bar{r}_1, \bar{r}_2, ..., \bar{r}_{N_a} | \mathcal{H}_1)$ and $p(\bar{r}_1, \bar{r}_2, ..., \bar{r}_{N_a} | \mathcal{H}_0)$ are the probability density functions (PDFs) of the data under hypotheses $\mathcal{H}_1$ and $\mathcal{H}_0$, respectively. Based on (8) and (15) and after some algebra, we decide $\mathcal{H}_1$ if

$$\begin{aligned} T' &= \sum_{i=1}^{N_a} \left\{ \bar{r}_i^H \bar{B} \bar{r}_i + \bar{r}_i^H \bar{g}_i + \bar{g}_i^H \bar{r}_i \right\} > \eta' \\ \bar{B} &= \tfrac{1}{\sigma_n^2} \bar{I}_{MQ_f} - \bar{C}^{-1}, \bar{g}_i = \bar{C}^{-1} \bar{d}_i \end{aligned} \tag{16}$$

In order to analyze the distribution of the test statistic, a non-data-dependent term $\sum_{i=1}^{N_a} \bar{g}_i^H \bar{B}^\dagger \bar{g}_i$ is added at both sides of (16), and the detector equation can be written as below:

$$T_{\mathrm{II}} = \sum_{i=1}^{N_a} \left\{ \left(\bar{r}_i + \bar{B}^\dagger \bar{g}_i \right)^H \cdot \bar{B} \cdot \left(\bar{r}_i + \bar{B}^\dagger \bar{g}_i \right) \right\} \begin{array}{l} >^{\mathcal{H}_1} \\ <_{\mathcal{H}_0} \end{array} \eta_{\mathrm{II}} \tag{17}$$

where † denotes the Moore-Penrose pseudoinverse. From (8) and (16), the following equations can be derived based on the SVD of $\bar{Y}$ mentioned in Section III-A:

$$\begin{aligned} \bar{C} &= \bar{U} \begin{bmatrix} \sigma^2 \sigma_e^2 \bar{\Xi} + \sigma_n^2 \bar{I}_n & \bar{0} \\ \bar{0} & \sigma_n^2 \bar{I}_{MQ_f - n} \end{bmatrix} \bar{U}^H \\ \bar{B} &= \bar{U} \begin{bmatrix} \frac{1}{\sigma_n^2} \bar{I}_n - \left(\sigma^2 \sigma_e^2 \bar{\Xi} + \sigma_n^2 \bar{I}_n \right)^{-1} & \bar{0} \\ \bar{0} & \bar{0} \end{bmatrix} \bar{U}^H \end{aligned} \tag{18}$$

Substituting (18) into (17), we can express the test statistic under $\mathcal{H}_0$ as below:

$$\begin{aligned} T_{\mathrm{II}} &= \sum_{i=1}^{N_a} \bar{z}_{0i}^H \begin{bmatrix} \frac{1}{\sigma_n^2} \bar{I}_n - \left(\sigma^2 \sigma_e^2 \bar{\Xi} + \sigma_n^2 \bar{I}_n \right)^{-1} & \bar{0} \\ \bar{0} & \bar{0} \end{bmatrix} \bar{z}_{0i} \\ &= \frac{1}{2} \sum_{i=1}^{N_a} \sum_{k=1}^{n} \frac{\sigma^2 \sigma_e^2 \beta_k}{\sigma^2 \sigma_e^2 \beta_k + \sigma_n^2} \left(2 \left| z_{0ik} \right|^2 \right) \qquad \text{Under } \mathcal{H}_0 \end{aligned} \tag{19}$$

where z_{0ik} is the k-th entry of the vector $\bar{z}_{0i} = \bar{U}^H \left(\bar{r}_i + \bar{B}^\dagger \bar{g}_i \right) \Big/ \sigma_n$. Denote γ_{0ik} the k-th element of the vector $\bar{U}^H \bar{B}^\dagger \bar{g}_i \Big/ \sigma_n$, which is given by

$$\gamma_{0ik} = \frac{\sigma^2 \sigma_n^2 \sigma_e^2 \beta_k + \sigma_n^4}{\sigma_n \sigma_e^2 \beta_k \left(\sigma^2 \sigma_e^2 \beta_k + \sigma_n^2 \right)} \varsigma_k h'_{ik} = \frac{\sigma_n h'_{ik}}{\sigma_e^2 \varsigma_k} \tag{20}$$

Following (8), it is not difficult to see that $\bar{z}_{0i} \sim \mathcal{CN} \left(\bar{U}^H \bar{B}^\dagger \bar{g}_i \Big/ \sigma_n, \bar{I}_{MQ_f} \right)$, and thus we have

$$2 \left| z_{0ik} \right|^2 \sim \chi_2^{'2} \left(2 \left| \gamma_{0ik} \right|^2 \right) = \chi_2^{'2} \left(\frac{2 \sigma_n^2 \left| h'_{ik} \right|^2}{\sigma_e^4 \beta_k} \right) \tag{21}$$

where $\chi_k^{'2}(\lambda)$ denotes a noncentral chi-square random variable with k degrees of freedom and noncentrality parameter λ. Notice that T_{II} is a weighted sum of noncentral chi-square random variables, and thus, it can be approximated as below by using the approximation technique mentioned before:

$$T_{\mathrm{II}} \sim \frac{1}{2} \sum_{i=1}^{N_a} \sum_{k=1}^{n} \frac{\sigma^2 \sigma_e^2 \beta_k}{\sigma^2 \sigma_e^2 \beta_k + \sigma_n^2} \chi_2^{'2} \left(\frac{2 \sigma_n^2 \left| h'_{ik} \right|^2}{\sigma_e^4 \beta_k} \right) \doteq \theta_0 \chi_{k_0}^2 \tag{22}$$

where χ_k^2 denotes a chi-square random variable with k degrees of freedom. The condition that the first two moments of both sides of (22) are the same leads to

$$\begin{aligned} &\frac{1}{2} \sum_{i=1}^{N_a} \sum_{k=1}^{n} \frac{\sigma^2 \sigma_e^2 \beta_k}{\sigma^2 \sigma_e^2 \beta_k + \sigma_n^2} \left(2 + \frac{2 \sigma_n^2 \left| h'_{ik} \right|^2}{\sigma_e^4 \beta_k} \right) = \theta_0 k_0 \\ &\frac{1}{4} \sum_{i=1}^{N_a} \sum_{k=1}^{n} \frac{\sigma^4 \sigma_e^4 \beta_k^2}{\left(\sigma^2 \sigma_e^2 \beta_k + \sigma_n^2 \right)^2} \cdot 2 \cdot \left(2 + \frac{4 \sigma_n^2 \left| h'_{ik} \right|^2}{\sigma_e^4 \beta_k} \right) = 2 \theta_0^2 k_0 \end{aligned} \tag{23}$$

Solving the above equation for the parameters θ_0 and k_0 yields the following expressions:

$$\begin{aligned}&\theta_0 = \Omega_0/\mu_0, \qquad k_0 = \mu_0^2/\Omega_0\\ &\mu_0 = \sum_{k=1}^{n} \sigma^2 \left(N_a\sigma_e^4\beta_k + \sigma_n^2\rho_k\right)/\left(\sigma^2\sigma_e^4\beta_k + \sigma_e^2\sigma_n^2\right)\\ &\Omega_0 = \sum_{k=1}^{n} \sigma^4\beta_k\left(N_a\sigma_e^4\beta_k + 2\sigma_n^2\rho_k\right)\Big/\left[2\left(\sigma^2\sigma_e^2\beta_k + \sigma_n^2\right)^2\right]\end{aligned} \tag{24}$$

Following (22), we can obtain the threshold for Detector II based on the choice of $\mathrm{Pr_{FA}}$:

$$\eta_{\mathrm{II}} = \theta_0 \mathcal{F}^{-1}_{\chi^2_{k_0}}\left(1 - \mathrm{Pr_{FA}}\right) \tag{25}$$

where $\mathcal{F}^{-1}_{\chi^2_k}$ is the inverse cumulative distribution function (CDF) of a chi-square random variable with k degrees of freedom. From (17) and (25), it is clear that the implementation of Detector II requires knowledge of $\bar{Y}$, $\hat{\bar{h}}_i$, and σ_e^2 at Array A in Fig.1. We next consider the alternate hypothesis. Based on (8), the received signal under $\mathcal{H}_1$ can be rewritten as $\bar{r}_i = \bar{d}_i + \bar{w}_i$ and $\bar{w}_i \sim \mathcal{CN}(\bar{0}_{MQ_f}, \bar{C})$. Thus, we have

$$\begin{aligned}T_{\mathrm{II}} = \sum_{i=1}^{N_a} \Big\{ &\left[\bar{C}^{-\frac{1}{2}}\bar{w}_i + \bar{C}^{-\frac{1}{2}}\left(\bar{d}_i + \bar{B}^{\dagger}\bar{g}_i\right)\right]^H \cdot \bar{C}^{\frac{1}{2}}\bar{B}\bar{C}^{\frac{1}{2}} \cdot\\ &\left[\bar{C}^{-\frac{1}{2}}\bar{w}_i + \bar{C}^{-\frac{1}{2}}\left(\bar{d}_i + \bar{B}^{\dagger}\bar{g}_i\right)\right]\Big\}\end{aligned} \tag{26}$$

Substituting (18) into (26) and letting $\bar{z}_{1i} = \bar{U}^H\left(\bar{C}^{-\frac{1}{2}}\bar{w}_i + \bar{C}^{-\frac{1}{2}}\left(\bar{d}_i + \bar{B}^{\dagger}\bar{g}_i\right)\right)$, we can express the test statistic T_{II} under $\mathcal{H}_1$ as below:

$$\begin{aligned}T_{\mathrm{II}} = &\sum_{i=1}^{N_a} \bar{z}_{1i}^H \cdot \begin{bmatrix} \frac{1}{\sigma_n^2}\bar{I}_n - \left(\sigma^2\sigma_e^2\bar{\Xi} + \sigma_n^2\bar{I}_n\right)^{-1} & \bar{0} \\ \bar{0} & \bar{0}\end{bmatrix} \cdot\\ &\begin{bmatrix} \sigma^2\sigma_e^2\bar{\Xi} + \sigma_n^2\bar{I}_n & \bar{0} \\ \bar{0} & \sigma_n^2\bar{I}_{MQ_f - n}\end{bmatrix} \cdot \bar{z}_{1i}\\ = &\frac{1}{2}\sum_{i=1}^{N_a}\sum_{k=1}^{n} \frac{\sigma^2\sigma_e^2\beta_k}{\sigma_n^2}\left(2\left|z_{1ik}\right|^2\right) \qquad \text{Under } \mathcal{H}_1\end{aligned} \tag{27}$$

where z_{1ik} is the k-th element of the vector $\bar{z}_{1i}$. Denote γ_{1ik} the k-th entry of the vector $\bar{U}^H\bar{C}^{-\frac{1}{2}}\left(\bar{d}_i + \bar{B}^{\dagger}\bar{g}_i\right)$, which is

$$\begin{aligned}\gamma_{1ik} = &\left(\sigma^2\sigma_e^2\beta_k + \sigma_n^2\right)^{-1/2}\Big\{1 + \left(\sigma^2\sigma_e^2\beta_k + \sigma_n^2\right)^{-1}\\ &\left(\frac{\sigma^2\sigma_e^2\beta_k}{\sigma^2\sigma_n^2\sigma_e^2\beta_k + \sigma_n^4}\right)^{-1}\Big\}\frac{\varsigma_k h'_{ik}}{1+\sigma_e^2} = \frac{\sqrt{\sigma^2\sigma_e^2\beta_k + \sigma_n^2}\cdot h'_{ik}}{\sigma_e^2\varsigma_k}\end{aligned} \tag{28}$$

Given $\bar{z}_{1i} \sim \mathcal{CN}\left(\bar{U}^H\bar{C}^{-\frac{1}{2}}\left(\bar{d}_i + \bar{B}^{\dagger}\bar{g}_i\right), \bar{I}_{MQ_f}\right)$, we have

$$2\left|z_{1ik}\right|^2 \sim \chi_2^{'2}\left(2\left|\gamma_{1ik}\right|^2\right) = \chi_2^{'2}\left(\frac{2(\sigma^2\sigma_e^2\beta_k + \sigma_n^2)|h'_{ik}|^2}{\sigma_e^4\beta_k}\right) \tag{29}$$

Similar to (22), we have the following approximation:

$$T_{\mathrm{II}} \sim \frac{1}{2}\sum_{i=1}^{N_a}\sum_{k=1}^{n}\frac{\sigma^2\sigma_e^2\beta_k}{\sigma_n^2}\chi_2^{'2}\left(\frac{2\left(\sigma^2\sigma_e^2\beta_k + \sigma_n^2\right)|h'_{ik}|^2}{\sigma_e^4\beta_k}\right) \doteq \theta_1\chi^2_{k_1} \tag{30}$$

Following the same procedure shown in (23) and (24), we can obtain the parameters θ_1 and k_1 for $T_{\rm II}$ under $\mathcal{H}_1$ as below:

$$\begin{aligned}
&\theta_1 = \Omega_1/\mu_1, \quad k_1 = \mu_1^2/\Omega_1 \\
&\mu_1 = \tfrac{\sigma^2}{\sigma_n^2\sigma_e^2} \sum_{k=1}^{n} \left\{ N_a\sigma_e^4\beta_k + \left(\sigma^2\sigma_e^2\beta_k + \sigma_n^2\right)\rho_k \right\} \\
&\Omega_1 = \tfrac{\sigma^4}{2\sigma_n^4} \sum_{k=1}^{n} \left\{ N_a\sigma_e^4\beta_k^2 + 2\beta_k\left(\sigma^2\sigma_e^2\beta_k + \sigma_n^2\right)\rho_k \right\}
\end{aligned} \tag{31}$$

Based on (30), the theoretical probability of detection of Detector II can be given by

$$\Pr_{\rm D,II} = 1 - \mathcal{F}_{\chi^2_{k_1}}\left(\tfrac{\eta_{\rm II}}{\theta_1}\right) \tag{32}$$

where $\mathcal{F}_{\chi^2_k}$ is the CDF of a chi-square random variable with k degrees of freedom.

C. Detector III: GLRT Detector

Detector III is the generalized likelihood ratio test (GLRT) detector, which is a practical approach when unknown parameters exist [18]. The GLRT detector replaces the unknowns with their maximum likelihood (ML) estimates, and the decision rule can be recast as below [14]:

$$\sum_{i=1}^{N_a} \bar{r}_i^H \bar{r}_i - \sum_{i=1}^{N_a} \min_{\bar{h}_1,\bar{h}_2,\ldots,\bar{h}_{N_a}} \left\| \bar{r}_i - \bar{Y}\bar{h}_i \right\|^2 \underset{<\mathcal{H}_0}{>^{\mathcal{H}_1}} \eta \tag{33}$$

where $\|\cdot\|$ stands for the Euclidean norm. Based on (7), we can derive the GLRT detector as follows:

$$T_{\rm III} = \sum_{i=1}^{N_a} \frac{2\bar{r}_i^H \bar{Y}\left(\bar{Y}^H\bar{Y}\right)^{\dagger}\bar{Y}^H\bar{r}_i}{\sigma_n^2} \underset{<\mathcal{H}_0}{>^{\mathcal{H}_1}} \eta_{\rm III} \tag{34}$$

Invoking the SVD of $\bar{Y}$, $T_{\rm III}$ under $\mathcal{H}_0$ can be written as

$$\begin{aligned}
T_{\rm III} &= \sum_{i=1}^{N_a} \left(\tfrac{2}{\sigma_n^2}\bar{r}_i^H\bar{U} \begin{bmatrix} \bar{I}_n & \bar{0} \\ \bar{0} & \bar{0} \end{bmatrix} \bar{U}^H\bar{r}_i \right) \\
&= \sum_{i=1}^{N_a}\sum_{k=1}^{n} \tfrac{2}{\sigma_n^2}\left|\psi_{0ik}\right|^2 \sim \chi^2_{2nN_a}
\end{aligned} \tag{35}$$

The above result comes from the fact that the vector $\bar{\psi}_{0i} = \bar{U}^H\bar{r}_i \sim \mathcal{CN}\left(\bar{0}_{MQ_f}, \sigma_n^2\bar{I}_{MQ_f}\right)$ and ψ_{0ik} is the k-th element of $\bar{\psi}_{0i}$. Following (35), we can obtain the threshold for the GLRT detector based on the choice of $\Pr_{\rm FA}$:

$$\eta_{\rm III} = \mathcal{F}^{-1}_{\chi^2_{2nN_a}}\left(1 - \Pr_{\rm FA}\right) \tag{36}$$

From (34) and (36), only the value of $\bar{Y}$ is required to be known for Detector III at Array A in Fig.1. We next calculate the distribution of T_{III} under $\mathcal{H}_1$. Let the vector $\bar{\psi}_{1i} = \bar{U}^H \bar{C}^{-\frac{1}{2}} \bar{r}_i$ and we can rewrite (34) as

$$\begin{aligned} T_{\mathrm{III}} &= \sum_{i=1}^{N_a} \frac{2}{\sigma_n^2} \left\{ \bar{\psi}_{1i}^H \bar{U}^H \bar{C}^{\frac{1}{2}} \bar{Y} \left(\bar{Y}^H \bar{Y} \right)^{\dagger} \bar{Y}^H \bar{C}^{\frac{1}{2}} \bar{U} \bar{\psi}_{1i} \right\} \\ &= \sum_{i=1}^{N_a} \frac{2}{\sigma_n^2} \left\{ \bar{\psi}_{1i}^H \begin{bmatrix} \sigma^2 \sigma_e^2 \bar{\Xi} + \sigma_n^2 \bar{I}_n & \bar{0} \\ \bar{0} & \bar{0} \end{bmatrix} \bar{\psi}_{1i} \right\} \\ &= \sum_{i=1}^{N_a} \sum_{k=1}^{n} \frac{1}{\sigma_n^2} \left(\sigma^2 \sigma_e^2 \beta_k + \sigma_n^2 \right) \left(2 \left| \psi_{1ik} \right|^2 \right) \end{aligned} \tag{37}$$

where ψ_{1ik} is the k-th entry of the vector $\bar{\psi}_{1i}$. Denote λ_{1ik} the k-th element of the vector $\bar{U}^H \bar{C}^{-1/2} \bar{d}_i$, which is given by

$$\lambda_{1ik} = \left(\sigma^2 \sigma_e^2 \beta_k + \sigma_n^2 \right)^{-\frac{1}{2}} \cdot \sigma^2 \varsigma_k h'_{ik} \tag{38}$$

Given $\bar{\psi}_{1i} \sim \mathcal{CN} \left(\bar{U}^H \bar{C}^{-\frac{1}{2}} \bar{d}_i, \bar{I}_{MQ_f} \right)$, we have

$$2 \left| \psi_{1ik} \right|^2 \sim \chi_2^{'2} \left(2 \left| \lambda_{1ik} \right|^2 \right) = \chi_2^{'2} \left(\frac{2\sigma^4 \beta_k |h'_{ik}|^2}{\sigma^2 \sigma_e^2 \beta_k + \sigma_n^2} \right) \tag{39}$$

Similar to (22), the test statistic can be approximated as

$$T_{\mathrm{III}} \sim \frac{1}{\sigma_n^2} \sum_{i=1}^{N_a} \sum_{k=1}^{n} \left(\sigma^2 \sigma_e^2 \beta_k + \sigma_n^2 \right) \chi_2^{'2} \left(\frac{2\sigma^4 \beta_k |h'_{ik}|^2}{\sigma^2 \sigma_e^2 \beta_k + \sigma_n^2} \right) \doteq \frac{\alpha}{\sigma_n^2} \chi_l^2 \tag{40}$$

Following the same procedure shown in (23) and (24), we can derive the parameters α and l for T_{III} under $\mathcal{H}_1$ as below:

$$\begin{aligned} &\alpha = b/a, \quad l = a^2/b \\ &a = \sum_{k=1}^{n} 2 \left\{ N_a \left(\sigma^2 \sigma_e^2 \beta_k + \sigma_n^2 \right) + \sigma^4 \beta_k \rho_k \right\} \\ &b = \sum_{k=1}^{n} 2 \left\{ N_a \left(\sigma^2 \sigma_e^2 \beta_k + \sigma_n^2 \right)^2 + 2\sigma^4 \left(\sigma^2 \sigma_e^2 \beta_k + \sigma_n^2 \right) \beta_k \rho_k \right\} \end{aligned} \tag{41}$$

Hence, based on (40), the theoretical $\mathrm{Pr}_{\mathrm{D,III}}$ is given by

$$\mathrm{Pr}_{\mathrm{D,III}} = 1 - \mathcal{F}_{\chi_l^2} \left(\frac{\eta_{\mathrm{III}} \sigma_n^2}{\alpha} \right) \tag{42}$$

IV. Waveform Design

In this section, we propose three approaches to design the retransmitted waveform $\bar{Y}$ in order to improve the system detection performance. Notice here that all the schemes discussed in this section are under the constraint $\mathrm{trace}(\bar{Y}\bar{Y}^H) = ME_s$ which limits the total transmitted power.

A. Conventional Signal Scheme

We first introduce the conventional signal (CS) scheme similar to that in [7] [8] for comparison purposes in the numerical results. In the CS scheme, the same waveform is retransmitted from Array B regardless of the available channel information. In this paper, we assume that the k-th element of the retransmitted signal vector $\bar{y}_m(f_q)$ in (4) is given by

$$y_{mk}(f_q) = \sqrt{\frac{E_s}{N_b Q_f}} \exp\left[j2\pi(k-1)(q-1)/Q_f\right] \tag{43}$$

where $k = 1, 2, ..., N_b$, $q = 1, 2, ..., Q_f$, and the normalization factor is employed here to meet the power constraint.

B. Time Reversal scheme

Before introducing the proposed waveform designs, we first briefly describe the TR scheme proposed in [7]–[9]. The numbers of snapshots during the probing and detecting phases are assumed to be the same, and for each snapshot, Array A transmits an incident waveform and the signals received by Array B are recorded, time reversed, power normalized, and transmitted back into the medium. The signal received by Array B at frequency f_q for the m-th snapshot is denoted by $\bar{x}_m(f_q)$ in (1), and the m-th retransmitted TR signal is

$$\bar{y}_m(f_q) = k_m \bar{x}_m^*(f_q) = k_m \left[\bar{H}^*(f_q)\bar{s}_m^*(f_q) + \bar{\varpi}_m^*(f_q)\right] \tag{44}$$

where $k_m = \sqrt{E_s \Big/ \sum_{q=1}^{Q_f} \|\bar{x}_m(f_q)\|^2}$ is a normalization factor to meet the power constraint and the superscript $*$ stands for the complex conjugate. The conjugation here results from the fact that time reversal in the time domain corresponds to phase conjugation in the frequency domain up to a phase shift (see, *e.g.*, [1]).

The noise level at Array B, *i.e.*, the variance of the white Gaussian noise $\bar{\varpi}_m(f_q)$, is assumed to be known in [7]–[9]. In this paper, instead, we assume that the estimated channel matrix $\hat{\bar{H}}(f_q)$ and the estimation error parameter σ_e^2 are known. In order to fairly compare the performance of different waveform schemes, we modified the TR scheme as follows:

$$\bar{y}_m(f_q) = \sqrt{E_s \Big/ \sum_{q=1}^{Q_f} \left\|\hat{\bar{H}}(f_q)\bar{s}_m(f_q)\right\|^2} \left[\hat{\bar{H}}^*(f_q)\bar{s}_m^*(f_q)\right] \tag{45}$$

Such a modification actually approximates $\bar{x}_m(f_q)$ as $\hat{\bar{H}}(f_q)\bar{s}_m(f_q)$, which is reasonable since $\hat{\bar{H}}(f_q)$ is estimated based on $\bar{x}_m(f_q)$ and σ_e^2 is a function of the noise level at Array B. We name this modified

TR scheme as the matched-filter (MF) scheme in this paper in order to avoid confusion. Following the procedure mentioned in Section II, we can generate the retransmitted MF signal matrix $\bar{Y}_{MF}$ by assembling all the MQ_f vectors $\bar{y}_m(f_q)$ appropriately. In general, the incident waveform can be any signal and in the simulations we adopt $s_{mk}(f_q) = \exp\left[j2\pi(k-1)(q-1)/Q_f\right]$ in (45) as in [9] where $s_{mk}(f_q)$ is the k-th entry of the vector $\bar{s}_m(f_q)$.

C. Waveform Design A: MF upper scheme

As demonstrated in [7]–[9], the TR scheme improves the system detection performance significantly. Our goal in this section is to further improve the performance by designing a waveform based on the MF scheme above, in order to maximize an upper bound of $\mathrm{Pr_D}$ for the GLRT detector. Before we proceed to the waveform design, several parameters are defined similar to (36) and (37):

$$\begin{aligned} &\eta_{\mathrm{L}} = \mathcal{F}^{-1}_{\chi^2_{2N_a}}\left(1-\mathrm{Pr_{FA}}\right), \quad \eta_{\mathrm{U}} = \mathcal{F}^{-1}_{\chi^2_{2\vartheta N_a}}\left(1-\mathrm{Pr_{FA}}\right) \\ &T_{\mathrm{U}} = \sum_{i=1}^{N_a}\sum_{k=1}^{\vartheta} \tfrac{1}{\sigma_n^2}\left(\sigma^2\sigma_e^2\beta_k+\sigma_n^2\right)\left(2\left|\psi_{1ik}\right|^2\right) \\ &= T_{\mathrm{III}} + \sum_{i=1}^{N_a}\sum_{k=n+1}^{\vartheta} \tfrac{1}{\sigma_n^2}\left(\sigma^2\sigma_e^2\beta_k+\sigma_n^2\right)\left(2\left|\psi_{1ik}\right|^2\right) \end{aligned} \tag{46}$$

where $\vartheta = \min(N_bQ_f, MQ_f)$ and the second term in the last row is defined as T_{D}. Since n is the rank of $\bar{Y}$ and β_k is the square of the k-th singular value of $\bar{Y}$, we have $1 \le n \le \vartheta$ and $\beta_k = 0$ when $k > n$. Therefore, $2\left|\psi_{1ik}\right|^2 \sim \chi_2'^2\left(2\left|\lambda_{1ik}\right|^2\right) = \chi_2^2$ for $k > n$ and hence $T_{\mathrm{D}} \sim \chi^2_{2N_a(\vartheta-n)}$. It is not difficult to derive the following inequalities:

$$\eta_{\mathrm{U}} \ge \eta_{\mathrm{III}} \ge \eta_{\mathrm{L}} > 0, T_{\mathrm{U}} = T_{\mathrm{III}} + T_{\mathrm{D}}, T_{\mathrm{III}} > 0, T_{\mathrm{D}} \ge 0 \tag{47}$$

The reason for defining the above parameters is that before the waveform design, it is impossible to know the rank of $\bar{Y}$, and thereby the threshold and test statistic in (36) and (37) can not be employed directly during the design process because of the unknown value of n. Following (47), we can derive the required upper bound of $\mathrm{Pr_D}$ for the GLRT detector as below:

$$\mathrm{Pr_D} \le \mathrm{Pr}\left\{T_{\mathrm{III}} \ge \eta_{\mathrm{L}}\right\} \le \mathrm{Pr}\left\{T_{\mathrm{U}} \ge \eta_{\mathrm{L}}\right\} \le \mathrm{E}\left[T_{\mathrm{U}}\right]/\eta_{\mathrm{L}} \tag{48}$$

where the last inequality arises from Markov's inequality [19]. Taking the expectation of T_{U} in (46) yields

$$\mathrm{E}\left[T_{\mathrm{U}}\right] = \frac{2\sigma^4}{\sigma_n^2}\sum_{k=1}^{\vartheta}\left[\frac{N_a\sigma_n^2}{\sigma^4} + \left(\frac{N_a\sigma_e^2}{\sigma^2}+\rho_k\right)\beta_k\right] \tag{49}$$

where $\rho_k = \sum_{i=1}^{N_a} |h'_{ik}|^2 = \sum_{i=1}^{N_a} \bar{v}_k^H \hat{\bar{h}}_i \hat{\bar{h}}_i^H \bar{v}_k$ and $\bar{v}_k$ is the k-th right-singular vector of $\bar{Y}_{MF}$ introduced in the last section. The entries of $\bar{\beta}$ are the eigenvalues of the Hermitian matrix $\bar{Y}\bar{Y}^H$, and thus the design criterion under the power constraint can be expressed as the following constrained maximization problem:

$$\begin{aligned} &\max_{\bar{\beta}} \sum_{k=1}^{\vartheta} \left(N_a \sigma_e^2/\sigma^2 + \rho_k\right) \beta_k \\ &\text{s.t.} \sum_{k=1}^{\vartheta} \beta_k = ME_s, \beta_k \geq 0, k = 1, 2, ..., \vartheta \end{aligned} \tag{50}$$

Moreover, considering the fact that $[N_a \sigma_e^2 \left(1 + \sigma_e^2\right) + \rho_k]$ is positive and taking into account the constraints, we can derive the following equation employing Abel's inequality [20]:

$$\begin{aligned} &\sum_{k=1}^{\vartheta} \left(N_a \sigma_e^2/\sigma^2 + \rho_k\right) \beta_k \\ &\leq \max\left\{\beta_1, \beta_1 + \beta_2, ..., \sum_{k=1}^{\vartheta} \beta_k\right\} \max\left\{\tfrac{N_a \sigma_e^2}{\sigma^2} + \rho_k\right\} \\ &= ME_s \cdot \left(N_a \sigma_e^2/\sigma^2 + \max\left\{\rho_k\right\}\right) \end{aligned} \tag{51}$$

From (51), it is easy to understand that the maximization of (50) is achieved by allocating all the available power to the eigenvalue β_k which corresponds to the largest ρ_k.

D. Waveform Design B: MF lower scheme

Now we design the second waveform by maximizing a lower bound of $\mathrm{Pr_D}$ for the GLRT detector based on the MF scheme. Similar to the last section, (47) leads to

$$\mathrm{Pr_D} \geq 1 - \Pr\left\{T_{\mathrm{III}} \leq \eta_{\mathrm{U}}\right\} \geq 1 - \tfrac{\Pr\{T_{\mathrm{III}} + T_{\mathrm{D}} \leq 2\eta_{\mathrm{U}}\}}{\Pr\{T_{\mathrm{D}} \leq \eta_{\mathrm{U}}\}} \tag{52}$$

In addition, recalling the definition of T_{D} and η_{U}, we have

$$\Pr\left\{T_{\mathrm{D}} \leq \eta_{\mathrm{U}}\right\} \geq 1 - \Pr\left\{\chi^2_{2N_a\vartheta} \geq \eta_{\mathrm{U}}\right\} = \mathrm{Pr_{FA}} \tag{53}$$

Substituting (53) into (52) and utilizing Markov's inequality, we express the required lower bound of $\mathrm{Pr_D}$ for the GLRT detector as

$$\mathrm{Pr_D} \geq 1 - \tfrac{\Pr\{T_{\mathrm{U}} \leq 2\eta_{\mathrm{U}}\}}{\mathrm{Pr_{FA}}} \geq 1 - \tfrac{\mathrm{E}\left[e^{-\sigma_n^2 T_{\mathrm{U}}}\right]}{e^{-2\sigma_n^2 \eta_{\mathrm{U}}} \cdot \mathrm{Pr_{FA}}} \tag{54}$$

Due to the fact that $[-\left(\sigma^2 \sigma_e^2 \beta_k + \sigma_n^2\right)] < 0$ and given the statistical independence of $2\left|\psi_{1ik}\right|^2$ for different values of i and k, the following equation can be obtained for the moment generating function of the noncentral chi-square distribution:

$$\begin{aligned} &\mathrm{E}\left[e^{-\sigma_n^2 T_{\mathrm{U}}}\right] = \prod_{k=1}^{\vartheta} \prod_{i=1}^{N_a} \mathrm{E}\left[e^{-\left(\sigma^2 \sigma_e^2 \beta_k + \sigma_n^2\right)\left(2|\psi_{1ik}|^2\right)}\right] \\ &= \prod_{k=1}^{\vartheta} \tfrac{\exp\left(\frac{-2\sigma^4 \beta_k \rho_k}{1 + 2\left(\sigma^2 \sigma_e^2 \beta_k + \sigma_n^2\right)}\right)}{\left[1 + 2\left(\sigma^2 \sigma_e^2 \beta_k + \sigma_n^2\right)\right]^{N_a}} \end{aligned} \tag{55}$$

Taking the logarithm and making use of the inequality $\log(1+x) > \frac{x}{1+x}$ when $x > -1$ and $x \neq 0$, we can express the waveform design criterion with the power constraint as below:

$$\begin{aligned} &\max_{\bar{\beta}} \sum_{k=1}^{\vartheta} \left\{ \frac{2\beta_k\rho_k + 2N_a(\sigma^2\sigma_e^2\beta_k+\sigma_n^2)}{1+2(\sigma^2\sigma_e^2\beta_k+\sigma_n^2)} \right\} \\ &\text{s.t.} \sum_{k=1}^{\vartheta} \beta_k = ME_s, \beta_k \geq 0, k = 1, 2, ..., \vartheta \end{aligned} \tag{56}$$

Applying the Karush-Kuhn-Tucker (KKT) conditions [21], the solution for the above design criterion can be given by

$$\beta_k = \frac{1+2\sigma_n^2}{2\sigma^2\sigma_e^2} \left(\frac{\sqrt{2\rho_k + 4\rho_k\sigma_n^2 + 2N_a\sigma^2\sigma_e^2}}{1+2\sigma_n^2}\xi - 1 \right)^+ \tag{57}$$

where $(a)^+ \triangleq \max(0, a)$ and ξ is chosen such that the power constraint is met:

$$\sum_{k=1}^{\vartheta} \left(\frac{\sqrt{2\rho_k+4\rho_k\sigma_n^2+2N_a\sigma^2\sigma_e^2}}{1+2\sigma_n^2}\xi - 1 \right)^+ = \frac{2ME_s\sigma^2\sigma_e^2}{1+2\sigma_n^2} \tag{58}$$

Obviously, this waveform design scheme utilizes the waterfilling strategy [15] to allocate power, and the larger the ρ_k is, the more power is allocated to the corresponding β_k.

REMARK 1: Both waveform designs introduced above select the values of β_k according to the ρ_k values, which are determined by the estimated channel vectors as well as the right-singular vectors of $\bar{Y}_{MF}$. Recalling the physical explanation of the SVD, we can split the design procedure into two separate parts. The "path directions" of the designed waveform are determined by the MF scheme, and the waveform design A and B allocate the retransmitted power to each direction according to the "path quality" following different design criteria. We emphasize this by naming the design schemes as "MF upper" and "MF lower", respectively. The reason for utilizing the MF scheme, *i.e.*, a modified TR scheme, is that [7]–[9] have shown that TR can improve the detection performance, and we want to achieve further optimization. Furthermore, although the theoretical derivation for both schemes are based on the GLRT detector, Detector I and II can also be employed when the designed waveforms are retransmitted from Array B, and their performance can be easily calculated using (14) and (32).

E. Waveform Design C: MI scheme

In this section, we design the waveform by maximizing the lower bound of the mutual information (MI) between the retransmitted and received signals. First of all, rewrite the $N_aQ_f \times 1$ received signal vector for one snapshot as

$$\begin{aligned} \bar{r} &= \left[\bar{r}^T(f_1), \bar{r}^T(f_2), \cdots, \bar{r}^T(f_{Q_f}) \right]^T = \bar{H}_Q^T\bar{y} + \bar{n} \\ \bar{y} &= \left[\bar{y}^T(f_1), \bar{y}^T(f_2), \cdots, \bar{y}^T(f_{Q_f}) \right]^T \end{aligned} \tag{59}$$

where the $N_a \times 1$ vector $\bar{r}(f_q)$ and the $N_b \times 1$ vector $\bar{y}(f_q)$ contain the signals received by all the N_a antennas of Array A and the signals retransmitted from all the N_b antennas of Array B at frequency f_q, respectively. The elements of the $N_a Q_f \times 1$ noise vector $\bar{n}$ are zero-mean complex Gaussian random variables with variance σ_n^2. The $N_b Q_f \times N_a Q_f$ matrix $\bar{H}_Q$ is a block diagonal matrix with the Q_f matrices $\bar{H}(f_q)$ arranged sequentially along its main diagonal blocks. We also define the $N_b Q_f \times N_a Q_f$ estimated channel matrix $\hat{\bar{H}}_Q$ in the same way. Assuming $\bar{y}$ is a random vector, the considered MI is $I\left(\bar{r}, \bar{y} | \hat{\bar{H}}_Q\right)$, which can be interpreted as the amount of uncertainty in the received signal $\bar{r}$ which is removed by knowing $\bar{y}$ given $\hat{\bar{H}}_Q$. Intuitively, the larger the MI, the less uncertain the received signal, and thus the better the system performance. Denoting $\bar{C}_{\bar{y}}$ the covariance matrix of $\bar{y}$ given $\hat{\bar{H}}_Q$ and following the procedure shown in Appendix I in [10], we can derive the lower bound of the MI as below:

$$I_{\mathrm{L}}\left(\bar{r}, \bar{y} | \hat{\bar{H}}_Q\right) = \log_2 \det\left[\bar{I}_{N_b Q_f} + \sigma^4 \hat{\bar{H}}_Q^* \bar{C}_\omega^{-1} \hat{\bar{H}}_Q^T \bar{C}_{\bar{y}}\right] \tag{60}$$

where the $N_a Q_f \times N_a Q_f$ matrix $\bar{C}_\omega$ is a block diagonal matrix, whose q-th diagonal block is a $N_a \times N_a$ matrix $\left[\sigma^2 \sigma_e^2 P(f_q) + \sigma_n^2\right] \cdot \bar{I}_{N_a}$ and $P(f_q) = \mathrm{E}\left[\bar{y}^H(f_q)\bar{y}(f_q)\right]$. We first express the eigenvalue decomposition of the Hermitian matrix $\hat{\bar{H}}^*(f_q)\hat{\bar{H}}^T(f_q)$ as $\bar{\mathcal{V}}(f_q)\bar{\mathcal{D}}(f_q)\bar{\mathcal{V}}^H(f_q)$, where the $N_b \times N_b$ matrix $\bar{\mathcal{V}}(f_q)$ is a unitary matrix and $\bar{\mathcal{D}}(f_q)$ is a diagonal matrix with N_b real and nonnegative eigenvalues $\Lambda_{q1}, \Lambda_{q2}, \cdots, \Lambda_{qN_b}$ (in decreasing order) as its diagonal entries. Next, we define the $N_b Q_f \times N_b Q_f$ block diagonal matrices $\bar{\mathcal{V}}_Q$ and $\bar{\mathcal{G}}_Q$, whose q-th diagonal blocks are $\bar{\mathcal{V}}(f_q)$ and $\sigma^4 \bar{\mathcal{D}}(f_q) / \left[\sigma_n^2 + \sigma^2 \sigma_e^2 P(f_q)\right]$, respectively. Thus, the lower bound of the MI in (60) can be rewritten as

$$I_{\mathrm{L}}\left(\bar{r}, \bar{y} | \hat{\bar{H}}_Q\right) = \log_2 \det\left[\bar{I}_{N_b Q_f} + \bar{\mathcal{G}}_Q \bar{\mathcal{Q}}\right] \tag{61}$$

where $\bar{\mathcal{Q}} = \bar{\mathcal{V}}_Q^H \bar{C}_{\bar{y}} \bar{\mathcal{V}}_Q$ is an $N_b Q_f \times N_b Q_f$ matrix. From Lemma 1 in [13], we know that (61) achieves its maximum when $\bar{I}_{N_b Q_f} + \bar{\mathcal{G}}_Q \bar{\mathcal{Q}}$ is diagonal. Remembering that the diagonal matrix $\bar{\mathcal{G}}_Q$ has nonnegative diagonal entries and $\bar{C}_{\bar{y}}$ is a covariance matrix, we conclude that $\bar{\mathcal{Q}}$ must be a diagonal matrix whose $\{(q-1)N_b + k\}$-th diagonal element is a nonnegative value $\mathcal{Q}_{qk}$, $q = 1, 2, ..., Q_f$ and $k = 1, 2, ..., N_b$. In addition, considering the power constraint $E_s = \mathrm{E}\left[\bar{y}^H \bar{y}\right] = \mathrm{trace}\left(\bar{\mathcal{Q}}\right)$, we can express the waveform design criterion maximizing the lower bound of the MI as below:

$$\begin{aligned} \max_{\bar{\mathcal{Q}}} \; & \sum_{q=1}^{Q_f} \sum_{k=1}^{N_b} \log_2\left\{1 + \tfrac{\sigma^4 \Lambda_{qk} \mathcal{Q}_{qk}}{\sigma_n^2 + \sigma^2 \sigma_e^2 P(f_q)}\right\} \\ \text{s.t.} \; & \sum_{q=1}^{Q_f} \sum_{k=1}^{N_b} \mathcal{Q}_{qk} = E_s \\ & \mathcal{Q}_{qk} \geq 0, \quad q = 1, 2, ..., Q_f, \quad k = 1, 2, ..., N_b \end{aligned} \tag{62}$$

Note that (62) is not a concave function due to the presence of $P(f_q) = \mathrm{E}\left[\bar{y}^H(f_q)\bar{y}(f_q)\right] = \sum_{k=1}^{N_b} \mathcal{Q}_{qk}$ in the denominator. However, for a fixed set of values for $P(f_q)$, the function becomes concave and thus it can be directly optimized. Hence, an iterative algorithm is proposed here, and the values of $P(f_q)$ are updated in each iteration until the algorithm converges. We initialize the algorithm by allocating equal power to all the Q_f frequencies, *i.e.*, $P(f_q, 0) = E_s/Q_f$ for $q = 1, 2, ..., Q_f$. For the i-th iteration, replacing $P(f_q)$ in (62) by $P(f_q, i-1)$ and applying the KKT conditions [21] leads to the solution

$$\mathcal{Q}_{qk}(i) = \left(\zeta(i) - \frac{\sigma_n^2 + \sigma^2\sigma_e^2 P(f_q, i-1)}{\sigma^4 \Lambda_{qk}}\right)^+ \tag{63}$$

where the water-level $\zeta(i)$ can be found by solving

$$\sum_{q=1}^{Q_f}\sum_{k=1}^{N_b}\left(\zeta(i) - \frac{\sigma_n^2 + \sigma^2\sigma_e^2 P(f_q, i-1)}{\sigma^4 \Lambda_{qk}}\right)^+ = E_s \tag{64}$$

Then, the values of $P(f_q)$ for the i-th iteration are updated as $P(f_q, i) = \sum_{k=1}^{N_b} \mathcal{Q}_{qk}(i)$ and the iteration ends if $\max|P(f_q, i) - P(f_q, i-1)| \leq \varepsilon$ for all the Q_f frequencies, where ε is a threshold with small value. Once all the $\mathcal{Q}_{qk}$ are determined, we have the covariance matrix $\bar{C}_{\bar{y}} = \bar{\mathcal{V}}_Q \bar{\mathcal{Q}} \bar{\mathcal{V}}_Q^H$.

Notice here that when $N_a < N_b$, a modification is required to be made to the above algorithm. Obviously, $\Lambda_{qk} = 0$ for $k = N_a + 1, N_a + 2, ..., N_b$, and from (62), it is clear that the corresponding $\mathcal{Q}_{qk}$ should be equal to zero in order to maximize the lower bound. Thus, when $N_a < N_b$, the limit of k is changed from N_b to N_a in (62)-(64) and the values of $\mathcal{Q}_{qk}$ are determined for $k = 1, 2, ..., N_a$ using the algorithm mentioned before. Next, setting $\mathcal{Q}_{qk} = 0$ for $k = N_a + 1, N_a + 2, ..., N_b$ gives us the $N_bQ_f \times N_bQ_f$ diagonal matrix $\bar{\mathcal{Q}}$.

Once $\bar{C}_{\bar{y}}$ is determined, we generate a set of $N_bQ_f \times 1$ deterministic vectors $\{\bar{y}_1, \bar{y}_2, \cdots, \bar{y}_M\}$ as the retransmitted signal vectors for the M snapshots. These vectors are appropriately designed such that their covariance matrix remains as $\bar{C}_{\bar{y}}$. The block diagonal structure of $\bar{C}_{\bar{y}}$ implies that the retransmitted signals at different frequencies are mutually orthogonal. Such orthogonality can be realized, for example, by designing the retransmitted signal using orthogonal frequency division multiplexing (OFDM) scheme [22]. Denoting the k-th column of $\bar{\mathcal{V}}(f_q)$ by $\bar{v}_k(f_q)$, we generate the signals transmitted by all the N_b antennas of Array B at frequency f_q for the m-th snapshot by utilizing an orthogonal basis as below:

$$\bar{y}_m(f_q) = \sum_{k=1}^{N_b} \bar{v}_k(f_q)\sqrt{\mathcal{Q}_{qk}}\mathcal{O}_{km}, \sum_{m=1}^{M} \mathcal{O}_{km}\mathcal{O}_{lm}^* = M\delta_{kl} \tag{65}$$

where $m = 1, 2, ..., M$, $k, l = 1, 2, ..., N_b$, and δ_{kl} represents the Dirac delta function. The $N_bQ_f \times 1$ signal vector $\bar{y}_m$ is obtained by sequentially stacking all the Q_f vectors $\bar{y}_m(f_q)$ into a vector. Walsh codes are adopted as the basis functions in the simulations, but other orthogonal bases can be employed

in principle. From (65), we can calculate that the covariance matrix of the generated vectors equals $\bar{C}_{\bar{y}}$ and the power constraint has been met. After all the M snapshots $\{\bar{y}_m\}$ are generated, the retransmitted signal matrix $\bar{Y}$ can be easily obtained by reshaping $\{\bar{y}_m\}$ appropriately. Its corresponding system performance for all the three detectors can be evaluated using the formulae provided in Section III.

REMARK 2: From the simulation we find that normally the iterative algorithm converges after a few iterations (less than 20 for $\varepsilon = 0.001$). However, at very low signal-to-noise ratios (SNRs) and when the difference between the largest two values of Λ_{qk} is very small, the algorithm can enter an endless loop by allocating all the power to their corresponding $\mathcal{Q}_{qk}$ in turn. From (63), it is not difficult to understand that this problem can happen when the difference between the numerators for two successive iterations $\sigma_e^2\left(1+\sigma_e^2\right)|P(f_q,i)-P(f_q,i-1)|$ is large enough. The lower the SNR, the larger the value of σ_e^2, and this is the reason why such a problem only occurs at very low SNRs. To solve this problem, we terminate the algorithm if the number of iterations exceeds a selected value and choose the results obtained in the last iteration as the final solution. This approach is reasonable since if there are two coefficients Λ_{qk} having similar values, then allocating the power to either of them leads to similar system performance.

V. Numerical Results and Discussion

In this section, numerical results are presented showing the target detection performance of a MIMO system with different detectors and retransmitted waveforms. We set $\mathrm{Pr_{FA}} = 0.001$ and define the SNR as $\mathrm{SNR} = E_s/\sigma_n^2$ with E_s normalized to 1. As mentioned before, the value of σ_e^2 depends on the estimation method and the waveform length during the probing phase, which is inversely proportional to the SNR at Array B [23]. Since we focus on the detection phase in this paper investigating the system performance when channel estimation error exists, we assume that the noise level at Array B is in proportion to that at Array A and set $\sigma_e^2 = \sigma_n^2$ in all the simulations. Note that the algorithms for both the detector and waveform designs are based on the estimated channel $\hat{\bar{H}}(f_q)$, which is the sum of the true channel and the estimation error. Therefore, we utilize a semi-analytical approach to obtain the system performance. That is, we generate $10,000$ realizations of the true channel and the estimation error matrix, calculate the corresponding $\mathrm{Pr_D}$ for each realization using (14), (32), and (42), and yield the theoretical system detection performance by averaging $\mathrm{Pr_D}$ over all the realizations.

We first examine the performance of a system with four sensors at both Arrays A and B, choosing $M = 5$ and $Q_f = 6$ for simulation purposes only. Fig.2 depicts the detection performance of the system employing different detectors when two designed waveforms, the MF lower and MI schemes, are adopted. The $\mathrm{Pr_D}$ recorded from Monte Carlo simulations is also presented. For each realization of the

estimated channel matrix, we generate 10,000 independent received signals, compute their test statistics, and compare them with the threshold. Obviously, the simulated results agree well with the theoretical values, validating the correctness of the derived formulae. Comparing the curves corresponding to the same waveform, we find that Detector II always performs the best, which is consistent with the fact that Detector II is the optimal detector. In addition, the performance difference between Detector I and Detector II decreases as the SNR becomes higher, *i.e.*, σ_e^2 is smaller. This can be explained by the fact that both the optimal detector when the channel matrix is known and Detector I are in the form of matched filters, and the only difference is that the former matches to the true channel $\bar{H}$ while the latter matches to the estimated channel $\hat{\bar{H}}$ [18]. When σ_e^2 has a small value, the estimation error in the estimated channel is insignificant, and thus the difference between the performance of Detector I and the optimal performance should be small. Furthermore, it is easily seen that Detector III performs the poorest at low SNR but is similar to the optimal detector when the SNR is high. This is because the GLRT detector estimates the unknown parameters first and then makes the detection decision based on it. Intuitively, the lower the SNR, the worse the estimation, which degrades the detection performance. However, although Detector II performs the best, it requires knowledge of $\bar{Y}$, $\hat{\bar{h}}_i$, and σ_e^2 at Array A. In contrast, as mentioned in Section III, the implementation of Detector I needs the information of $\bar{Y}$ and $\hat{\bar{h}}_i$, while for Detector III only $\bar{Y}$ is required to be known.

We next compare the detection performance of the systems retransmitting different waveforms as shown in Fig.3 and Fig.4 for low and high SNRs, respectively. Here, Detector II is employed for all the scenarios. We also provide the system performance recorded from Monte Carlo simulations following the same procedure mentioned before, and there is a very good agreement between the theoretical and simulated performance. Obviously, the MF scheme provides much better performance than the CS approach, and all the three proposed waveform designs further improve the system performance significantly with respect to the MF scheme. We start by comparing the MF upper and lower schemes. At low SNR, the MF upper is superior, while the MF lower is preferred when SNR is high. In addition, the MF lower always outperforms the MF approach, but the MF upper performs worse than the MF scheme when SNR is high enough. Such results are reasonable since that one should concentrate all the available power on the path with the best quality in order to overcome the high level of noise at low SNR, which is the idea of the MF upper method. As the SNR becomes higher, the noise level and consequently the estimation error parameter σ_e^2 decreases, and thus allocating power to several paths according to their amplitudes, *i.e.*, the waterfilling strategy utilized in the MF lower approach, leads to better detection reliability because of the spatial diversity gain. Furthermore, it is clear from Fig.3 and Fig.4 that the MI scheme outperforms

all the other waveform designs and should be selected for precise target detection, *e.g.*, the probability of detection $\mathrm{Pr_D} \geq 0.7$. Although all the three designed waveforms bring in significant performance improvements, we point out that such enhancement is achieved at the price of knowing the channel estimation error parameter σ_e^2 *a priori*.

We proceed to investigate the impact of the number of antennas at Array A N_a, the number of antennas at Array B N_b, and the number of snapshots M on the detection performance for the proposed three waveform designs. The SNR is fixed at 0dB for the next three figures, and the number of snapshots M equals to 5 for Fig.5 and Fig.6. First of all, it is clear that for all the scenarios considered in Fig.5, Fig.6, and Fig.7, the MI scheme provides the best detection performance, and the MF lower approach outperforms the MF upper method. Next, we compare the slopes of the curves corresponding to different waveforms for the same N_b in Fig.5, and the larger the slope is, the more effect N_a has on the corresponding waveform design. In other words, for the same increase in the value of N_a, the MI scheme provides the greatest performance improvement, and the MF lower method achieves more enhancement than the MF upper approach does. Similarly, we can draw the same conclusions for both N_b and M by observing Fig.6 and Fig.7. Hence, the MI scheme is the best among the three waveform design approaches since it not only performs the best but also realizes the largest performance enhancement for the same increase in the value of N_a, N_b, or M, and in that sense, the MF lower scheme is better than the MF upper approach.

VI. Conclusions

In this paper, we investigated the target detection performance of a bistatic wideband MIMO system, whose detection process is similar to the TR procedure. Based on the estimated channel and a parameter indicating the quality of the estimation obtained during the probing phase, the retransmitted waveform and the detector are designed. Three detectors are developed, whose theoretical thresholds and probabilities of detection are derived in closed form. Three schemes are proposed to design the retransmitted waveform with a power constraint, which maximizes the upper and lower bound of the probability of detection of the GLRT detector, and the lower bound of the MI between the retransmitted signal and the received signal, respectively. Numerical results showing the detection performance of a MIMO system involving the designed detectors and retransmitted waveforms are presented. It is shown that the optimal detector performs the best but it requires more *a priori* information than the conventional detector does. The performance difference between the conventional and the optimal detector increases as the estimation quality becomes poorer. The GLRT detector performs the poorest but demands the least amount of *a*

priori information. All the three waveform design approaches further improve the system performance with respect to the MF approach at the price of knowing the quality of channel estimation *a priori*. The MF upper scheme works the best at low SNR, but is outperformed by the MF lower approach as the SNR increases. However, the MI scheme consistently provides the minimum target detection probability in all the simulation scenarios that were tested.

REFERENCES

[1] M. Fink, "Time reversal of ultrasonic fields - part I: Basic principles," *IEEE Trans. Ultrason., Ferroelectr., Freq. Control*, vol. 39, no. 5, pp. 555–566, Sept. 1992.

[2] C. Prada, F. Wu, and M. Fink, "The iterative time reversal mirror: A solution to self-focusing in the pulse echo mode," *IEEE J. Acoust. Soc. Am.*, vol. 90, no. 2, pp. 1119–1129, Aug. 1991.

[3] L. Borcea, G. Papanicolaou, C. Tsogka, and J. Berryman, "Imaging and time reversal in random media," *Inverse Problems*, vol. 18, pp. 1247–1279, 2002.

[4] R. C. Qiu, C. Zhou, N. Guo, and J. Q. Zhang, "Time reversal with MISO for ultra-wideband communications: Experimental resutls," *IEEE Antennas Wireless Propag. Lett.*, vol. 5, pp. 269–273, 2006.

[5] G. Shi and A. Nehorai, "Maximum likelihood estimation of point scatterers for computational time-reversal imaging," *Commun. Inf. Syst.*, vol. 5, no. 2, pp. 227–256, 2005.

[6] A. J. Devaney, "Super-resolution processing of multi-static data using time reversal and MUSIC," 2000. [Online]. Available: http://www.ece.neu.edu/faculty/devaney

[7] J. M. F. Moura and Y. Jin, "Detection by time reversal: Single antenna," *IEEE Trans. Signal Process.*, vol. 55, no. 1, pp. 187–201, Jan. 2007.

[8] J. M. F. Moura, Y. Jin, D. Stancil, J. G. Zhu, A. Cepni, Y. Jiang, and B. Henty, "Array processing using time reversal: Experimental and performance," *IEEE Int. Conf. Signal Process. (ICASSP '06)*, vol. 4, pp. 1053–1056, May 2006.

[9] Y. Jin, J. M. F. Moura, and N. O'Donoughue, "Time reversal transmission in MIMO radar," *Proc. 41th Asilomar Conf. Signals, Systems, Computers, Pacific Grove, CA*, pp. 2204–2208, 2007.

[10] T. Yoo and A. Goldsmith, "Capacity and power allocation for fading MIMO channels with channel estimation error," *IEEE Trans. Inf. Theory*, vol. 52, no. 5, pp. 2203–2214, May 2006.

[11] T. E. Klein and R. G. Gallager, "Power control for the additive white Gaussian noise channel under channel estimation errors," *in Proc. IEEE Int. Symp. Inf. Theory (ISIT)*, p. 304, Jun. 2001.

[12] A. Soysal, "Optimum transmit strategies for Gaussian multi-user MIMO systems with partial CSI and noisy channel estimation," Ph.D. dissertation, University of Maryland, 2008.

[13] Y. Yang and R. S. Blum, "MIMO radar waveform design based on mutual information and minimum mean-square error estimation," *IEEE Trans. Aerosp. Electron. Syst.*, vol. 43, no. 1, pp. 330–343, Jan. 2007.

[14] A. D. Maio and M. Lops, "Design principles of MIMO radar detectors," *IEEE Trans. Aerosp. Electron. Syst.*, vol. 43, no. 3, pp. 886–898, Jul. 2007.

[15] D. Tse and P. Viswanath, *Fundamentals of wireless communication*. New York: Cambridge University Press, 2005.

[16] E. Fishler, A. Haimovich, R. S. Blum, L. J. Cimini, D. Chizhik, and R. A. Valenzuela, "Spatial diversity in radars-Models and detection performance," *IEEE Trans. Signal Process.*, vol. 54, no. 3, pp. 823–838, Mar. 2006.

[17] G. E. P. Box, "Some theorems on quadratic forms applied in the study of analysis of variance problems," *The Annals of Mathematical Statistics*, vol. 25, no. 2, pp. 290–302, Jun. 1954.

[18] S. M. Kay, *Fundamentals of statistical signal proceesing: Detection Theory*. Upper Saddle River, NJ: Prentice-Hall PTR, 1993.

[19] T. M. Cover and J. A. Thomas, *Elements of information theory*, 2nd ed. New York: Wiley, 2005.

[20] [Online]. Available: http://mathworld.wolfram.com/Abelsinequality.html

[21] S. Boyd and L. Vandenberghe, *Convex optimization*. New York: Cambridge University Press, 2004.

[22] A. F. Molisch, *Wireless Communications*. Chichester: John Wiley & Sons, 2006.

[23] V. Tarokh, A. Naguib, N. Seshadri, and A. R. Calderbank, "Space-time codes for high data rate wireless communication: Performance criteria in the presence of channel estimation errors, mobility, and multiple paths," *IEEE Trans. Commun.*, vol. 47, no. 2, pp. 199–207, Feb. 1999.

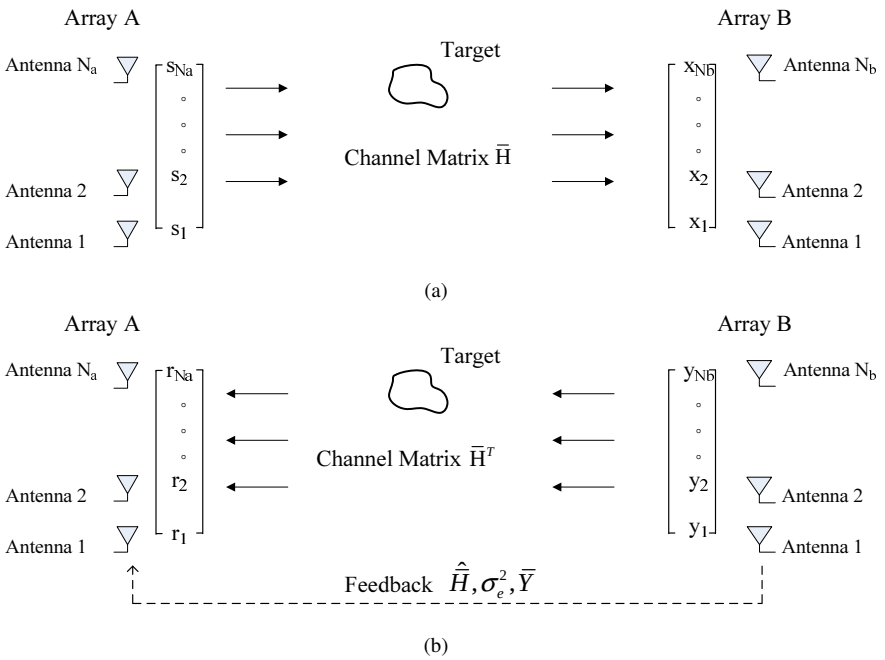

Fig. 1. Description of the (a) probing and (b) detecting process of the MIMO system

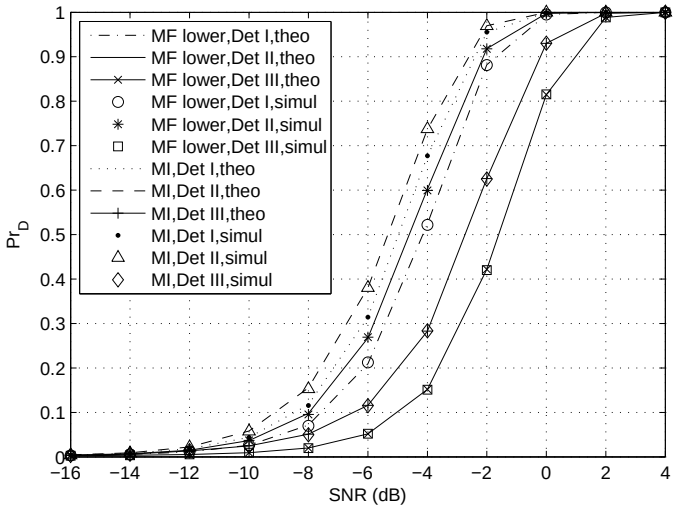

Fig. 2. $\mathrm{Pr_D}$ versus SNR for systems with different detectors

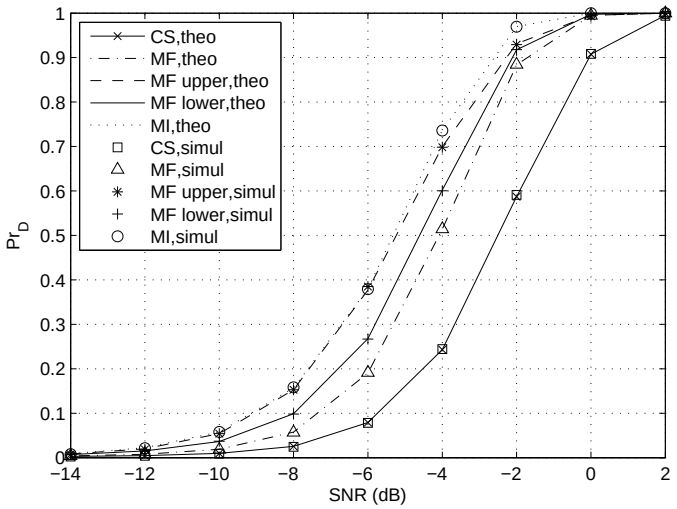

Fig. 3. $\mathrm{Pr_D}$ versus SNR for systems with different retransmitted waveforms

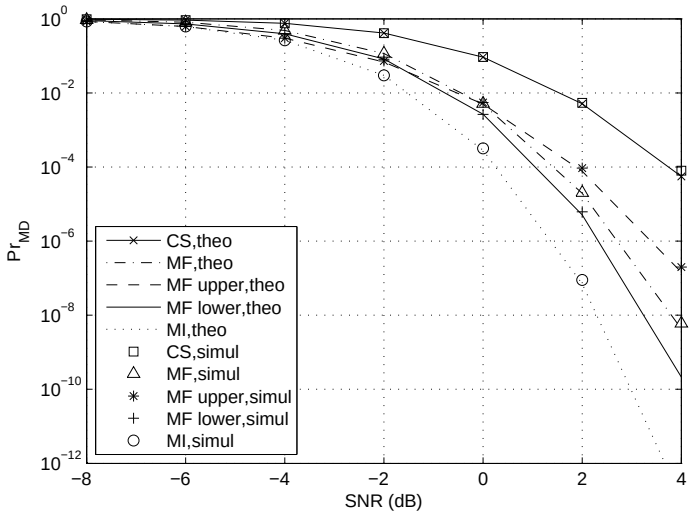

Fig. 4. $\mathrm{Pr}_{\mathrm{MD}}$ versus SNR for systems with different retransmitted waveforms

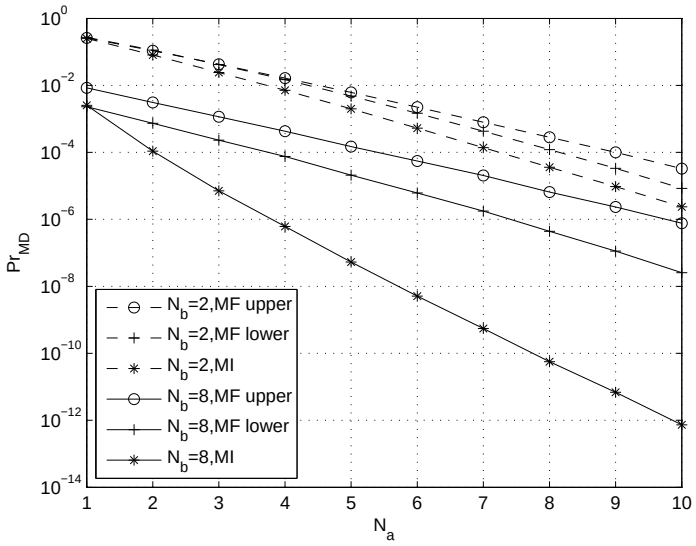

Fig. 5. $\mathrm{Pr}_{\mathrm{MD}}$ versus N_a for systems with different retransmitted waveforms when $M = 5$, SNR $=$ 0dB, and Detector II is employed

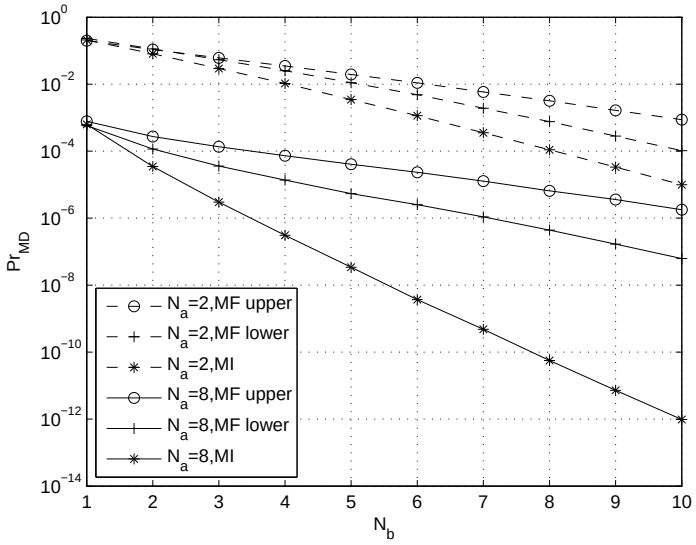

Fig. 6. $\mathrm{Pr}_{\mathrm{MD}}$ versus N_b for systems with different retransmitted waveforms when $M = 5$, SNR $= 0$dB, and Detector II is employed

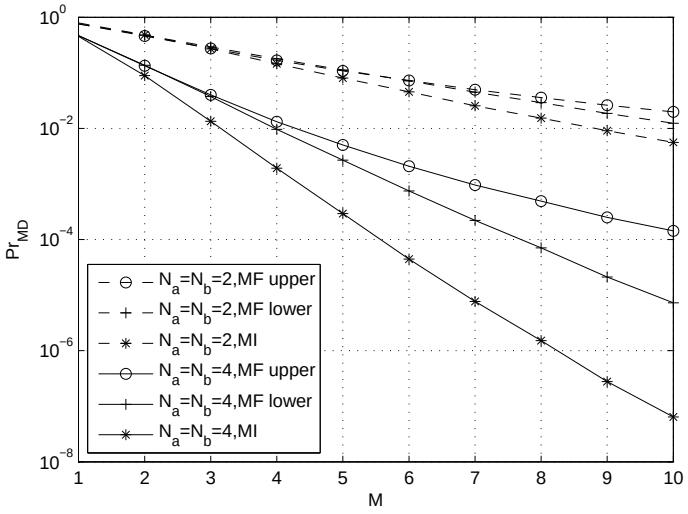

Fig. 7. $\mathrm{Pr}_{\mathrm{MD}}$ versus M for systems with different retransmitted waveforms when SNR $= 0$dB and Detector II is employed

IEEE SIGNAL PROCESSING LETTERS, VOL. 15, 2008

Predicted Detection Performance of MIMO Radar

Chaoran Du, John S. Thompson, *Member, IEEE*, and Yvan Petillot

***Abstract*—It has been shown that multiple-input multiple-output (MIMO) radar systems can improve target detection performance significantly by exploiting the spatial diversity gain. We introduce the system model in which the radar target is composed of a finite number of small scatterers and derive the formula to evaluate the theoretical probability of detection for the system having an arbitrary array-target configuration. The results can be used to predict the detection performance of the actual MIMO radar without time-consuming simulations.**

***Index Terms*—Detection performance, finite scatterers model, multiple-input multiple-output (MIMO), radar, spatial diversity.**

I. Introduction

MOTIVATED by the advantages offered by multiple-input multiple-output (MIMO) systems in communications, Fishler *et al.* [1], [2] proposed that MIMO techniques can also be applied in radar scenarios to improve performance by exploiting the so-called spatial diversity gain defined in communication theory [3]. However, it is assumed that the rectangular-shape target is composed of an infinite number of random scatterers in [1], and the gains of all the scatterers are random variables with the same distribution. Hence, such a model is not convenient to be employed when the target comprises several significant scatterers at different spatial locations, which implies that a finite scatterers model should be used instead. Although in [2] the finite scatterers model is utilized, it assumes that the scatterers are laid out as a linear array which is parallel to the antenna array.

In this letter, we implement the MIMO radar system assuming that the target is modeled by a finite number of scatterers without limitation on the locations. The main contribution of this letter is the derivation of a formula to calculate the theoretical probability of detection for a MIMO radar having an arbitrary array-target configuration, while [1] presents the detection performance for only four special configurations. This theoretical result makes it possible to predict the actual MIMO radar performance before implementing expensive experiments and avoiding time-consuming simulations. Furthermore, the preferable MIMO array configuration could be selected for different scenarios by comparing the predicted performance of various configurations.

This letter is organized as follows. In Section II, we develop the system model of the MIMO radar. We then apply this model to formulate the detection problem and generate the equation to compute the probability of detection. Analysis of two extreme channel models and simplified expressions for two special cases are also shown in Section III. The next section examines numerical results and provides some discussion. Section V gives the conclusions.

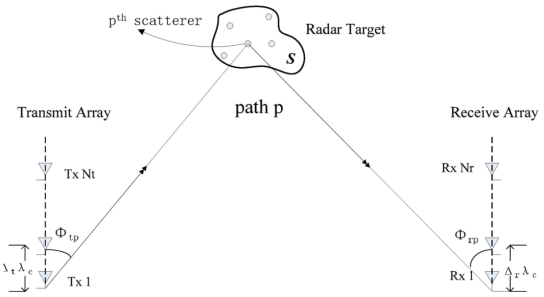

Fig. 1. Configuration of the finite scatterers channel model.

II. System Model

A. Channel Model

Uniform linear arrays of antennas [3] are employed at both transmitter and receiver with N_t and N_r elements, respectively. The antenna separations are $\Delta_t\lambda_c$ and $\Delta_r\lambda_c$, where λ_c is the carrier wavelength and Δ_t and Δ_t are the normalized transmit and receive antenna spacing in wavelengths. We assume that all the signals are narrow band and that distances between scatterers and both transmitter and receiver are much larger than the dimensions of the antenna arrays, that is, we operate in the far field.

The radar target can be viewed as the finite point-like scatterers model illustrated in Fig. 1. It is assumed that there are N_s random and independent scatterers uniformly distributed over the target area S, and N_s is also the number of independent multipaths because of the assumption of a "single-bounce" propagation model. As shown in Fig. 1, path p is defined by angle of departure (AoD) Φ_{tp}, angle of arrival (AoA) Φ_{rp}, complex path gain a_p, and distance between T$\times$ 1 and R$\times$ 1 along the path d_p.

Manuscript received July 5, 2007; revised September 10, 2007. This work was supported by the Scottish Funding Council for the Joint Research Institute with Edinburgh and the Heriot-Watt Universities, which is a part of the Edinburgh Research Partnership (ERP). The Ph.D. studies of C. Du were supported by the ERP. The associate editor coordinating the review of this manuscript and approving it for publication was Dr. Andreas Jakobsson.

C. Du and J. S. Thompson are the Institute for Digital Communications, Joint Research Institute for Signal and Image Processing, School of Engineering and Electronics, University of Edinburgh, Edinburgh EH9 3JL, U.K. (e-mail: C.Du@ed.ac.uk; John.Thompson@ed.ac.uk).

Y. Petillot is with the Joint Research Institute for Signal and Image Processing, School of Engineering and Physical Sciences, Heriot-Watt University, Edinburgh, EH14 4AS, U.K. (e-mail: Y.R.Petillot@hw.ac.uk).

Digital Object Identifier 10.1109/LSP.2007.910312

Based on above assumptions, the channel matrix $\bar{H}$, which is an $N_r \times N_t$ matrix, is given by [3]

$$\bar{H} = \sum_{p=1}^{N_s} a_p \exp\left(-\frac{j2\pi d_p}{\lambda_c}\right) \bar{\Psi}_r(\Omega_{rp}) \bar{\Psi}_t^H(\Omega_{tp}) \quad (1)$$

$$\bar{\Psi}_\varepsilon(\Omega_{\varepsilon p}) = \begin{bmatrix} 1 \\ \exp(-j2\pi\Delta_\varepsilon\Omega_{\varepsilon p}) \\ \vdots \\ \exp(-j2\pi(N_\varepsilon - 1)\Delta_\varepsilon\Omega_{\varepsilon p}) \end{bmatrix}. \quad (2)$$

In (2), ε represents either r or t, $\Omega_{rp} = \cos\Phi_{rp}$ and $\Omega_{tp} = \cos\Phi_{tp}$, and the superscript H denotes the conjugate transpose. We assume that each path gain a_p can be a zero-mean complex Gaussian random variable with variance ϖ_{p}^2 and assume that the sum of all the variances equals to one.

B. Signal Model

It is supposed that the kth transmitter transmits a signal $\sqrt{(E)/(N_t)}s_k(t)$, where $||s_k(t)||^2 = 1$ and E is the total transmitted power. The normalizing coefficient is employed to make sure that the total transmitted power and the average received power at each element are not affected by the number of transmit antennas. Furthermore, all the transmitted signals are orthogonal, which is equivalent to the fact that $\int s_j(t)s_i(t)dt = \delta_{ij}$, where δ_{ij} is a dirac delta function. Denote the transmitted signals by an $N_t \times 1$ vector $\bar{s} = [s_1 s_2 \cdots s_{N_t}]^T$, the received signals and the additive white Gaussian noise at all the receiver antennas by an $N_r \times 1$ vector $\bar{r} = [r_1 r_2 \cdots r_{N_r}]^T$ and an $N_r \times 1$ vector $\bar{n} = [n_1 n_2 \cdots n_{N_r}]^T$, respectively, where the superscript T represents transpose and $\bar{n} \sim CN(\bar{0}_{N_r}, \sigma_n^2 \bar{I}_{N_r})$. Here $\bar{0}_{N_r}$ is a $N_r \times 1$ all-zeros vector and $\bar{I}_{N_r}$ is a $N_r \times N_r$ identity matrix. The system model can be written as follows:

$$\bar{r} = \sqrt{\frac{E}{N_t}}\bar{H}\bar{s} + \bar{n}. \quad (3)$$

Together with the channel matrix $\bar{H}$ given by (1), we can measure the value of the observed signals $\bar{r}$, from which the target detection decision will be made after applying an appropriate detector.

The optimal MIMO radar detector given by [1] can be expressed as follows:

$$||\bar{x}||^2 \underset{<_{\mathcal{H}_0}}{>^{\mathcal{H}_1}} \delta \quad (4)$$

where the alternate hypothesis $\mathcal{H}_1$ and null hypothesis $\mathcal{H}_0$ are that the target does or does not exist, respectively, and δ is a threshold determined by the probability of false alarm. The $N_r N_t \times 1$ matrix $\bar{x}$ is the output of a bank of matched filters, which is written as [1]

$$\bar{x} = \begin{cases} \bar{n} & \mathcal{H}_0 \\ \sqrt{\frac{E}{N_t}}\bar{h} + \bar{n} & \mathcal{H}_1 \end{cases} \quad (5)$$

where the $N_r N_t \times 1$ channel vector $\bar{h}$ is composed of all the entries of the channel matrix $\bar{H}$ and the $N_r N_t \times 1$ noise vector $\bar{n} \sim CN(\bar{0}_{N_r N_t}, \sigma_n^2 \bar{I}_{N_r N_t})$.

From (4) and (5), it is easy to understand that the probability of detection Pr_D of the MIMO radar depends on the distribution of $||\bar{x}||^2$. Thus, the problem of predicting the detection performance of the MIMO radar turns into the calculation of the probability density function (PDF) of $||\bar{x}||^2$, which will be discussed in the next section.

III. Detection Performance

In this section, we first derive the formula to calculate the theoretical probability of detection for a MIMO radar system with an arbitrary array-target configuration. Following that is the analysis of two extreme channel models with respect to the level of correlation of the channel matrix, and then simplified expressions of the formula for two special cases are provided.

A. General MIMO Radar

The general MIMO radar can be modeled by the system mentioned in the last section without any other restriction. First of all, we consider $||\bar{x}||^2$ given $\mathcal{H}_0$. Recall from [1, equation (26)] that the distribution of $||\bar{x}||^2$ is a chi-square random variable with $2N_r N_t$ degrees of freedom as follows:

$$||\bar{x}||^2 \sim \frac{\sigma_n^2}{2}\chi^2_{(2N_r N_t)} \quad \mathcal{H}_0. \quad (6)$$

We proceed to the case under the alternate hypothesis $\mathcal{H}_1$. Firstly, we define the $N_r N_t \times 1$ vector $\bar{\beta} = \bar{h} + \sqrt{\frac{N_t}{E}}\bar{n}$. It is easy to verify that $\bar{\beta}$ has zero mean, and the square matrix $\bar{M} = E[\bar{\beta} \cdot \bar{\beta}^H]$ is the covariance matrix of $\bar{\beta}$, that is, $\bar{\beta} \sim CN(\bar{0}_{N_r N_t}, \bar{M})$. Substituting (1) gives

$$M(m,n) = \sum_{s=1}^{N_s} \varpi_{\mathrm{s}}^2 \{\exp[-j2\pi(p-u)\Delta_r\Omega_{rs}] \cdot \exp[j2\pi(q-v)\Delta_t\Omega_{ts}]\} + \frac{N_t}{E}\sigma_n^2\delta_{mn} \quad (7)$$

where $m = (p-1)N_t + q$ and $n = (u-1)N_t + v, p, u = 1, 2, \ldots, N_r; q, v = 1, 2, \ldots, N_t$. Therefore, for any set of parameters in the channel matrix given by (1), we can easily compute the covariance matrix $\bar{M}$. $\bar{M}$ can be rewritten as $\bar{U}\bar{\Lambda}\bar{U}^H$, where $\bar{\Lambda}$ is a diagonal matrix whose kth diagonal element is the corresponding eigenvalue λ_k of $\bar{M}$ and $\bar{U}$ is a unitary matrix. We define a $N_r N_t \times 1$ vector $\bar{\gamma} = \bar{U}^H\bar{\beta}$, and then according to the property of linear transforms of complex normal distributed random vectors, the distribution of $\bar{\gamma}$ is given by

$$\bar{\gamma} \sim CN(\bar{0}_{N_r N_t}, \bar{U}^H\bar{M}\bar{U}) = CN(\bar{0}_{N_r N_t}, \bar{\Lambda}). \quad (8)$$

Considering the fact that $\bar{\Lambda}$ is the covariance matrix of $\bar{\gamma}$ and is a diagonal matrix, it is safe to conclude that all the elements of $\bar{\gamma}$ are uncorrelated and the kth element γ_k has the distribution $CN(0, \lambda_k)$. Notice that $||\bar{\gamma}||^2 = ||\bar{\beta}||^2$, and then the original problem of calculating $||\bar{x}||^2$ becomes the evaluation of $||\bar{\gamma}||^2$. The reason why we apply such a transform is that the elements of $\bar{x}$ could be correlated for some scenarios. The uncorrelated nature of the elements of $\bar{\gamma}$ simplifies the calculation process dramatically.

According to the above analysis, $\|\bar{x}\|^2$ can be viewed as the sum of a set of N_rN_t independent random variables $\{\alpha_k\}$, and $\alpha_k \sim (E)/(N_t)(\lambda_k)/(2)\chi^2_{(2)}$. We further define $C_k = E/(N_t)\lambda_k$ and assume there are N distinct values $\{C_m\}$ of all the N_rN_t values, and C_m has corresponding algebraic multiplicity μ_m [4]. Thus, the characteristic function of $\|\bar{x}\|^2$ can be expressed as follows [6]:

$$\Gamma(v) = \prod_{m=1}^{N} \frac{1}{(1-jvC_m)^{\mu_m}} \quad \left(\sum_{m=1}^{N} \mu_m = N_rN_t\right). \quad (9)$$

Given the fact that the characteristic function of a random variable x is the Fourier transform of the PDF of x with a sign inverse in the complex component, it is possible to derive the PDF of $\|\bar{x}\|^2$ through the inverse Laplace transform of (9) with the substitution $s = -jv$. Following [4], the PDF of $\|\bar{x}\|^2$ given $\mathcal{H}_1$ is given by

$$p(\|\bar{x}\|^2) = \sum_{m=1}^{N}\sum_{n=1}^{\mu_m} \frac{A_{m,n}}{(\mu_m - n)!}(\|\bar{x}\|^2)^{\mu_m - n} e^{\frac{-\|\bar{x}\|^2}{C_m}} \quad (10)$$

where the coefficient $A_{m,n}$ is written as [5]

$$A_{m,n} = \frac{1}{(n-1)!}\left[\frac{d^{n-1}}{ds^{n-1}} \frac{\prod_{m=1}^{N}\left(\frac{1}{C_m}\right)^{\mu_m}}{\prod_{p=1,p\neq m}^{N}\left(s+\frac{1}{C_p}\right)^{\mu_p}}\right]\Bigg|_{s=-\frac{1}{C_m}}. \quad (11)$$

As mentioned before, for a given noise level, the threshold δ can be determined by Pr_{FA}, while Pr_D is computed from the value of δ and the PDF of $\|\bar{x}\|^2$ under $\mathcal{H}_1$. Using the upper incomplete Gamma function, we can express Pr_D as follows:

$$Pr_D = \sum_{m=1}^{N}\sum_{n=1}^{\mu_m} A_{m,n} C_m^{\mu_m - n+1} e^{\frac{-\delta}{C_m}} \sum_{p=0}^{\mu_m - n} \frac{\left(\frac{\delta}{C_m}\right)^p}{p!} \quad (12)$$

$$\delta = \frac{\sigma_n^2}{2} F^{-1}_{\chi^2_{(2N_rN_t)}}(1 - Pr_{FA}) \quad (13)$$

where $F^{-1}_{\chi^2_{(2N_rN_t)}}$ denotes the inverse cumulative distribution function of a chi-square random variable with $2N_rN_t$ degrees of freedom. The above equation demonstrates that it is possible to predict the performance of the MIMO radar system without implementing costly experiments. In addition, the comparison between the theoretical performance of different configurations provides us the principle based on which to design the best MIMO system for various scenarios. We further investigate the relationship between the correlation of the channel matrix and the distribution of eigenvalues $\{\lambda_k\}$, and then show the simplified expressions of Pr_D for two special cases.

B. Analysis of Extreme Channel Models

Recall that the additive white Gaussian noise is independent of the channel, then $\bar{M}$ can be rewritten as

$$\bar{M} = E[\bar{\beta}\cdot\bar{\beta}^H] = E[\bar{h}\cdot\bar{h}^H] + \frac{N_t}{E}\sigma_n^2 \bar{I}_{N_rN_t}. \quad (14)$$

It is clear that the eigenvalues $\{\lambda_k\}$ of $\bar{M}$ are closely related to the correlation matrix of the vector $\bar{h}$ including N_rN_t channel matrix entries $\{h_i\}$. This correlation matrix depends on the specific configuration of the radar system. However, we can compute its value under the following two extreme cases.

1) Entries Are Totally Uncorrelated: Invoking the assumption that the sum of all the variances of the path gains is one, it is not difficult to verify that $E[h_i \cdot h_i*] = 1$, where $*$ denotes the conjugate, in other words, the diagonal elements of the correlation matrix are one. Moreover, the totally uncorrelated condition illuminates that all the non-diagonal elements of $E[\bar{h}\cdot\bar{h}^H]$ are zero. This results in the diagonal matrix $\bar{M} = (1+(N_t)/(E)\sigma_n^2)\bar{I}_{N_rN_t}$. Hence, there exists N_rN_t eigenvalues $\{\lambda_k\}$, and they all have the same value $\lambda = 1 + (N_t)/(E)\sigma_n^2$. Making use of the simplified formula introduced in the next section, we can evaluate Pr_D easily.

2) Entries Are Fully Correlated: Similar to the calculation in the previous subsection, we know that the diagonal elements of the correlation matrix are one. The condition of full correlation demonstrates that all the non-diagonal elements are also equal to one, that is, $E[\bar{h}\cdot\bar{h}^H]$ is an all-ones matrix. Therefore, $\bar{M}$ has N_rN_t eigenvalues, in which $\lambda_1 = N_rN_t + (N_t)/(E)\sigma_n^2$ and the other $N_rN_t - 1$ eigenvalues have the same value $\lambda_2 = (N_t)/(E)\sigma_n^2$.

The magnitudes of the correlation values $M(m,n)$ in (7) depend on the distribution of the angles Ω_t and Ω_r of each path and the array interelement spacing. If Ω_t and Ω_r for all the paths are the same, then we get the fully correlated case. The correlation decreases as the range of angles increases for the same array spacing. For any non-zero angle spread, increasing antenna spacing has the effect of decreasing the correlation [3].

C. Formulae of Pr_D for Two Special Cases

Here, in order to simplify the computation, we display the compact form of (12) for two special cases: all the eigenvalues $\{\lambda_k\}$ are different or are the same.

1) Eigenvalues Are Different: In this case, the number of distinct eigenvalues is $N = N_rN_t$ and all the algebraic multiplicity μ_m are one. As a result, (10) is rewritten as

$$p(\|\bar{x}\|^2) = \sum_{m=1}^{N_rN_t} \frac{\prod_{p=1,p\neq m}^{N_rN_t} \frac{C_m}{C_m - C_p}}{C_m} \cdot e^{-\frac{\|\bar{x}\|^2}{C_m}}. \quad (15)$$

Therefore, the probability of detection is given by

$$Pr_D = \sum_{m=1}^{N_rN_t}\left(\prod_{p=1,p\neq m}^{N_rN_t} \frac{C_m}{C_m - C_p}\right)\cdot e^{-\frac{\delta}{C_m}}. \quad (16)$$

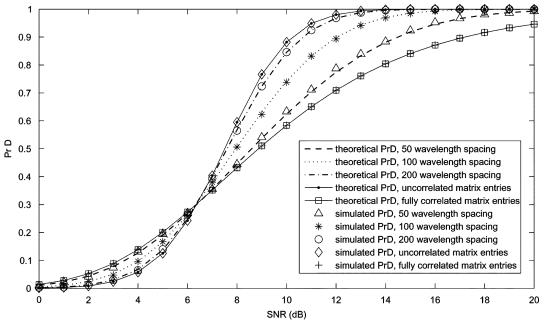

Fig. 2. Theoretical and simulated Pr_D as a function of the SNR.

2) Eigenvalues Are the Same: In this case, the N_rN_t eigenvalues have the same value λ, so (9) can be expressed as follows:

$$\Gamma(v) = \frac{1}{\left(1 - jv\frac{E}{N_t}\lambda\right)^{N_rN_t}} \tag{17}$$

which results in the conclusion that $||\overline{x}||^2 \sim (E)/(N_t)(\lambda)/(2)\chi^2_{(2N_rN_t)}$. Consequently, the probability of detection is given by

$$Pr_D = 1 - F_{\chi^2_{(2N_rN_t)}}\left(\frac{2N_t\delta}{E\lambda}\right) \tag{18}$$

where $F_{\chi^2_{(2N_rN_t)}}$ denotes the cumulative distribution function (CDF) of a chi-square random variable with $2N_rN_t$ degrees of freedom. This result matches [1, equation (29)].

IV. Numerical Results and Discussion

A simulation of a MIMO radar system has yielded several numerical results that are provided in this section. We consider a system with two transmitting antennas and four receiving antennas, and the target area has circular shape with radius r_0, within which 64 scatterers are uniformly distributed. The carrier frequency of the signal is 10 GHz, and the size of antenna array is much smaller than the distances between the target and both the transmitter and receiver, which are in the order of 3–5 km. The probability of false alarm is set to be a constant value $Pr_{FA} = 10^{-6}$.

First of all, we validate the theoretical results of Pr_D obtained from (12) for various configurations. Fig. 2 depicts the theoretical probability of detection as a function of the average received SNR when $r_0 = 15m$, and the five configurations considered involve the two extreme models mentioned in Section III-B and three models whose array interelement spacings are 50, 100, and 200 wavelengths, respectively.

Fig. 2 also shows the Pr_D recorded from simulations for the same five scenarios, and the total number of tests for each case is 10 000. Obviously, the simulated results agree well with the theoretical values, which confirms the correctness of formula (12).

Observing the figure, we find that the curves corresponding to the two extreme channel models set bounds for the system performance. In other words, all the configurations with specific element spacings lie between these two ideal scenarios. Moreover, the performance curve is closer to the full correlation case as the spacing decreases, while closer to the uncorrelated case as the spacing becomes larger, which agrees with the analysis of the relation between antenna interelement spacing and the channel matrix correlation shown in Section III-B.

It can be seen in Fig. 2 that at low SNR, a system with densely spaced antennas outperforms the ones whose interelement spacing is large, while at high SNR, the latter performs better. Furthermore, the system with large antenna spacing is always preferred when the detection performance is acceptable, i.e., PrD is large enough. This is because that at low SNR, the received power affects target detection performance the most, while the number of diversity paths is the dominating factor at high SNR.

V. Conclusion

In this letter, we introduced the MIMO radar system assuming that the target is modeled as the sum of a finite number of random and independent scatterers. A formula to calculate the theoretical probability of detection for a MIMO radar having arbitrary array-target configuration was derived, and it was validated by simulation results.

References

[1] E. Fishler, A. Haimovich, R. S. Blum, L. J. Cimini, D. Chizhik, and R. A. Valenzuela, "Spatial diversity in radars-models and detection performance," *IEEE Trans. Signal Process.*, vol. 54, no. 3, pp. 823–838, Mar. 2006.

[2] E. Fishler, A. Haimovich, R. S. Blum, D. Chizhik, L. J. Cimini, and R. A. Valenzuela, "MIMO radar: An idea whose time has come," in *Proc. IEEE Int. Conf. Radar*, Apr. 2004, pp. 71–78.

[3] D. Tse and P. Viswanath, *Fundamentals of Wireless Communication*. New York: Cambridge Univ. Press, 2005.

[4] M. V. Clark, L. J. Greenstein, W. K. Kennedy, and M. Shafi, "Matched filter performance bounds for diversity combining receivers in digital mobile radio," *IEEE Trans. Veh. Technol.*, vol. 41, no. 4, pp. 356–362, Nov. 1992.

[5] I. J. Nagrath and M. Gopal, *Control Systems Engineering*. New York: Wiley, 1982.

[6] J. G. Proakis, *Digital Communications*, 4th ed. Boston, MA: McGraw-Hill, 2001.

DETECTION PERFORMANCE OF MIMO RADAR WITH REALISTIC TARGET MODELS

Chaoran Du, John Thompson, Bernard Mulgrew
School of Engineering and Electronics
The University of Edinburgh
Edinburgh, EH9 3JL, UK
{C.Du, John.Thompson, B.Mulgrew}@ed.ac.uk

Yvan Petillot
School of Engineering and Physical Sciences
Heriot-Watt University
Edinburgh, EH14 4AS, UK
Y.R.Petillot@hw.ac.uk

***Abstract*—We simulate a multiple-input multiple-output (MIMO) radar system involving a realistic target, which is a life-size land vehicle modeled using a EM simulator FEKO. Numerical results showing the detection performance of a MIMO radar are provided, which is measured based on multiple realizations of the channel matrix generated using the available FEKO data. The results validate in a practical setting the improvements in detection performance available from MIMO radar configurations.**

MIMO radar, detection performance, spatial diversity, finite scatterers model

I. INTRODUCTION

Motivated by the advantages offered by MIMO systems in communications, Fishler et al. [1, 2] proposed that MIMO techniques can also be applied in radar scenarios to improve performance by exploiting the so-called spatial diversity gain defined in communication theory [3]. However, the rectangular-shape target is assumed to be composed of an infinite number of random scatterers in [1], and the gains of all the scatterers are random variables with the same distribution. Such a model is neither realistic nor convenient to be employed given that in practice the target actually comprises several significant scatterers at different spatial locations. In [4], we model the target by a finite number of scatterers without limitation on the locations, whose reflectivity coefficients are assumed to be random variables. [1] presents the detection performance of a MIMO radar system with four special configurations, while the probability of detection for a MIMO radar having an arbitrary array-target configuration can be computed using formulae derived in [4]. These numerical results show that the MIMO radar whose array interelement spacing is large always outperforms the ones with densely spaced antennas for high SNRs and hence high detection probabilities, e.g., 0.5 or higher.

The main contribution of this paper is that we set up a MIMO radar system involving a realistic target, and simulate the detection performance of the system with different configurations, validating the conclusions presented in [1, 4] which are based on theoretical and mathematical target models. To the authors' knowledge, this is the first effort of its kind in the open literature. The target considered here is a life-size land vehicle, which is modeled using a computer aided electromagnetic (EM) simulator FEKO [5]. We emphasize that although we are working with FEKO data, rather the "real" data collected from experimental field trials, the former is a common practical choice as the availability of the real data is very limited [5]. The system model used in this paper is similar to that in [4] where, however, the gains of the scatterers composing the target are assumed to be zero-mean complex Gaussian random variables.

This paper is organized as follows. We first introduce the system configuration of a MIMO radar, and then develop its channel model, signal model, and the target detector which is utilized in the simulation. In Section IV, numerical results showing the target detection performance of a MIMO radar system with various configurations are provided, followed by some discussion. These results are obtained based on multiple realizations of the channel matrix generated using the available FEKO data. Section V gives the conclusions.

II. SYSTEM CONFIGURATION

Mishra [5] modeled four types of life-size land vehicles using a computer aided EM simulator FEKO, and formatted bistatic SAR images through appropriate post-processing of the results. These four targets are the armoured personal carrier (APC), the main battle tank (MBT), the stinger launcher (STR), and the land missile launcher (MSL). In this section, we build up a bistatic MIMO radar system having a 3-dimensional (3D) configuration based on Mishra's work, including a realistic target model.

In Mishra's simulation, for each run, the 3D target is illuminated by the transmitter for a range of frequencies, and the transmitter is fixed at a certain azimuth and elevation with a given polarization. The EM simulator generates the surface current on the provided CAD model of the target, based on which the scattered field in a given polarization at the receiver is obtained and stored. The receiver has a fixed elevation and varying azimuth angle through 0° to 360° with a predetermined angular step. The FEKO data collected from each run then are post-processed, generating 2D SAR images of the target viewed by the fixed transmitter and rotating receiver with different azimuth.

For certain polarizations of transmitter and receiver, several 50×50 matrices are available to form images of a given type of

target viewed by a pair of transmitter and receiver at different locations. As the values of matrix entries indicate the reflectivities of different parts of the target, it is reasonable to assume that the target is composed of a finite number of point-like scatterers, whose reflectivity coefficients change as the locations of transmitter and receiver vary. In other words, for each pair of transmitter and receiver locations, the target is modeled by a 10*m*×10*m* rectangular area *S* as shown in Fig.1, in which there are 2500 point-like scatterers $\{s_{i,j}\}$, whose reflectivity coefficients $\{a_{i,j}\}$ are the values of the (*i, j*) entries of the corresponding 50×50 matrix. The origin of the *xy*-plane is at the centre of the target, and the coordinates $(x_{i,j}, y_{i,j})$ of the scatterer $s_{i,j}$ are $(j\times0.2-5.1, i\times0.2-5.1)$.

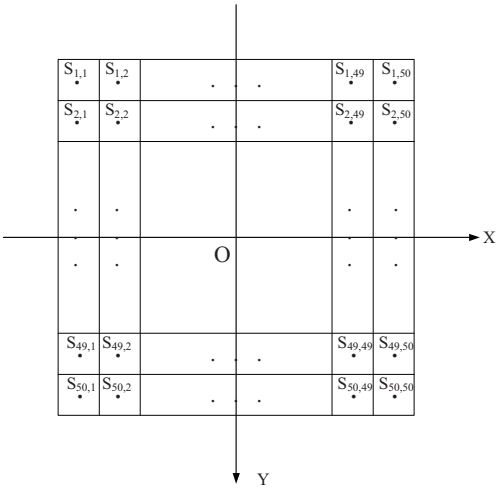

Figure 1. Finite scatterers model of the target.

Therefore, we can set up the MIMO radar system as illustrated in Fig.2, where uniform linear arrays of antennas [3] are employed at both transmitter and receiver with N_t and N_r elements, respectively. The antenna separations are $\Delta_t\lambda_c$ and $\Delta_r\lambda_c$, where λ_c is the carrier wavelength and Δ_t and Δ_r are the normalized transmit and receive antenna spacing in wavelengths. R_{t0} and R_{r0} are the distances between the centre of the target and the first antenna of the transmitting and receiving array, respectively. Notice the fact that these two values do not need to be the same. In Fig.2, the rectangular area *S* in the *xy*-plane is the 10*m*×10*m* target model illustrated in Fig.1. Because of the limited FEKO data, the elevation of transmitter and receiver, θ_t and θ_r, can be either 10° or 15°, and the transmitter azimuth φ_t can be one of the following six values 0°, 60°, 120°, 180°, 240°, and 300°, while the receiver azimuth φ_r can be any one among 500 values, from 0° to 360° with a step of 0.72°. For any of the aforementioned system configuration, the target can be APC, MBT, STR, or MSL, and the polarizations of the transmitter and receiver can be either horizontal or vertical.

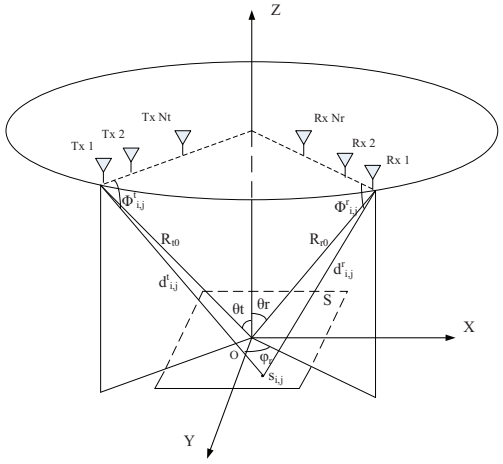

Figure 2. Configuration of the MIMO radar system.

III. SYSTEM MODEL

A. Channel Model

We assume that all the signals are narrowband and that distances between scatterers and both transmitter and receiver are much larger than the dimensions of the antenna arrays, that is, we operate in the far field. As shown in Fig.2, the path through the scatterer $s_{i,j}$ is defined by angle of departure (AoD) $\Phi^t_{i,j}$, angle of arrival (AoA) $\Phi^r_{i,j}$, reflectivity coefficient $a_{i,j}$, distance between Tx 1 and $s_{i,j}$, $d^t_{i,j}$, and distance between $s_{i,j}$ and Rx 1, $d^r_{i,j}$. Then, for a MIMO radar having the configuration described in the last section with any combination of all the possible parameters, we can calculate the $N_r\times N_t$ channel matrix **H** as below [3, 4]:

$$\mathbf{H}=\sum_{i=1}^{50}\sum_{j=1}^{50}a_{i,j}\exp\left[-\frac{j2\pi d_{i,j}}{\lambda_c}\right]\boldsymbol{\Psi}_r\left(\Omega^r_{i,j}\right)\boldsymbol{\Psi}_t^H\left(\Omega^t_{i,j}\right) \quad (1)$$

$$\boldsymbol{\Psi}_\varepsilon(\Omega^\varepsilon_{i,j})=\begin{bmatrix}1\\ \exp\{-j2\pi\Delta_\varepsilon\Omega^\varepsilon_{i,j}\}\\ \vdots\\ \exp\{-j2\pi(N_\varepsilon-1)\Delta_\varepsilon\Omega^\varepsilon_{i,j}\}\end{bmatrix} \quad (2)$$

where ε represents either r or t, $\Omega_{i,j}^{\varepsilon} = \cos(\Phi_{i,j}^{\varepsilon})$, $d_{i,j} = d_{i,j}^{t} + d_{i,j}^{r}$, and the superscript H denotes the conjugate transpose. Geometrical computation gives us the following equations:

$$d_{i,j}^{\varepsilon} = \sqrt{(R_{\varepsilon 0}\sin\theta_{\varepsilon})^2 + (x_{\varepsilon} - x_{i,j})^2 + (y_{\varepsilon} - y_{i,j})^2} \tag{3}$$

$$\Omega_{i,j}^{\varepsilon} = \frac{\left(d_{i,j}^{\varepsilon}\right)^2 - R_{\varepsilon 0}^2\cos(2\theta_{\varepsilon}) - x_{i,j}^2 - y_{i,j}^2}{2R_{\varepsilon 0}\sin\theta_{\varepsilon} d_{i,j}^{\varepsilon}} \tag{4}$$

where $x_{\varepsilon} = R_{\varepsilon 0}\sin\theta_{\varepsilon}\sin\varphi_{\varepsilon}$ and $y_{\varepsilon} = R_{\varepsilon 0}\sin\theta_{\varepsilon}\cos\varphi_{\varepsilon}$.

B. Signal Model

It is supposed that the kth transmitter transmits a signal $\sqrt{E/N_t}s_k(t)$, where E is the total transmitted power. The normalizing coefficient is employed to make sure that the total transmitted power and the average received power at each element are not affected by the number of transmit antennas. Furthermore, all the transmitted signals are orthogonal, which is equivalent to the fact that $\int s_j(t)s_i(t)dt = \delta_{ij}$, where δ_{ij} is a Dirac delta function. An $N_r \times 1$ vector $\mathbf{r} = \begin{bmatrix} r_1 & r_2 & \cdots & r_{N_r} \end{bmatrix}^T$ denotes the received signals, which is given by

$$\mathbf{r} = \sqrt{\frac{E}{N_t}}\mathbf{H}\cdot\mathbf{s} + \mathbf{w} \tag{5}$$

where the $N_t \times 1$ vector $\mathbf{s} = \begin{bmatrix} s_1 & s_2 & \cdots & s_{N_t} \end{bmatrix}^T$ and the $N_r \times 1$ vector $\mathbf{w} = \begin{bmatrix} w_1 & w_2 & \cdots & w_{N_r} \end{bmatrix}^T$ stands for the transmitted signals and the additive white Gaussian noise at all the receiver antennas, respectively. Here $\mathbf{w} \sim \mathcal{CN}(\mathbf{0}_{N_r}, \sigma_n^2\mathbf{I}_{N_r})$, the superscript T denotes transpose, $\mathbf{0}_{Nr}$ is a $N_r \times 1$ all-zeros vector, and $\mathbf{I}_{Nr}$ is a $N_r \times N_r$ identity matrix. Let the received signal $\mathbf{r}$ go through a bank of matched filters, and denote the output by a $N_rN_t \times 1$ vector $\mathbf{x}$, which can be written as follows [1, 4]:

$$\mathbf{x} = \begin{cases} \mathbf{n} & \mathcal{H}_0 \\ \sqrt{\frac{E}{N_t}}\mathbf{h} + \mathbf{n} & \mathcal{H}_1 \end{cases} \tag{6}$$

where the alternate hypothesis $\mathcal{H}_1$ and null hypothesis $\mathcal{H}_0$ are that the target does or does not exist, respectively. The $N_rN_t \times 1$ channel vector $\mathbf{h}$ is composed of all the entries of the channel matrix $\mathbf{H}$, and the $N_rN_t \times 1$ noise vector $\mathbf{n} \sim \mathcal{CN}(\mathbf{0}_{N_rN_t}, \sigma_n^2\mathbf{I}_{N_rN_t})$. Together with the channel matrix $\mathbf{H}$ given by (1), we can measure the value of the $\mathbf{x}$, from which the target detection decision will be made.

In [1, 4], $\mathbf{h}$ is assumed to be a zero-mean complex Gaussian random vector with known covariance matrix, and thus, the theoretical probability of detection $\mathrm{Pr_D}$ of a MIMO radar can be calculated. In this paper, however, the channel gains are calculated using the FEKO data and the distributions are unknown. Therefore, we make the detection decision for each realization of $\mathbf{h}$ by viewing it as a deterministic vector, and obtain the $\mathrm{Pr_D}$ of a MIMO radar by averaging over multiple realizations. Because the entries of $\mathbf{h}$ are not known in advance, we resort to the generalized likelihood ratio test (GLRT) approach which replaces the unknown parameters by their maximum likelihood estimates [6]. In other words, the decision rule of the GLRT can be stated as follows

$$\frac{\max_{\mathbf{h}} p\left(\mathbf{x}|\mathcal{H}_1, \mathbf{h}\right)}{p\left(\mathbf{x}|\mathcal{H}_0\right)} \underset{\mathcal{H}_0}{\overset{\mathcal{H}_1}{\gtrless}} \gamma \tag{7}$$

where $p\left(\mathbf{x}|\mathcal{H}_1, \mathbf{h}\right)$ and $p\left(\mathbf{x}|\mathcal{H}_0\right)$ denote the probability density function (pdf) of the data given $\mathbf{h}$ under $\mathcal{H}_1$ and under $\mathcal{H}_0$, respectively. Given the complex Gaussian distribution of $\mathbf{n}$, it is not difficult to obtain the radar detector which can be expressed as

$$T = \|\mathbf{x}\|^2 \underset{\mathcal{H}_0}{\overset{\mathcal{H}_1}{\gtrless}} \delta \tag{8}$$

where δ is a threshold ensuring the required probability of false alarm $\mathrm{Pr_{FA}}$. As the distribution of $\|\mathbf{x}\|^2$ under $\mathcal{H}_0$ is a chi-square random variable with $2N_rN_t$ degrees of freedom, we can calculate the threshold which is given by

$$\delta = \frac{\sigma_n^2}{2} F_{\chi^2_{(2N_rN_t)}}^{-1}\left(1 - \mathrm{Pr_{FA}}\right) \tag{9}$$

where $F_{\chi^2_{(2N_rN_t)}}^{-1}$ denotes the inverse cumulative distribution function of a chi-square random variable with $2N_rN_t$ degrees of freedom. Then, the detection decision can be made by comparing the value of $\|\mathbf{x}\|^2$ with δ.

IV. SIMULATION AND NUMERICAL RESULTS

In this section, we present numerical results showing the target detection performance of a MIMO radar system with

different antenna spacings. The performance is measured based on multiple realizations of the channel matrix generated using the available FEKO data. Note the fact that there are several approaches to generate channel realizations, and here we just employ a simple one, as our major objective is to validate the advantages of a MIMO radar when a realistic target is considered.

In all the following simulations, the target is a MBT, the polarizations of both the transmitter and receiver are horizontal, the elevation of the receiver is 10°, and the elevation and azimuth of the transmitter is 10° and 0°, respectively. Numerical results for the scenarios with other combinations of the parameters can also be obtained using corresponding FEKO data. We consider a system with two transmitting antennas and four receiving antennas, the carrier frequency of the signal is 1 GHz, and the probability of false alarm is set to be a constant value $\mathrm{Pr}_{\mathrm{FA}} = 10^{-6}$. The channel matrix **H** is normalized such that the average energy returned from the target is one. The SNR is therefore defined as the ratio between the transmitted power *E* and the noise level per receiving antenna σ_n^2.

When the system parameters are fixed at the above values, 500 matrices with size 50×50 are available, whose entries are the reflectivity coefficients $\{a_{i,j}\}$ of all the 2500 scatterers $\{s_{i,j}\}$ composing the target. Each matrix corresponds to a receiver location with the azimuth φ_r varying from 0° to 360° at a step of 0.72°. We observe that those images, viewed by a fixed transmitter and a rotating receiver whose azimuth changes within a small variation range, are quite similar. In other words, the coefficients $\{a_{i,j}\}$ would not change dramatically for a few successive receiver azimuth steps when other parameters remain the same. Furthermore, from (1)-(4), it is obvious that, with the selected polarizations, elevations and azimuths of the transmitter and receiver, $\{a_{i,j}\}$ are fixed and the value of channel matrix **H** changes as the values of R_{t0} and R_{r0} vary. The conditions on choosing R_{t0} and R_{r0} are quite loose, as long as they are large enough that the system is operated in the far field, but not so large that the target would not be viewed as a point target.

The detection performance for various MIMO radar configurations is shown in Fig.3, and these systems are almost the same, except that the antenna spacings Δ_t and Δ_r are 0.5, 100, 200, and 500 wavelengths, respectively. For each configuration, we generate 3000 realizations of **H** by assigning 10 successive values to φ_r from 32.4° to 38.88° with a step of 0.72° (denoted range I), and allocating 300 arbitrary values to R_{t0} and R_{r0} respectively for each angular value. R_{t0} and R_{r0} are selected to be between 3 ~ 5 km.

Observing the figure, we find that at low SNR, a system with densely spaced antennas outperforms the ones whose interelement spacing is large, while at high SNR the latter performs better. Furthermore, the system with large antenna spacing is always preferred when the detection performance is acceptable, *i.e.*, $\mathrm{Pr}_D > 0.5$. This is because that at low SNR, the received power affects target detection performance the most, while the number of diversity paths is the dominating factor at high SNR.

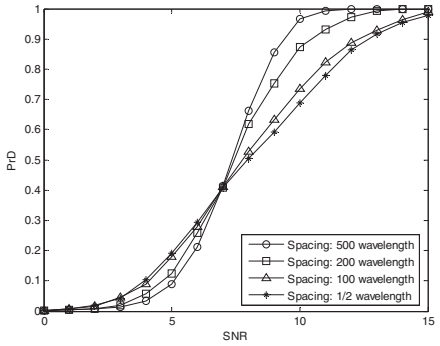

Figure 3. Pr_D as a function of the SNR for angular range I, 2 Tx, 4 Rx antennas, Tx/Rx interelement spacings varied simultaneously.

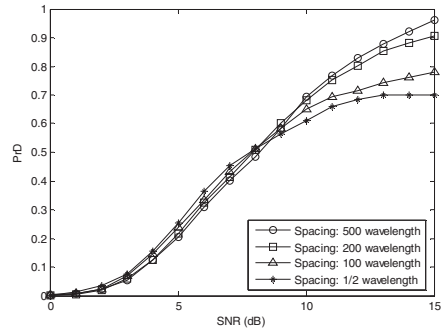

Figure 4. Pr_D as a function of the SNR for angular range II, 2 Tx, 4 Rx antennas, Tx/Rx interelement spacings varied simultaneously.

The receiver azimuth φ_r can only be one of the 500 values which are integer multiples of 0.72° when the data record is used directly. As mentioned before, $\{a_{i,j}\}$ are similar for a few successive receiver azimuths when other parameters remain unchanged. Hence, we can generate several realizations of **H** where φ_r could be any value by using linear interpolation. In other words, for an arbitrary φ_{r0} that is not an integer multiple of 0.72°, we first find two values φ_{rl} and φ_{ru}, which is the lower and upper bound of φ_{r0}, respectively. Here $\varphi_{rl} = \lfloor \varphi_{r0} / 0.72^\circ \rfloor \times 0.72^\circ$ and $\varphi_{ru} = \varphi_{rl} + 0.72^\circ$, where $\lfloor k \rfloor$ represents the largest integer smaller than *k*. The reflectivity coefficients corresponding to φ_{rl} and φ_{ru} are available, denoted by $\{a_{i,j}^l\}$ and $\{a_{i,j}^u\}$, respectively. We calculate the reflectivity of each scatterer $a_{i,j}^0$ when the receiver azimuth is φ_{r0} by using interpolation between the corresponding two

values of $a_{i,j}^{l}$ and $a_{i,j}^{u}$. Notice here that the real and imaginary parts of $\{a_{i,j}^{0}\}$ are interpolated separately.

Fig.4 depicts the detection performance of a MIMO radar system with different configurations. The difference between this figure and Fig.3 is the new angular range (range II) of the look angle, *i.e.*, 10 successive values are assigned to φ_r here from 176.4° to 182.88° with a step of 0.72°. Similar to Fig.3, we find from Fig.4 that the system with sparsely spaced arrays performs better at high SNR, and this configuration should always be chosen when $Pr_D > 0.6$. This result agrees well with the conclusions drawn in [1, 4], where the realizations of the channel matrix are obtained based on theoretical and mathematical target models. However, it is obvious that the radar system has different detection performance from various observe angles, and the performance improvement brought in by the MIMO configuration is also different. Therefore, we now consider Fig.5, which displays the detection performance when the target is viewed from various receiver look angles at a fixed SNR.

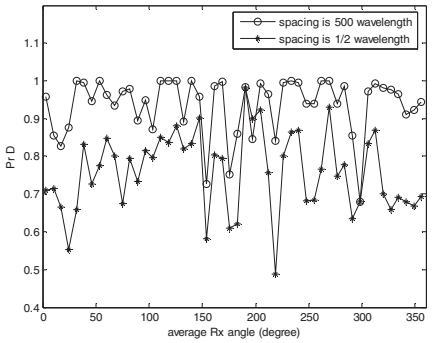

Figure 5. Pr_D as a function of the look angle at SNR=15dB, 2 Tx, 4 Rx antennas, Tx/Rx interelement spacings varied simultaneously.

In this simulation, we divide 360° into 50 equal-sized angular sections and obtain the corresponding Pr_D values. Each Pr_D value comes from 3000 realizations of **H** utilizing the interpolation approach mentioned before. These realizations are computed with different R_{t0} and R_{r0}, and various receiver azimuth chosen arbitrarily from the corresponding angle section. From Fig.5, it is clear that, except for a few observation angles, a MIMO radar with large antenna spacing always provides better detection performance, and for most angles, the performance improvement resulting from the MIMO configuration is significant. For those few observation angles where the MIMO configuration is worse, the performance difference is small, and we believe this is because the target scattering is not rich enough when it is viewed from those specific angles. In addition to the better average performance with the angle, we find from Fig.5 that the MIMO configuration also provides performance with less variability, *i.e.*, the performance is less dependent on the look angle, which makes it more attractive.

V. CONCLUSIONS

In this paper, we introduce the configuration of a MIMO radar system including a target, which is a life-size land vehicle modeled using an EM simulator FEKO. Numerical results showing the target detection performance are presented, which is measured based on multiple realizations of the channel matrix generated utilizing the available FEKO data. Comparisons of the detection performance of a MIMO radar with different antenna spacings show that a system with a large array interelement spacing always performs better for high SNRs and hence high detection probabilities, e.g., 0.6 or higher. These numerical results obtained using FEKO data validate the conclusion drawn in previous papers where the target is characterized by theoretical target models.

ACKNOWLEDGMENT

We acknowledge the support of the Scottish Funding Council for the Joint Research Institute with Edinburgh and the Heriot-Watt Universities, which is a part of the Edinburgh Research Partnership (ERP). Chaoran Du gratefully acknowledges the support of the ERP in funding her PhD studies.

REFERENCES

[1] E. Fishler, A. Haimovich, R. S. Blum, L. J. Cimini, D. Chizhik, and R. A. Valenzuela, "Spatial diversity in radars - Models and detection performance," IEEE Trans. Signal Process., vol. 54, no. 3, pp. 823-838, Mar. 2006.

[2] E. Fishler, A. Haimovich, R. S. Blum, D. Chizhik, L. J. Cimini, and R. A. Valenzuela, "MIMO radar: An idea whose time has come," Proc. of the IEEE Int. Conf. on Radar, pp. 71-78, Apr. 2004.

[3] D. Tse and P. Viswanath, Fundamentals of wireless communication, New York: Cambridge University Press, 2005.

[4] C. Du, J. Thompson, and Y. Petillot, "Predicted detection performance of MIMO radar," IEEE. Signal Process. Lett., vol. 15, pp. 83-86, 2008.

[5] A. K. Mishra and B. Mulgrew, "Database generation of bistatic ground target signatures," IEEE/ACES Conference on Wireless Communication and Applied Computational Electromagnetics, pp. 523-528, Apr. 2005.

[6] S. M. Kay, Fundamentals of Statistical Signal Processing: Detection Theory, Upper Saddle River, NJ: Prentice-Hall PTR, 1993.

DETECTION AND DIRECTION FINDING PERFORMANCE OF HYBRID BISTATIC RADAR

Chaoran Du, John S. Thompson
School of Engineering and Electronics
The University of Edinburgh
Edinburgh, EH9 3JL, UK
{C.Du, John.Thompson}@ed.ac.uk

Yvan R. Petillot
School of Engineering and Physical Sciences
Heriot-Watt University
Edinburgh, EH14 4AS, UK
Y.R.Petillot@hw.ac.uk

***Abstract*—The conventional phased-array radar provides coherent processing gain while the MIMO radar exploits spatial diversity gain to improve the system performance. We investigate a hybrid bistatic radar combining these two configurations to take advantage of both gains. The probability of detection of the hybrid system is derived, and the CRB and the MSE of the maximum likelihood estimation for both angle of departure and angle of arrival are evaluated to assess the direction finding performance.**

MIMO, phased-array radar, spatial diversity, coherent processing gain, target detection, direction finding, CRB, MSE

I. INTRODUCTION

Two major challenges in radar theory are the target detection and parameter estimation problems. In practice, the performance of a radar system is limited by target scintillations or "fading" [1]. For target detection, the conventional phased-array radar addresses this target "fading" problem by cohering a narrow beam toward the target direction, which can realize coherent processing gain to maximize the received energy reflected by the target. While for direction finding, we collect multiple independent snapshots to average out scintillation effects to improve the estimation accuracy. A new architecture called the MIMO radar proposed by Fishler et al. in [2] can overcome the deep fading problem by exploiting the spatial diversity gain defined in communication theory [3]. It is demonstrated in [2] that, for target detection, the MIMO radar system outperforms the phased-array radar at high signal-to-noise (SNR) while the latter performs better when the SNR is low. It is also shown in [4] and [5] that the MIMO radar leads to significant improvements in angle-of-arrival (AoA) estimation accuracy because widely-separated antennas at the transmitter observe different aspects of the target.

In this paper, we investigate the best architecture for a radar system which is used for both target detection and direction finding, particularly when the total number of transmitting and receiving antennas is fixed. A hybrid bistatic radar combines the phased-array and the MIMO radar configurations, providing a balance between the coherent processing gain and the spatial diversity gain. In addition, the hybrid radar is a general system model, which can be used to describe various practical radar configurations, including the MIMO and phased-array configurations as special and extreme cases. Although the architecture of the multistatic coherent sparse aperture system proposed in [6] is similar to the hybrid bistatic radar, they utilized the point-like target assumption and focus on processing the received data at a central processor coherently rather than exploring the spatial diversity of the target. The system configuration discussed in [7] is the same as that in this paper, but the major aim of [7] is to propose spatial spectral estimators to detect the target and estimate propagation parameters. In this paper a parametric approach is applied and our emphasis is to explore the performance of the system accounting for both the diversity gain and the coherent processing gain in order to find the best configuration. In [7], the target direction is only denoted by a "target location parameter" whose manifold is not formally defined, and linearly independent waveforms are assumed to be transmitted from all the antennas. In this paper, however, we define the target direction by two parameters, angle-of-departure (AoD) and AoA, and assume that each array transmits one of a set of orthogonal waveforms and the antennas of each array operate as a beamformer cohering a beam toward the estimated AoD. In this way, as mentioned in [8], extra coherent processing gain can be achieved compared with fully independent waveforms case at the price of estimating the AoD first. We want to investigate the effect different configurations have on system performance and so we wish to measure the gains that the hybrid radar system can realize. The theoretical expressions presented in this paper provide both the detection and estimation performance of a hybrid radar system. These equations can be used to select the best architecture for a given specific scenario, considering factors such as the number of antennas, the SNR values, and the required precision of the application.

This paper is organized as follows. In Section II we introduce the hybrid radar system model. The target detection problem is formulated and a closed form expression to compute the theoretical probability of detection is derived in section III. We then discuss the initialization process during which the AoD is estimated, and assess the estimation performance by measuring the average CRB. Next, the average and outage CRBs for AoA estimation are presented, assuming that the AoD information is available at the transmitter. Numerical results and some discussion are shown in Section V, and conclusions are drawn in Section VI. Readers may refer to [9] for more details.

II. SYSTEM MODEL

Similar to the system configuration in [7], the narrowband hybrid bistatic radar considered here has M_t antenna arrays at the transmitter and M_r arrays at the receiver, and the array separations are large enough such that different arrays observe different aspects of the target. Each array is a uniform linear array (ULA) of antennas with N_t elements at the transmitter and N_r elements at the receiver, which has the same configuration as that of a conventional phased-array radar with closely spaced sensors. We assume that the whole system works in the "far field", *i.e.*, the dimension of each array and the array separations are much smaller than the distances between the target and both the transmitter and receiver. Denote the transmitted signals and the additive white Gaussian noise by **e**(t) and **n**(t), respectively, and the received signal can be written as

$$\mathbf{r}(t) = \mathbf{H} \cdot \mathbf{e}(t) + \mathbf{n}(t) \tag{1}$$

where $\mathbf{n}(t) \sim \mathcal{CN}(\mathbf{0}_{M_r N_r}, \sigma_n^2 \mathbf{I}_{M_r N_r})$ and here $\mathbf{I}_k$ denotes a $k \times k$ identity matrix. The channel matrix is given by

$$\mathbf{H} = \begin{bmatrix} \mathbf{C}_{11} & \mathbf{C}_{12} & \cdots & \mathbf{C}_{1M_t} \\ \mathbf{C}_{21} & \mathbf{C}_{22} & & \vdots \\ \vdots & & \ddots & \vdots \\ \mathbf{C}_{M_r 1} & \cdots & \cdots & \mathbf{C}_{M_r M_t} \end{bmatrix} \tag{2}$$

where the $N_r \times N_t$ matrix $\mathbf{C}_{up}$ can be expressed as below:

$$\mathbf{C}_{up} = \beta_{up} \mathbf{\Psi}_r(\Phi_u^r) \mathbf{\Psi}_t^T(\Phi_p^t)$$

$$\mathbf{\Psi}_\varepsilon(\Phi_\varsigma^\varepsilon) = \begin{bmatrix} 1 \\ \exp\left\{ j2\pi\Delta_\varepsilon \sin(\Phi_\varsigma^\varepsilon) \right\} \\ \vdots \\ \exp\left\{ j2\pi(N_\varepsilon - 1)\Delta_\varepsilon \sin(\Phi_\varsigma^\varepsilon) \right\} \end{bmatrix} \tag{3}$$

where the superscript T denotes the transpose of a matrix, ε is either t or r, and correspondingly ς is either p or u. Here p=1,2,…,M_t, and u=1,2,…,M_r. Δ_t and Δ_r are the normalized transmit and receive interelement spacings in wavelengths, and β_{up} is the fading coefficient between the pth transmit array and the uth receive array. Here Φ_p^t is the AoD of the path from the first element of the pth transmit array to the center of the target area, and Φ_u^r is the AoA of the path from target center to the first antenna of the uth receive array. We adopt the statistical model proposed in [2] in this paper, and hence a fading coefficient vector $\boldsymbol{\beta}$ is defined such that $[\boldsymbol{\beta}]_{(u-1)M_t+p} \triangleq \beta_{up}$ and $\boldsymbol{\beta} \sim \mathcal{CN}(\mathbf{0}_{M_r M_t}, \mathbf{I}_{M_r M_t})$, where $\mathbf{0}_k$ represents a $k \times 1$ all-zeros vector. Note here that the vector $\boldsymbol{\beta}$ is the key MIMO definition, suggesting that each array constitutes one element of a MIMO system. On the other hand, (3) follows the phased-array definition, implying that each array itself works as a conventional phased-array radar.

We further assume that each of the M_t transmit arrays transmits a different waveform, which are collectively denoted by $\mathbf{b}(t) = \left[b_1(t), b_2(t), \cdots, b_{M_t}(t) \right]^T$. In addition, the pth transmitting array utilizes its corresponding beamformer $\mathbf{a}_p$ to steer toward the estimated target direction $\tilde{\Phi}_p^t$, where $\mathbf{a}_p = \mathbf{\Psi}_t^*(\tilde{\Phi}_p^t)$, the superscript * stands for the complex conjugate and p=1,2,…,M_t. Therefore, the transmitting signals are given by

$$\mathbf{e}(t) = c_0 \left[b_1(t)\mathbf{a}_1^T \quad b_2(t)\mathbf{a}_2^T \quad \cdots \quad b_{M_t}(t)\mathbf{a}_{M_t}^T \right] \tag{4}$$

where $c_0 = \sqrt{\frac{E_s}{M_t N_t}}$ and E_s is the transmitted power. The normalizing coefficient is employed here to make sure that the total transmitted power and the average received power at each element are not affected by the number of transmit antennas.

III. TARGET DETECTION PERFORMANCE

In this section, we derive a closed form expression to evaluate the theoretical probability of detection of a hybrid bistatic radar. In order to exploit coherent processing gain at both the transmitter and receiver to improve the target detection performance, we assume that the uth receiving array, similar to that of the transmitter, utilizes its corresponding beamformer to steer toward the estimated target direction $\tilde{\Phi}_u^r$. Denote the uth receiving beamformer by $\mathbf{g}_u = \mathbf{\Psi}_r^*(\tilde{\Phi}_u^r)$, and assume that the transmit waveforms are mutually orthogonal over L samples, *i.e.*, $\int b_j(t) b_i(t) dt = L\delta_{ij}$. Here u=1,2,…,M_r and δ_{ij} is the Dirac delta function. The output of the uth beamformer is given by

$$y_u(t) = \sqrt{\frac{E_s}{M_t N_t}} \mathbf{g}_u^T \sum_{k=1}^{M_t} \mathbf{C}_{uk} \mathbf{a}_k b_k(t) + \mathbf{g}_u^T \mathbf{n}_u(t) \tag{5}$$

where $\mathbf{n}_u(t)$ denotes the noise at the elements of the uth receiving array and $\mathbf{n}_u(t) \sim \mathcal{CN}(\mathbf{0}_{N_r}, \sigma_n^2 \mathbf{I}_{N_r})$. Following [2], the optimal detector makes the detection decision based on a $M_r M_t \times 1$ vector $\mathbf{x}$, which is the output of a bank of matched filters, that is, $[\mathbf{x}]_{(u-1)M_t+p} = \int y_u(t) b_p(t) dt$, where u=1,2,…,M_r and p=1,2,…,M_t. The theoretical probability of detection of a hybrid radar system can be expressed as below:

$$\mathrm{Pr_D} = 1 - F_{\chi^2_{(2M_tM_r)}}\left(\frac{2\xi}{\frac{E_s L^2 N_r^2 N_t^2}{M_t N_t} + LN_r\sigma_n^2}\right) \quad (6)$$

$$\xi = \frac{LN_r\sigma_n^2}{2} F^{-1}_{\chi^2_{(2M_tM_r)}}\left(1 - \mathrm{Pr_{FA}}\right)$$

where ξ is the threshold determined by the required probability of false alarm $\mathrm{Pr_{FA}}$, $F^{-1}_{\chi^2_{(2M_tM_r)}}$ and $F_{\chi^2_{(2M_tM_r)}}$ denotes the inverse cumulative distribution function and the cumulative distribution function of a chi-square random variable with $2M_tM_r$ degrees of freedom, respectively. Here it is assumed that all the beamformers steer toward the true target direction, and then the full coherent processing gain N_rN_t can be realized. We provide the detection performance when only the estimated target direction is available in our journal paper [9], which is not presented here due to the space limitation.

The three systems discussed in [2] actually are special cases of the hybrid bistatic radar system, *i.e.*, the hybrid radar is the MIMO radar when N_t=N_r=1, the phased-array radar when M_t=M_r=1, and the MISO radar when N_t=M_r=1. The corresponding equations to calculate ξ and $\mathrm{Pr_D}$ for all these extreme cases derived from (6) matches the results in equations (28), (29), (34), (35), (38) and (39), respectively, in [2].

IV. DIRECTION FINDING PERFORMANCE

In this section, the performance of the hybrid radar as a direction finding system to estimate the AoD and AoA based on the received signal reflected from the target is examined. We focus our attention on the CRB of the hybrid system with various configurations, which provides a benchmark against which the performance of any unbiased estimator can be compared [11]. In order to avoid spatial aliasing, we set Δ_t=Δ_r=0.5 in this section [3][12]. It is noted that in this paper, we only consider a simple scenario where the target is viewed as a point source by each antenna array, which then estimates the target direction. However, our analysis could be easily extended to a more complicated problem of estimating the nominal direction of a distributed target [13].

A. Initialization

In order to realize coherent processing gain, the transmitter needs to known the AoD to steer toward the target direction. Hence, an "initialization" stage is required with no *a priori* knowledge about the channel available, during which the AoD is estimated. The transmitted signal model described in (4) cannot be employed in the procedure of estimating AoD since the direction knowledge of the transmitting beamformers is not known. Instead, orthogonal waveforms are transmitted from all the antennas to realize the AoD estimation [14][15]. As a special example of orthogonal waveforms, the time-division multiplexing (TDM) process is utilized in this paper, which is described as follows: At time t_1, the first element of the first transmitting array transmits the signal s and the received signals at all the M_rN_r receiving antennas are recorded. Then, at time t_2, the second element of the first array transmits s and again all the received signals are stored. This operation is repeated until the last transmitting antenna is excited at time $t_{M_tN_t}$. Here we assume that $|s|^2$=1 and that the scintillation coefficients are constant during the initialization process. Note that the "far field" assumption implies that the differences between the AoD Φ_p^t for different transmitting arrays are so small that they can be neglected, *i.e.*, $\Phi_1^t \doteq \Phi_2^t \doteq \cdots \Phi_{M_t}^t$. Similar statement applies to the AoA as well, and hence, we denote the AoD and AoA by Φ_t and Φ_r, respectively. After recording all the $M_rN_rM_tN_t$ received signals, we combine them into one $N_t \times 1$ data record with $M_rN_rM_t$ snapshots, which can be shown as below following (1) to (4)

$$\mathbf{y}(k) = \boldsymbol{\gamma}_t(\Phi_t)\beta_{up}\gamma_r(v)s + \mathbf{n}(k) \quad (7)$$

where the qth entry of the $N_t \times 1$ vector $\boldsymbol{\gamma}_t(\Phi_t)$ is $\exp\{j\pi(q-1)\sin(\Phi_t)\}$; $\gamma_r(v) = \exp\{j\pi(v-1)\sin(\Phi_r)\}$; k = (u-1) N_rM_t+ (v-1) M_t+ p; u = 1, 2,…, M_r; v = 1,2,…, N_r and p=1,2,…,M_t. $\mathbf{n}(k) \sim \mathcal{CN}(\mathbf{0}_{N_t}, \sigma_n^2\mathbf{I}_{N_t})$ and β_{up} is an entry of the vector $\boldsymbol{\beta}$, which is the same as that in (3). The estimated AoD $\hat{\Phi}_t$ is obtained by using the maximum likelihood (ML) estimator, which is given by [16]

$$\hat{\Phi}_t = \arg\max_{\Phi_t'} \sum_{k=1}^{M_rN_rM_t} \left|\boldsymbol{\gamma}_t^H(\Phi_t')\mathbf{y}(k)\right|^2 \quad (8)$$

where the superscript H denotes the conjugate transpose. We use the Cramer-Rao lower bound on the variance of any AoD estimator $\hat{\Phi}_t$ to compare the estimation performance, which is denoted by $\mathrm{CRB}(\Phi_t|\boldsymbol{\beta})$. The notation indicates that the value is conditioned on the unknown parameters $\boldsymbol{\beta}$ [5]. By using Theorem 4.1 provided in [17], the CRB conditioned on the scintillation coefficients can be expressed as

$$\mathrm{CRB}(\Phi_t|\boldsymbol{\beta}) = \frac{\sigma_n^2}{\|\boldsymbol{\beta}\|^2} \cdot \frac{6}{N_rN_t\pi^2\cos^2(\Phi_t)(N_t^2-1)} \quad (9)$$

Note here that $\|\boldsymbol{\beta}\|^2 \sim \frac{1}{2}\chi^2_{(2M_rM_t)}$. Similar to [5], the average CRB (ACRB) can be computed by averaging the CRB with respect to $\boldsymbol{\beta}$, which is given by

$$\mathrm{ACRB}(\Phi_t)=\frac{\sigma_n^2}{M_r M_t-1}\cdot\frac{6}{N_r N_t\pi^2\cos^2(\Phi_t)(N_t^2-1)} \quad (10)$$

B. AoA Estimation

Now we proceed to assess the performance of the hybrid radar system for estimating the AoA. Since the estimated AoD is available after the initialization process, each transmit array employs a beamformer to steer toward the target direction to exploit coherent processing gain. Here we assume that the transmitter knows the true target direction, *i.e.*, $\hat{\Phi}_t=\Phi_t$. The performance of the hybrid radar when the error in estimating AoD is taken into account is investigated in [9]. The interested reader may refer to [9] for more details, in which the CRB formulae and corresponding numerical results are presented, indicating that the estimation error in AoD resulting from the initialization stage may not decrease the performance of estimating AoA dramatically.

We assume that the waveforms which are mutually orthogonal over L samples have been used as the transmit waveform $\mathbf{b}(t)$, and matched filters of duration L samples for each distinct waveform are applied to the received signals. Following (1) to (4), we can obtain a $N_t\times 1$ data record with M_rM_t snapshots as below:

$$\mathbf{y}_{up}=\sqrt{\frac{E_s N_t L^2}{M_t}}\boldsymbol{\gamma}_r(\Phi_r)\beta_{up}+\mathbf{n}_{up} \quad (11)$$

where β_{up} is the $\{(u-1)M_t+p\}$th entry of the vector $\boldsymbol{\beta}$ defined in Section II, u=1,2,…,M_r, and p=1,2,…,M_t. The vth element of the $N_r\times 1$ vector $\boldsymbol{\gamma}_r(\Phi_r)$ is $\exp\{j\pi(v-1)\sin(\Phi_r)\}$ and $\mathbf{n}_{up}\sim\mathcal{CN}(\mathbf{0}_{N_r},L\sigma_n^2\mathbf{I}_{N_r})$. The ML estimator applied to estimate AoA $\hat{\Phi}_r$ can be written as [16]

$$\hat{\Phi}_r=\arg\max_{\Phi_r'}\sum_{u=1}^{M_r}\sum_{p=1}^{M_t}\left|\boldsymbol{\gamma}_r^H(\Phi_r')\mathbf{y}_{up}\right|^2 \quad (12)$$

The CRB conditioned on $\boldsymbol{\beta}$ can be calculated by using Theorem 4.1 provided in [17], which is given by

$$\mathrm{CRB}(\Phi_r|\boldsymbol{\beta})=\frac{6}{L\pi^2\cos^2(\Phi_r)(N_r^2-1)}\cdot\frac{M_t\sigma_n^2}{E_s N_r N_t\|\boldsymbol{\beta}\|^2} \quad (13)$$

Therefore, the average CRB of Φ_r can be expressed as

$$\mathrm{ACRB}(\Phi_r)=\frac{6}{L\pi^2\cos^2(\Phi_r)(N_r^2-1)}\cdot\frac{M_t\sigma_n^2}{E_s N_r N_t(M_rM_t-1)} \quad (14)$$

From (14), it is obvious that the ACRB is unable to indicate the direction finding performance of the system when M_r=M_t=1. Hence, we proceed to examine the outage CRB proposed in [5], which is denoted by $\mathrm{CRB}_{out=p}(\Phi_r)$. The outage CRB for a given probability p means that the probability of finding an estimator whose MSE is less than $\mathrm{CRB}_{out=p}(\Phi_r)$ is p [5]. Following [5], $\mathrm{CRB}_{out=p}(\Phi_r)$ can be evaluated from (13) by replacing $\|\boldsymbol{\beta}\|^2$ with $\frac{1}{2}F^{-1}_{\chi^2_{(2M_tM_r)}}(p)$.

Note here that although orthogonal waveforms are utilized in this paper, the transmitted signals can also be modelled by a Gaussian random process in the hybrid radar as that in [5], *i.e.*, $\mathbf{b}(t)\sim\mathcal{CN}(\mathbf{0}_{M_t},\mathbf{I}_{M_t})$. The AoA is estimated based on the signals received by all the receive antennas, which are given by

$$\mathbf{r}(t)=\sqrt{\frac{E_s N_t}{M_t}}\left[\mathbf{I}_{M_r}\otimes\boldsymbol{\gamma}_r(\Phi_r)\right]\boldsymbol{\Gamma}\mathbf{b}(t)+\mathbf{n}(t) \quad (15)$$

where the symbol $\otimes$ denotes the Kronecker product, the $M_r\times M_t$ matrix $\boldsymbol{\Gamma}=\left[\boldsymbol{\beta}_1\ \ \boldsymbol{\beta}_2\ \ \cdots\ \ \boldsymbol{\beta}_{M_r}\right]^T$, $\boldsymbol{\beta}_u\sim\mathcal{CN}(\mathbf{0}_{M_t},\mathbf{I}_{M_t})$, u = 1, 2,…, M_r, and $\mathbf{n}(t)\sim\mathcal{CN}(\mathbf{0}_{M_rN_r},\sigma_n^2\mathbf{I}_{M_rN_r})$. Following a derivation similar to that in [18], we can obtain the CRB of AoA condition on $\boldsymbol{\Gamma}$, which is shown as below:

$$\mathrm{CRB}(\Phi_r|\boldsymbol{\Gamma})=\frac{6}{L\pi^2\cos^2(\Phi_r)(N_r^2-1)}\left\{\frac{E_s N_r N_t\|\boldsymbol{\Gamma}\|^2}{M_t\sigma_n^2}-M_t+\mathrm{Re}\left[\mathrm{trace}\left(\mathbf{I}_{M_t}+\frac{E_s N_r N_t}{M_t\sigma_n^2}\boldsymbol{\Gamma}^H\boldsymbol{\Gamma}\right)^{-1}\right]\right\}^{-1} \quad (16)$$

V. NUMERICAL RESULTS

In this section, we examine the performance of a hybrid radar system with eight antennas at both the transmitter and receiver. Fig. 1 depicts the probability of miss-detection $\mathrm{Pr}_{\mathrm{MD}}$ calculated by using (6) for various system configurations. First of all, we compare the curves corresponding to the systems having the same M_t and three different values of M_r. The configuration with M_r=1 works the best at low SNR, and the system with one sparsely-spaced receive array (M_r=8, N_r=1) outperforms the others as the SNR increases, which is always preferred when the detection performance is acceptable, *e.g.*, $\mathrm{Pr}_{\mathrm{MD}}$ is less than 10^{-4}. Then we consider the scenarios with a fixed M_r and various M_t. Similarly, the system having a phased-array configuration at the transmitter performs the best at low SNR, while systems with larger M_t achieve lower $\mathrm{Pr}_{\mathrm{MD}}$ as the SNR increases. However, when M_r is large, the system

with large M_t performs the best only at relatively high SNR, and at that SNR value Pr_{MD} is comparatively low, *e.g.*, lower than 10^{-6}, which is unnecessary or even impossible in the real radar system. In addition, we can find that the improvement on detection performance by enlarging M_r for a fixed transmitter configuration is more obvious than that by increasing M_t when the receiver is unchanged. Therefore, a hybrid radar system, whose transmitter consists of a few antenna arrays and widely spaced elements at the receiver, provides better target detection performance than either the MIMO radar or the phased-array radar for practical values of Pr_{MD}.

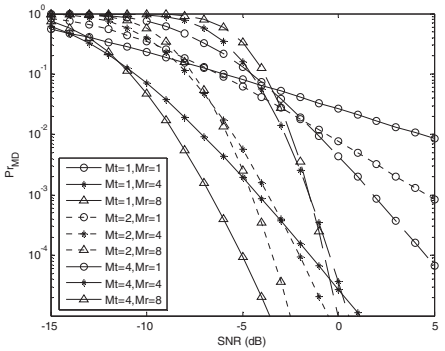

Figure 1. Pr_{MD} versus the SNR for various configurations.

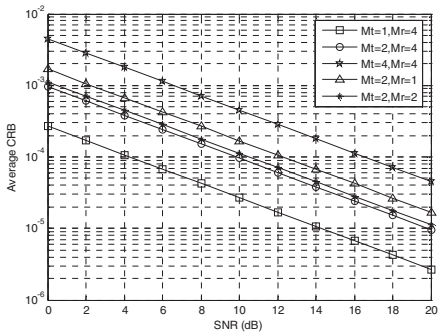

Figure 2. Average CRB of AoD versus the SNR for various configurations.

Next, we proceed to investigate the direction finding performance. Fig. 2 shows the average CRB of AoD calculated by using (10) for a hybrid system with various configurations. Notice here that M_t cannot be eight since no AoD estimation is possible during the initialization process when there is only one single antenna for each transmit array. It is obvious that for the same M_r, the smaller the value of M_t of a system, the lower the ACRB, while the ACRB decreases as M_r becomes larger for a fixed M_t. Thereby, in order to estimate the AoD more precisely, the phased-array configuration (M_t=1) should be selected for the transmitter while increasing the number of receive arrays M_r improves performance.

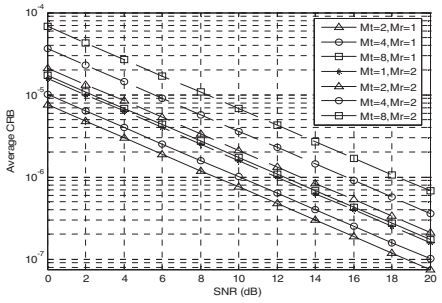

Figure 3. Average CRB of AoA versus the SNR for various configurations.

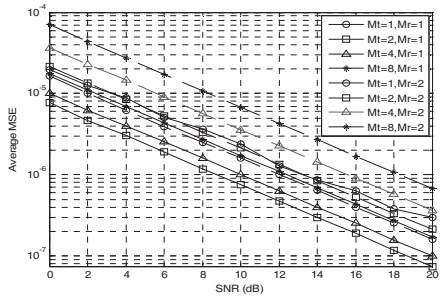

Figure 4. Average MSE of the ML estimator for AoA versus the SNR.

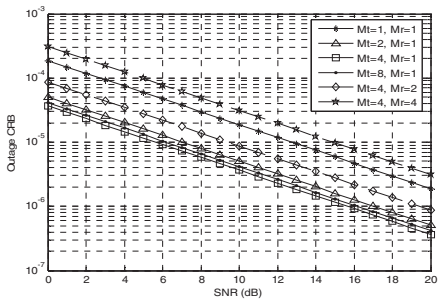

Figure 5. Outage CRB of AoA for systems with various configurations.

Fig. 3 represents the average CRB of AoA evaluated by (14) for different systems when the number of snapshots is assumed to be 80. In Fig. 4, the simulated average MSE of AoA for various configurations employing the ML estimator is shown. The estimated AoA is obtained from (12) and the simulated results are given by averaging the $\mathrm{MSE}\left|\hat{\boldsymbol{\Phi}}_r - \boldsymbol{\Phi}_r\right|^2$ for 100,000 realizations of the channel matrix **H**. Obviously, the theoretical ACRB results shown in Fig. 3

agree well with the corresponding simulated curves in Fig. 4. We also find that the smaller the value of Mr, the better the estimation of AoA. For the systems with the same receiver configuration M_r=1, the one with M_t=2 transmit arrays achieves the lowest average MSE, indicating that the total gain achieved by combining the spatial diversity gain provided by the 2 arrays and the coherent processing gain obtained by the 4 antennas of each array outweighs the diversity gain, or the processing gain realized by the 8 antennas in the MIMO or the phased-array configurations.

Finally we will compare the system performance by using the outage CRB rather than the ACRB since the latter does not exist when M_r=M_t=1. Fig. 5 shows the $\mathrm{CRB}_{out}(\Phi_r)$ when p=0.01. Observing the results for systems whose number of transmit arrays M_t is fixed at 4, we find that the radar with smaller M_r always performs better, which agrees with the conclusion drawn before. Hence, an array with closely-spaced antennas is usually preferred at the receiver for estimating the AoA. Then we compare the performance of systems with M_r=1, and see that the hybrid radar with 4 transmit arrays performs better than the system whose transmitting antennas are far from each other (M_t=8) or are closely located (M_t=1). Results for the system performance taking into account estimation errors in the AoD can be found in [9].

Based on previous discussion, we find that the best configuration for estimating AoD is the exact opposite of that for finding AoA. Although the performance of AoD estimation during the initialization process will affect the direction finding performance overall given the fact that the AoD information is required at the transmitter in order to cohere a beam toward the target detection, we validate in [9] that the estimation error in AoD caused by the initialization would not decrease the performance of estimating AoA significantly. It can be seen that the best hybrid configuration for a radar system is not the same for different detection and estimation applications. A hybrid system which is a compromise of these configurations would be the best choice to optimize jointly the detection and estimation performance. The best hybrid radar configuration for a specific scenario varies depending on the given number of antennas, the SNR value considered, the required precision, *etc.*, which can be evaluated by the theoretical expressions presented in this paper.

VI. CONCLUSIONS

In this paper, we investigated the hybrid bistatic radar system, which is a combination of the conventional phased-array and MIMO radar configurations. A closed form expression to evaluate the theoretical probability of detection of the hybrid system is derived, and the direction finding performance is examined by measuring the average CRB and outage CRB for estimating AoD and AoA. For a radar system having a fixed number of transmitting and receiving antennas, which is used for both target detection and direction finding, we suggest that a hybrid configuration should be employed, and the total gain achieved by combining the spatial diversity gain provided by the antenna arrays together and the coherent processing gain obtained by each array outweighs the diversity gain, or the processing gain realized by the antennas in pure MIMO or phased-array configurations.

ACKNOWLEDGMENT

We acknowledge the support of the Scottish Funding Council for the Joint Research Institute with Edinburgh and the Heriot-Watt Universities, which is a part of the Edinburgh Research Partnership (ERP). Chaoran Du gratefully acknowledges the support of the ERP in funding her PhD studies.

REFERENCES

[1] M. Skolnik, Introduction to Radar Systems, 3rd ed., New York: McGraw-Hill, 2002.

[2] E. Fishler, A. Haimovich, R. S. Blum, L. J. Cimini, D. Chizhik, and R. A. Valenzuela, "Spatial diversity in radars - Models and detection performance," IEEE Trans. Signal Process., vol. 54, no. 3, pp. 823-838, Mar. 2006.

[3] D. Tse and P. Viswanath, Fundamentals of wireless communication, New York: Cambridge University Press, 2005.

[4] E. Fishler, A. Haimovich, R. S. Blum, D. Chizhik, L. J. Cimini, and R. A. Valenzuela, "MIMO radar: An idea whose time has come," Proc. of the IEEE Int. Conf. on Radar, pp. 71-78, Apr. 2004.

[5] N. H. Lehmann, E. Fishler, A. Haimovich, R. S. Blum, D. Chizhik, L. J. Cimini, and R. A. Valenzuela, "Evaluation of transmit diversity in MIMO-Radar direction finding," IEEE Trans. Signal Process., vol. 55, no. 5, pp. 2215-2225, May 2007.

[6] D. R. Kirk, J. S. Bergin, P. M. Techau, and J. E. Don Carlos, "Multi-static coherent sparse aperture approach to precision target detection and engagement," IEEE Int. Radar Conf., pp. 579-584, May 2005.

[7] L. Xu and J. Li, "Iterative generalized-likelihood ratio test for MIMO radar," IEEE Trans. Signal Process., vol. 55, no. 6, pp. 2375-2385, June 2007.

[8] A. S. Fletcher and F. C. Robey, "Performance bounds for adaptive coherence of sparse array radar," presented at the 11th Conf. Adaptive Sensors Array Process., Lexington, MA, Mar. 2003.

[9] C. Du, J. Thompson, and Y. Petillot, "Detection and direction finding performance of hybrid bistatic radar," in preparation.

[10] C. Du, J. Thompson, and Y. Petillot, "Predicted detection performance of MIMO radar," IEEE. Signal Process. Lett., vol. 15, pp. 83-86, 2008.

[11] S. M. Kay, Fundamentals of Statistical Signal Processing: Estimation Theory, Upper Saddle River, NJ: Prentice-Hall PTR, 1993.

[12] A. M. Sayeed, "Deconstructing multiantenna fading channels," IEEE Trans. Signal Process., vol. 50, no. 10, pp. 2563-2579, Oct. 2002.

[13] S. Valaee, B. Champagne, and P. Kabal, "Parametric localization of distributed sources," IEEE Trans. Signal Process., vol. 43, no. 9, pp. 2144-2153, Sept. 1995.

[14] D. W. Bliss and K. W. Forsythe, "Multiple-input multiple-output (MIMO) radar and imaging: degrees of freedom and resolution," Proc. 37th Asilomar Conf. Signals, Systems, Computers, Pacific Grove, CA, vol. 1, pp. 54-59, Nov. 2003.

[15] F. C. Robey, S. Coutts, D. Weikle, J. C. McHarg, and K. Cuomo, "MIMO radar theory and experimental results," Proc. 37th Asilomar Conf. Signals, Systems, Computers, Pacific Grove, CA, vol. 1, pp. 300-304, Nov. 2004.

[16] H. Krim and M. Viberg, "Two decades of array signal processing research," IEEE Signal Process. Mag., vol. 13, no. 4, pp. 67-94, Jul. 1996.

[17] P. Stoica and A. Nehorai, "MUSIC, maximum likelihood, and Cramer-Rao bound", IEEE Trans. Acoust., Speech, Signal Process., vol. 37, no. 5, pp. 720-741, May 1989.

[18] P. Stoica, E. G. Larsson, and A. B. Gershman, "The stochastic CRB for array processing: A testbook derivation," IEEE Signal Process. Lett., vol. 8, no. 5, pp. 148-150, May 2001.

DETECTOR AND WAVEFORM DESIGN OF MIMO SYSTEM

Chaoran Du[a], John S. Thompson[a], Yvan R. Petillot[b]

[a]Institute for Digital Communications, Joint Research Institute for Signal & Image Processing, School of Engineering and Electronics, The University of Edinburgh, Edinburgh, EH9 3JL, UK.
[b]Joint Research Institute for Signal & Image Processing, School of Engineering and Physical Sciences, Heriot-Watt University, Edinburgh, EH14 4AS, UK.

Chaoran Du
Institute for Digital Communications, Joint Research Institute for Signal & Image Processing, School of Engineering and Electronics, Room 2.01, AGB Building, King's Buildings, The University of Edinburgh, Edinburgh, EH9 3JL, UK
Email: C.Du@ed.ac.uk
Fax: +44 (0)131 6506554

Abstract: *It has been shown that time reversal (TR), which is developed in the acoustics domain, can also improve the detection performance of a radar system. However, the TR technique is no longer a good choice when the noise level is high since the retransmitted signal contains significant noise components. We investigate a multiple input-multiple output (MIMO) detection process similar to TR detection, during which a waveform designed based on the estimated channel and a parameter indicating the quality of the estimation given a priori is retransmitted, and the detector determines the presence or absence of a target. We develop three detectors, whose theoretical thresholds are derived in closed form. Two schemes are proposed to design the retransmitted waveform with constraints on signal power. We compare the detection performance of different detectors, showing that the detector performing the best has the highest complexity, while the detector with the poorest performance demands the least amount of a priori information. Numerical results also present that both the designed waveforms achieve significant performance gains compared with the signal utilized in the TR process.*

Keywords: *MIMO, time-reversal, target detection, detector design, waveform design*

1. INTRODUCTION

The time-reversal (TR) technique, extended from the concept of phase-conjugation in optics, has attracted increasing interest for a broad range of applications. The unique feature of TR is that it can turn multipath effects, traditionally a drawback for target detection and imaging, into a benefit, which is very similar to the multiple-input multiple-output (MIMO) concept developed in communications. In the TR approach, a signal is first radiated through the medium, then the backscattered signal is recorded, time reversed, energy normalized, and retransmitted [1]. Recently, Moura *et. al.* explored the MIMO radar target detection problem using TR, showing that TR detection provides significant gains over conventional detection [2,3]. This results from the fact that the transmitter reshapes the waveform to match the channel during the TR process. However, the retransmitted signal in Moura's algorithm contains noise components, and it is obvious that if the noise level is high, the TR technique is no longer a good choice. Furthermore, [2,3] did not derive analytical expressions for the threshold and probability of detection of the TR detection, which were determined instead by Monte Carlo simulations.

We investigate a MIMO detection process similar to the TR detection in this paper. That is, during the probing phase, an incident wave is first transmitted into the medium and an estimated channel matrix with estimation error is obtained. It is assumed that a parameter indicating the quality of the estimation is given *a priori*, which can be appropriately chosen depending on the noise level, the channel dynamics, and estimation strategies, *etc.* [4]. Then, a waveform designed using the estimated channel and the estimation quality parameter under power constraints, instead of the TR signal used in Moura's scheme, is retransmitted, and finally the detector determines the presence or absence of a target. Note here that similar to the TR detection, it is assumed that the channel remains static during the probing and detecting phases.

2. SYSTEM MODEL

We consider a wideband bistatic MIMO sonar (or radar) system including a pair of arrays A and B as shown in Fig.1, which has N_a and N_b sensors, respectively. The channel frequency response is denoted by a $N_b \times N_a$ matrix $\bar{H}(f_q)$, q=1,2,…,Q_f, where the (k,l)-th entry of $\bar{H}(f_q)$ is the frequency response of the channel between the k-th sensor of array B and the l-th sensor of array A at the discrete frequency f_q. We adopt the statistical MIMO model here, that is, the entries of the channel matrix are assumed to be zero-mean circularly symmetric complex Gaussian (ZMCSCG), and they are normalized to have unit variance. The random target response results from the multipath effect, which arises from different propagation mechanisms. For example, the multipaths are due to a rich scattering environment surrounding point-like targets in [3], while in [5], the distributed target itself leads to multipath propagation.

As shown in Fig.1, the target detection process has two steps, and an estimated channel matrix $\hat{\bar{H}}(f_q)$ is obtained after the probing phase. In this paper, we consider the situation where minimum mean square error (MMSE) estimation is employed, and denote the estimation error as $\bar{E}(f_q) = \bar{H}(f_q) - \hat{\bar{H}}(f_q)$, whose entries are ZMCSCG with variance σ_e^2.

Note here that knowing the value of σ_e^2 requires noise power estimation and knowledge of the waveform length during the probing phase. Then, using the properties of MMSE estimation, the entries of $\hat{\bar{H}}(f_q)$ can be shown to be ZMCSCG with variance 1-σ_e^2 [4]. Since the focus of this paper is to design different detectors and retransmitted waveforms and study their effects on the target detection performance of the MIMO system, we assume that the estimated channel matrix and the quality parameter σ_e^2 are given *a priori*, and we concentrate on investigating the detection performance of the second step.

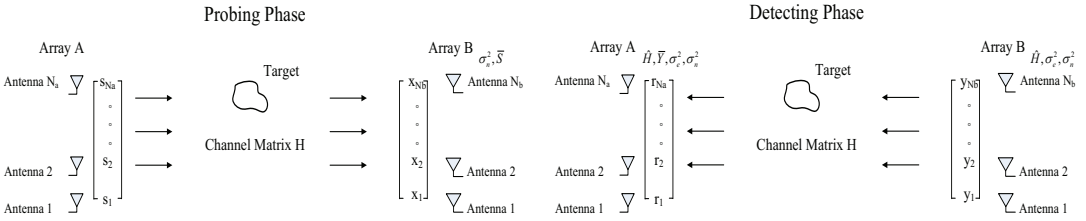

Fig.1: Description of the probing and detecting process of the MIMO system

It is assumed that array B transmits M snapshots in the second stage, during which the channel remains the same. Grouping the M snapshots received by the i-th sensor of array A at all the Q_f frequencies yields an $MQ_f \times 1$ vector, which is given by

$$\begin{aligned} &\bar{r}_i = \bar{Y} \cdot \bar{h}_i + \bar{n}_i, \\ &\bar{Y}(f_q) = \left[\bar{y}_1(f_q) \quad \bar{y}_2(f_q) \quad \cdots \quad \bar{y}_M(f_q) \right]^T, \bar{h}_i = \left[\bar{h}_i^T(f_1) \quad \bar{h}_i^T(f_2) \quad \cdots \quad \bar{h}_i^T(f_{Q_f}) \right]^T \end{aligned} \tag{1}$$

where i=1,2,…,N_a, q=1,2,…, Q_f, and the superscript T denotes the transpose of a matrix. Here, the $MQ_f \times N_b Q_f$ matrix $\bar{Y}$ is a block diagonal matrix whose diagonal blocks are $\bar{Y}(f_1)$, $\bar{Y}(f_2)$,…, $\bar{Y}(f_{Q_f})$, the $N_b \times 1$ vector $\bar{y}_m(f_q)$ is the m-th snapshot retransmitted from array B at frequency f_q, $\bar{h}_i(f_q)$ is the i-th column of $\bar{H}(f_q)$, and $\bar{n}_i$ represents the corresponding additive white Gaussian noise, whose entries are ZMCSCG with variance σ_n^2. Similarly to $\bar{h}_i$, we can obtain N_a estimated channel vectors $\hat{\bar{h}}_i$ and error vectors $\bar{e}_i$ by stacking the corresponding columns of $\hat{\bar{H}}(f_q)$ and $\bar{E}(f_q)$ into $N_b Q_f \times 1$ columns, respectively, and $\bar{h}_i = \hat{\bar{h}}_i + \bar{e}_i$. The detector at array A decides whether or not a target exists based on the values of all the signals $\bar{r}_i$ received by the N_a sensors.

3. DETECTOR DESIGN

The target detection problem of the MIMO system can be described as follows:

$$\text{Under } H_0: \ \bar{r}_i = \bar{n}_i; \qquad \text{Under } H_1: \ \bar{r}_i = \bar{Y} \cdot \hat{\bar{h}}_i + \bar{Y} \cdot \bar{e}_i + \bar{n}_i \tag{2}$$

where i=1,2,…,N_a, and the alternate hypothesis H_1 and null hypothesis H_0 are that the target does or does not exist, respectively. In this section, we develop three approaches to detect the

target: the conventional detector, the optimal detector, and the generalized likelihood ratio test (GLRT) detector. Only the key equations are presented here due to space limitation, and interested readers may refer to [6] for the detailed derivation.

It is well known that the optimal detector for a known signal in white Gaussian noise is the matched filter, and such a detector is denoted as Detector I, whose performance is examined when estimation error exists. The conventional detector given by [7] can be expressed as

$$T_{\mathrm{I}} = \mathrm{Re}\Big(\sum_{i=1}^{N_a} \overline{d}_i^{H} \overline{r}_i\Big) \underset{H_0}{\overset{H_1}{\gtrless}} \eta_{\mathrm{I}}, \quad \overline{d}_i = \overline{Y} \cdot \hat{\overline{h}}_i, \quad \eta_{\mathrm{I}} = \sqrt{\frac{\sigma_n^2 \sum_{i=1}^{N_a} \overline{d}_i^{H} \overline{d}_i}{2}} \cdot Q^{-1}(\mathrm{Pr}_{\mathrm{FA}}) \tag{3}$$

where the superscript H denotes the conjugate transpose of a matrix, $\mathrm{Pr}_{\mathrm{FA}}$ is the required probability of false alarm, and $\mathrm{Q}^{-1}(\mathrm{x})$ stands for the inverse Gaussian right-tail function. Clearly, Detector I demands the information of $\overline{Y}$ and $\hat{\overline{h}}_i$ to decide the existence of targets. Note here that the detector matches to the estimated channel $\hat{\overline{h}}_i$ instead of the true channel $\overline{h}_i$ as in [7], and this is because only the estimated channel is available at arrays A and B.

Next, we proceed to design Detector II, which is the likelihood ratio test (LRT) detector. The LRT detector is the optimal solution in the Neyman-Pearson sense [7]. After some algebra, the optimal detector can be described as below:

$$\begin{aligned} T_{\mathrm{II}} &= \sum_{i=1}^{N_a} \left\{ \left(\overline{r}_i + \overline{B}^{\dagger} \overline{g}_i \right)^{H} \cdot \overline{B} \cdot \left(\overline{r}_i + \overline{B}\ \overline{g}_i \right) \right\} \underset{H_0}{\overset{H_1}{\gtrless}} \eta_{\mathrm{II}} \\ \overline{d}_i &= \overline{Y} \cdot \hat{\overline{h}}_i, \ \ \overline{C} = \sigma_e^2 \overline{Y}\overline{Y}^{H} + \sigma_n^2 \overline{I}_{MQ_f}, \ \ \overline{B} = \frac{1}{\sigma_n^2} \overline{I}_{MQ_f} - \overline{C}^{-1}, \ \ \overline{g}_i = \overline{C}^{-1} \overline{d}_i \end{aligned} \tag{4}$$

where the superscript † denotes the pseudoinverse, and $\overline{I}_k$ stands for a $k \times k$ identity matrix.

It is reasonable to assume that T_{II} under both hypotheses have Gamma distributions as it has a quadratic form in Gaussian random variables, *i.e.*, $T_{\mathrm{II}} \sim \Gamma(k_0, \theta_0)$ under H_0 and $T_{\mathrm{II}} \sim \Gamma(k_1, \theta_1)$ under H_1, where $\Gamma(k, \theta)$ denotes the Gamma distribution with the shape parameter k and scale parameter θ. Hence, the theoretical threshold of the optimal detector can be given by

$$\begin{aligned} \eta_{\mathrm{II}} &= F^{-1}_{\Gamma(\mu_0^2/\Omega_0, \Omega_0/\mu_0)} \left(1 - \mathrm{Pr}_{\mathrm{FA}}\right) \\ \mu_0 &= \sum_{i=1}^{N_a} \left\{ \sigma_n^2 \mathrm{trace}(\overline{B}) + \overline{g}_i^{H}\ \overline{B}^{\dagger} \overline{g}_i \right\}, \quad \Omega_0 = \sum_{i=1}^{N_a} \left\{ \sigma_n^4 \mathrm{trace}(\overline{B}^{H} \overline{B}) + 2\sigma_n^2 \overline{g}_i^{H} \overline{g}_i \right\} \end{aligned} \tag{5}$$

where $F^{-1}_{\Gamma(k,\theta)}$ denotes the inverse cumulative distribution function (CDF) of the Gamma random variable with parameters k and θ. From (4) and (5), it is clear that the implementation of Detector II requires knowledge of $\overline{Y}$, $\hat{\overline{h}}_i$, and σ_e^2 at array A.

Detector III is the GLRT detector, which is a practical approach when unknown parameters exist [7]. The GLRT detector replaces the unknowns with their maximum likelihood (ML) estimates, and in our case, it is given by

$$T_{\mathrm{III}} = \sum_{i=1}^{N_a} 2\overline{r}_i^H \overline{Y}\left(\overline{Y}^H\overline{Y}\right)^{\dagger}\overline{Y}^H\overline{r}_i \Big/ \sigma_n^2 \underset{<_{H_0}}{\overset{>^{H_1}}{}} \eta_{\mathrm{III}}, \quad \eta_{\mathrm{III}} = F^{-1}_{\chi^2_{2nN_a}}\left(1-\mathrm{Pr}_{\mathrm{FA}}\right) \tag{6}$$

where n is the rank of $\overline{Y}$, i.e., $n = \mathrm{rank}(\overline{Y}) \le \min\left(MQ_f, N_BQ_f\right)$, and $F^{-1}_{\chi^2_k}$ is the inverse CDF of a central chi-square random variable with k degrees of freedom. Obviously, only the value of $\overline{Y}$ is required to be known for Detector III. We next consider T_{III} under H_1. Denote by $\overline{U}\overline{\Sigma}\overline{V}^H$ the singular value decomposition (SVD) of $\overline{Y}$, where the $MQ_f \times MQ_f$ matrix $\overline{U}$ and $N_bQ_f \times N_bQ_f$ matrix $\overline{V}$ are unitary matrices, and $\overline{\Sigma}$ is an $MQ_f \times N_bQ_f$ diagonal matrix with n positive singular values $\varsigma_1, \varsigma_2, ..., \varsigma_n$ of $\overline{Y}$ (in decreasing order) on the diagonal. Defining an $n \times 1$ vector $\overline{\beta}$, whose k-th entry β_k is the square of the corresponding singular value of $\overline{Y}$, *i.e.*, $\beta_k = \varsigma_k^2$, we can rewrite (6) as below:

$$T_{\mathrm{III}} = \sum_{i=1}^{N_a}\sum_{k=1}^{n}\frac{1}{\sigma_n^2}\left(\sigma_e^2\beta_k + \sigma_n^2\right)\gamma_{ik}, \quad \gamma_{ik} \sim \chi_2^{'2}\left(\lambda_{ik}\right), \quad \lambda_{ik} = 2\beta_k\left|h_{ik}^{'}\right|^2 \Big/ \left(\sigma_e^2\beta_k + \sigma_n^2\right) \tag{7}$$

where $|.|$ denotes the modulus of a complex number, $h_{ik}^{'}$ is the k-th element of the vector $\overline{h}_i^{'} = \overline{V}^H\hat{\overline{h}}_i$, and $\chi_k^{'2}(\lambda)$ stands for a noncentral chi-square random variable with k degrees of freedom and non-centrality parameter λ. Notice here that T_{III} is a weighted sum of several noncentral chi-square random variables, and it is difficult to derive a closed form for its distribution. In order to calculate the theoretical $\mathrm{Pr_D}$, we approximate T_{III} using a common technique which has been widely adopted in statistics and engineering. This approach approximates a weighted sum of chi-square variables by a single one with different degree of freedom and a scaling factor, which are carefully chosen such that the first two moments remain the same. Therefore, the test static of the GLRT detector can be expressed as below:

$$T_{\mathrm{III}} \sim \frac{\alpha}{\sigma_n^2}\chi_l^2, \quad \alpha = b/a, \quad l = 2a^2/b, \quad \rho_k = \sum_{i=1}^{N_a}\left|h_{ik}^{'}\right|^2 \tag{8}$$

$$a = \sum_{k=1}^{n}\left\{N_a\left(\sigma_e^2\beta_k + \sigma_n^2\right) + \beta_k\rho_k\right\}, \quad b = \sum_{k=1}^{n}\left\{N_a\left(\sigma_e^2\beta_k + \sigma_n^2\right)^2 + 2\left(\sigma_e^2\beta_k + \sigma_n^2\right)\beta_k\rho_k\right\}$$

4. WAVEFORM DESIGN

In this section, we propose two approaches to design the retransmitted waveform $\overline{Y}$ by maximizing the upper and lower bound of the $\mathrm{Pr_D}$ of the GLRT detector developed in the last section, respectively. The design criteria are under the constraint $\mathrm{trace}(\overline{Y}\overline{Y}^H) = MQ_fE_s$ which limits the total transmitted power. As defined in the last section, entries of $\overline{\beta}$ are actually the eigenvalues of the Hermitian matrix $\overline{Y}\overline{Y}^H$, and thus, the power constraint can be rewritten as $\sum_{k=1}^{n}\beta_k = MQ_fE_s$, and $\beta_k \ge 0,\ k = 1, 2, ..., n$. The first waveform is designed to maximize the upper bound, which is obtained by utilizing Markov's inequality, *i.e.*, $\mathrm{Pr_D} = \Pr\{T \ge \eta\} \le E[T]/\eta$.

Substituting (7) into the above equation and recalling the power constraint, we can express the design criterion for waveform design I as the following constrained maximization problem:

$$\max_{\vec{\beta}} \sum_{k=1}^{n} \left(N_a \sigma_e^2 + \rho_k \right) \beta_k, \quad \text{s.t.} \sum_{k=1}^{n} \beta_k = MQ_f E_s, \quad \beta_k \geq 0, \ \ k = 1, 2, ..., n \tag{9}$$

Applying Abel's inequality, we find that the maximization of (9) is achieved by allocating all the available power to the eigenvalue β_k which corresponds to the largest ρ_k.

Next, we design the second waveform based on the lower bound. Again, adopting Markov's inequality leads to the bound $\Pr_D = 1 - \Pr\left\{ -\sigma_n^2 T \geq -\sigma_n^2 \eta \right\} = 1 - \Pr\left\{ e^{-\sigma_n^2 T} \geq e^{-\sigma_n^2 \eta} \right\} \geq 1 - E\left[e^{-\sigma_n^2 T} \right] \Big/ e^{-\sigma_n^2 \eta}$. After some derivation, we can describe the problem of maximizing the lower bound as below

$$\max_{\vec{\beta}} \sum_{k=1}^{n} \left\{ \frac{2\beta_k \rho_k + 2N_a \left(\sigma_e^2 \beta_k + \sigma_n^2 \right)}{1 + 2(\sigma_e^2 \beta_k + \sigma_n^2)} \right\}, \quad \text{s.t.} \sum_{k=1}^{n} \beta_k = MQ_f E_s, \ \ \beta_k \geq 0, \ \ k = 1, 2, ..., n \tag{10}$$

This constrained optimization problem can be solved by employing the Karush-Kuhn-Tucker (KKT) conditions [9], and the waveform design II can be given by

$$\beta_k = \left(1 + 2\sigma_n^2 \right) \Big/ 2\sigma_e^2 \left(\xi \sqrt{2\rho_k + 4\rho_k \sigma_n^2 + 2N_a \sigma_e^2} \Big/ \left(1 + 2\sigma_n^2 \right) - 1 \right)^{+} \tag{11}$$

where $(a)^{+} = \max(0, a)$ and ξ is chosen such that the constraint is met, *i.e.*, $\sum_{k=1}^{n} \beta_k = MQ_f E_s$. It is clearly seen that this design scheme utilizes the waterfilling strategy [4] to allocate the power, and the larger the ρ_k is, the more power is allocated to its corresponding β_k.

5. NUMERICAL RESULTS AND DISCUSSION

In this section, we present numerical results showing the target detection performance of a MIMO system with four sensors at array A and two sensors at array B. We choose the number of snapshots M = 2 and the number of frequencies Q_f = 4 for simulation purposes. The signal-to-noise ratio (SNR) is defined as $\text{SNR} = E_s / \sigma_n^2$, and the probability of false alarm is set to be a constant value $\Pr_{FA}$=0.01. Notice here that the algorithms for both the detector and waveform design are based on a known estimated channel, which is actually a realization of the random vector. Therefore, a semi-analytical approach is utilized to obtain the system performance. In other words, we generate 10,000 realizations of the estimated channel matrix, calculate the corresponding $\Pr_D$ for each realization, and determine the system detection performance by averaging $\Pr_D$ over all the realizations.

Fig.2 depicts the detection performance of systems employing different detectors at array A for two values of σ_e^2. The waveform adopted here is the normalized TR signal, and the normalization is used to meet the power constraint. For each σ_e^2, any difference in performance results from the detector design only since the retransmitted signals are the same for all systems. Observing the curves, we find that Detector II performs the best under any

circumstance, which is consistent with the fact that Detector II is the optimal detector in the Neyman-Pearson sense. In addition, the performance difference between Detector I and Detector II increases as the estimation quality becomes lower, *i.e.*, σ_e^2 is larger. This can be explained that Detector I is effectively a matched filter to the signal $\overline{Y}\hat{\overline{h}}_i$, while the optimal detector is a filter matching to the true signal $\overline{Yh}_i$ when the channel matrix is known [7]. Therefore, the difference between the performance of Detector I and the optimal performance should be small when the error in the estimated channel is insignificant, and this happens when σ_e^2 is small. Furthermore, it is easily seen that Detector III performs the poorest at low SNR but is similar to the optimal detector when the SNR is high. This is because the GLRT detector actually estimates the unknown parameters first and then makes the detection decision based on those estimates. Intuitively, the lower the SNR, the worse the estimation, which leads to worse detection performance. However, although Detector II performs the best, it has the highest complexity and it requires knowledge of $\overline{Y}$, $\hat{\overline{h}}_i$, and σ_e^2 at array A. In contrast, as mentioned in Section 3, the implementation of Detector I needs the information of $\overline{Y}$ and $\hat{\overline{h}}_i$, while for Detector III only $\overline{Y}$ is required to be known.

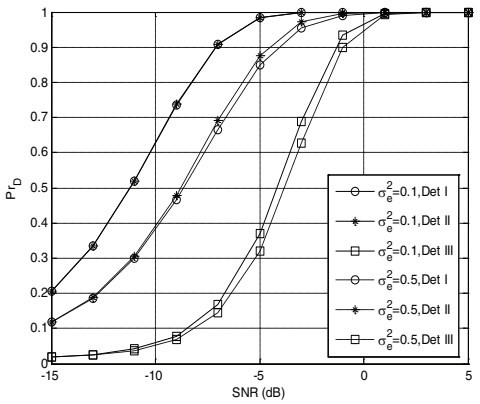

Fig.2: Pr_D versus SNR for systems with different detectors

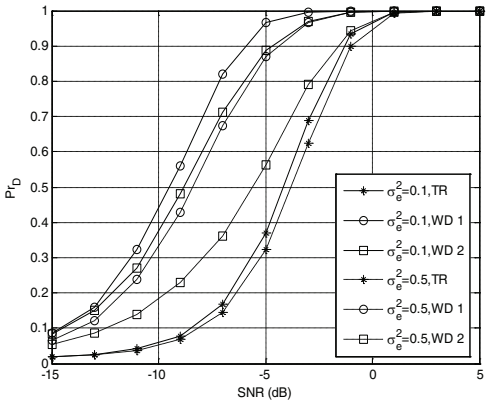

Fig.3: Pr_D versus SNR for systems with different retransmitted waveforms

We next examine the detection performance of the systems retransmitting different waveforms with two values of σ_e^2 as shown in Fig.3. Here, Detector III is employed for all scenarios, and any difference in performance arises from the designed waveforms only. In Fig.3, the labels TR, WD1, and WD2 correspond to the normalized TR signal, the waveform design I, and the waveform design II proposed in the last section, respectively, and all the waveforms have the same transmitted power constraint. Obviously, the designed waveforms improve the system performance significantly with respect to the TR signal. Specifically, for Pr_D =0.8, the performance gap between waveform design I and the TR signal is about 5dB when $\sigma_e^2 = 0.1$ and 4dB when $\sigma_e^2 = 0.5$, while the performance gain achieved by waveform design II compared with the TR signal is about 4dB when $\sigma_e^2 = 0.1$ and 1.5dB when $\sigma_e^2 = 0.5$. Nevertheless, from the waveform design algorithms, we realize that such significant performance improvement is achieved at the price of knowing the quality of channel estimation σ_e^2 *a priori*. We emphasize here that although both the waveforms are designed based on the GLRT detector, the semi-analytical Pr_D of the systems employing Detector I and

Detector II can also be obtained when the designed waveforms are retransmitted from array B, and similarly, both waveforms achieve considerable performance gains. These numerical results are available in [6], but are not presented here due to the space limitation.

6. CONCLUSIONS

In this paper, we investigated the target detection performance of a bistatic wideband MIMO system, whose detection process is similar to the TR procedure. Based on the estimated channel and a parameter indicating the quality of the estimation obtained during the probing phase, the retransmitted waveform and the detector are designed. Three detectors are developed, whose theoretical thresholds are derived in closed form. Two approaches are proposed to design the retransmitted waveform with signal power constraint, which maximize the upper and lower bound of the probability of detection of the GLRT detector, respectively. Numerical results demonstrate that the optimal detector performs the best but demands the largest amount of *a priori* information. The performance difference between the conventional and the optimal detector increases as the estimation quality becomes lower. The GLRT detector performs the poorest at low SNR but is similar to the optimal detector at high SNR. Both the designed waveforms achieve significant performance gains compared with the TR signal at the price of knowing the quality of channel estimation *a priori*.

7. ACKNOWLEDGEMENTS

We acknowledge the support of the Scottish Funding Council for the Joint Research Institute with Edinburgh and the Heriot-Watt Universities, which is a part of the Edinburgh Research Partnership (ERP). Chaoran Du gratefully acknowledges the support of the ERP in funding her PhD studies.

REFERENCES

[1] C. Prada, F. Wu, and M. Fink, The iterative time reversal mirror: A solution to self-focusing in the pulse echo mode, *IEEE J. Acoust. Soc. Am.*, 90(2), pp.1119-1129, 1991

[2] J. M. F. Moura and Y. Jin, Detection by time reversal: Single antenna, *IEEE Trans. Signal Process.*, 55(1), pp.187-201, 2007

[3] Y. Jin and J.M.F. Moura, Time reversal transmission in MIMO radar, *Proc. 41th Asilomar Conf. Signals, Systems, Computers*, Pacific Grove, CA, pp.2204-2208, 2007

[4] T. Yoo and A. Goldsmith, Capacity and power allocation for fading MIMO channels with channel estimation error, *IEEE Trans. Inf. Theory*, 52(5), pp.2203-2214, 2006

[5] E. Fishler, R.S. Blum, L.J. Cimini, and D. Chizhik, Spatial diversity in radars-Models and detection performance, *IEEE Trans. Signal Process.*, 54(3), pp.823-838, 2006

[6] C. Du, J.S. Thompson, and Y.R. Petillot, Detector and waveform design of MIMO system, in preparation

[7] S.M. Kay, *Fundamentals of statistical signal processing: Detection Theory*, Upper Saddle River, NJ: Prentice-Hall PTR, 1993

[8] M. Nakagami, The m-distribution-A general formula of intensity distribution of rapid fading, *Statistical Methods in Radio Wave Propagation*, pp.3-36, 1960

[9] S. Boyd and L.Vandenberghe, *Convex Optimization*, Cambridge University Press, 2004